A Distributed Tactile System for Humanoid Robot Hands

Alexander Schmitz

A thesis submitted in partial fulfillment
of the requirements for the degree of
Doctor of Philosophy

University of Sheffield

2011

To my parents

ABSTRACT

The lack of sensitive skin for the hands of humanoid robots has proven to be a key limitation preventing human-like performance in tasks that require controlled physical manipulation of unmodeled objects in uncontrolled environments. While a large number of sensing technologies exist, it is not trivial to incorporate them into the hands of humanoid robots. This is because of the limited space available in such hands, which makes it difficult to preserve the other functions of the hand while integrating the sensors. Not only the transducers need to be small, also the space for the connected wires needs to be taken into account. Therefore, embedded electronics and distributed computation are crucial.

This thesis presents the smallest existing artificial fingertip that incorporates a distributed pressure sensor with integrated digitisation. In particular, 12 sensors based on capacitive technology are included in the fingertip. Due to the integrated digitisation, only 4 wires need to be connected to each fingertip. Concerning the morphology, to support human-like grasping, the fingertips have a curved shape similar to human fingertips, and moreover the fingertips are compliant. The fingertips have been embedded together with a sensitive palm into the hands of the humanoid robot iCub. The palms are based on the same technology as the fingertips, which facilitates the integration. Each hand has in total 108 taxels. The sensors have already been installed on a number of iCubs. To achieve this, also the ease of production and the installation mechanism of the fingertips had to be optimized. The hysteresis and drift in the measurements have been addressed, which are common problems for capacitive pressure sensors. Experiments with both the fingertips and the palm have been performed and it could be shown that the sensors have good characteristics and can be used to grasp unmodeled, fragile objects.

ACKNOWLEDGMENTS

Firstly, I want to thank my supervisor, Dr. Tony Dodd, who has read many drafts of this work, gave me a lot of advice and was constantly available when questions came up. I also want to thank Prof. David Owens, who assisted me in the beginning of my PhD and was my former supervisor at the ACSE. Without his help it would have been impossible to start my thesis.

I also thank the people at the Italian Institute of Technology, where I spend a lot of time during my thesis and who provided constant support. In particular, I want to thank Dr. Lorenzo Natale, who was looking after my work while I was at the IIT. Many discussions with him proved to be fruitful for coming up with ideas and improvements. I also want to thank Dr. Marco Maggiali who was developing a tactile sensor for the palms of the robot in parallel. We exchanged many ideas and I could use the microcontroller board he had developed for his sensor. Dr. Marco Randazzo was using a conductive silicone for his actuators, which I could use with some modifications for the fingertips. Dr. Maurizio Biso supervised my attempts to develop a more conductive silicone. The electronics department, in particular Bruno Bonino and Claudio Lorini, assisted me in realizing the printed circuit boards. Dr. Ravinder Dahiya permitted the use of two of his experimental setups for initial experiments with the fingertips. Many other people supported my stay at the Italian Institute of Technology, in particular Prof. Giorgio Metta, Prof. Giulio Sandini, Prof. Darwin Caldwell, Dr. Francesco Nori and Perla Maiolino.

Also numerous other colleagues helped me in many different ways, for example in proof reading my papers, providing me with ideas or letting me use some of their equipment. In addition, I want to thank the assistive staff for making my PhD possible. Finally, I thank my family and friends for providing consistent support during the years of my PhD!

This work was funded by the European Commission as part of the following projects: RobotCub (IST-FP6-004370), Poeticon (ICT-FP7-215843) and RoboSkin (ICT-FP7-231500).

CONTENTS

LIST OF FIGURES

LIST OF TABLES

LIST OF ACRONYMS

CAN Controller–Area Network

CB Carbon Black

CDC Capacitance to Digital Converter

DMAC Dimethylacetamide

DOM Degree Of Motion

I^2C Inter-Integrated Circuit

MWCNT Multi-Wall Carbon Nanotubes

PCB Printed Circuit Board

PVDF Polyvinylidene Fluoride

SWCNT Single-Wall Carbon Nanotubes

Taxel Tactile element, one sensitive zone, one sensing point

THF Tetrahydrofuran

Chapter 1

INTRODUCTION

1.1 Motivation

Even though the sense of touch is crucial for humans, most humanoid robots lack tactile sensing. In this work, the tactile sensing abilities of the robot iCub have been improved. Such abilities will support the humanoid's object grasping and manipulation skills. They provide essential information for adapting the grasp for a particular task, and can additionally be used to actively explore an object in the hand. By integrating tactile and visual information while interacting with objects, it will be possible to obtain robot-specific representations of objects, and, more generally, of the interaction of the robot with its environment. Moreover, when humanoids work with humans, tactile skin is crucial for safety, and tactile feedback can be used to interact with the robot.

While many different modes of transduction have been explored (for an overview see for example [1][2]), integrating tactile sensors into robotic hands remains challenging. This is because the sensors should not only give reliable measurements, but they should also be integrated into little space without obstructing the other functions of the robot. Therefore, one has to focus not only on the transducer, but also on other factors like digitization and wiring [2]. Most of the sensors that have been integrated into the fingertips of humanoid robots are three- or six-axis force torque sensors (in Section 2.3.1 an overview of sensors that have been integrated into humanoid fingertips will be given). While they also provide information about forces tangential to the sensor surface, they do not give distributed information about the contact area. Moreover, it is difficult to integrate them into fingertips as small as those of the iCub[1]. Other robots integrate distributed tactile sensors, but most of them are too big to be installed on the fingertips of iCub, too, or they cannot be fitted to a fingertip with a human like shape, or they are not compliant. Most of the sensors that have densely distributed tactile elements can be produced only for flat surfaces or at most for cylindrical

[1] In any case, if three- or six-axis force torque sensors can be designed at a later stage small enough for the fingers of iCub, the different sensor modalities would complement each other.

surfaces. In general, few sensors have integrated electronics and the wiring is an unsolved problem for them. Those that have integrated electronics usually use components that would be too big for small humanoid hands. Moreover, many sensors are cumbersome to produce and have been fabricated only as prototypes. Finally, many of the sensors described in the literature are not sensitive enough, or their characteristics have not been published. As a conclusion, no solution was available that fulfilled all requirements (stated in Section 1.3), and therefore it became necessary to develop a viable solution for the iCub robot as part of this thesis, which at the same time would increase the knowledge and the possibilities of artificial tactile sensing in general.

1.2 Context

The sensors described in this thesis have been designed to be mounted on the hands of the humanoid robot iCub. iCub has been designed with the goal of creating an open hardware/software robotic platform for research in embodied cognition [3]. Its design has been mainly developed within the RobotCub project[2], a European funded project with the aim of studying natural and artificial cognitive systems [4]. At the current state, the iCub robot has a total of 53 actuated degrees of freedom, 6 in each leg, 7 in each arm, 6 in the head, 3 in the waist and 9 for each hand, see Figure 1.1. The robot is about 1m tall, which is roughly the size of a three and a half years old child. It is equipped with an active stereo vision system, microphones, acceleration sensors in the head and joint position sensors in most of the joints [5].

The hand of iCub is roughly 14 *cm* long and 6 *cm* wide. It has five underactuated fingers (see Figure 1.2) actuated by 9 motors. Two motors control independently the motion of the proximal and medial phalanges of the index finger; the most distal phalange is mechanically coupled with the medial one to bend in a human-like way when the finger closes. The same configuration is repeated for the middle finger. Ring and little fingers are coupled together and are driven by only one motor. The thumb is actuated by three motors: it can rotate around the palm and flex at the level of proximal and medial phalanges. Finally, another motor controls the abduction of the index, ring and little finger. Seven of the nine motors for the hand are located in the forearm. The wrist has three additional actuated degrees of freedom. Most joints in the hand are instrumented with Hall effect position sensors in addition to the incremental encoders in the motors. Details about the coupling of

[2]RobotCub was a project funded by the European Commission under the sixth framework programme (FP6) by Unit E5: Cognitive system, interaction and Robotics.

the joints can be found in Section 2.4.

In order to enhance the object manipulation skills of iCub, a tactile sensor system was to be integrated into its hands. Therefore, a capacitive pressure sensor system with 108 taxels has been integrated into the hand of iCub, i.e. into all fingertips and the palm, see Figure 1.2. The palm (developed mainly by Dr. Marco Maggiali) consists of four triangular modules, which can be used to cover generic curved surfaces and can be used to cover also other parts of the robot body [6]. The small size and the desired curved shape of the fingertips on the contrary made it necessary to design a specific solution that fits on the fingers of iCub: each fingertip is 14.5 mm long and 13 mm wide and high. It has a round shape that resembles a human fingertip.

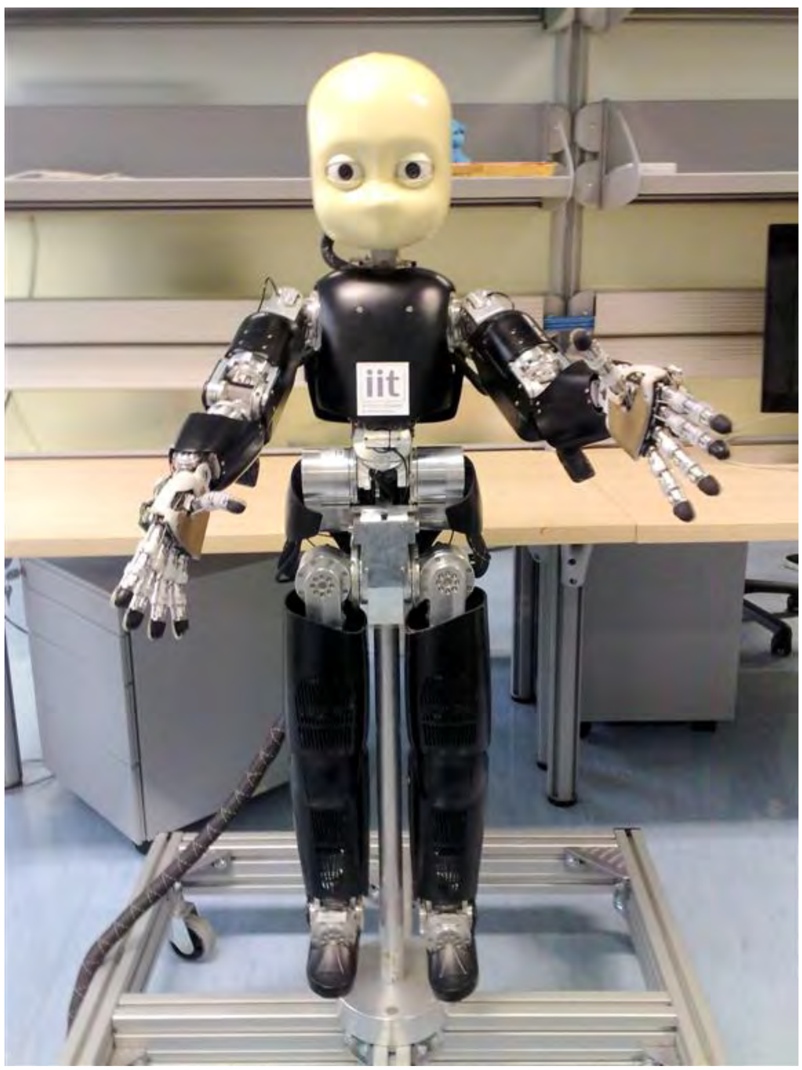

Figure 1.1: **The humanoid robot iCub.** It has 53 controllable degrees of freedom.

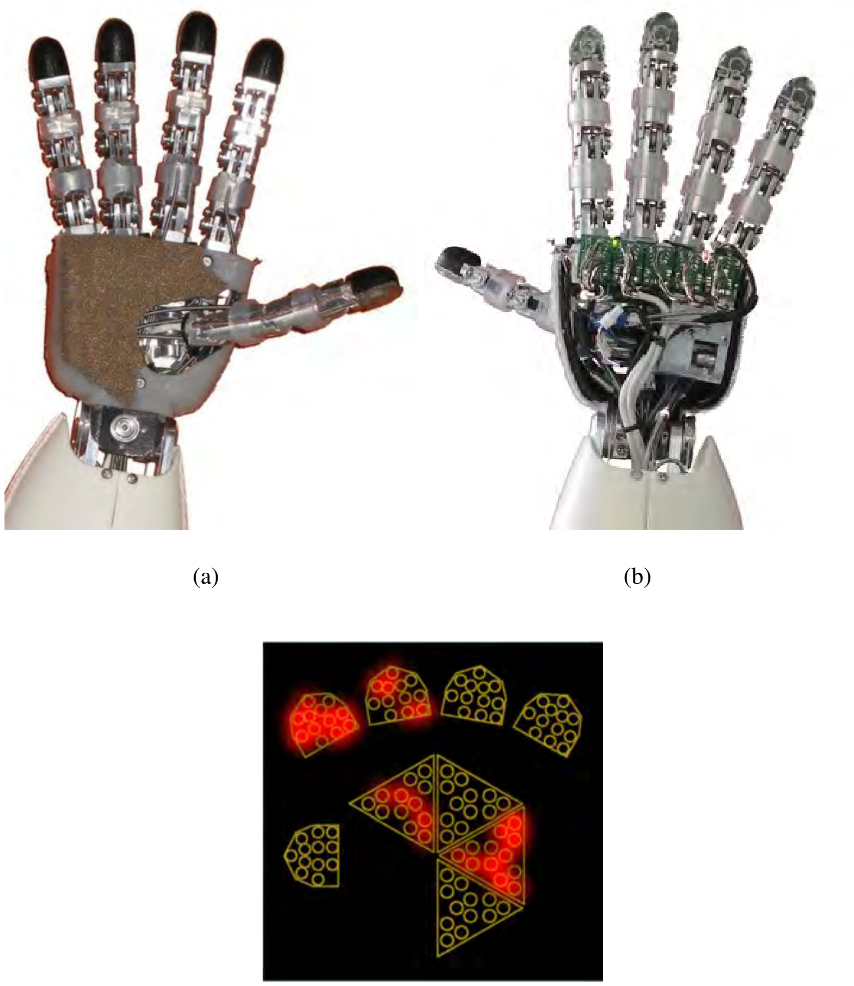

(a) (b)

(c)

Figure 1.2: **The hand of the humanoid robot iCub.** Each fingertip has 12 taxels and in addition the palm has 48 taxels. Overall each hand has a sensory system with 108 taxels. In **(a)** the hand is seen from the front and in **(b)** from the back. In **(c)** a screenshot from the visualization of the measurements of the tactile sensor system is shown. It also shows a schematic representation of how the sensors are distributed on the fingertips and the palm.

1.3 Aims and Objectives

The goal was to construct *a cutaneous distributed tactile pressure sensor system for the fingertips of iCub*, which can be integrated together with a sensitive palm into the hands of the robot. The information from these sensors could be used to perceive the strength, shape and localization of the contact with an object that the robot is grasping. Several requirements have to be fulfilled so that the sensors can be integrated into the fingertips of the humanoid robot iCub.

- The space for the fingertips is limited; therefore, the design has to be compact.

- The electronics for the digitization of the sensor signals should be included in the fingertip. In this way, the sensor readings from several tactile elements can be transmitted over the same wire and fewer wires have to be connected to the fingertip. A reduced number of wires is a key benefit for the implementation on the robot, because an excessive amount of wires would use too much of the space available in the hand and would impede the dexterity of the hand. In addition, digitization close to the transducer also reduces the noise in the sensor measurements. This is because analogue signals transmitted over long wires are more prone to interference and signal degradation. In an analogue signal, any change to the signal influences the message, while in a digital line, as long as the bits can be correctly interpreted as either a zero or one (even if for example the voltage slightly changes), the message is not corrupted.

Furthermore, the morphology of the fingertip should be similar to a human fingertip, as this would be beneficial while studying human like grasping. This causes additional challenges for the sensor.

- The shape should resemble those of human fingertips. Therefore, and as the goal is a cutaneous sensor, the transducer of the sensor has to be able to conform to compound curves. Conformability to curved geometries is a challenge for current production mechanisms. Most standard production methods are not suitable as they only work on two-dimensional flat surfaces.

- Compliance also at the surface level of the end effector can aid grasping. Therefore, in order to make the fingertips compliant, the sensor should be soft.

Moreover, there are several requirements concerning the production and maintenance, as the fingertips are intended to be installed on a number of robots.

- The sensor should be easy to produce, requiring as little manual labour as possible.

- The sensors should be robust to increase the lifetime of the fingertips, and the sensor characteristics should be stable.

- In case the sensor breaks it should be possible to repair or to replace it easily.

Concerning the quality of the measurements, the ultimate goal is to achieve or even exceed human like sensing. If this is not possible, the aim is to excel comparable, state of the art, artificial tactile sensors. The following factors contribute to the overall quality of the measurements:

- The human finger has a sensitivity of about 0.1 g per mm2 (or about 1 kPa) [7]. In order for the robot to achieve a similar performance, a number of factors have to be taken into account: the noise in the sensor measurements should be as low possible, with a good signal to noise ratio. The sensor should show low hysteresis and low drift, including long term drift, due to degradation of the sensor; the existent systematic errors should be compensated. Nonlinearity in the sensor response also has to be identified and compensated. As a result, the sensor should provide accurate and repeatable measurements, the sensor should be sensitive to low pressure and have a good resolution, and the measurements should not be effected by other properties than the pressure applied to the sensor.

- Moreover, the sensor should have a good response time and a high sampling frequency. The frequency response should be stable over the relevant frequencies. Humans can distinguish two stimuli if they have an interval of about 5.5 ms [8].

- Furthermore, the range of the sensor should cover the forces necessary for object manipulation. Humans use pressures from 10 to 100 *kPa* while handling objects [9].

- A distribute cutaneous sensor has the benefit that it can be used to localize where pressure is applied to the fingertip, to identify the shape of the contact area, and also to distinguish separate contacts. In order to achieve human like performance, the spatial resolution should be about 1 *mm* for the fingertips, but can be as low as 5 *mm* for other parts like the palm [2]. Moreover, in humans the whole skin is covered with tactile sensors. Also in the robot, at least for the fingertips, the whole area should be covered with sensors. As a result, no touch event should be missed, because the contact happens in an insensitive surface area.

1.4 List of Novel Contributions

This thesis presents first a fingertip for a humanoid robot, which integrates a distributed pressure sensor. A major issue during the development was the limited space that is available for the senor. The resulting sensor is compact, compliant and shaped like a human fingertip. It has 12 taxels, local A/D conversion and needs to be interfaced with few wires. The fingertips have been integrated together with a palm, which has been developed by Dr. Marco Maggiali, into the hands of a humanoid robot. Tests have been performed to show that the sensor has favourable characteristics and algorithms have been implemented to compensate the hysteresis and drift, which commonly affect capacitive sensors [2]. Experiments with the robot prove that the sensors can be used to grasp unmodeled, fragile objects.

- **C 1: Miniaturisation** - For the first time a distributed tactile sensing system with integrated digitisation has been incorporated into a fingertip as small as the one presented in this thesis.

- **C 2: Multi-curved shape** - The fingertips have a shape similar to a human fingertip. Most of the other fingertips that are described in the literature are flat, consist of a combination of flat surfaces, or are at most cylindrical.

- **C 3: Integration** - As only few other systems before, the fingertips together with the palm have been successfully integrated into the hands of a humanoid robot. They work together as a complete solution without impeding the other functions of the robot (like its dexterity).

- **C 4: Manufacturing** - The manufacturing process was optimized to make it possible to fabricate the sensor reliably, easily and fast. The sensors were not only produced as prototypes, but already five robots have been equipped with the sensors.

- **C 5: Evaluation** - Many different aspects of the sensors have been experimentally evaluated. For most of the other sensors, which have been integrated into humanoid robots in the past, only limited data concerning their characteristics is available.

- **C 6: Drift and hysteresis compensation** - Both usually affect capacitive sensors and in this thesis compensation algorithms have been successfully implemented and evaluated. Especially hysteresis compensation algorithms are often only tested by loading and unloading the sensor once. In this thesis, the algorithm has been examined during multi-step, cyclic loading with varying time intervals.

The work presented in this thesis has also been made available in the following publications:

1. Schmitz, A., Maggiali, M., Randazzo, M., Natale, L. and Metta, G. (2008) A Prototype Fingertip with High Spatial Resolution Pressure Sensing for the Robot iCub. Proceedings of the 8th IEEE-RAS International Conference on Humanoid Robots, Daejeon, Korea

2. Schmitz, A., Maggiali, M., Natale, L., Bonino, B. and Metta, G. (2010) A Tactile Sensor for the Fingertips of the Humanoid Robot iCub. 2010 IEEE/RSJ International Conference on Intelligent Robots and Systems (IROS 2010), Taipei, Taiwan

3. Schmitz, A., Maggiali, M., Natale, L. and Metta, G. (2010) Integrating Tactile Sensors into the Hands of the Humanoid Robot iCub. Workshop on Representations for Object Grasping and Manipulation, 2010 IEEE International Conference on Robotics and Automation (ICRA 2010), Anchorage, Alaska, USA

4. Schmitz, A., Maggiali, M., Natale, L. and Metta, G. (2010) Touch Sensors for Humanoid Hands. Special Session on the Role of Tactile Sensing in Human-Robot Interaction, 19th IEEE International Symposium in Robot and Human Interactive Communication (Ro-Man 2010), Viareggio, Italy

5. Schmitz, A., Pattacini, U., Nori, F., Natale, L., Metta, G. Sandini, G. (2010) Design, Realization and Sensorization of the Dexterous iCub Hand. 2010 IEEE-RAS International Conference on Humanoid Robots (Humanoids 2010), Nashville, Tennessee, USA

6. Natale, L., Nori, F., Metta, G., Fumagalli, M., Ivaldi, S., Pattacini, U., Randazzo, M., Schmitz, A. and Sandini, G. (submitted) Studying Developmental Robotics on the iCub Platform, Book chapter, in IMCLEVER roadmap book

7. Schmitz, A., Maiolino. P., Maggiali, M., Natale, L., Cannata G. and Metta, G. (2011) Methods and Technologies for the Implementation of Large Scale Robot Tactile Sensors. Transactions on Robotics, Special Issue on Robotic Sense of Touch.

The first version of the fingertips can be found in [10] and the final version in [11]. The integration on the robotic hands and a comparison of the characteristics of the fingertips and the palm was presented at [12] and shown in detail in [13]. In [14] first grasping experiments were performed to evaluate the sensor system. In [14] further experimental results, algorithms for hysteresis and drift compensation and grasping with tactile feedback are presented.

1.5 Collaborative Work

The tactile sensor for the palm has been developed by Dr. Marco Maggiali. He has also designed and programmed the microcontroller board that is used to communicate with the CDC chips. Dr. Marco Randazzo was using a conductive material for his actuators, which I could use with some modifications for the fingertips. The experimental setups used for the tests with the first fingertip prototype have been designed by Dr. Ravinder Dahiya. The electronics department of the IIT, especially Bruno Bonino and Claudio Lorini, assisted me in realizing the printed circuit boards for the fingertips. In particular, they implemented my PCB designs in the Gerber format so that they could be realized by an external company. The version of the inner support that should have been able to be soldered onto the PCB was implemented by Technimold Servizi. Other people with whom I exchanged ideas that influenced the design of the sensors are listed in the acknowledgments.

1.6 Thesis Outline

This section provides an overview of the rest of the thesis.

1.6.1 Chapter 2

In Chapter 2 background information on tactile sensing in humans and robots is presented. First, it is shown why tactile sensors are beneficial and also the benefits of passive compliance are explored. Humans have an elaborate tactile sensing system that far outperforms any available system for robots; therefore, the kinds of sensors that the human skin incorporates are briefly presented. Also tactile sensing is defined. While a human-like tactile sensing system for humanoid robots is still missing, a number of robots include tactile sensors, and a selection of them is presented. Also the iCub hand is explained in detail, as the sensors presented in this thesis have been designed specifically for this hand.

1.6.2 Chapter 3

Chapter 3 compares the different possibilities that were considered for the sensors for iCub. To arrive at viable solution for iCub, the first challenge was to find a transduction principle that would enable the use of electronics small enough to be integrated in the iCub fingertips. After having found a suitable solution for the electronics, materials for the transducer had to be selected, both conductive and non-conductive. Moreover, due to the fact that the fingertips were to be installed on a number of robots, the manufacturing process had to be optimised; especially the fabrication of the inner electrodes was challenging. Also the factors that have to be taken into account while designing the experimental setup and the test procedure are listed.

1.6.3 Chapter 4

Chapter 4 shows the implementation of the ideas from Chapter 3. First, the working principle of the capacitive sensor is explained: the transducer is made out of several layers and the use of each one of them is shown. The electronics that perform the digitization and that manage the transmission on a serial bus are presented. The characteristics of the material for the dielectric are listed. Subsequently, several experiments are described that were performed to find a conductive and flexible composite for the capacitive sensor. Before the final solution for the fingertip, several other design methods have been explored. The final version of the fingertip is based on a flexible PCB. The construction process and how the fingertip can be mounted on iCub will be shown.

1.6.4 Chapter 5

Tests have been performed to show the characteristics and usability of the sensor. First, the experimental setup is described, which was used to determine the characteristics of the sensor. Experiments were performed with the fingertips, but the curved shape makes it hard to get clean experimental results. Also the palm was tested, for which it is easier to obtain clear results. The sensor measurements drift, probably due to temperature changes. An algorithm is presented that has been implemented to compensate for this drift. Subsequently, the spatial resolution of the sensor is shown, the dependence on the contact area is explored as well as the difference in the response of different taxels. Furthermore, the noise and the stability of the sensor measurements are investigated and the resulting sensitivity of the sensor is shown. An algorithm is presented to compensate for the nonlinearity and viscoelastic behaviour of the silicone foam. This algorithm is evaluated and it performs reasonably well.

Furthermore, grasping experiments with the fingertip sensors were performed. In the first set of experiments a preprogrammed grasp was used and it could be shown that the sensor measurements are repeatable and can be used to detect touch. In the second experiment a fragile, unmodeled object (a plastic cup) was grasped with tactile feedback without deforming it.

1.6.5 Chapter 6

In Chapter 6 the conclusion is presented and the key benefits of the fingertips are listed. Even though the results are generally satisfying, there are many ways to improve the sensors that still have to be explored. Several possibilities are shown which would enhance the reliability of the fingertips and the ease of the production process. Moreover, not all the characteristics of the sensor have been fully explored yet. The future work is presented in Section 6.1.

Chapter 2

BACKGROUND

In this chapter it will be discussed in more detail why tactile sensors are useful for humanoid robots (see Section 2.1). In this context also the importance of compliance for grasping will be explained. Subsequently, in Section 2.2, it will be shown which tactile sensing capabilities humans possess and also a definition of tactile sensing will be given. Section 2.3 will give a brief overview of existing touch sensor technologies and show several of them that have been incorporated in humanoid robots. Finally, in Section 2.4, the iCub hand will be described in detail, since the tactile sensor introduced in this thesis has been specifically designed for this hand. A flowchart of the overall structure of this chapter is presented in Figure 2.1.

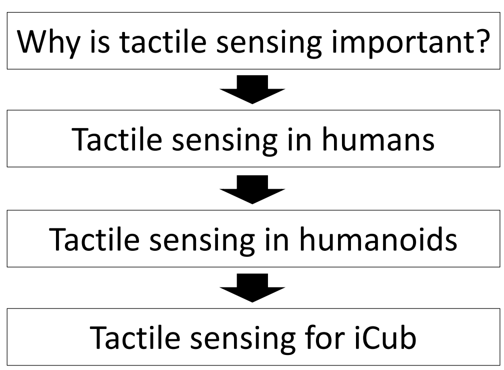

Figure 2.1: **Outline of Chapter 2.**

2.1 The Need for a Compliant Tactile Sensor

Robots can manipulate objects quickly, precisely and reliably in controlled settings, such as industrial environments. However, they often fail to achieve such abilities in unknown environments, or with novel objects. Humans, on the other hand, are consistently skilful at such actions. One of the reasons why current robotic systems lag behind is that they lack accurate and precise tactile feedback for force control. In general, the sense of touch is useful for a number of reasons:

1. Precise manipulation and grasp control.
2. Safe interaction with the environment.
3. Exploration of real world objects.
4. Acquiring a sense of self and the surrounding space.

In the following, a closer look at each of those points will be given. Subsequently, it will be shown why also compliance is desirable for manipulation and how it can be combined with tactile sensing.

2.1.1 Precise Manipulation and Grasp Control

Tactile feedback is a key requirement for grasping and manipulating objects as it gives the most direct information about the contact with an object. In many real life situations knowing the exact position and the precise shape of the object beforehand is impossible; planning the grasp in advance becomes challenging. Instead, adapting the grasp with the help of tactile feedback allows for a more stable grasp. It also allows for necessary adjustments due to non visible parameters of the object, like its stiffness, and changing contact parameters during object manipulation and object deformation. The information gathered through touch is hard if not impossible to obtain through other sensory modalities [15].

The need for tactile sensing becomes obvious while observing humans that have lost their sense of touch: it becomes almost impossible for them to hold objects or use tools [16]. Also the artificially induced temporary loss of the sense of touch makes it hard for test subjects to maintain a stable grasp [17]. Like humans, humanoid robots are expected to adapt to novel objects and changes in the environment.

2.1.2 Safe Interaction with the Environment

In unknown or changing environments a robot can easily damage itself or its surrounding if it cannot sense impacts. For instance, it can move against objects or grasp fragile objects too forcefully. Most robotic hands are position controlled, due to a lack of appropriate sensors and difficulty in creating good force actuators. This can lead to large forces if an obstacle is encountered, for example when a rigid object is grasped: the hand tries to reach its target posture despite the counteracting force, which might lead to a failure of the actuator or the destruction of the object.

Safety becomes a major issue especially if a robot is sharing its workspace with a human. This is the case for humanoid robots, which are intended to interact with humans in the future: they could for example take care of the increasing amount of elderly people or perform complex household tasks [18]. Especially when working with humans, robots need to be able to reliably detect touch and measure the forces they exert. Contact sensing provides the most direct feedback to control contact forces both in voluntary and involuntary interactions with the environment. Also a compliant skin increases the safety, which will be discussed in Section 2.1.5.

2.1.3 Exploration of Real World Objects

Tactile information can be used to actively explore an object in-hand [19]. Thus, it is possible to obtain information about objects that is hard or even impossible to acquire through other sensing modalities such as vision or sound [20]. This is important because grasping and object manipulation do not depend only on visible properties such as size, orientation and shape, but also, for example, on weight, slipperiness, texture and hardness. Humans use size to estimate weight, but also have a rich memory of objects [21]. Even visible features, such as the shape and the edges of an object, are sometimes easier to detect with haptic sensors [22][23].

In general, object manipulation enables active object exploration and induces sensory-motor correlations. Many researchers see perception as an active process, where a human or robot actively structures its own sensory input by manipulating the world to obtain "good" sensory data, enabling categorization, adaptation and learning (see for example [24][25][26]). Therefore, sensing not only aids action, but acting also aids sensing. It has been shown that active object exploration gives more information than passively sensing objects [27]. For example, when pushing or moving an object, everything that moves together and does not belong to the robot can be seen as a single physical entity, and therefore segmentation becomes easier [26]. Also the size of objects can be easier compared, as all the objects can be held in the same distance. In [20] features were extracted from the tactile information gained through grasping, and the grasped objects were successfully assigned to categories.

The knowledge gained through tactile exploration is specific knowledge, which enables a robot to act efficiently in the real world: many researchers today believe that intelligent behaviour does not require full world models and knowledge about every aspect of the environment [28]; instead, models of the interaction with the world are necessary, which are specifically designed to enable prospective actions. For example, in goal-directed hand movements the brain has to plan parts of the movement before it starts: when humans grasp objects, already during reaching they shape the hand according to the size and the function of the object [29]; this adjusting of the opening of the hand (called "*preshaping*" [30]) leads to a dynamic coupling between reaching and grasping. The way humans grasp objects depends on visible features like the size and shape of the object, but also on non-visible features, and even on the intended use of the object. According to all this information, whenever we grasp an object, we have to choose one out of the many different possible grasps; furthermore, grasping is just one of many different interaction possibilities with an object, broadening the available choices of what to do even more. *Affordances*, a term introduced by Gibson [24], is used to refer to the possible interactions between a robot and a particular object, for example whether the robot can lift or push an object. When objects are used to accomplish goals, they are elevated to the status of tools. As the same object can be used in a variety of ways to accomplish different goals, interaction possibilities are flexible and context dependent. To make a robot less dependent on his creator and more autonomous, the robot should be able to learn new affordances itself [31].

Being able to behave efficiently in the world through prospective actions is of such importance, that it even influences high level cognitive skills like categorization and planning, which were traditionally believed to be independent from the specific interaction possibilities somebody possess. There is increasing evidence that humans and animals form *categories* according to their special needs to interact with the world. Accordingly, objects might fall into the same category because they can be used to accomplish the same task, not because they look similar. It could be concluded that the possible interactions with an object actually constitute its meaning, which is also increasingly proven by experimental data [32][25][33]: when we see an object, our brain anticipates the different interaction possibilities, and that is what constitutes a certain category. Moreover, literature on *simulation theory* indicates that even abstract thinking is closer to object manipulation than traditionally believed: we may use the same neural mechanisms for thinking about actions that we use for actually performing actions [34][35]. Humans and animals use forward models to predict the sensory feedback resulting from executing a particular movement: emulation circuits calculate a forward mapping from control signals to the (anticipated) consequences of executing the control command [36]. Likewise, *sequential behaviour planning* can be seen as a forward offline simulation of subsequent actions [37].

Evidence for the close relationship between action and cognition also comes from neuroscience. Two types of neurons of special interest have been in found in the Area F5 in the ventral premotor cortex of monkeys. *Canonical neurons* [38] are both active when grasping an object in a certain way and when looking at an object that can be grasped this way. They are therefore a neuronal analogue of affordances, and can be used to foresee possible interactions with an object and prepare oneself accordingly. *Mirror neurons* [39] are both active when manipulating an object and when seeing someone else doing the same object manipulation. They are therefore considered to be important for understanding others (including their intentions and their state of mind) and imitating them. These two types of neurons provide evidence that neural processes are action specific.

2.1.4 Acquiring a Sense of Self and the Surrounding Space

A fundamental ability for a robot is to learn about itself. Reminiscent of what has been talked about in the last section, this is a basic requirement for interacting with the environment, but here the focus is more on the robot itself, and its action in space. For instance, the robot has to be able to learn the causal relationships between commands to its motors and the resulting posture. In this way, it learns what kind of sensory activity is caused by its own movements and in turn this ability allows to generate actions based on their intended effect [40][41]. For example in [42] a sensor-motor map is learned that enables a humanoid robot to perform reaching movements. These are the beginnings of what could be considered a “sense of self”.

Another aspect is how a robot can acquire knowledge about the extent and configuration of its own body. Tactile sensors are essential in this regard, and are important for the sense of self in general (examples will be given in the following). When a robot can detect self collisions and contact with its surrounding, this can be used for self exploration. By exploiting the correlations between touch and vision, the physical extent of the robot’s body, the location of the body in the environment and the correlation of the body parts to each other can be analyzed.

In humans, the internal representation of the location of our limbs and their spatial extension is classically referred to as *body schema*. It is generally acknowledged that proprioception (including kinaesthesia and the vestibular sense), but also the efference copy, vision and touch are essential for the body schema. For example, it is possible to move the sense of self-ownership humans feel for their own body from the real human hand to a plastic one, by hiding the real hand and simultaneously tapping the real and the plastic hand [43]; this shows the importance of tactile sensation for the body schema. It has been claimed that the body schema not only assists in the feeling of self-ownership of body parts, but also in controlling our spatial actions. In addition to giving information about the starting position of a movement, it should also assist for example to judge whether to duck when passing through a door [44].

It is believed that humans have no unitary representation of space, but numerous spatial maps that participate in the control of movement, some of which are body-part centred [45]. Recent research concerning the control of movements has been especially interested in the peripersonal space immediately surrounding our body parts. This map can be used to determine whether an object can be reached or whether we are going to hit an object in our environment when performing a certain movement. The integration of stimuli from various sensory modalities (i.e. visual, tactile and proprioceptive) is necessary for constructing the peripersonal space: animal studies have shown multimodal neurons in the F4 region of the brain that react for example to touch within a certain tactile receptive field, and also to visual stimuli near the corresponding body part[44]. The closer the visual stimulus is to the tactile receptive fields, the stronger the neurons react. The visual receptive field is not retinotropic but moves with the body part. In other words, the visual-haptic receptive field is anchored to the body part and it is independent of the relative position of the eyes and the body part. It has also been shown that tool use, which extends reachable space, modifies the peripersonal space [44]. Evidence for cross-modal spatial interactions between vision and touch in humans comes from the change of response time by spatial incongruent distracters and by spatial cues of other modalities. Also observations of brain-damaged patients exhibiting spatial extinction point to the importance of cross-modal interaction [44]. A robot that learns about its own body structure with the help of internal models is presented in [46]. In [47] a body schema for a humanoid robot is acquired through the integration of visual and tactile information; in this case the joint positions and orientations are learned. In [48] an algorithm is proposed to autonomously locate the position of taxels on the body.

2.1.5 Passive Compliance

Another important aspect when designing a robotic hand is compliance. Compliance reduces mechanical impedance and helps against the inherent delay of feedback control, which is often too slow to affect control appropriately if unforeseen events occur [49][50]. Therefore, a number of researchers have started to emphasize the role of passive compliance (for example through the use of elastic materials) for dealing with uncertainties [51][52][53]. Compliance has the benefit of providing immediate response without any time-delay and no computational effort. The fact that passive compliance is achieved through the mechanical structure and not through computation makes it also more robust, which is important for applications where safety is an issue. Even in the absence of sophisticated control, passive compliance facilitates movements in unknown environments.

Due to these factors, passive compliance can aid grasping. The grasping problem is addressed by a "cooperation" of the controller and the morphology of the robot. A compliant hand leads to the compensation of small errors in the configuration of the grasp. This allows, for example, faster force-controlled grasping movements[1] and a more robust handling of objects. It creates grasp adaptability and stability, and provides protection against impacts [54]. While describing the UB Hand 3, Lotti et al. [55] state that, "The rough manipulation experiments performed so far ... when performed with a previous device with very reduced compliance (the UB Hand 2, 1995) ... proved to be very critical and many times were failing. Now they succeed, even in presence of incomplete sensory feedback and simplified control algorithms." The UB Hand 3 uses elastic joints and a soft layer covers the endoskeletal structure. In general, compliance in robotic hands can be achieved and is desirable at both the joint and the surface level: on the one hand, an elastic transmission system (e.g. flexible tendons or tendons with springs, see for example [54]), or actuators that are intrinsically flexible generate compliant joints; on the other hand, an elastic skin or cover enables shape adaptation directly at the contact with the object. An evaluation method for compliant and underactuated hands is presented in [56].

Even though passive compliance is generally favourable for working in unknown environments, it can also cause limitations. Particularly important for us, it can hamper the sensor performance [1], leading to a loss in sensitivity, temporal, and potentially also spatial resolution. The adverse effects are even more pronounced if the compliant material is attached on top of the transducer, as it will dissipate part of the energy. Therefore, to minimize the negative effects of compliance, it would be

[1] On the other hand, compliance can make position control more difficult.

beneficial if the transducer itself was compliant. The sensors presented in this thesis are intrinsically compliant, because they incorporate a soft dielectric. In the experiments, presented in Section 5, it can be seen that the compliant material in the sensor presented in this thesis leads to hysteresis in the measurements; however, a compensation algorithm for this behaviour will be presented, and even though no full analysis of the temporal behaviour has been performed (in particular, the frequency response has not been measured yet), the fast initial response of the sensor is satisfying. Moreover, the sensor exhibits a good sensitivity and spatial resolution. Within the work presented in this thesis it was aimed to increase the compliance of the fingertip further by producing a version of the fingertip for which also the support of the transducer can be made flexible (as described in Section 4.4.4), but so far no fully working prototype has been produced and tested yet; thus it cannot be stated how this would have influenced the sensor measurements.

2.2 Tactile Sensing in Human Hands and its Definition

A source of inspiration for artificial tactile systems is the human sense of touch. It far outperforms any artificial system, it includes more sensing modalities than traditionally believed, and it includes distributed data processing. Even though the importance of the sense of touch for humans is often underrated, its loss is hard or even impossible to compensate through other senses, as it has already been discussed in Section 2.1.1. In the following, tactile sensing will be defined, and its functioning in humans will be presented.

2.2.1 Definition of Tactile Sensing

While touch is widely known as one of the traditional five senses, the feeling of touch in humans is in fact comprised of several sensory modalities. As a result, there is considerable disagreement regarding the definition of touch and tactile sensing. An overview over various definitions is given in [2]. The sensor organs which contribute to the sense of touch include mechanoreceptors (pressure, vibration, shape, softness, texture, shear force), thermoreceptors (temperature), nociceptors (pain), as well as the kinesthetic sensors (posture and movement). As in [2], for this thesis all these modalities, which give information about the contact with an object, will be included in the definition of tactile sensing. Mechanoreceptors, thermoreceptors, and nociceptors are cutaneous sensors[2] because they are located in the skin, and they are exteroceptive sensors, because they are sensitive

[2]Other cutaneous sensors are for example the chemical sensors in the nose.

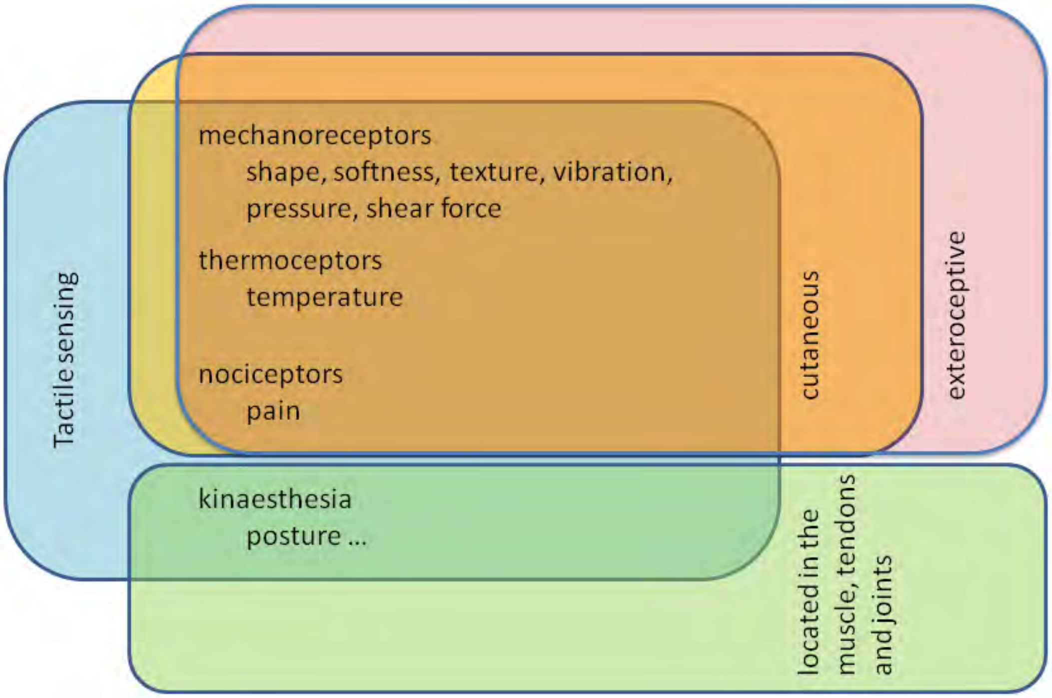

Figure 2.2: **Sensor modalities involved in tactile sensing.** Cutaneous sensors are located in the skin; kinesthetic sensors are located in the muscles, tendons and joints.

to stimuli originating from the environment[3]. On the contrary, the kinesthetic sensors are located in the muscles, tendons and joints, as it will be discussed in the next section. An overview of the different sensory modalities contributing to tactile sensing is given in Figure 2.2.

Dahiya et al. [2] define tactile sensing as the "detection and measurement of contact parameters in a predetermined contact area and subsequent preprocessing of the signals at the taxel level, i.e., before sending tactile data to higher levels for perceptual interpretation." They thereby stress particularly the fact that tactile information is processed and selected at various stages before it reaches the brain. An overview of this process is given in Figure 2.3.

2.2.2 Kinaesthesia

Kinaesthesia is the sense of muscle movement (muscle length and tension) and joint movement [16]; also the efference copy adds to the kinesthetic sense [57]. It gives information about the position and

[3]Indeed, cutaneaous sensors are also interoceptive sensors, as they respond also for example to vasodilation, such as blushing.

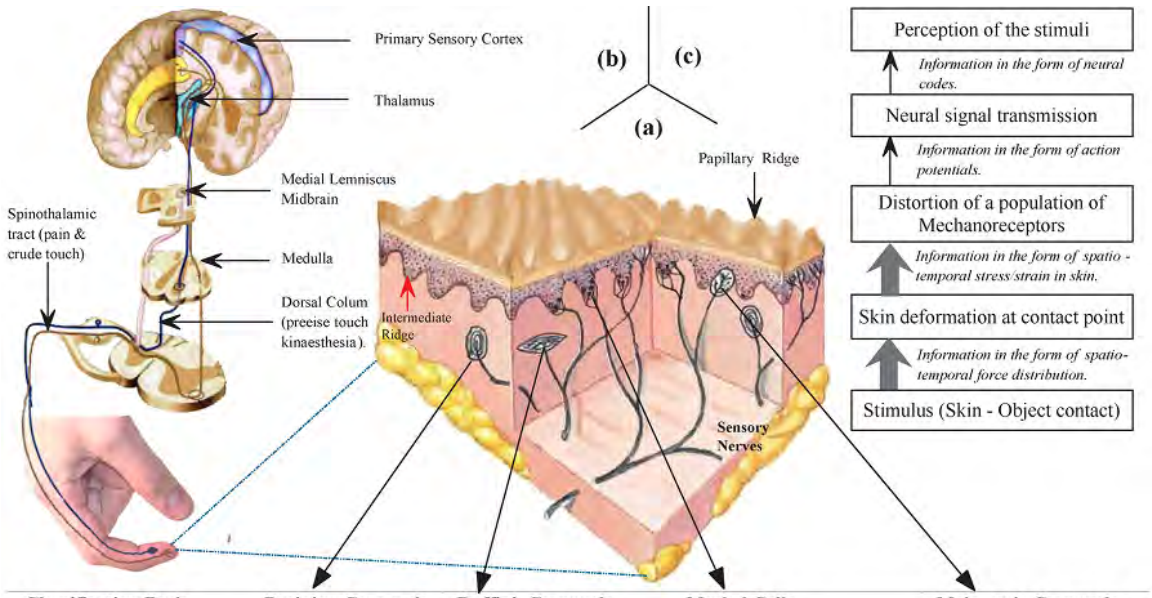

Classification Basis		Pacinian Corpuscle	Ruffini Corpuscle	Merkel Cells	Meissner's Corpuscle
Type		FA II	SA II	SA I	FA I
Adaptation Rate		Fast	Slow	Slow	Fast
Spatial Acuity (mm)		10+	7+	0.5	3-4
Vibration/rapid indent. threshold	Best(μm)	0.01	40	8	2
	Mean(μm)	0.08	300	30	6
Stimuli Frequency (Hz)		40-500+	100-500+	0.4-3	3-40
Conduction Velocity (m/s)		35-70	35-70	40-65	35-70
Effective Stimuli		Temporal changes in the skin deformation	Sustained downward Pressure; Lateral skin stretch; Skin slip.	Spatial deformation; Sustained pressure; Curvature, edge, corners.	Temporal changes in skin deformation
Sensory Function		High frequency vibration detection; Tool use.	Finger position; Stable grasp; Tangential Force; Motion direction	Pattern/form detection; texture perception; Tactile flow perception.	Low frequency vibration & motion detection; Grip control; Tactile flow perception.

Figure 2.3: **Tactile sensing in humans, in particular mechanoreceptors.** Picture taken from [2]. **(a)** The illustration shows several different types of tactile mechanoreceptors embedded in the skin, and the table below gives some characteristics of them. **(b)** The tactile signals are processed at several stages before they arrive at the brain. In **(c)** the process is shown how a stimulus forms a perception.

movement of the body parts, which is important for motion control. Proprioception is often used synonymously for kinaesthesia [16]; but kinaesthesia clearly excludes the vestibular sense, the sense of balance and acceleration of the human body, located in the inner ear. Kinaesthesia is usually not counted as an exteroceptive sensor; still, it can be used to gain information about the external world, for example, the position of the fingers reveals information about the shape of an grasped object and the force necessary to lift the object can be used to estimate its weight. Indeed, Charles Scott Sherrington [58], who coined the term proprioception, defined proprioception as a third category, besides internal and external sensors. Yet, in humans the sensitivity for mechanical fingertip events through proprioception is low [15].

Different receptors contribute to kinestethic perception: muscle spindles signal changes in the muscle length and are situated parallel with the muscle fibres. Golgi tendon organs are located in the tendons and react to changes in muscle tension. A number of mechanoreceptors in and around the joints gather information about the limb position and the joint movement. However, the functioning of these receptors is not well understood, and some joints can measure movement but not their static position [16]. Remarkably, humanoid robots outperform humans concerning kinaesthesia [2].

2.2.3 Mechanoreceptors in the Skin

The human sensors most related to the artificial sensors presented in this thesis are the mechanoreceptors in the skin. They are also the sensors which correspond most closely to the classic concept of *touch*. Mechanoreceptors can measure a variety of contact parameters, including shape, softness, texture, vibration, tangential and normal force. The human skin incorporates several types of receptors to measure all these characteristics; different sensors measure light and hard pressure, sustained and changing pressure, they are located at different depths in the skin and the size of the receptive fields (the extent of body area to which a sensor is receptive) varies. The table at the bottom of Figure 2.3 gives an overview of the tactile sensors found in the human skin. A fast-adapting (FA) receptor is most active during changing stimuli, while a slow-adapting (SA) receptor is receptive to continuous stimuli. In addition, also mechanorecepting free nerve endings can detect pressure and stretch, and hair follicle receptors detect the position of the hairs. As in humans, probably also for humanoids a single transduction principle is not sufficient to measure all contact parameters. Varied sensors modalities, that can measure both static and dynamic stimuli, and additionally the direction of force, are necessary [2].

An overview over the spatial, temporal as well sensitivity limits of human tactile sensing is given in [2]. Together they affect the capability to recognize objects [57]. The density of tactile sensors in the human skin is not uniform: an adult has about 241 low threshold mechanoreceptive units per square centimetre in the fingertips and only 58 in the palm [59]. As a result, humans can detect that two contact points are separate from each other when they are only 1 *mm* apart in the fingertips, but the palm has a spatial sensitivity which is 5.7 to 8.8 times worse than in the fingerpad [60]. On the belly, two pressure points have to be as far apart as 30 *mm* to be recognized as separated from each other. Concerning temporal resolution, [8] report that subjects can detect vibrations up to about 700 Hz and that two stimuli need to be separated by about 5.5 *ms* to distinguish them. As stated in [2], a temporal separation of 30-50 *ms* of two events occurring at different locations is necessary to detect them as non-simultaneously. Regarding sensitivity, the human finger has a sensitivity of about 0.1 *g* per mm^2 (or about 1 *kPa*) [7]. According to [9], about 10 to 100 *kPa* is the range suitable for object manipulation. In [2] sources are cited that state that normal manipulation involves forces from 15 to 90 *g wt* and that a force sensitivity range of 1-1000 *g wt* is desirable for various exploratory tasks (like very often in the literature, only force but not pressure measures are given).

2.3 State of the art - Previous Work

Many touch sensors have been described in the literature, using various different methods of transduction. Yet, few sensors have been integrated into humanoid robots and even less have gone beyond the prototype stage. This is because "they are too big to be used without sacrificing dexterity or because they are slow, fragile, lack elasticity, lack mechanical flexibility, and lack robustness" [2]. Transitioning a single tactile element or a small matrix prototype to a solution suitable for a robotic hand poses several challenges. Therefore, while designing a sensor, one has to focus not only on the transducer, but also on embedded electronics, distributed computation, wiring, ease of production and robustness.

This review will focus on sensors that have been installed on robots. For a more in depth discussion of different transduction technologies and integration issues please refer to Nicholls and Lee [61], Lee and Nicholls [1] and Puangmali et al. [62]. An overview over aspects of tactile sensing that are important for robotic manipulation can be found in [63]. A comparison of several robotic hands can be found in [64]. More recently, Argall and Billard [65] reviewed tactile sensing for human robot interaction, and Dahiya et. al [2] provide a survey of tactile sensing in humans and robots.

2.3.1 Sensors for Robot Hands

The limited space in robotic hands imposes severe design constraints and therefore only a limited number of them incorporate tactile sensors. Several hands that include tactile sensors will be presented, sorted according to the transduction principle which is employed for their tactile sensors; as some hands including several sensor modalities (for example, nearly all of them employ some sort of proprioceptive sensing), this is only a rough separation.

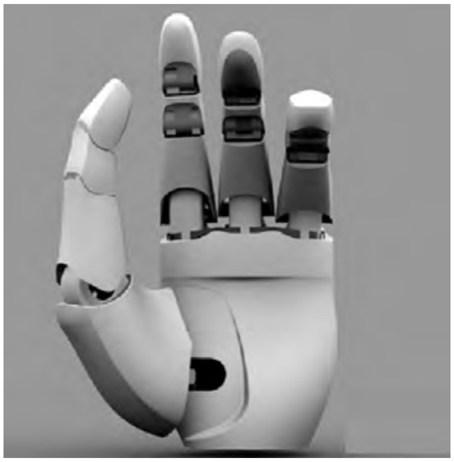

(a)

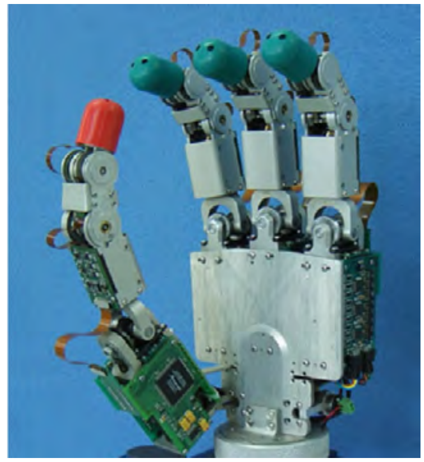

(b)

(c)

(d)

Figure 2.4: **The DLR-HIT hand, (a)** with and **(b)** without the cover. **(c)** and **(d)** shows the 6-axis force-torque sensor with included electronics. The pictures are taken from [66] and [67].

Force-Torque Sensors

Several groups have included 3-axis force sensors (for example the Paloma hand [68]) or even 6-axis force sensors (for example the DLR-HIT hand [66]) into the fingertips of robotic hands. These sensors can localize touch only to an extent and cannot give information about the contact shape, but on the other hand they can measure not only normal but also tangential forces. The DLR-HIT hand (see Figure 2.4) is a further development of DLR hand 2, which has been incorporated in the humanoid Justin. The hand consists of three fingers and one thumb, and all the actuators are located in the digits and the palm; the hand is 1.4 times bigger than a human hand. In addition

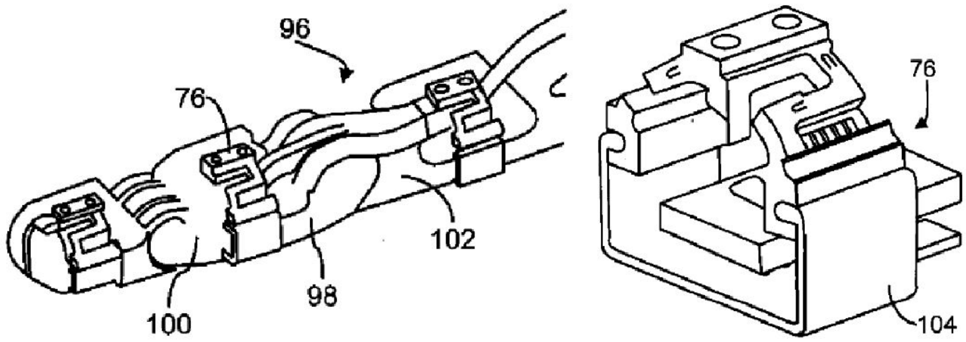

(a) (b)

Figure 2.5: **Load cells in the hands of the Robonaut 2.** **(a)** All phalanges are equipped with loadcells. **(b)** shows a single loadcell. Pictures taken from [71].

to the six-dimensional finger tip force torque sensor (strain gauge sensors) each finger has 3 joint torque sensors (strain gauge sensors), 3 joint position sensors (Hall effect sensors), 3 motor position sensors (Hall effect sensors) and 2 temperature sensors. A major problem with 6-axis force sensors is their size: for example, the one in the DLR-HIT hand is 16 *mm* long and has a diameter of 20 *mm*. Yet, they managed to miniaturize the hand in the form of the DLR-HIT hand 2 [67], which lacks a degree of freedom for the thumb. ATI claims to produce the smallest commercially available 6-axis transducer in the world, the Nano17 [69]. It is 14 *mm* high and 17 *mm* wide, but it does not include all the electronics, unlike the sensor in DLR-HIT hand. Miniaturized 6-axes force sensors were also included in the four fingertips of the human-sized robot hand described in [70]. The hand of the recently developed Robonaut 2 [71] manages to incorporate six-axis load cells in all phalanges of its fingers, see Figure 2.5, yet no embedded electronics are mentioned. Several other robotic hands have force-torque sensor in addition to distributed surface sensors [72][73][74][18] and will be presented in more detail in the following sections.

Skin Based on Hall Effect Sensors

The hand of the robot James [54] has 20 joints and 8 motors, which are located in the forearm. Besides the magnetic incremental encoders in all motors, Hall effect sensors (custom made) measure the total position of each of the 15 joints for flexion and 2 sensors measure the adduction/abduction of the thumb and the fingers, respectively. Hall effect sensors are also used to measure the force exerted on the skin. Each fingertip has two such sensors and 7 more are spread on phalanges, as

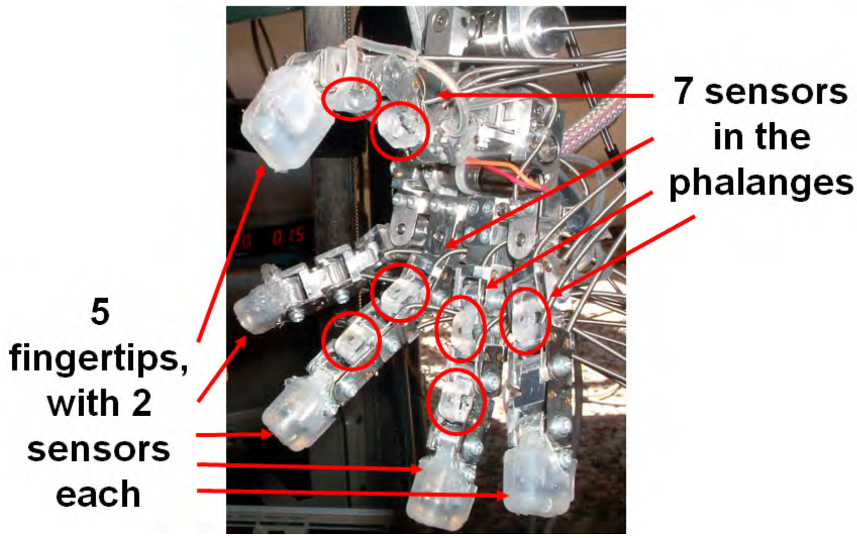

Figure 2.6: **The hand of the humanoid robots James.** 17 Hall effect sensors measure the force exerted by the hand. The picture is taken from [54].

Figure 2.7: **The hand of the humanoid robot Obrero.** It includes 40 dome like sensors made from silicone rubber. The position of a magnet in the tip of each dome is sensed by 4 Hall effect sensor located in the base of the dome.

depicted in Figure 2.6. An air gap in the silicone skin adds to the log shaped response curve of these sensors. The data acquisition card for all the Hall effect sensors is mounted in the back of the hand and is interfaced to the CAN bus. These sensors are intrinsically compliant. The hand has been used to grasp objects with a simple algorithm and to classify objects according to the sensory information from its proprioceptive and exteroceptive sensors. The Obrero hand [23] has 40 contact points which embed 4 Hall effect sensors each, as shown in Figure 2.7. The sensors are able to measure a minimum normal force of 0.098 N. The hand uses Series Elastic Actuators and has 8

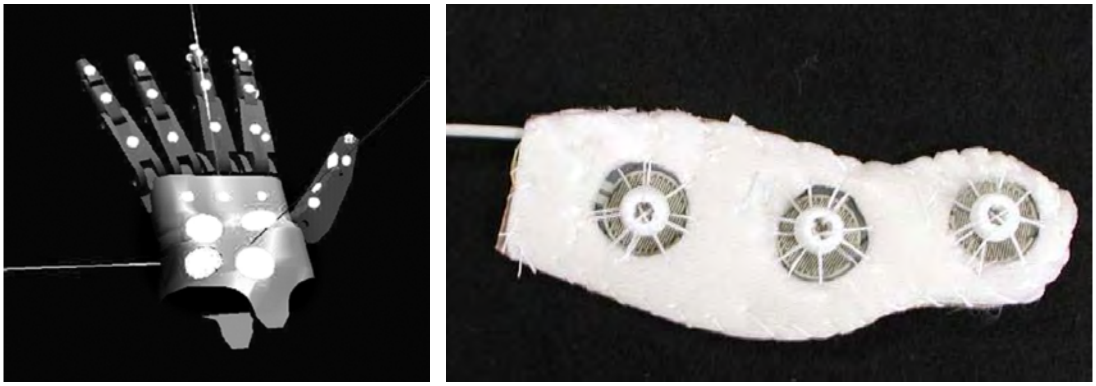

Figure 2.8: **The Robonaut hand and its tactile sensors.** The location of the sensors is shown. The sensors are mounted as a glove. Plastic beads above the sensors help against the loss in sensitivity due to the compliance of the glove.

joints driven by 5 motors. Position feedback is obtained by potentiometers in all joints and encoders in the motors. Moreover, in the base of the palm an infrared proximity sensor is mounted.

On/Off Taxels

The Cyber hand [72] incorporates distributed on/off taxels (activation force $< 15\ mN/mm^2$). They are placed on a bendable foil and give information about the contact location and size, but not the amount of applied force. This drawback is compensated by the fact that the fingers also include small three axis force sensors. In addition, the hand includes joint position sensors (Hall effect sensors in all joints) and tensiometers in the tendons. No electronics are embedded in the fingers. A version of this hand, the RoboCasa Hand No. 1 (RCH-1), has been incorporated into the humanoid robot WE-4RII [75].

Sensors Based on a Thin Film Piezoresistive Layer

A tactile glove has been developed for the Robonaut 1 hand [76], which includes force sensing resistors (FSR) from *Interlink Electronics* and sensors based on *Quantum Tunnelling Composite* from *Peratech*[4], with 33 taxels in total, see Figure 2.8. Plastic beads had to be mounted above the sensors, because otherwise the softness of the glove greatly reduced their sensitivity. The stiff backing of the force sensing resistors made it difficult to fit them to the curved shape of the hand. A small version

[4]Quantum Tunnelling Composite will be discussed later while describing the Shadow hand.

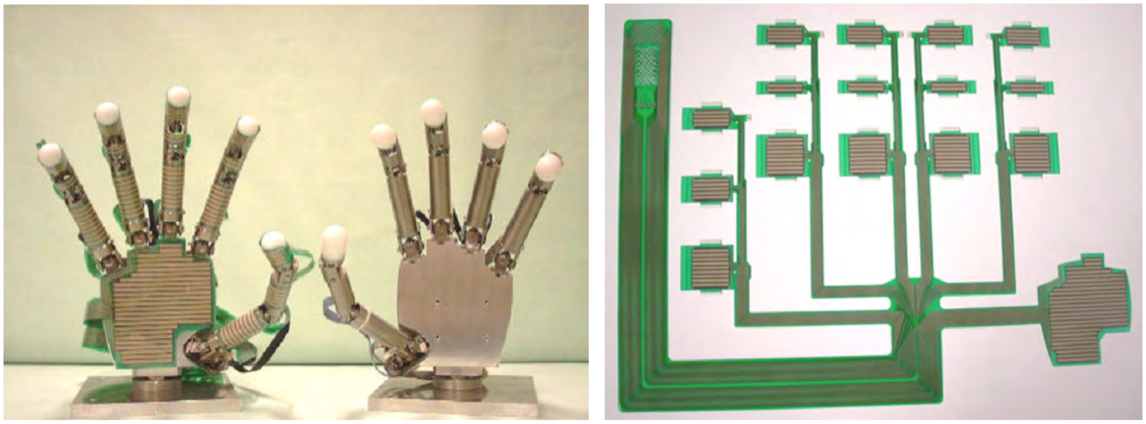

Figure 2.9: **GIFU III hand and its distributed tactile sensor.** In addition it has 6 axis force-torque sensors in the fingertips. Pictures taken from [73].

(approx. 0,25” diameter) could have been installed in the smaller segments of the hand, but this limited the sensed area. In general, force sensing resistors from *Interlink Electronics* are available in different shapes and sizes [77]. The basis of the force sensing resistor is a piezoresistive layer that decreases its resistance with an increase in applied force; FSRs are thin and not compliant. FSR sensors (23 in total) were also integrated in the Belgrade/USC hand [78]. The DLR 1 hand [79] included “x,y,z pads” in all finger phalanges: tactile foils based on FSR indicated both the amount and the position (averaged centre) of the applied pressure. A bendable 16×16 matrix sensor for the finger segments of the UTAH/MIT hand based on force sensing resistors is described in [80][5]. Thin film force sensors based on piezoresistivity are also available from *TekScan*; both single and distributed pressure sensors can be purchased. The distributed sensors are offered in many different forms [81], for example as the *Grip* system, which fits on a human hand and includes 349 sensing elements [82]. All these systems include no local data processing.

The GIFU III hand [73] not only has 6-axis force sensors in its fingertips, but also includes a skin with 859 pressure sensing points based on pressure sensitive piezo-resistive ink, see Figure 2.9. The servomotors for all 16 degrees of freedom are located within the hand. As a result, the hand is considerably bigger than a human hand: from the wrist till the end of the longest finger the hand is 25 *cm* long. The sensitive skin is only 0.2 *mm* thick and can conform to flat and cylindrical shapes. The electrodes are in a grid pattern. The palm, the thumb, and the each of the other fingers have 313,

[5]Another tactile sytem for the UTAH/MIT hand will be discussed later.

Figure 2.10: **The MAC hand and its tactile sensors.** Eight identical modules are located within the fingers.

126 and 105 detecting points each, respectively. The insensitive area is 49.1%. The maximum load is about $2.2 \times 10^{-3}\ N/m^2$, the resolution is 8 bits, the sampling cycle is 10ms/frame and the response characteristic is more than 1 kHz. It includes no local data processing and the sensor cables from all the transducers are routed along the fingers and the palm. Moreover, the skin is not compliant.

Pressure Sensitive Rubber

The four fingers of the MAC hand [74][83] include 8 identical modules; each module has embedded electronics and incorporates a 3-axis force sensor in addition to a pressure sensitive rubber (which changes is resistance according to pressure) with 64 sensing elements, as depicted in Figure 2.10. Yet, the sensor is not compliant and the modules would be too big to be included into small humanoid hands. Tactile sensors based on pressure sensitive rubber (in addition to joint torque sensors) were also included in the hand described in [84]; each finger incorporates 242 sensing elements (size: 3.4×1.8 mm). The motors are included in the fingers and the hand is considerably bigger than a human hand (33 *cm* long). The finger segments seem to include a multiplexer and an amplifier, but not the digitisation electronics. The hand described in [85] includes 686 pressure sensing points, but no local data acquisition is performed. A highly flexible transducer (the sensing electrodes consist of conductive wires that are stitched on pressure sensitive rubber) was mounted on a robot hand and is presented in [86]. Distributed pressure sensors for round fingertips are presented in [87]; only the multiplexers are included. A flat version[6] of this sensor system [88] for the *SCHUNK Dextrous*

[6] Also a slightly bend version is available.

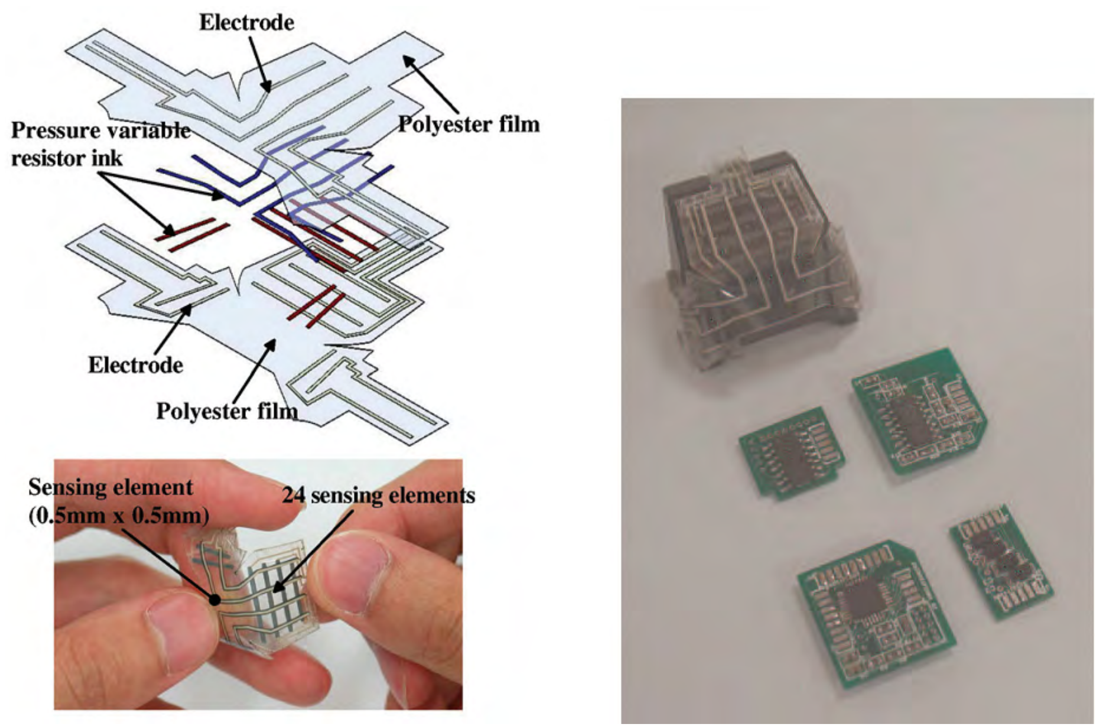

Figure 2.11: **Tactile sensors in the fingertips of the SKKU hand II.** The distributed pressure sensor was based on pressure sensitive ink. The electronics were included in the fingertips, but the fingertips were considerably bigger than the fingertips of iCub.

Hand SDH is commercially available from *Weiss Robotics* [89] and has also been included into other grippers [90][91] and anthropomorphic robot hands [92].

Combined Piezoelectric and Piezoresistive Sensors

PVDF (polyvinylidene fluoride) is a piezo-electric material that generates voltage in response to the changes in the applied mechanical stress. The SKKU hand II [93] includes sensors based on PVDF in addition to sensors based on pressure sensitive ink from *Creative Materials*. Both are located on a thin and flexible substrate, see Figure 2.11. The distributed pressure sensor consists of 24 sensing elements (size: 0.5×0.5 *mm*), and the PVDF sensor consists of two PVDF strips. The PVDF sensor was used to detect dynamic response such as slippage. The fingertips also include the electronics, which is facilitated by the fact that the fingertips are considerably bigger than human ones. In [92] the flat tactile sensing modules based on pressure sensitive rubber from *Weiss Robotics*, which were already discussed before, were enhanced with a dynamic sensor based on PVDF and were included

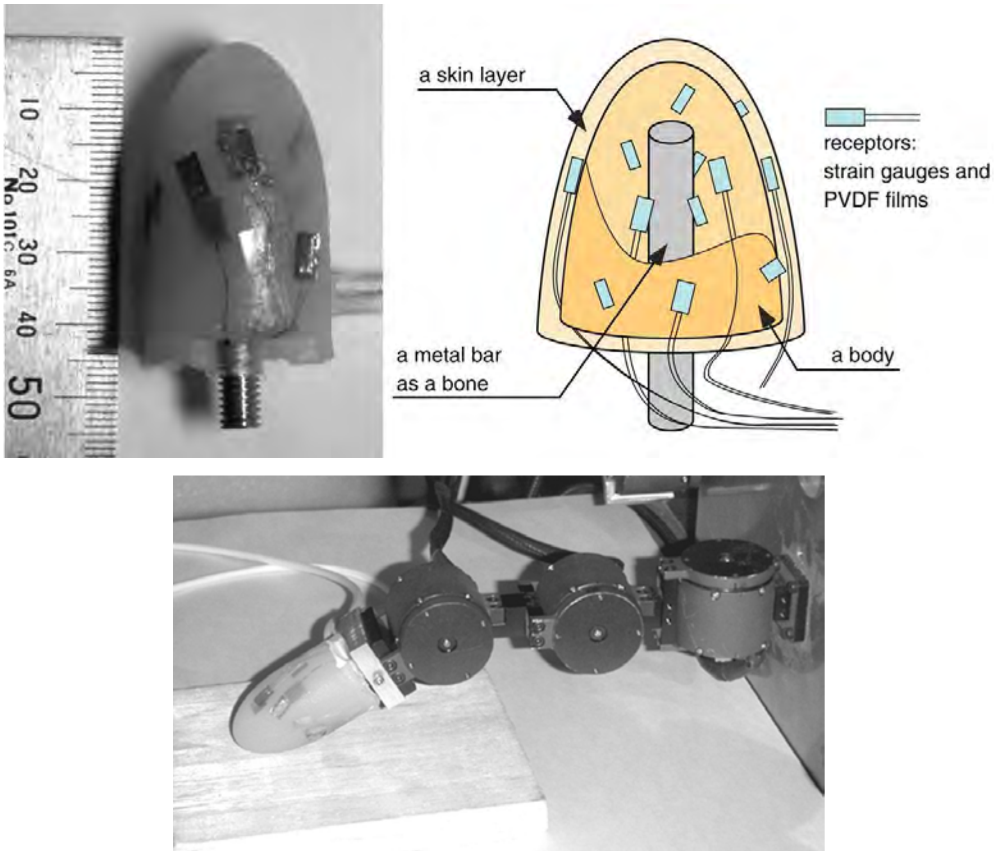

Figure 2.12: **Fingertip with randomly distributed strain gauges and PVDF films.** Six strain gauges and six PVDF films are in the skin layer, and equally many sensors are deeper inside the fingertip. The pictures are taken from [95].

in an anthropomorphic robotic hand. To enhance the sensitivity of the dynamic sensor, cylindrical shaped knobs were added to the cover of the sensor. A small fingertip which includes both static (based on a thin FSR film) and dynamic (based on PVDF) sensor is presented in [94]. Knobs are added to the surface of the fingertip to enhance the sensor response. The system was included in a three-fingered robot manipulator. Both the sensors described in [92] and [94] use distributed data processing, but no local digitisation.

Hosoda et al. [95] built an anthropomorphic robotic fingertip with randomly distributed strain gauges and PVDF films embedded in silicone rubber, see Figure 2.12. Six strain gauges and six PVDF films are in the skin layer, and equally many sensors are deeper inside the fingertip, summing up to 24 sensors. The fingertip has a diameter of 2.5 *cm* and a length of 4.5 *cm*. The authors argue that the different sensor modalities and the different depths they are embedded in provide more information than a single type of sensor could provide. As discussed in Section 2.2, also the human skin has different sensors for static and dynamic pressure (strain and strain velocity) in different layers of the skin. The fingertip was not mounted on a robotic hand, but experiments have been carried out for discriminating several materials through pushing and rubbing. Five out of eight tested materials could be distinguished through a combination of the available sensory information. They formed separate groups in the feature space and could therefore be recognized through supervised learning.

Quantum Tunnelling Composite

Distributed tactile skin sensors are in development for the fingertips of the Shadow hand [96][97]. The fingertip of the thumb includes 34 taxels, and the fingertips of the other fingers have 22 taxels each. The fingertips have a three-dimensional curved shape; the tactile elements are approximately evenly distributed, have an average diameter of 3.3 mm and there are no gaps between the taxels (see Figure 2.13). The tactile sensors are based on Quantum Tunnelling Composite, which changes its resistance according to pressure (like the thin film force sensing resistors and the pressure sensitive rubber already discussed before). The fingertips have embedded electronics for digitizing the measurements. Unfortunately, it is difficult to assess the quality of the measurements as little has been published about it. The Shadow hand C5 uses pneumatic actuators that are located in the forearm; they move the 20 degrees of freedom of the hand and the wrist in an antagonistic fashion, resulting in adjustable compliance of the actuation system. The pressure in each actuator is sensed and the hand also includes joint position sensors (Hall effect sensors with 0.2 degrees resolution) [98].

2.3.2 Large Scale Tactile Sensors for Humanoids

Here work is presented that has focused on the design of large area tactile sensors for humanoid robots. Particularly in such cases the need for local data processing becomes evident. One of the first conformable and scalable sensitive skin systems was proposed by Ohmura and Kuniyoshi [99], see Figure 2.14. It is still one of the few solutions that is based on self-contained modules with integrated digitisation, so that the modules do not need to be connected to a microcontroller board for digitisation. Instead, the signals are locally digitized within the module, which allows modules also to be connected to each other. The modules are based on a flexible substrate and have a tree shape like form to conform to different shapes. Therefore, it is possible to adjust the covered area without

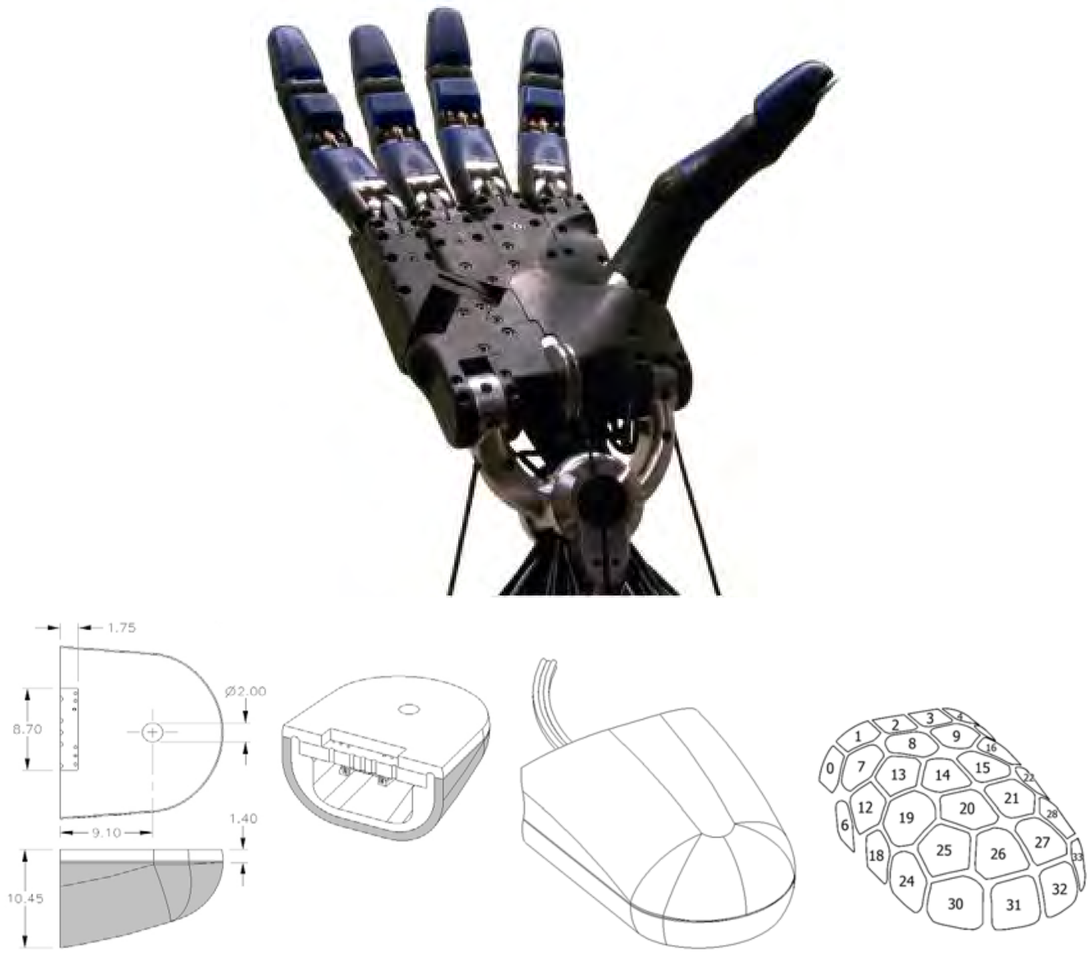

Figure 2.13: **The shadow hand and its fingertip sensors.** The tactile sensors in the fingertips are based on Quantum Tunnelling Composite and the fingertips also have embedded electronics. The sensor system for the thumb is depicted; the dimensions are given in *mm*. The pictures are taken from [96] and [97].

the need of specifically designing modules for each body part. On the downside, the digitization is performed by a microcontroller (which would be too big to be included into the small modules used for the iCub) and in general the modules used by Ohmura and Kuniyoshi are big, making it difficult to incorporate them into small body parts. Moreover, the spatial resolution is low. The sensing elements are photo reflectors covered by urethane foam. Because of their high power consumption the sampling frequency had to be reduced to achieve feasible power consumption: it takes 51.2 *ms* to sample the maximum possible number of sensing elements. 1864 sensing elements have been installed on a humanoid robot [100]. Also the tactile system that has been developed for the robot RI-MAN uses flexible PCBs with a tree-like shape to conform to curved surfaces [101]. The tactile elements are commercially available piezoresistive semiconductor pressure sensors, and the measurements show less hysteresis than those of Ohmura and Kuniyoshi. To reduce the number of wires, the sensor modules include multiplexers. Nevertheless, the modules need to be connected individually to controller boards, as the sensor modules themselves include no digitisation electronics. Five modules with 8 *times* 8 sensing elements have been installed on the robot.

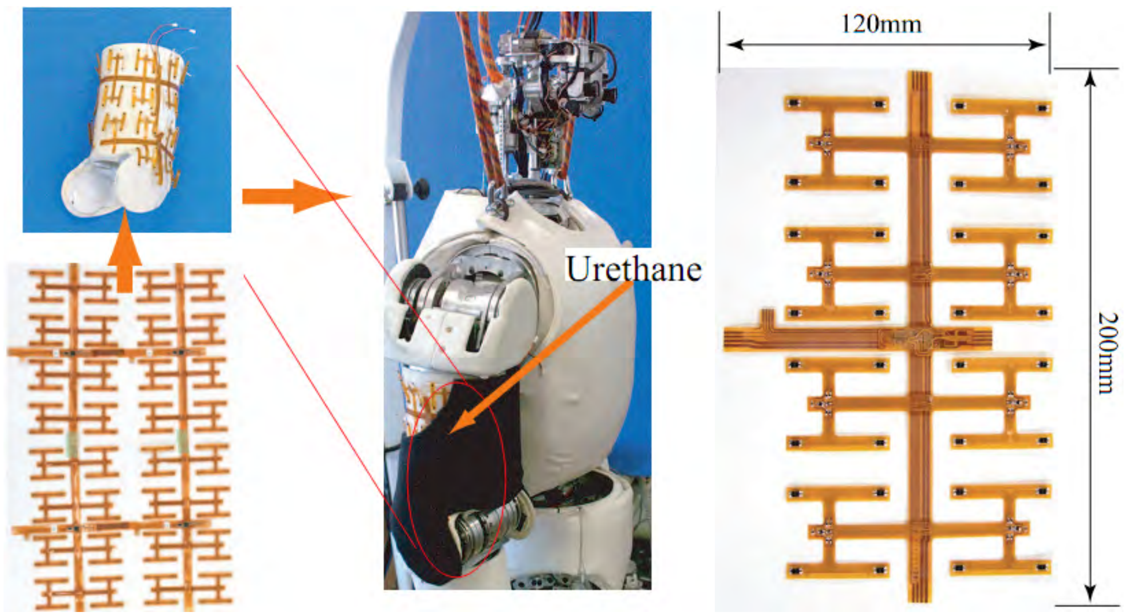

Figure 2.14: **Tactile system from Ohmura et al.** The robot includes 1864 optical tactile sensors; the tactile system is based on modules with embedded digitization. The pictures are taken from [99].

In the robot ARMAR-III custom-made matrices of sensors with piezo-resistive rubber cover the shoulder, lower and upper arm [102][103], see Figure 2.15(a). Smaller matrices are used for the fingers; two different systems are presented in [87] and [92] and have already been discussed above. The sensors include multiplexers, and also relatively small modules for the digitisation have been designed. In the robot Kotaro [104] tactile sensing is achieved through flexible bandages (two flexible PCBs with an intermediate layer of pressure sensitive conductive rubber) with 64 taxels each, as shown in Figure 2.15(b). The hands are sensorized with pressure sensitive conductive rubber foam, which can be used to form complex 3D shapes and gives a fleshy tactile impression. The tactile sensors in Kotaro have no integrated data acquisition electronics.

Sensors based on PVDF (which measure dynamic but not static forces) are embedded in the

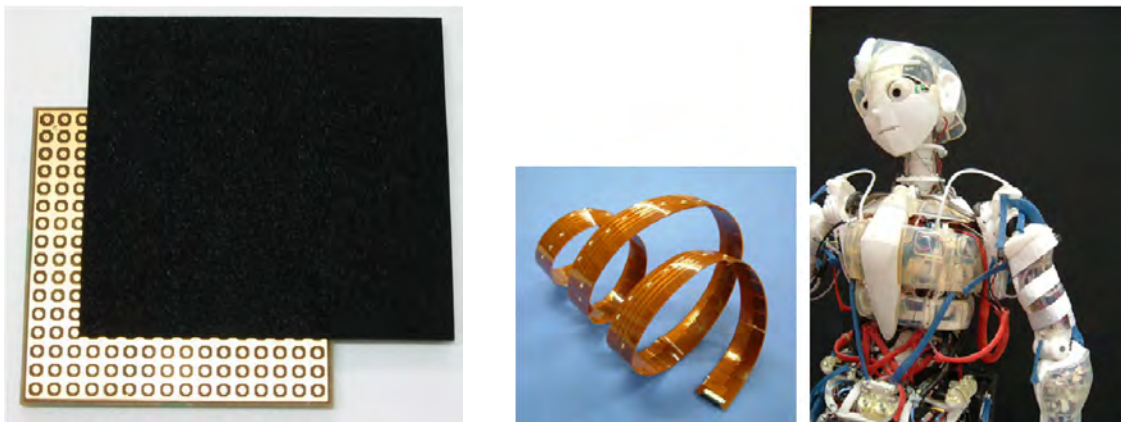

(a) (b)

Figure 2.15: **Tactile systems for ARMAR-III and Kotaro. (a)** A prototype of the tactile sensing matrix used for ARMAR-III. Electrodes are just below the pressure conductive rubber, which is several *mm* thick. **(b)** Kotaro uses flexible bandages based on pressure conductive rubber with 64 taxels per bandage. The pictures are taken from [102] and [104].

Robovie series, see Figure 2.16. The skin consists of four layers: thin silicone rubber, piezoelectric film (PVDF), thick silicone rubber and urethane foam. The first version of Robovie-IIS included 48 sensing elements, the second 276 [105]; Robovie-IV had 56 [106] and Robovie-IIF 276 [107] taxels. The spatial resolution is low (the smallest sensing elements are 3×3 *cm* big). The same research group developed a similar tactile system for the anthropomorphic robots Repliee R1 [108] and Repliee Q2 [109]. Finally, the CB2 humanoid robot [110] is covered all over the robot's body with 197 taxels based on PVDF films, which were placed between a layer of urethane foam covering the mechanical parts and the outer silicone layer [110], as depicted in Figure 2.17. While the PVDF tactile sensors have been implemented on many different robots and have been successfully integrated in a soft skin, the spatial resolution is low and the taxels have to be installed individually.

2.3.3 *Stretchable Sensors*

Another challenge is the development of sensors that are not only bendable, but also stretchable. This would increase the conformability to compound curved shapes and they could also be used to cover joints. In [112] a stretchable, flexible, large area "E-skin" which includes both thermal and pressure sensors is presented. It is formed by a net-like structure; when the structure is stretched, the many square-holes of the net are deformed into diamonds. The structure was shown to be able

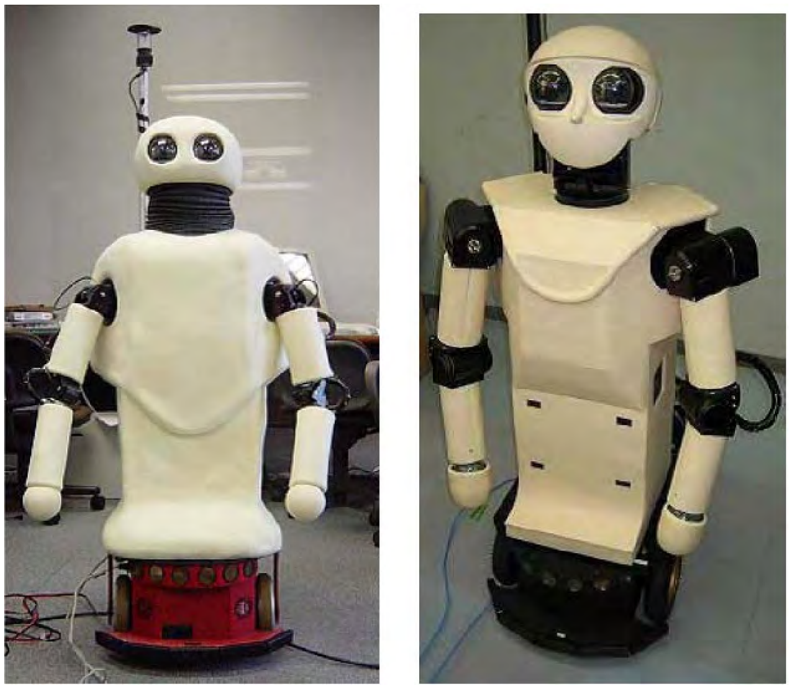

Figure 2.16: **Robovie-IIS.** Robovie-IIS had in its first version 48 taxels based on PVDF, in the second version 276. The pictures are taken from [111]

to conform to the surface of an egg. In the intersection areas of the net the sensors are located: the pressure sensors are based on pressure sensitive rubber and the thermal sensors are formed using organic diodes. The periodicity of the sensors is 4 *mm*. A pressure of 30 *kPa* can be reliably detected. According to the authors, issues of the perforated configuration are that the sensor array cannot be stretched biaxially or in all directions, and the stretchability is limited to 25 to 30% because the utilised materials are not inherently stretchable. In [113] a stretchable tactile distribution sensor that employs Electrical Impedance Tomography (EIT) is presented. This method was originally used in medical imaging and requires no wiring in the sensing area: electrodes at the boundary of a conductive sheet inject electrical current from different pairs of neighbouring electrodes and at the same time measure the electrical potentials. The resistance distribution can be estimated based on the concept of Inverse Problem Analysis. The authors also tackled the problem of the sensitivity to stretch: most conductive rubbers are sensitive to both stretch and pressure, and it is not trivial to distinguish them. This causes limitations if the sensor is employed above a joint. While dynamic calibration due to simultaneous information about the joint angle is possible, it is often complex and not feasible. Therefore, the authors also introduce pressure sensitive stretch insensitive material.

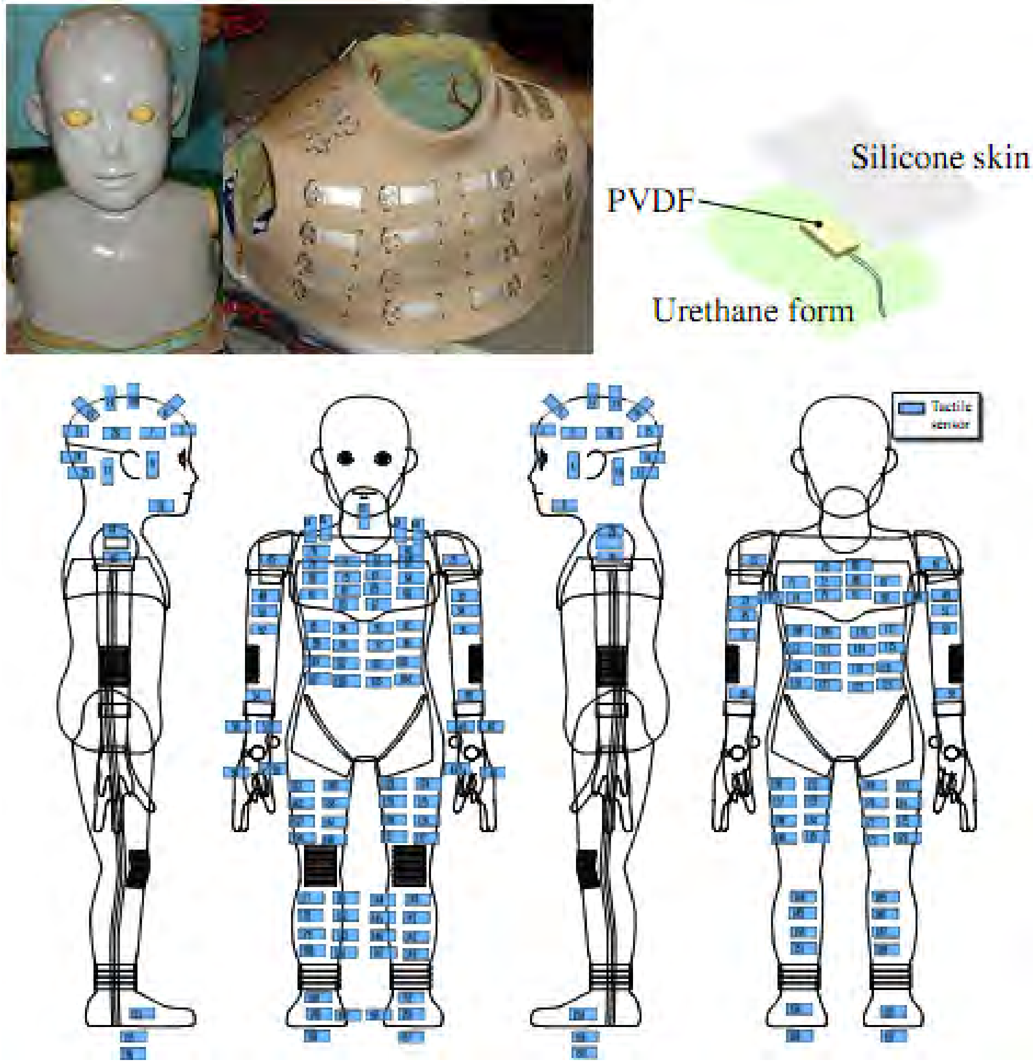

Figure 2.17: **CB2.** CB2 incorporates 200 PVDF patches. The pictures are taken from [110].

The resulting structure can be stretched to around 140% of its original size in both directions and can be placed above a human elbow. Forces of 10 N over an area with 20 mm diameter could be detected as well as the location of multiple contacts [114]. A downside of the sensor is the high power consumption, which is a limitation for autonomous mobile robots that are powered by batteries. While no large scale integration of such sensors has been performed yet, it would be interesting to implement them in the future above the joints of robots.

2.3.4 Touch Sensors Based on Capacitive Technology

Capacitive pressure sensors have already been explored for some time. One of the first were Miyazaki and Ishida [115] who used a capacitive sensor to measure vertical foot force. Capacitive sensors cannot only be used to detect pressure, but for example in [116] a 3-axis sensor is proposed. Using capacitive technology, sensor matrices with very high spatial resolutions can be produced: Gray and Fearing [117] implemented an 8×8 capacitive tactile sensing array within 1 mm^2; in [118] 300dpi and 500dpi capacitive tactile imaging arrays are reported. Integrated tactile-thermal sensors are reported in [119] and [120]: a matrix of thermal sensors is located beneath the capacitive tactile matrix. In [121] an artificial skin based on capacitive technology with interesting characteristics like no apparent hysteresis and low noise was presented. However, none of these solutions has been integrated into a robotic system. A system using small brushes of fibres was integrated into a robot gripper and was described to have high sensitivity [122]. The fibres were mounted on a diaphragm and the capacitive sensors were used for dynamic measurements. In addition, a matrix sensor based on piezoresistive foil was used for static measurements. A tactile system based on capacitive sensing was developed for the robot Paro [123].

An interesting early implementation of capacitive sensors into the UTAH/MIT dextrous hand is reported in [124]. In total, the hand incorporated 744 taxels. The measurements were digitised locally in the finger segments; each phalange included excitation electronics, analogue filters, a Motorola 6811 microcontroller and interface electronics. Electronics like this would be too big to be included into a hand as small the one of iCub (the UTAH/MIT dextrous hand was about twice as big as a human hand (28×21 cm) and had only four digits [75]). Concerning the transducer, early prototypes of the sensor were matrix based: conductive stripes below the dielectric were perpendicular to the ones above the dielectric [125]. In the version of the sensor included in the hand however, the conductive layer above the dielectric consisted of floating electrodes. Because of this, the sensitivity was reduced. The authors state that this solution was adopted due to “the possibility of a contact breakage with conductive strips”. Two electrodes below the dielectric were used to obtain the measurements: one was excited, the other one was measured. Such a solution occupies more space than a matrix or a method in which the same electrode is exited and measured, as it is the case in the sensor presented in this thesis. Furthermore, the sensors in the UTAH/MIT hand seem to have included no shielding layer (even though in [125] the necessity of such a layer is stated), which exposed the sensor to stray capacitance. Interestingly, the dielectric was very thin and included air gaps, to increase the compressibility of the dielectric.

Recently a number of products like laptop trackpads, MP3 players, computer monitors and cell phones have been using capacitive technology to detect and localize human touch, for example the "iPod-touch" [126]. Therefore, small dedicated A/D converter chips have been made commercially available, for example the AD7147 [127]. Those chips can collect and digitize the measurements from several capacitive sensors in very limited dimensions. To the best of my knowledge, and also according to [2], such chips are not available for other transduction modes such as pressure sensitive rubber or Hall effect sensors. Instead, several larger electronic components are necessary to acquire a digital signal that can be sent over a serial bus.

Pressure Profile Systems is a company that sells capacitive pressure sensors [128]. The "RoboTouch" system has been included in the robots PR2 [128] and TWENDY-ONE [18]. TWENDY-ONE has 241 pressure sensing points based on capacitive technology in each of its hands and 134 sensor points on its arms and upper body, as shown in Figure 2.18. Moreover, the skin is compliant and the fingertips have a round shape and also include a six-axis force sensor. However, the fingers are considerably bigger than human fingers and to the best of my knowledge no data has been published concerning the performance of the sensors.

2.3.5 Discussion of Previous Work

Several tactile systems have been integrated into humanoid robots and described in the literature. Some of them are modular and include hierarchical data processing. Yet, the modules are usually big and cannot be installed on small robot parts, furthermore in many cases the spatial resolution is low, or the modules cannot communicate between themselves and need to be individually interfaced in a star network. Instead, small sensor modules are necessary (therefore, even small microcontrollers would be too big) that can also communicate between themselves (therefore, locally integrated multiplexers are not sufficient). For some promising systems no data concerning their performance or details about their implementation has been published yet.

2.4 iCub Hand

In this section the actuation structure of the iCub hand will be described in detail. The hand of iCub is roughly 14 *cm* long and 6 *cm* wide. Differently from other projects, the hand has been specifically designed for the iCub and therefore an exceptional level of integration was achieved allowing high

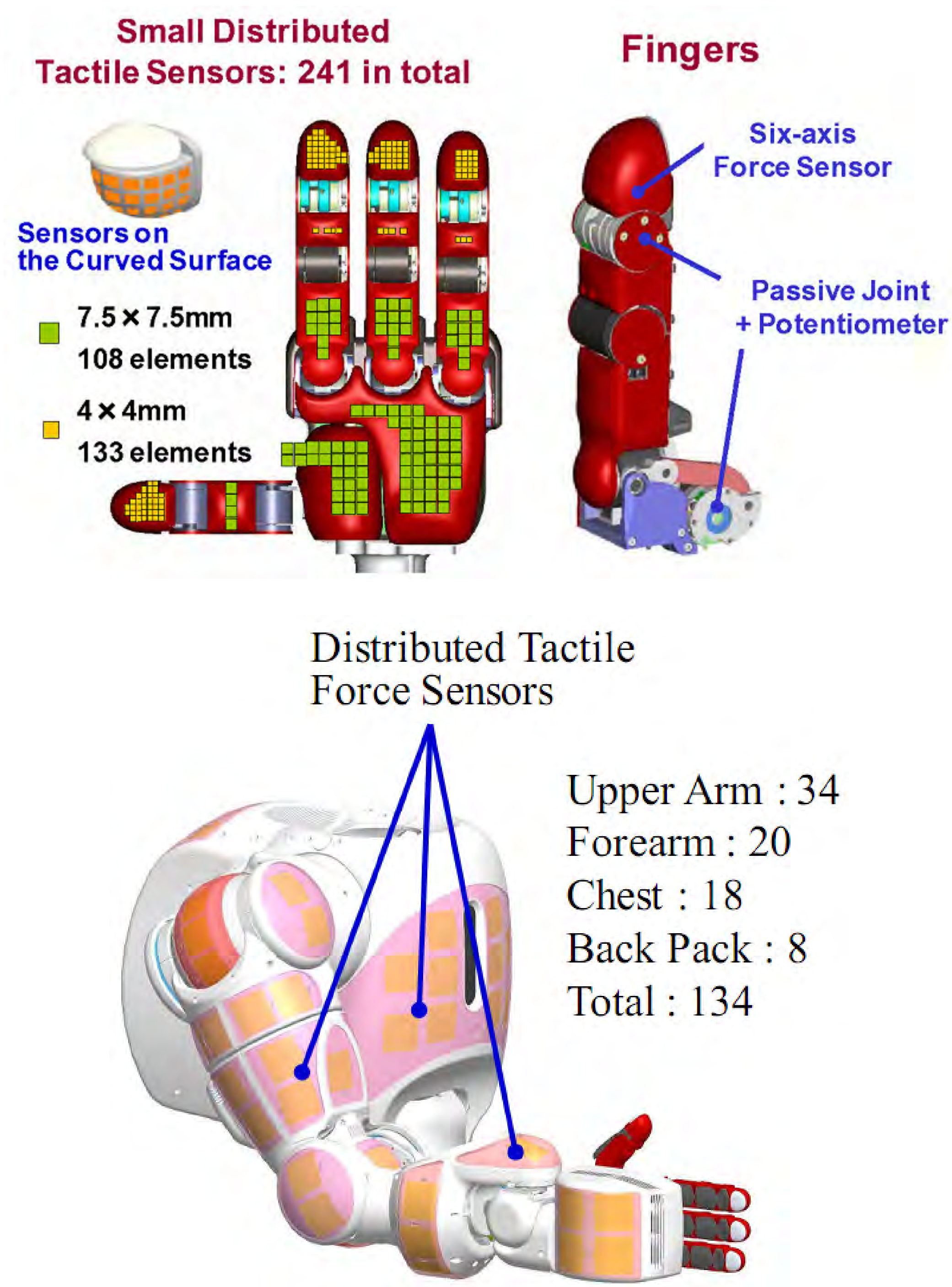

Figure 2.18: **Tactile sensors in TWENDY-ONE.** Distributed tactile sensors based on capacitive technology have been incorporated in TWENDY-ONE. Pictures taken from [18].

dexterity and sensorization in limited dimensions. Early versions of the hand were presented in [129] and [130].

2.4.1 The hand actuation system

The hand actuation system is based on tendons. This solution was adopted because it allowed maintaining a sufficient dexterity in the available space. Most of the motors are integrated in the forearm and the associated tendons are routed through the wrist. Only two motors are embedded in the palm. The adopted tendon actuation can be divided into two different classes: *open-ended* tendon drives and *closed-loop* tendon drives (see [131] for details).

The typical closed-loop actuation structure relies on a pulley attached to the motor: a stainless steel tendon[7] is twined around the pulley and is *routed to the joint and back to the motor* using custom made guide-wires. These guide-wires basically consists of long Teflon-coated springs (1*mm* in diameter) inside which the tendons slide. Therefore, the closed-loop configuration uses the tendon for moving the joint in both directions of motion. On the contrary, in the open-ended actuation system the tendon is only used to rotate the joint in one direction (usually flexion) while a spring is in charge of rotating the joint back (extension). The rotation of the motor flexes the joint and compresses the spring; the counter-rotation releases the potential energy accumulated in the spring and extends the joint.

The hand has 19 joints. Its dimensions (155*mm* long; 75*mm* wide at the widest part of the palm; and 40*mm* thick, including the electronic boards in the back of the hand) and ranges of motion (90° for all joints except for the abduction of the fingers, which is for all fingers together around 50°) were inspired by those of a human hand. Most of the human hand joints have been replicated. The thumb has four joints: two of them are located in the carpometacarpal (CMC) joint while the other two joints are in the metacarpophalangeal (MP) joint and in the interphalangeal (IP) joint respectively. Similarly, the remaining four fingers (index, middle, ring and little) have four joints each: two located in the metacarpophalangeal (MP) joint and the other two in the proximal interphalangeal (PIP) joint and in the distal interphalangeal (DIP) joint respectively (see Figure 2.19 for a detailed description).

The actuation of all these 19 joints is obtained using 9 DC motors, 7 of which are embedded in

[7]Commercial steel cables produced by Carlstahl [132] with a diameter of 0.63*mm* were used. Also other materials such as Dyneema [133] were tested but were eventually not chosen because of their tendency to wear on the motor pulley.

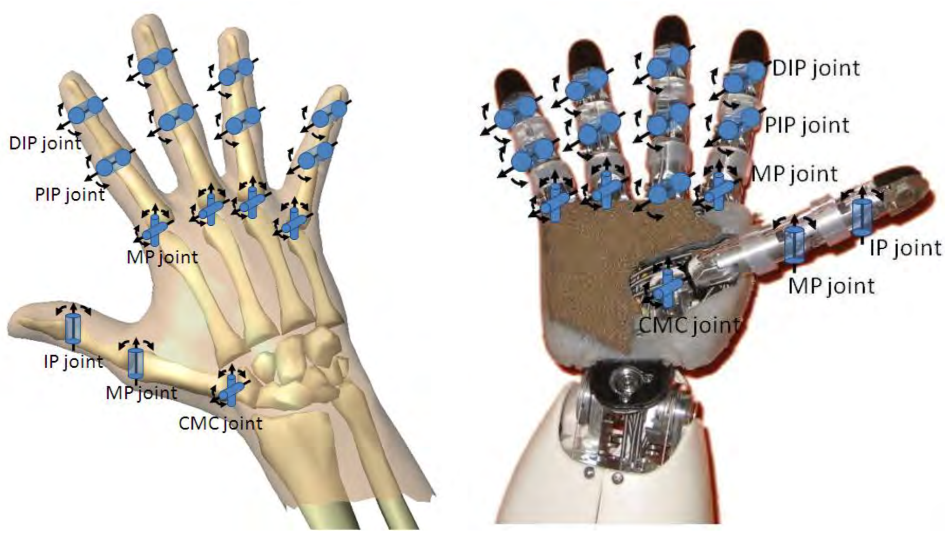

Figure 2.19: **Left**: a sketch of the human hand with its joints; joints name for the middle, ring and little fingers are the same indicated for the index finger. **Right**: a picture of the iCub hand with all its joints; notice the analogy with the human hand joints.

the forearm and 2 in the hand. Therefore, certain degrees of motion (DOM) are obtained by coupling different joints so that they are moved by a single motor in a synergistic fashion (see Figure 2.20 and 2.21). Only the abduction of the fingers is coupled tightly, the others elastically, resulting in some passive degrees of freedom. Even though this is a major difference between the iCub hand mechanics and the human hand biomechanics, the idea of reducing the overall number of motors by creating suitable synergies was suggested by well established studies on typical grasping strategies [134]. Following this principle, the Robonaut hand for example has fingers with more degrees of actuation for fine manipulation and fingers with fewer actuators that mainly serve power grasps [76]. In the following, a detailed description of the joints couplings is given; particularly, the finger MP abduction coupling, the thumb MP-IP coupling, the index PIP-DIP coupling, the middle PIP-DIP coupling and finally the ring-little fingers coupling are described.

Fingers MP Abduction Coupling

A single motor embedded in the hand is used to actuate the index (abbreviated *ind*), ring (*rng*) and little (*ltl*) fingers abduction/adduction movements. The mechanism is basically a closed-loop tendon drive with the tendon twined around the index, ring and little finger pulleys in order to coordinate their movements (see Figure 2.22). Given a rotation θ_m of the motor, the MP abduction/adduction

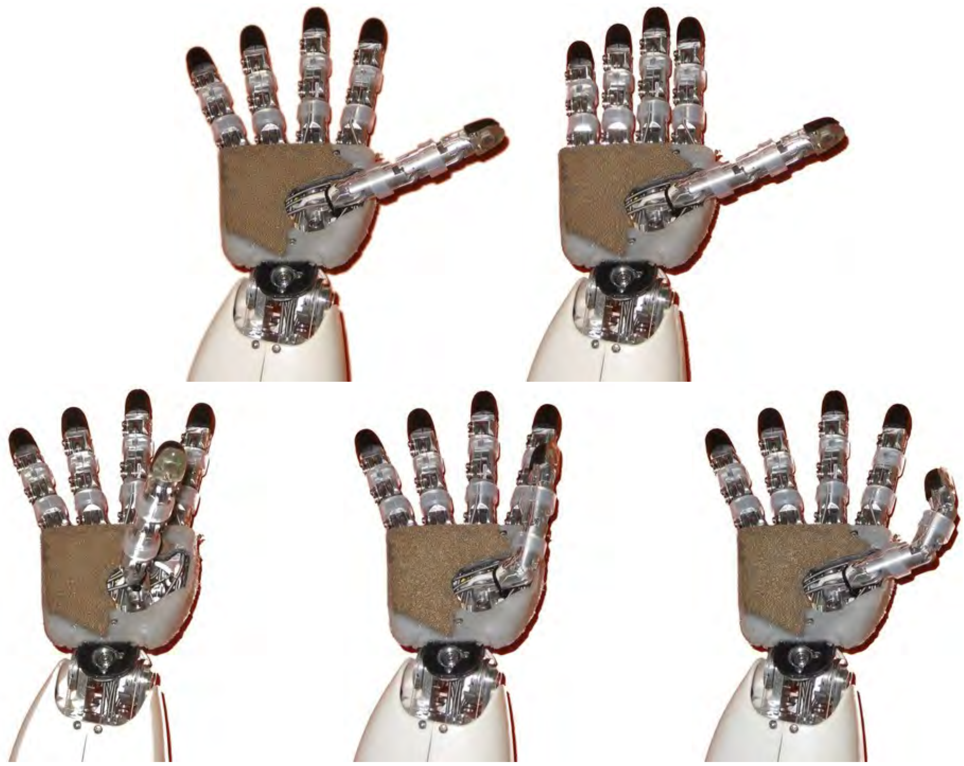

Figure 2.20: 4 DOMs of the iCub hand. From the top-left corner (reading order): (1) initial configuration for all successive postures; (2) (index, middle, ring, little) fingers MP abduction, (3) thumb MP opposition, (4) thumb MP abduction, (5) thumb MP-IP coupling.

displacement for each finger is given by the following formulas:

$$\theta_{ind} = \frac{r_m}{r_{ind}} \theta_m, \qquad \theta_{rng} = -\frac{r_m}{r_{rng}} \theta_m, \qquad \theta_{ltl} = -\frac{r_m}{r_{ltl}} \theta_m \tag{2.1}$$

where θ_{finger} is the finger MP abduction/adduction displacement, $r_m = 3.25mm$ is the radius of the motor pulley, r_{finger} is the radius of the finger pulley ($r_{ind} = 4.75mm$, $r_{rng} = 4.75mm$, $r_{ltl} = 3.5mm$). Therefore, the radii of the joint pulleys determine the finger coordination.

Thumb MP-IP Coupling

The thumb distal joints are actuated by an open-ended tendon drive. The coupling of the joints is obtained by winding the cable around both the MP and the IP joints (see Figure 2.22 right). A torsional spring in both the MP and IP joints accumulates energy when the motor is pulling the cable, thereby flexing the joints. This potential energy is then used for extending the finger. At the equilibrium configuration and *in absence of external forces*, the position of the MP-IP joints (θ_{mp},

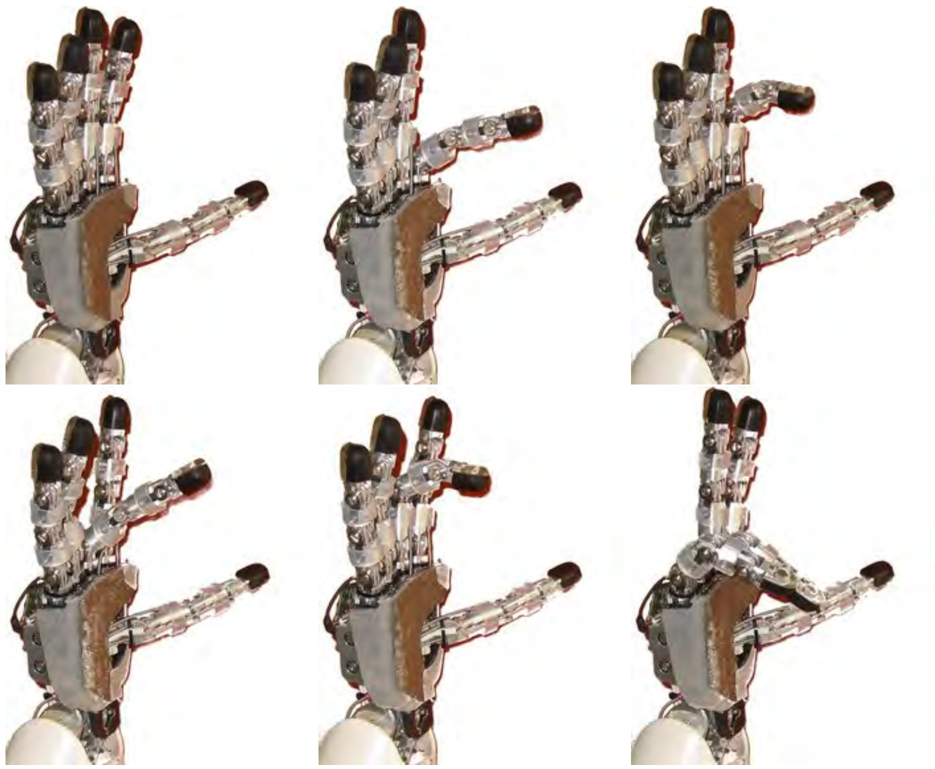

Figure 2.21: 5 DOMs of the iCub hand. From the top-left corner (reading order): (1) initial configuration for all successive postures; (2) index MP flexion, (3) index PIP-DIP coupling, (4) middle MP flexion, (5) middle PIP-DIP coupling, (6) ring-little fingers coupling.

θ_{ip}) is related to the position of the motor (θ_m) by the following rules:

$$\theta_{mp} = \frac{k_{ip}}{k_{mp}+k_{ip}}\frac{r_m}{r_{mp}}\theta_m, \quad \theta_{ip} = \frac{k_{mp}}{k_{mp}+k_{ip}}\frac{r_m}{r_{ip}}\theta_m \tag{2.2}$$

where k_{ip} and k_{mp} are the stiffnesses of the torsional springs attached to the IP and MP joints, r_m is the radius of the motor pulley and $r_{ip} = r_{mp}$ are the radii of the IP and MP joint pulleys.

Index and Middle PIP-DIP Coupling

The index finger distal joints (PIP and DIP) are actuated by a single motor according to the same actuation structure described for the thumb MP and IP joints. The same actuation structure has also been adopted for the distal joints of the middle finger.

Ring and Little Finger Joint Coupling

The little and ring finger joints (MP flexion/extension, DIP and PIP joints) are moved by a single motor with a suitable coupling mechanism. In the current configuration, a closed-loop tendon moves a linear slider; the slider is then used to pull simultaneously two open-ended tendon drives: one tendon moves the little finger; the other tendon actuates the ring finger. Specifically, each tendon actuates the MP (flexion/extension), DIP and PIP joints according to a three joints extension of the coupling mechanism used in the thumb, index and middle finger distal joints (see Figure 2.22 (a)). In this case (at steady state and in absence of external forces) the motor position θ_m and the joint positions θ_{mp}, θ_{dip} and θ_{pip} satisfy the following equations (holding for both ring and little fingers):

$$\theta_{mp} = \frac{1}{k_{mp}} \frac{1}{\frac{1}{k_{mp}} + \frac{1}{k_{pip}} + \frac{1}{k_{dip}}} \frac{r_m}{r_{mp}} \theta_m, \tag{2.3}$$

$$\theta_{pip} = \frac{1}{k_{pip}} \frac{1}{\frac{1}{k_{mp}} + \frac{1}{k_{pip}} + \frac{1}{k_{dip}}} \frac{r_m}{r_{pip}} \theta_m, \tag{2.4}$$

$$\theta_{dip} = \frac{1}{k_{dip}} \frac{1}{\frac{1}{k_{mp}} + \frac{1}{k_{pip}} + \frac{1}{k_{dip}}} \frac{r_m}{r_{dip}} \theta_m, \tag{2.5}$$

where k_{mp}, k_{pip} and k_{dip} are the stiffnesses of the torsional springs attached to the MP, PIP and DIP joints, r_m is the radius of the motor pulley, $r_{mp} = r_{pip} = r_{dip}$ are the radii of the MP, PIP and DIP joint pulleys.

Uncoupled Joints

4 out of the 19 joints are driven by a single motor without any coupling. These joints are the thumb CMC opposition, the thumb CMC abduction/adduction, the index MP flexion/extension and the middle MP flexion/extension. For these joints the actuation structure consists of a closed-loop tendon drive and therefore the position of the motor θ_m is related to the position of the joint θ_m by the following formula:

$$\theta_m = \frac{r_m}{r_j} \theta_j, \tag{2.6}$$

where r_m and r_j are the radius of the motor pulley and of the joint pulley respectively.

Summary

The overall hand actuation structure is summarized in Table 2.1.

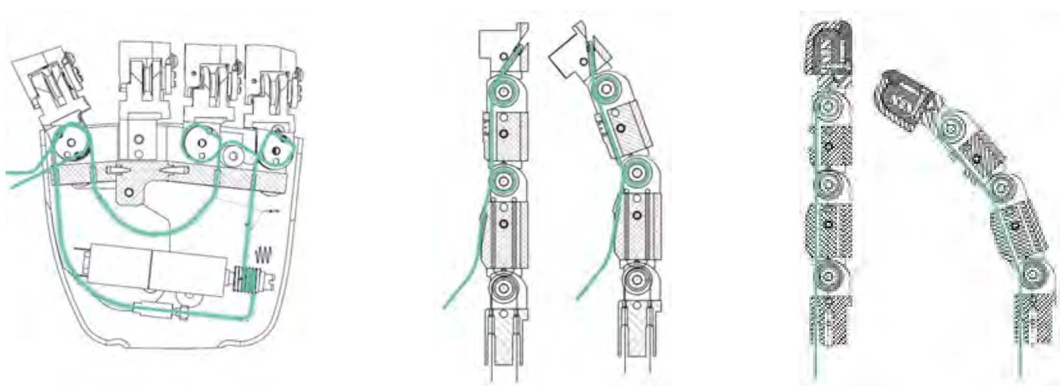

(a) (b) (c)

Figure 2.22: **Coupled joints actuation schemas.** **(a)** A cross section of the fingers MP abduction/adduction actuation scheme. The configuration is a closed-loop tendon drive; the tendon path is highlighted in cyan. The joint pulley radii and the tendon winding direction (clock-wise or counter clock-wise) determine the value and the sign of the coefficients in Eq. (2.1). **(b)** A cross section of the distal joints actuation scheme (thumb MP-IP, index and middle PIP-DIP coupling). The configuration is an open-ended drive. The tendon path is highlighted in cyan. The left figure shows the straight finger while the bottom refers to the flexed finger. The coordination of the two joint movements by means of a single motor is obtained by torsional springs; steady state configuration in absence of external forces is give by Eq. (2.2). The picture shows the flexion steady state configuration when $k_{ip} = k_{mp}$. **(c)** A cross section of the ring finger and little finger actuation scheme. The design is an open-ended tendon drive similar to the one used for the thumb, index and middle fingers distal joints shown in (b), but in this case three joints are coupled together instead of two.

Table 2.1: **A tabular representation of the synergies used to move the 19 joints by means of 9 motors.** The 19 joints are reported on the horizontal axis where thumb CMC_1 is the thumb opposition, thumb CMC_2 is the thumb abduction/adduction, MP_1 is the abduction/adduction and MP_2 is the flexion/extension. The 9 DOMs are reported in the vertical axis. If a DOM contributes to moving a certain joint then the corresponding entry in the table differs from "-" and it contains a reference to the equation that describes the relationship between the motor and joint position.

	Joints																		
DOM	thumb				index				middle			ring				little			
	CMC_1	CMC_2	MP	IP	MP_1	MP_2	PIP	DIP	MP_2	PIP	DIP	MP_1	MP_2	PIP	DIP	MP_1	MP_2	PIP	DIP
Finger MP abduction	-	-	-	-	(2.1)	-	-	-	-	-	-	(2.1)	-	-	-	(2.1)	-	-	-
Thumb MP opposition	(2.6)	-	-	-	-	-	-	-	-	-	-	-	-	-	-	-	-	-	-
Thumb MP abduction	-	(2.6)	-	-	-	-	-	-	-	-	-	-	-	-	-	-	-	-	-
Thumb MP-IP coupling	-	-	(2.2)	(2.2)	-	-	-	-	-	-	-	-	-	-	-	-	-	-	-
Index MP flexion	-	-	-	-	-	(2.6)	-	-	-	-	-	-	-	-	-	-	-	-	-
Index PIP-DIP coupling	-	-	-	-	-	-	(2.2)	(2.2)	-	-	-	-	-	-	-	-	-	-	-
Middle MP flexion	-	-	-	-	-	-	-	-	(2.6)	-	-	-	-	-	-	-	-	-	-
Middle PIP-DIP coupling	-	-	-	-	-	-	-	-	-	(2.2)	(2.2)	-	-	-	-	-	-	-	-
Ring-little coupling	-	-	-	-	-	-	-	-	-	-	-	-	(2.3)	(2.4)	(2.5)	-	(2.3)	(2.4)	(2.5)
Position Measurement	✓	✓	✓	✓	✓	✓	✓	✓	✓	✓	✓		✓	✓	✓		✓	✓	✓

2.4.2 The phalangeal position sensors

The positions of 17 out of 19 hand joints (indicated with ✓ in Table 2.1) are measured with tiny Hall effect sensors (SS495A Honeywell, Figure 2.23(b)) whose analogue output is converted to digital by a custom made board (see Figure 2.23(a)). This board has been produced in two different (symmetric) form factors in order to be optimally embedded in the right and left hand. The 12 bits analogue to digital conversion of the 17 signals relies on a 16 bit DSP Microchip (dsPIC30F4013) and on a multiplexer (ADG659). The digital data is transmitted to the control board via a CAN-bus.

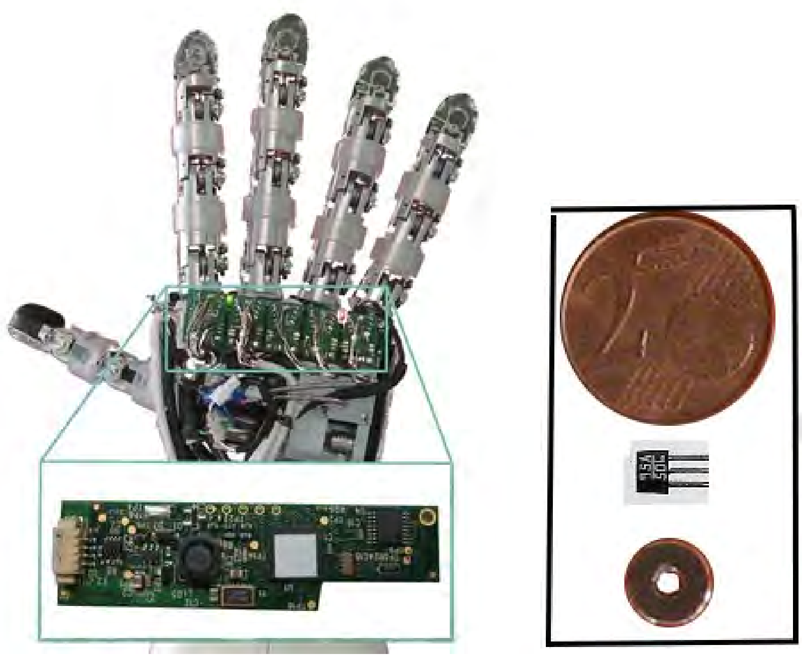

(a) (b)

Figure 2.23: **Hall effect sensor.** **(a)** A picture of the hand with a zoom on the embedded board designed to collect the analogue data from the 17 (Hall effect) position sensors. **(b)** A picture of the analogue Hall effect sensor together with the ring-shaped magnet used to generate the magnetic field sensed by the sensor. Magnets are positioned at each joint with the sensor underneath the magnet.

2.5 Conclusion of the Background

In this chapter, first the importance of tactile sensing was explored. Moreover, it was explained why morphological factors such as compliance are relevant for object manipulation. Next, touch sensing in humans was discussed, and some measures concerning sensitivity, spatial and temporal resolution in humans were given, which could serve as benchmark for humanoids. Subsequently, an overview of tactile sensing solutions for robots was given, and the limitations of those systems were discussed. It became clear that artificial systems lack far behind the capabilities of humans. Moreover, no sensors are available that would fit all the requirements given in Section 1.3. Finally, the iCub hand was presented.

Chapter 3

MOTIVATION AND METHODOLOGY

In the previous section, the importance of tactile sensing was shown. Also the benefit of compliant skin was discussed. While humans have a large number of sensors in their skin, in particular their fingertips, the integration of many tactile sensors still remains a challenge for robotic systems. In Section 2.3 several tactile systems were shown that have been integrated into humanoid robots, yet they have various problems (as explained already in Section 2.3.5, and they are not able to fulfil the requirements as listed in Section 1.3. To arrive at viable solution for iCub, the first challenge was to find a transduction principle that would enable the use of electronics small enough to be integrated in the iCub fingertips, as discussed in Section 3.1. After having found a suitable solution for the electronics, materials for the transducer had to be selected, both non-conductive (see Section 3.2) and conductive (see Section 3.3). Moreover, due to the fact that the fingertips were to be installed on a number of robots, the manufacturing process had to be optimised; especially the fabrication of the inner electrodes was challenging, as described in Section 3.4. While design the experimental setup and the test procedure, a number of factors had to be taken into account, listed in Section 3.5.

3.1 Interfacing and Electronics

Many different transduction principles and technologies have been explored in the past [1]. However, it is not trivial to scale from a single tactile element (or even a matrix of sensor elements) to a high number of spatially distributed sensors embedded in a robotic skin. This is because the sensors should not only give reliable measurements, but they should also be integrated into little space without obstructing the other functions of the robot. One has to focus not only on the transducer, but also embedded electronics and distributed computation are necessary to facilitate the integration in the robot, otherwise an overwhelming amount of wires would impede the dexterity of the robot.

Most of the sensors that have been integrated into the fingertips of humanoid robots are three- or six-axis force torque sensors (compare Section 2.3). While they also provide information about forces tangential to the sensor surface, they do not give distributed information about the contact area. Moreover, it is difficult to integrate them into fingertips as small as those of iCub[1].

Already in the past several distributed tactile sensing solutions with embedded electronics have been integrated into humanoid robots, as shown in Section 2.3. Many of these sensor systems use integrated multiplexers, but no local digitization. Therefore, less, but still several wires (for 12 sensors it would require 7 wires) are necessary, and an extra module for the digitization needs to be installed on the robot, which requires extra space. Other systems also have integrated digitization, but the electronic components that are used (like microcontrollers) are too big to be installed into a space as small as the fingertips of iCub. Therefore, in the past, no distributed tactile sensors with local digitization have been incorporated into a fingertip as small as the one of iCub. The fingertips that are closest to the requirements for the iCub fingertips are those of the Shadow hand and the robot TWENDY-ONE. Yet, the sensors for the Shadow hand are based on Quantum Tunneling Composite, and the technology is still under development and little information about it is available. TWENDY-ONE uses capacitive sensing. The fingertips are much bigger than those of iCub, and not much has been published about the characteristics of the robot's sensors.

After having performed a survey of the possible solutions, it was discovered that only for capacitive sensors dedicated chips are available, that are able to collect and digitize a number of sensor measurements, and that are at the same time small enough for the fingertips of iCub. Using a commercially available chip is preferential to designing an own specialized one, because off-the-shelf components are cheap, thoroughly tested, and their use reduces the development time off the overall project. The capacitance to digital converter chip AD7147 from *Analog Devices* is able to acquire 12 measurements of capacitance. The resulting taxel density would be as good as the one of the leading comparable fingertips, as the fingertips of the Shadow hand and of TWENDY-ONE. The use of this chip also has the benefit that in parallel to the fingertips a palm was being developed, which uses the same technology. As the goal was an integrated tactile system for the hand of iCub, this made the integration of the palm and the fingertips easier. Furthermore, capacitive sensors can be made intrinsically compliant, which is beneficial for object manipulation, as explained in Section 2.1.5. Yet, several technological challenges have to be solved, before the capacitive technology can be used for the fingertips. The chips are usually used for flat touchscreen devices, and the sensors

[1] In any case, if three- or six-axis force torque sensors can be designed at a later stage small enough for the fingers of iCub, the different sensor modalities would complement each other.

are only responsive to human touch. In the following Sections, the different aspects of designing a transducer for curved shapes that is sensitive also to non-conductive objects will be discussed. In particular, the electrodes for the capacitive sensor should be covered by a dielectric layer and a flexible, conductive layer.

3.2 Dielectric Material

While choosing the dielectric material, several factors have to be considered, that will be presented in the following.

1. *Moulding:* it should be possible to mould the material into the multi-curved shape of the dielectric layer for the fingertip. This excludes ready-made sheets of dielectric material.

2. *Strain:* it is beneficial if the dielectric exhibits a high strain as result of applied pressure. This is because the capacitive sensor measures displacement, and therefore a higher strain results in a more sensitive sensor. On the other hand, the material that is chosen should enable the sensor to measure the whole range of pressures that can be expected during object manipulation (as discussed in Section 2.2, humans manipulate objects normally with about up to 100 *kPa*). Therefore, a sufficient change of strain (not necessarily uniform, as also the relationship of displacement to capacitance is inversely proportional) over the whole range of pressures is necessary. Depending on the material that is chosen, also the moulding process can influence the resulting softness of the dielectric layer.

   The softness of the dielectric is also important for the compliance and safety of the robot.

3. *Dielectric constant:* the higher the dielectric constant, the more sensitive the sensor will be.

4. *Homogeneity:* it is beneficial if the dielectric layer has a homogenous hardness, so that all taxels have the same sensitivity. Big air gaps like in the fingertips of the robot James (see Section 2.3.1) make the layer softer, but non-homogenous.

5. *Diffusion:* the influence of pressure on the deformation of the dielectric should be local. Otherwise, it will lead to cross talk between the taxels. In particular, elastomers are generally non-compressible and when pressure is applied to them in one place, material radiates to the surrounding areas.

6. *Viscosity:* viscosity in the dielectric leads to hysteresis in the sensor measurements. Hysteresis is detrimental to sensors, and therefore materials with less viscosity are preferable as dielectrics for the sensor. Even if the viscosity of the dielectric can be modelled and its influence on the sensor measurements can be compensated, unless the model is absolutely perfect, it is beneficial if the viscosity is as low as possible, in order to reduce the influence of errors in the model. Furthermore, it is beneficial if the material reacts fast to pressure changes, so that touch can be detected fast and high frequencies can be measured. Moreover, it makes the behaviour planning of the robot harder, if the softness of the fingertips varies due to its viscosity (for example, the skin should not be harder when grasping an object shortly after another grasping action).

7. *Endurance:* the material should be robust and not change its properties over time, in order to avoid creep in the measurements and to give the sensor a long lifetime.

In general, elastomers (like silicones or natural rubber) could be used for the dielectric layer, because they are elastic, can be moulded and are not electrically conductive. Sometimes they are moulded to include cavities, so that the resulting dielectric layer becomes compressible and softer [124]. Also because of their compressibility, foams are used. Moreover, foams are in general preferable to bulk elastomers concerning viscosity, because gas in general is several orders of magnitude less viscous than solid materials. Especially closed-cell silicone foams demonstrate excellent properties, also concerning hysteresis [121].

3.3 Flexible, Electrically Conductive Material

In order to enable the sensor to respond to objects irrespective of their electrical conductivity, it is necessary to have a conductive layer above the dielectric layer (as explained in further detail in Section 4.1). To reduce the development time, commercial products should be used, but only few commercial materials are available that fulfil all requirements: electrically conductive, flexible, adhesive to the dielectric material and can be applied on curved surfaces. In general, the search for conductive, flexible materials is still an open research field. Conductive dopants that are often used to make elastomers conductive include carbon black, silver and particles plated with silver. Recently, several researchers have started using carbon nanotubes as conductors (depending on their structure, they can be highly conductive). Common methods to apply the material are spraying, moulding, sputtering and many others.

3.4 Manufacturing

One of the requirements is that the shape of the robotic fingertips should resemble those of a multi-curved human fingertip. With very few exemptions (the fingertips of the Shadow hand and of TWENDY-ONE, for both of which limited information is available) the distributed tactile systems that are available are flat, a combination of several flat surfaces or at most cylindrical (compare Section 2.3). A problem while designing a multi-curved sensor system is that most production methods are not able to produce three dimensional electronic structures. For example the cylindrical sensors are usually produced as flat sheets, which are subsequently bent. Moreover, it has to be taken into account that the fingertip sensors for iCub are to be produced in large numbers (for ten iCubs or even more). Therefore, the ease and speed of production have to be considered. Furthermore, robustness is an issue, as the sensors will be used by different laboratories for diverse experiments, over extended amounts of time.

For the capacitive fingertip sensor, especially the fabrication of the inner electrodes and their connection to the chip are challenging, due to the small size and round shape of the electrodes. The electrodes could be directly applied onto the inner support in an automatic way with syringes, stamps, sputtering or spraying through masks. To achieve a multi-curved dielectric layer, it could be moulded. For the outer conductive layer, spraying would be a commonly used method that requires relatively little work.

3.5 Experimental Design

The sensor response is influenced by a number of factors. Some of them are intrinsic to the design of the sensor, some of them are influenced by the choice of the dielectric. In any case, all of them are important for a full understanding of the sensor response and they should be investigated individually or taken into account while designing the experimental setup.

1. *Sensitivity:* it has to be measured how the sensor reacts to varying pressure, and which is the minimal detectable pressure (considering the noise in the sensor measurements).

2. *Responsiveness only to perpendicular force:* the sensor responds only to the normal component of the applied force[2]. Therefore, to make the results of different experiments comparable, the angle of pressure has to be held constant; in particular, force should only be applied perpendicular to the sensor surface, in order to make the sensor measurements comparable to the reference measurements from the loadcells, used in the experiments.

3. *Contact Area:* in general, the sensor is a pressure sensor: given that the contact area is far larger than the electrode area on the inner support, the size of the contact area does not influence the measurements, as long as the ratio of perpendicular force and area stays constant. But if one reduces the contact area progressively, and the borders of the contact area approach and finally cross the boarders of the underlying electrode, the size of the contact area starts to influence the measurements at one point, even if the pressure is held constant. This principle is illustrated in Figure 3.1. The distance from the borders of the electrode, which starts influencing the sensor measurements, has to be experimentally determined.

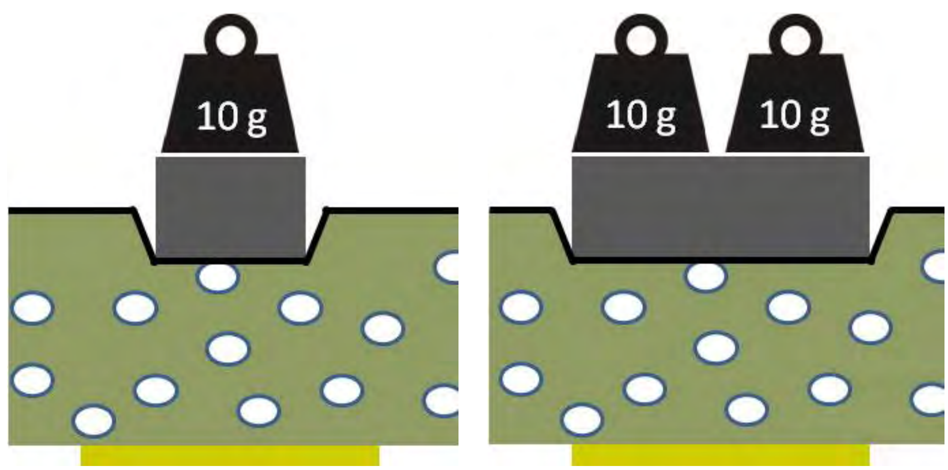

(a) (b)

Figure 3.1: **Illustration of the influence of the contact area.** Silicone foam (greenish) is sandwiched by two electrodes (gold and black). The pressure is the same in (a) as in (b): the force is twice as big, and so is the contact area. The sensor response can be expected to be stronger in (b) than in (a), because the sensor measures the distance between the two electrodes, and a relevant part of the black electrode is closer to the golden electrode.

[2]Indeed, this can be assumed but it was never verified with the experimental setup. For example, a six axis force load cell would have been necessary to evaluate the influence of non-perpendicular forces on the measurements, but the cost of such a load cell were prohibitive.

4. *Difference in response between different taxels:* it has to be evaluated whether different taxels respond differently. It would be beneficial if all taxels respond in the same way, otherwise they would have to be individually calibrated.

5. *Cross-talk:* the cross-talk between the taxels has to be evaluated. It could be caused either by effects intrinsic to the capacitive technology or due to material properties.

6. *Non-linearity:* in addition to the factors described above, the static response of the sensor to a certain pressure depends on a number of factors. (1) The sensor measures capacitance, and capacitance is inversely proportional to displacement. (2) The displacement in turn depends on the stress-strain relationship of the dielectric: stress, the force exerted per unit area, causes strain, a relative displacement: the compressive pressure applied to the sensor surface results in a specific distance between the electrodes above and below the silicone foam. This stress-strain relationship depends on the dielectric material (some have in a certain pressure range a linear relationship, other materials have an inversely proportional relationship). As a result of all these factors, the pressure to sensor response relationship depends on the choice of the dielectric and is not easily predictable; it is not clear whether the sensor will respond linearly and if at all, in which range. Therefore, the pressure vs. sensor measurement relationship has to be experimentally evaluated.

7. *Hysteresis:* Ideal springs are purely elastic, but other materials also exhibit a time dependent viscous behaviour. The viscosity of the dielectric layer has an influence on the sensor measurements. For example, even when the applied pressure is constant, the distance between the electrodes above and below the dielectric decreases with time, thereby influencing the capacitance measurements. This causes for example hysteresis in the measurements[3]. If possible, this behaviour should be modelled and the influence on the sensor measurements should be compensated.

8. *Drift:* one factor that could cause drift in the sensor measurement is for example the fact that many capacitive pressure sensors are sensitive to temperature (see for example [127]). While probably also the sensitivity is slightly influenced by temperature, the most important aspect

[3]No other factors that cause hysteresis in the sensor have been identified yet.

is the change of the baseline. The drift in the sensor measurements should be studied (for example, do all taxels drift in the same way?) and its influence on the sensor measurements should be compensated, if possible.

9. *Temporal Resolution:* It should be evaluated how fast the sensor responds to pressure changes, and moreover it would be interesting how the sensitivity changes when the sensor is stimulated with higher frequencies.

10. *Repeatability:* it should be evaluated whether the measurements are repeatable, i.e. whether always the same capacitance is measured for the same pressure (after having considered all factors above).

Due to these requirements, the following things have to be taken into account for the experimental setup. It should be possible to apply pressure with a probe to the sensor at different places. Ideally, the probe should have five degrees of freedom, so that it can reach the whole fingertip surface. Also the work area has to be sufficiently big. It should be possible to precisely control and monitor the position and rotation of the probe, preferably automatically with a robot. Furthermore, the setup has to include a load cell, to provide reference force measurements. A static loadcell is preferable to a dynamic one, as also the capacitive sensor delivers static measurements. Nevertheless, it would be good if frequencies up to 500 Hz or higher could be measured, because this is also the maximum frequency of the AD7147 chip. The range of the loadcell should be around 500 g, as those are the forces that are intended to be applied to the capacitive sensor. The sensitivity of the loadcell should be higher than the one of the capacitive sensor. If a single axis loadcell is used, the angle with which the pressure is applied has to be exactly controlled. A six-axis force-torque sensor would be preferential, in order to release this constraint. Moreover, it should be possible to use probes with different sizes.

The costs of a 5 axis degree of freedom robot and a 6 axis loadcell are prohibitively high. Therefore, it was decided to use a robot with only 3 degrees of freedom and a single axis loadcell. Already a robot with 3 DOF costs at least around 5000 Euro. Concerning the loadcell, off-centre static loadcells with a suitable range were available at the laboratory, and were therefore used. The maximal frequency of the loadcell is far lower than 500 Hz. Therefore, not all, but still many of the characteristics that are described above can be evaluated with the resulting experimental setup.

3.6 Conclusion

In this chapter, it was presented how the goal of building fingertips for iCub was approached. The different factors that have to be taken into consideration during the different stages of designing the fingertips were described. Following these criteria, in the next chapter it will be shown how the fingertips were implemented.

Chapter 4

IMPLEMENTATION OF THE FINGERTIP ARCHITECTURE

In this chapter, the implementation of the ideas from the previous chapter concerning the construction of the fingertip is shown. First, the working principle of the capacitive pressure sensor and the structure of the transducer are presented in Section 4.1. The digitisation of the sensor measurements is explained in Section 4.1.1. Afterwards, the dielectric layer is presented in Section 4.2. The search for a flexible, electrically conductive material is discussed in Section 4.3. Several versions of the fingertip were designed before the final one, as particularly the 12 inner electrodes proved to be challenging to fabricate in a fast and reliable way, as presented in Section 4.4. In the first version the electrodes were fabricated and connected to the PCB manually (see Section 4.4.1), afterwards it was intended to solder them to the PCB (Section 4.4.2), or to connect them to the PCB with a conductive foil (Section 4.4.3). Also a version with a soft inner support was designed, as presented in 4.4.4. The final version of the fingertip is based on a flexible PCB, as explained in Section 4.4.5. In Section 4.5, the installation of the fingertips on iCub is shown. A conclusion of the implementation is drawn in Section 4.6.

4.1 Capacitive Pressure Sensor for the iCub Hand

As discussed in Section 3.1, it was decided to base the distributed pressure sensors for iCub on capacitive technology. The transducer needs to have a particular structure, so that it can respond to all objects irrespective of their conductivity. In particular, the transducer consists of a soft dielectric sandwiched by electrodes. When pressure is applied to the sensor, the distance between the electrodes above and below the dielectric changes, and the capacitance changes accordingly (capacitance is a function of distance). In each fingertip and in each module in the palm (discussed in Appendix A), 12 electrodes below the dielectric form the taxels. On the contrary, above the di-

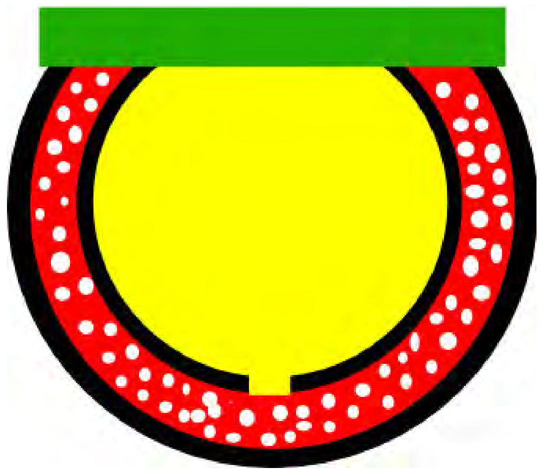

Figure 4.1: **A section of the fingertip.** The inner core is yellow, the silicon foam is red and the conductive material black. Also the PCB is shown in green.

electric one conductive layer covers the whole surface. This layer serves as the common electrode above the dielectric for all the taxels. It is connected to ground (and will therefore be called "ground layer" in the following). This ground layer enables the sensor to respond to objects irrespective of their electrical properties. It also reduces the electronic noise coming from the environment, in particular the stray capacitance, which can be a problem for capacitive pressure sensor systems [2]: stray capacitance refers to the fact that any two adjacent conductors act as a capacitor, and therefore without proper shielding any conductor close to the sensors would influence the measurements. In order to achieve a shape that resembles a human fingertip, in the artificial fingertips the transducer surrounds the inner support of the fingertip, see Figure 4.1.

4.1.1 Digitisation of the sensor measurements

The capacitive measurements are digitized locally: each fingertip and each triangular module in the palm incorporates a printed circuit board (PCB) with the electronics to obtain 12 measurements of capacitance and to send them over a serial bus. To perform the digitization, a capacitance to digital converter (CDC) (*AD7147* from *Analog Devices*, [127]) is mounted on the PCB. The chip provides 16 bit measurements and sends them over an I^2C serial interface. Each chip can be assigned with a 2 bit address; therefore up to 4 chips can communicate over the same serial bus. Using a serial bus is a critical advantage since it reduces the amount of wires and electrical connections that are required. As a result only 4 wires travel along the side of the fingers to small boards at the back of the hand.

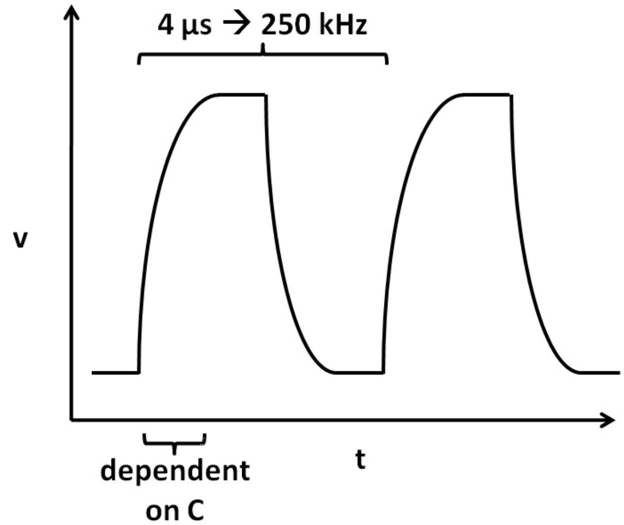

Figure 4.2: **Capacitance measurements.** The capacitor is charged until a certain threshold is reached. The charge time depends on the capacitance.

These boards relay the data from all five fingertips to a microcontroller board[1]. The microcontroller unit collects the measurements from all the CDC chips and sends the measurements through a CAN bus to the PC104 in the iCub head.

The CDC chip samples the capacitance at 250 *kHz*, see Figure 4.2. The excitation signal is applied to the same electrode from which also the measurements are taken, see Figure 4.3. The measurements that are sent over the serial bus are the result of an averaging process: the mean of either 192, 384 or 768 samples (depending on how the registers in the chip are set) is output. Therefore, from each chip 12 measurements of capacitance can be obtained at about 100, 50 or 25 Hz, respectively. The chip can be also set to measure an average of the 12 taxels at around 500 Hz (limited by the bandwidth of the serial bus).

The chip also provides an active shield signal, which is preferential to passive shielding in a grounded capacitive sensor like ours [135]. If the shield layer in the PCB is passive (connected to ground), the stray capacitance of the passive shield can be much greater than that of the transducer, which affects the range of the sensor and makes the measurements more susceptible to environmental influences. An active shield is in phase with the excitation of the sensor, driven at the same DC level as the capacitive sensor [136]. As a result, there is no potential between the shield layer and

[1]The microcontroller board has been designed by Marco Maggiali.

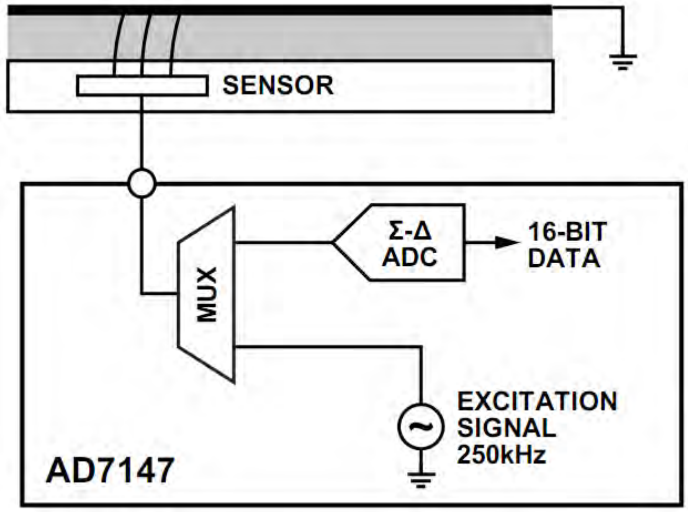

Figure 4.3: **Capacitance sensor schema.** When pressure is applied to the plane connected to ground, it gets closer to the sensor electrode. The picture is modified from [127].

the sensor electrode and traces, which also eliminates the capacitance [137].

Already in the earliest implementations of the fingertips it could be seen that out of the 16 measurement bits that the CDC chips send, the lowest 3 bits are affected by noise, and that the range the highest 5 bits provide is not used. Therefore, the microcontroller board sends only 8 bit measurements over the CAN bus, where one measurement unit corresponds to 2.88 fF (calculated according to Figure 18 in [127]). In these remaining 8 bits the sensor measurements usually oscillate between 2 neighbouring values (due to noise, but also due to the delta-sigma analogue to digital conversation used by the CDC chip). Yet, in few taxels the noise can be up to ± 3 measurement units of the baseline. The cause of this could be traced back to the soldering quality of the CDC: if a pin is not perfectly aligned with its soldering pad (at the current stage the CDCs are soldered manually onto the PCB), the sensor measurements are affected by larger noise. The noise will be further evaluated later on in the experiments (see Section 5.1.3).

4.2 Dielectric Layer

According to the criteria listed in Section 3.2, several materials were tested for their adequacy as a dielectric for the capacitive pressure sensor. Sheets of readymade foil like in [121] could not be used as a product is required that can be moulded into a multi-curved shape. Natural rubber proved to be not sufficiently soft. *Ecoflex 00-30* or *Ecoflex 00-10* from *Smooth-On* are softer, but *Ecoflex 00-10* is covered by an oily film even when it is fully cured. More importantly, simple tests showed that the silicone foam *Soma Foama 15* from *Smooth-On* exhibits less hysteresis than the bulk silicones made out of *Ecoflex 00-30* or *Ecoflex 00-10*: it was obvious even through observations with the naked eye that the bulk materials took several seconds to return to their original shape after being shortly pressed, while no such effect was visible in the silicone foam. The addition of the softener *Slacker* from *Smooth-On* to *Ecoflex 00-30* or *Ecoflex 00-10* even increased the viscosity of the two products. In general, *Soma Foama 15* has many characteristics that make it a good choice for the dielectric layer:

1. *Moulding: Soma Foama 15* can be easily moulded. Moreover, it adheres to many materials to which it is in contact during the moulding process, and if the adhesion is strong enough, no additional adhesive is necessary to glue it to the inner support.

2. *High, nonlinear strain: Soma Foama 15* is very soft and easily compressible. The fact that the foam includes gas bubbles, could also lead to interesting properties in the sensor. The sensor measures capacitance, and capacitance has an inversely proportional relationship to displacement. According to Boyle's law, the gas entrapped in the foam has also an inversely proportional relationship between pressure and the gases' volume (which in our case relates to displacement). Therefore, if the dielectric behaves like an ideal gas, the relationship between pressure and capacitance is linear. [2]

3. *Viscosity:* According to the preliminary experiments described above, *Soma Foama 15* is preferable to the other products that were tested. Also in [121] closed-cell silicone foams are described to demonstrate excellent properties concerning hysteresis. In Section 5.1.3, the time dependent behaviour of the sensor due to the viscoelasticity of the silicone foam will be investigated in detail.

[2] But the overall stress-strain relationship of the closed-cell silicone foams depends on both the elasticity of the gas entrapped in the silicone foam and the elasticity of the silicone itself. The elastic response of silicone to uniaxial compression can be modelled like a hyperelastic material [138]. Moreover, as the gas is initially easier compressible than the silicone, for lower pressure the elasticity of the silicone foam depends mainly on the properties of the gas, while in later stages it increasingly depends also on the silicone. Therefore, it is difficult to predict the overall relationship between pressure and capacitance (in particular, whether it is linear, and if, in which range).

4. *Diffusion:* Foam is compressible (unlike bulk silicone, which as a result of uniaxial pressure expends in the other dimensions), and therefore is beneficial to minimize the cross-talk between the taxels.

5. *Endurance:* silicones in general are chemically inert, are resistant to oxygen and UV-light, and are often used where durability is demanded [139]. Like all elastomers, silicones have a high yield point (the stress at which a material stops being elastic and instead begins to deform plastically). Therefore, also silicone foam can be expected to be robust.

By looking at this list, the choice of silicone foam as the dielectric can be justified. Silicones are usually durable, and silicone foam is softer than bulk silicone and shows less hysteresis. The silicone foam is also easy to process and mould, and it adheres itself to many surfaces with which it has contact during the moulding process. The softness of the silicone foam also makes the surface of the hand compliant. However, the foam exhibits also bad qualities:

1. *Inhomogeneity:* The density of the foam can vary from sample to the next, if not the exact same amount of material is used. Also within one sample the density varies a bit (the size of the bubbles slightly varies). Moreover, at the edges of the silicone foam layer, the foam could be softer, as it is less constricted by neighbouring foam, and also during the moulding process the holes through which excessive foam can exit are located there. Furthermore, it could be observed that *Soma Foama 15* that has spent more time on the shelf before the moulding process will be less soft, less adhesive and also the viscosity changes.

2. *Work time:* The foam cures within less than a minute, therefore the moulding process has to be very fast.

3. *Dielectric constant:* The gas in the foam dominates its dielectric constant, and the dielectric constant of gas is low. It was tried to add fillers to the foam, but this made the foam much stiffer, without changing its dielectric constant too much[3]. Preliminary tests with an ionic liquid showed that the dielectric constant could be doubled without causing negative mechanical effects.

[3] I peformed preliminary experiments, but a set of more thorough experiments was performed by Perla Maiolino.

Nevertheless, it was decided to use the silicone foam (in its original form), because it was sufficiently good and other problems in the sensor were more urgent. Yet, in the future, the sensor could be more sensitive or more homogenous by improving the dielectric, as discussed in Section 6.1.2.

The thickness of the silicone foam was decided to be 2 *mm* (for both the fingertips and the palm), in order for the sensor to be sufficiently compliant: the thicker the foam layer, the more compliant the sensor, but the less sensitive it is[4].

As a final note, it was discovered that the softness of the foam also depends on the mould used during the fabrication process: the more holes the mould has, through which excessive silicone foam can exit during the moulding process, the softer the resulting foam will be (it will be less dense). The mould has been to be designed taking this into consideration.

4.3 Flexible, Electrically Conductive Layer

Initially, the use of commercially available conductive materials was intended for the conductive layer above the silicone foam. However, the commercial products that were tested did not fulfil the expectations, as described in more detail below. Therefore, experiments with self-made composites with carbon nanotubes as the conductive dopant were performed (listed in detail below), but also those experiments proved ineffective. Furthermore, non-functionalized silver nanopowder (<100 *nm* particle size) from *Sigma Aldrich* proved ineffective as the conductive dopant, as it did not disperse in the solvents tetrahydrofuran, toluene and ethanol. There are many possibilities to improve the results, but due to time constraints they could not be investigated yet. Finally, the self-made composite based on silicone and carbon black was used for the fingertips, even though the conductivity of this material is rather low. The reliability of the flexible conductive layer remains the biggest limiting factor of the fingertips, as discussed in Section 5.1.4.

- *Commercial Materials*

  Few materials were purchasable that are flexible, electrically conductive and adhesive to silicone (the same is true for materials that are adhesive to latex, which was also an option before the silicone foam was chosen). The following materials were tested, but none proved effective: *102-32* silicone based electrical conductive adhesive from *Creative Materials*, *FIP-II*

[4]As capacitance is inversely proportional to distance, the sensor would be probably twice as sensitive if the dielectric layer is only 1 *mm* thick.

silver/copper silicone composite from *Tecknit* and *Teckbond-C* silver plated/copper filled silicone adhesive also from *Tecknit*. The electrical conductivity was too low for our application, the adhesion to silicone was weak and the flexibility insufficient.

- *Experiments with Carbon Nanotubes*

The experiments with carbon nanotubes as the conductive dopant are summarized in Table 4.1. These experiments were performed under the guidance of Maurizio Biso. The first column states the type of carbon nanotubes used for that trial: single-walled carbon nanotubes (SWCNT; purity $>$ 90wt%) from *Cheap Tubes Inc.*, multi-walled carbon nanotubes (MWCNT; purity $>$ 99wt%) from *Nanocyl S.A.* and single-walled carbon nanotubes produced by Maurizio Bisio according to the procedure described in [140], which was named SW-Prato. In some of the tests ionic liquid 1-butyl-3-methylimidazolium tetrafluoroborate ($BMIMBF_4$) was used, as ionic liquids in general and this one in particular are often used together with carbon nanotubes to improve their dispersibility, see for example [141]. The third column states the employed solvent: tetrahydrofuran (THF; purity $\geq$ 99.9%), dimethylacetamide (DMAC; purity $\geq$ 99.5%) and 4-methyl-2-pentanone (pentanone, purity $\geq$ 99.9%), all from *Sigma Aldrich*. To disperse the carbon nanotubes and the ionic liquid in the solvent a *Sonicator 4000* from *QSONIX* was used. Different elastomers were added to the dispersed carbon nanotubes: *CAF 4* from *Rhodia-Silicones*, Sil-Poxy from *Smooth-On* or polyvinylidene fluoride (PVDF; molecular weight (M_r) $\sim$530000) from *Fluka*. Before adding the elastomer by stirring, it was dissolved in THF (in general we tried to use as little THF as possible; specifying the exact quantity of solvent is difficult, as THF evaporates fast). Some of the resulting composites quickly segregated before they could be applied (as noted in Table 4.1). If not stated otherwise, the composite was applied on *Ecoflex 00-30* silicone from *Smooth-On*, but in one case PVDF was used, and in another case also *Soma Foama 15* from *Smooth-On*. The goal was to spray the composite with an airbrush on the silicone, but many composites did not adhere to the *Ecoflex 00-30*, but instead were blown off from the *Ecoflex 00-30*. If successful, patches were sprayed which had a diameter of around 4 *cm*. Instead of spraying, in some experiments the composite was casted on flat silicone inside a Petri dish (inner diameter 5.7 *cm*), which was subsequently heated at 70°C; still, casting is not a feasible approach for the fingertip as it is not flat, and could only be used for preliminary experiments. The resistance was tested

Table 4.1: Experiments to create a conductive elastomer with carbon nanotubes.

Nanoparticle	Ionic liquid	Solvent	Elastomer + extra solvent	Sprayable	Adhesion	Resistance	Flexibility
0.5mg SWCNT		3ml THF	none	no (gets blown away)	no (can be wiped off)		
20mg MWCNT		20ml THF	114mg CAF 4	yes	good	200 kΩ	no
20mg MWCNT	200mg IL	20ml THF	114mg CAF 4	yes (but the composite was not homongenous)	no	300 kΩ	no
20mg SW-Prato		6g THF	0.2g CAF 4	yes (but the composite was not homongenous)	good	130 kΩ	
20mg SW-Prato		6g THF	0.2g Sil-Poxy	yes (mix looks more homogeneous than with CAF)	good	30 kΩ	good
30mg SWCNT	70mg IL	10ml DMAC	70mg PVDF	poured on silicone, cast and heat at 70°C	no (Ecoflex 00-30 and PVDF)	**100** Ω	bendable, but not stretchable
30mg SWCNT	88mg IL	7ml THF	0.3g Sil-Poxy	poured on Ecoflex 00-30, cast and heat at 70°C		150 kΩ	
30mg SWCNT	75mg IL	6ml DMAC	0.3g Sil-Poxy	poured on Ecoflex 00-30, cast and heat at 70°C	good	200 Ω - 1 kΩ	good
30mg SWCNT	75mg IL	6ml DMAC	0.6g Sil-Poxy	half poured on Ecoflex 00-30		20 kΩ	
30mg SWCNT	75mg IL	6ml DMAC	0.6g Sil-Poxy	no (gets blown away), both on Ecoflex 00-30 and Soma Foama 15			
30mg SWCNT	75mg IL	6ml DMAC, reduced on hot plate	0.6g SilPoxy	no (gets blown away)			
30mg SWCNT	78mg IL	7ml Pentanone	0.3g Sil-Poxy	yes (from an increased distance)	good	30 kΩ	good

with an Ohmmeter (the probes had a distance of about 1 *cm*). As the experiments described here were only preliminary, the area of the conductive patch, the distance of the probes and the thickness of the conductive material were not precisely measured, and therefore the conductivity of the materials can only be stated approximately. To test whether the conductor is flexible, it was stretched to approximately 120% of its original size and was subsequently checked for mechanical damage and degradation in the electric conductivity. Materials that could not be sprayed could not be tested for their characteristics and some materials with a high resistivity were immediately discarded and not further tested.

One of the samples had a low resistance of about 100 Ω, but the material was not adhesive to silicone. Another problem was that the solvent DMAC, with which good results were achieved, has a high boiling temperature, which makes it difficult to spray. In conclusion, none of the trials proved to be an applicable solution for the fingertips.

- *Carbon Black/ Silicone Composite*

  The best results were obtained with a self-made mixture of *Rhodorsil CAF 4* silicone from *Bluestar Silicones*[5] and carbon-black particles *Vulcan XC72* from *Cabot*. It is a further development of a conductive material based on carbon-black particles originally used by Dr. Marco Randazzo [142]. The resulting composite is elastic, adhesive to silicone and electrically conductive (about 10kΩ measured between two points at the maximum distance found on the fingertips). It easily conforms to the round shape of the fingertip. To spray this material the solvent tetrahydrofuran was used (in earlier versions toluene was used, but toluene is more toxic, and therefore tetrahydrofuran is preferable). The production process is described in detail in Section 6.

4.4 Manufacturing

While constructing the fingertip, particular challenges were the fabrication of the 12 inner electrodes and their connection to the PCB. This was mainly due to the small size and curved shape of the fingertip. Most standard production methods for electrodes are targeted for flat surfaces and are therefore not suitable to produce three-dimensional electrodes. In order to apply the conductive

[5] *CAF 4* silicone was previously produced by *Rhodia Silicones*, until *Rhodia* sold its silicone department to the *BlueStar* cooperation. The products used for early versions of the fingertips were therefore produced by *Rhodia Silicones*.

material automatically on the electrode areas, syringes, stamps and masks have been unsuccessfully tried. The main problem was to keep the electrodes separate, as the employed conductive inks tended to conjoin due to the small distances between the electrode areas. Therefore, in the first successful approach, described in Section 4.4.1, the electrodes had to be produced manually: the inner support was completely covered with electrically conductive ink and the electrodes were separated with a file. A working prototype of the fingertip was built and used for first experiments, testing its response to changing pressure. However, the construction process was work intensive and prone to errors. Therefore, an automatic way of producing the 12 electrodes was attempted, with materials that would have allowed the soldering of the inner support with the electrodes onto the PCB (see Section 4.4.2). Even after improving the PCB, several problems rendered this approach unsuccessful. In an attempt that produced several working fingertips, the electrodes (which were again painted with conductive ink on the inner support) were electrically connected to the PCB with the help of a z-axis conductive foil, as described in Section 4.4.3. Nonetheless, even this approach was quite work intensive, and it usually took several attempts to produce a working fingertip. Moreover, the fingertips worked only for limited amounts of time. In parallel, a version of the fingertip with a flexible inner support made from silicone (see Section 4.4.4) was produced. This approach would have increased the compliance of the fingertip, but the construction process proved to be even more difficult than with a hard inner support.

For the final version of the fingertip, the PCB was made flexible and also included the round pads for the 12 taxels, thereby eliminating the need to connect them in an extra working step to the PCB. This solution proved to be robust. In Section 4.4.5 the production process of the final version of the fingertip is explained step by step and in Section 4.5

4.4.1 Version 1: Deposition of the Electrodes by Hand and Connecting them with Short Wires

In the first tentative approach the 12 electrodes were painted by hand on the inner support of the fingertip. Raised lines between the 12 areas make it possible to remove excessive paint between the 12 areas (see Figure 4.4 and Figure 4.5). A first version of the PCB was designed, which was very small, as depicted in Figure 4.6.

The production process is as follows.

1. The inner core is produced. This was done initially by an external contractor (*Terza Dimensione*) using 3D printing and subsequently with an in-house 3D printer (Elite from *Dimen-*

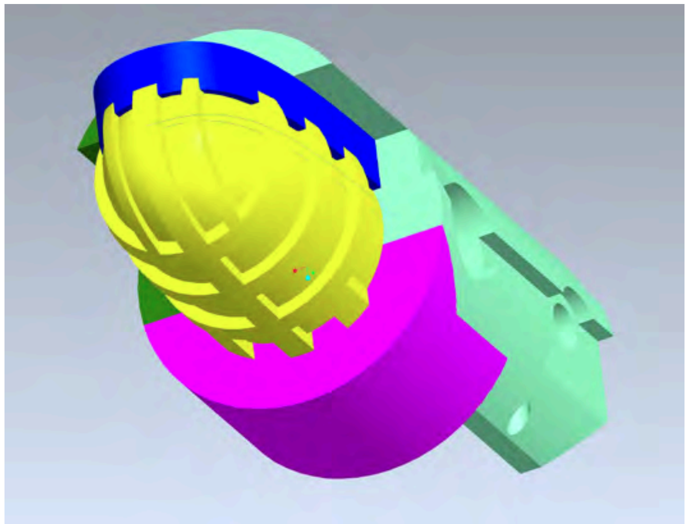

Figure 4.4: **A section of the internal structure of the fingertip:** the inner core/electrodes support (yellow), the aluminium phalange (green), the PCB in blue and the cover silicone (only partially shown, in purple).

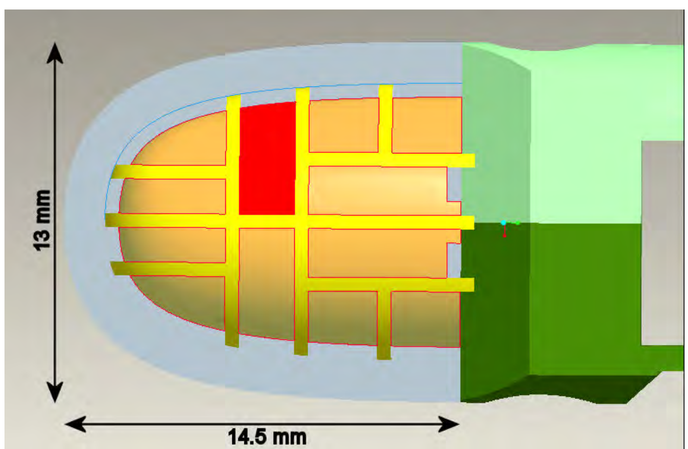

Figure 4.5: **Drawing of the inner core and the silicone foam from below.** The electrodes, which act as the receptive fields, are highlighted in orange. The silicone foam is also visible, shaded in grey, to show to overall size of the fingertip. Taxel 4, which is referred to in Figure 4.13 and 4.14, is shown in red.

sion). The spatial resolution of those printers is lower than the one used for the final version.

2. The inner core is covered with silver conductive paint from *Electrolube*. Due to the small

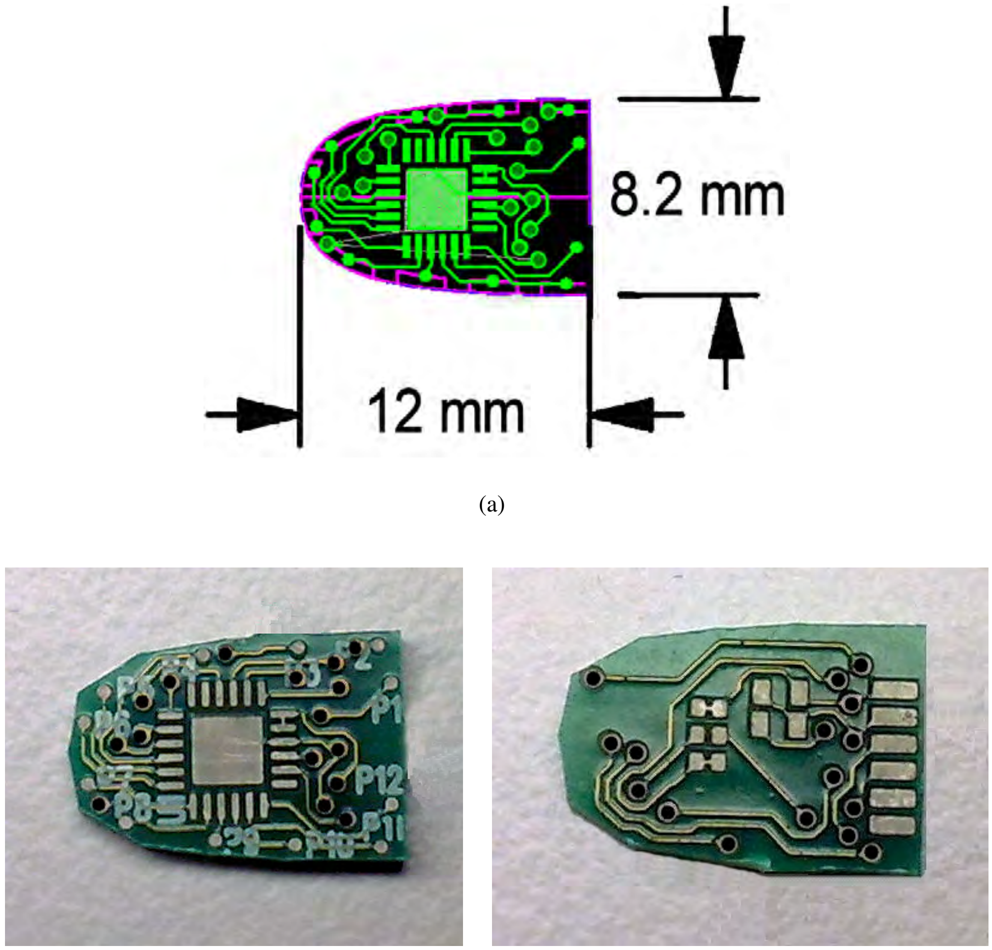

(a)

(b) (c)

Figure 4.6: **First PCB for the fingertip.** In **(a)** the schematic of the PCB shows the dimensions of the PCB. **(b)** and **(c)** depict the two sides of the PCB.

size of the electrodes and the low viscosity of the silver paint[6] it is impossible to apply the material only on the electrode areas. Excessive conductive material between the electrodes is therefore removed with a file. This is possible as the inner support is a bit raised between the electrode areas (see Figure 4.4 and Figure 4.5).

3. Short wires are soldered on the PCB, one for each of the 12 electrodes. The PCB is attached to the inner support with glue. One has to pay attention not to break off the wires during this process.

[6]Also two other conductive paints were tested, but they were even more difficult to apply: Conductive Pen (with micro tip) from *circuitworks* and Silver Conductive Paint from *RS components*.

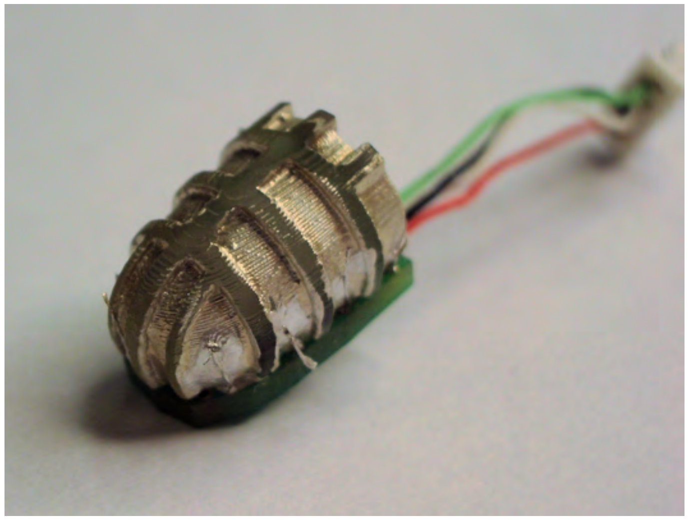

Figure 4.7: **A picture of the hard fingertip prototype without its outer layer.** One can see the inner core and the PCB. The taxels are made of conductive ink (silver).

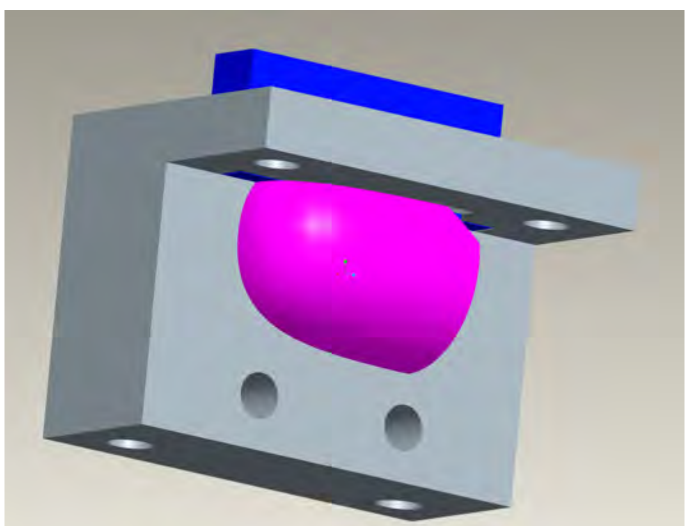

Figure 4.8: **Schematic drawing of the mould for the silicone foam layer.** One part of the mould is hidden, to show the silicone foam (purple).

4. To electronically connect the electrodes to the PCB, the wires are pressed against the corresponding electrode on the inner support and are fixated with a drop of silver ink. Excessive silver ink between the electrodes has to be again removed with a file. For a picture of the fingertip at this stage please refer to Figure 4.7.

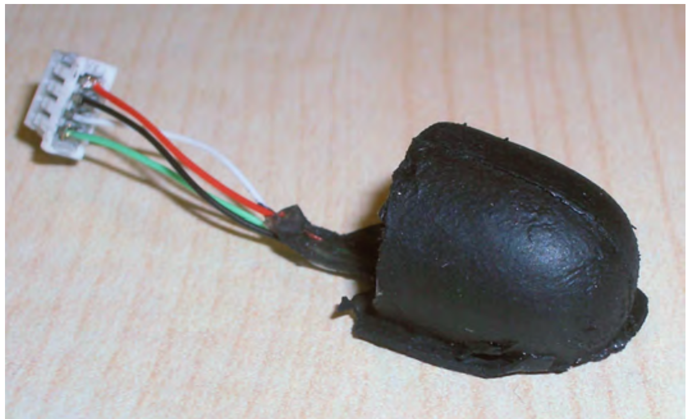

Figure 4.9: **A picture of the first version of the fingertip.** The outer conductive layer is black because of a carbon black-silicone deposition made to create a flexible conductor. The fingertip includes a capacitive pressure sensor with 12 taxels. The PCB with the electronics is included in the fingertip.

5. In the mould for the outer layer (as depicted in Figure 4.8) a small amount of *Ecoflex 00-30* from *Smooth-On* is poured and spread on all surfaces so that it covers the whole inner side of the mould with a thin layer. This will be outside of the silicone foam and enables the silicone foam to be removed from the mould later on. In addition, it is used to obtain a smooth outer surface[7]. The silicone is cured in an oven.

6. The inner support with the PCB is inserted into the mould and fixated in the proper position. The silicone foam is poured into the remaining space of the mould. This is a very time critical process, as the silicone foam cures within a couple of seconds. The excessive silicone foam is removed. The procedure is similar to the final one described in Section 4.4.5.5.

7. Finally, the outer conductive layer is sprayed. The procedure is similar to the final one described in Section 4.4.5.7. Yet, a major difference is that in the first prototype no connection to the ground is available for the outer electrode layer. Instead it was intended to connect the outer electrode layer with a wire to the ground. The final result can be seen in Figure 4.9.

[7]This step is not necessary in the final procedure anymore, as for the final version EasyRelease 200 from *Smooth-On* was used, which makes it easy to remove the fingertip later from the mould. The problem with open bubbles which cause non smooth surfaces also appears less often now and is solved by refabricating the silicone layer in those cases.

Figure 4.10: **Experimental setup with dynamic load cell used to measure the response of the sensor.** Initial tests have been performed with a shaker moving the fingertip vertically with a sinusoidal profile. The data obtained from one of the receptive fields was compared to the force measured by a PCB 208 C01 dynamic load cell.

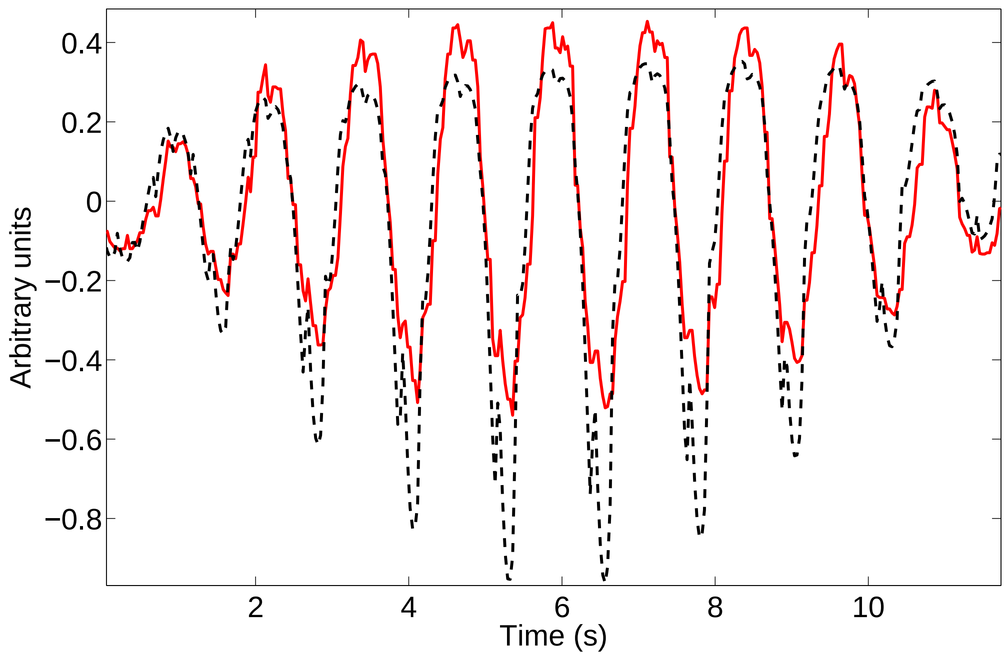

Figure 4.11: **The scaled output of the dynamic load cell (black, dashed) and the capacitive pressure sensor (red).** The shaker moved the fingertip vertically with a sinusoidal profile, and simultaneously the amplitude was modulated sinusoidally. One can clearly see the similarities between the two measurements. The different amplitudes of the two signals stem solely from the different output ranges of the sensors.

Experiments with the First Prototype

Initial tests have been performed with the first prototype. Test setups developed by Ravinder Dahiya were used (see for example [143]). In the first experiment, a solenoid pushes the fingertip periodically against a load cell (PCB 208 C01 dynamic load cell from *PCB Piezotronics*, see Figure 4.10); the amplitude and the frequency of the vibration can be controlled. The load cell measures the change in force between the probe and the surface of the fingertip; slowly changing and static force cannot be measured. The data was collected using a Labview program. The data obtained from taxel 4 of the fingertip was compared to the force measurements from the load cell.

Figure 4.11 reports the collected data and shows that the two are qualitatively similar (values are scaled to facilitate comparison). This plot also shows the dynamic response of the sensor, although more tests would have been required to properly measure its frequency response. It is difficult to specify the response of the sensor to a certain pressure given these results, as it will be explained in

Figure 4.12: **Test setup with a load cell that can measure static forces.** The off-centre load cell (3 kg AL series, from Laumas) and the micrometer (TESA Micromaster IP54) are shown.

the discussion.

In a second set of experiments an off-centre load cell was used (3 kg AL series, from Laumas[8]) suitable to measure static forces. Pressure is applied with a micrometer (TESA Micromaster IP54) by moving a cylindrical metal probe vertically against the sensor. The micrometer position can also be manually monitored. When it is moved downward, it applies pressure to the fingertip (see Figure 4.12). The fingertip is mounted on the load cell; the pressure is calculated as the ratio of the force over the contact area. The contact area was estimated to be constant and to correspond to the size of the probe, i.e. 18.6 mm^2.

The probe moved in small steps of $0.1mm$ each, to cover the available range. In each step, data was collected from the fingertip and the load cell for about 5 seconds and then the position of the

[8] www.laumas.com

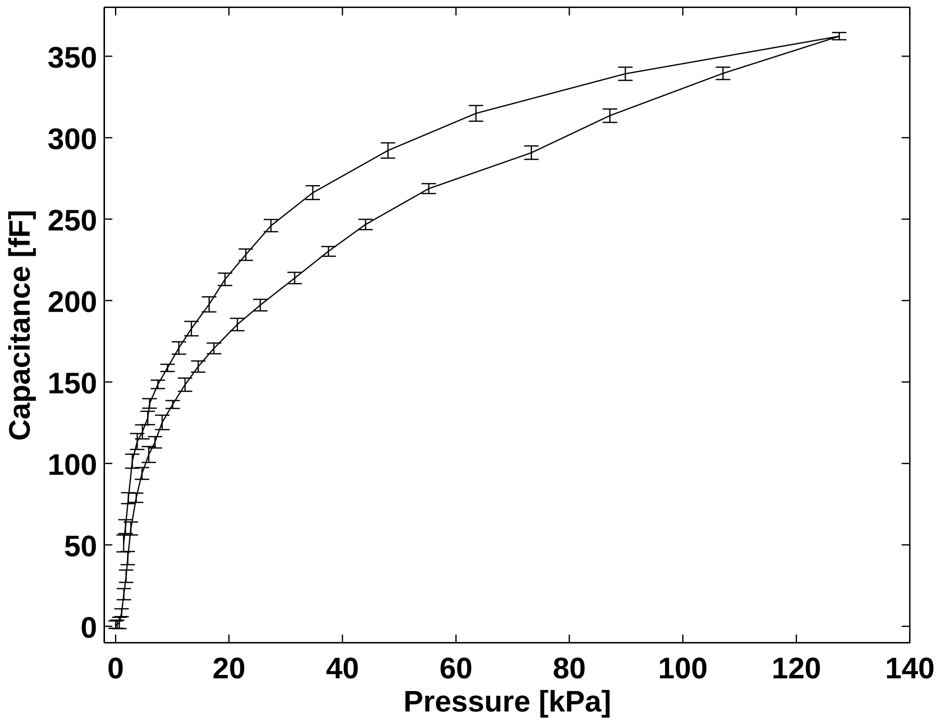

Figure 4.13: **The output of one of the receptive fields vs. the pressure as calculated from the measurements of the load cell.** The pressure was increased and decreased is small steps, by moving a probe by means of a micrometer in steps of 0.1 *mm* toward and then away from the fingertip. For each step the average measurement of taxel 4 (the taxel placed directly below the probe) together with the standard deviation is shown. One can clearly see a nonlinear response of the capacitive sensor, with a higher sensitivity for lower pressures. Moreover, hysteresis in the sensor measurements is visible: the measurements while stepwise increasing the pressure are clearly different than while releasing it. Possible causes for the nonlinearity and hysteresis are discussed in Section 4.4.1.

probe was manually changed. Figure 4.13 shows the output of the taxel immediately below the probe (taxel 4) and the measured pressure. Figure 4.14 reports data collected when continuously increasing and decreasing the stimulus several times over the course of a couple of minutes. The figure shows how much the measurements change between repetitions. As with the dynamic loadcell, also with these experiments it is difficult to define the response of the sensor to a certain pressure, as it will be discussed below.

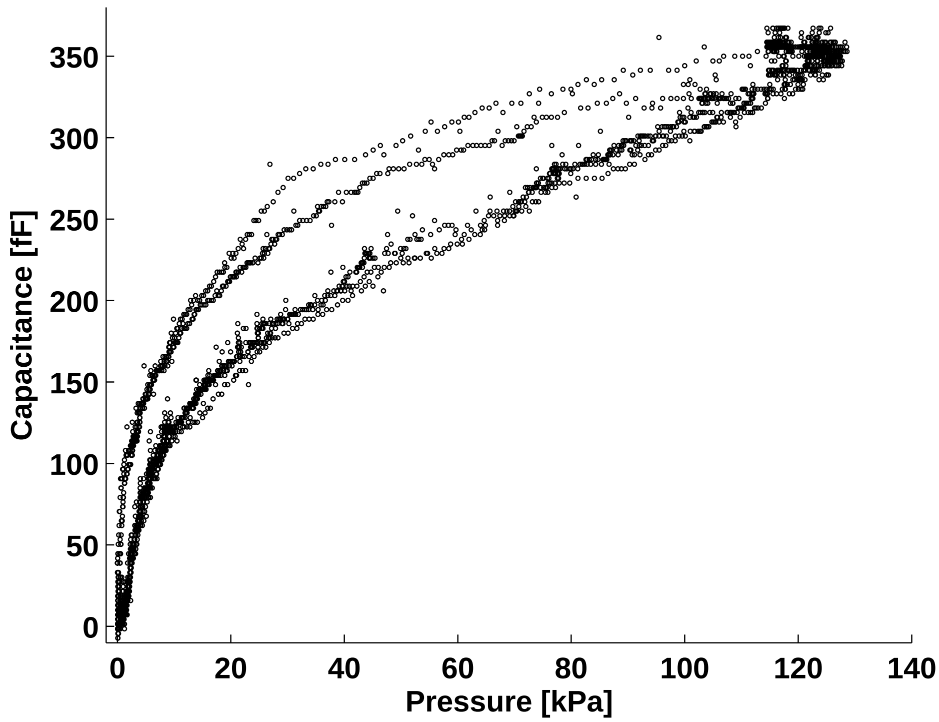

Figure 4.14: **The output of one of the receptive fields vs. the pressure as calculated from the measurements of the load cell.** The pressure was increased and decreased uniformly. The process was repeated three times in a row.

Discussion of the experiments

The dynamic loadcell used in the first experiment only measures changes in force and can therefore be used only for qualitative comparisons to the fingertip sensor. The second set of experiments shows the following characteristics of the sensor: a rather low noise level (seen in Figure 4.13 as low standard deviations compared to the range of outputs), a monotonic relationship between pressure and sensor response, hysteresis and nonlinearity. Yet, with the results from the experiments it is impossible to determine the response of the sensor to a certain pressure. This is due to two factors that influence the sensor measurement in an unquantified way: contact area and viscoelasticity.

The contact area and the electrode area of taxel 4 only partially overlap. As explained in Section 3.5, the contact area and the exact position of the probe with respect to the taxel influence the measurements. Therefore, the results of the experiments are only valid for the particular probe size and position used in the experiment. Furthermore, the probe is flat, while the fingertip is curved;

therefore, the contact area depends on the force with which the probe pushed against the fingertip (the contact area gets bigger when the probe is pushed harder against the fingertip sensor). Only when the probe is already pushed about 0.5 mm inside the foam, all the probe is in contact with the fingertip surface.

Concerning the hysteresis of the sensor, the sensor exhibits a time dependent behaviour due to the viscoelasticity of the silicone foam (explained in Section 3.5). This effect is clearly visible as a difference in the measurements while decreasing and increasing the force. Less obvious, it already affects the measurements while increasing the force. The force was increased stepwise, without time for the foam to recover in between. The effect of the viscoelasticity gets stronger with increased time as well as with increased force. As a result, in the experiments, the higher the force, the stronger the influence of the viscoelasticity on the sensor measurements was. As the effects of the viscoelasticity cannot be precisely quantified with the given experiments, especially for higher forces the response of the sensor to a certain pressure cannot be specified. To show the initial response of the sensor to a certain pressure, it would have been necessary to always measure the response after the silicone foam has fully recovered before to its original state. In addition, the viscoelasticity of the silicone foam should be studied independently. Due to the viscoelasticity of the foam it can be expected that the pressure changes, even if the probe is steady, and therefore an experiment would be necessary in which the probe is held constant for extended amounts of time, and the change in the loadcell and capacitance sensor measurements are monitored. This experiment was conducted for the final version of the fingertip, as discussed in more detail in Section 5.1.3.

The sensor also exhibits a nonlinear response. Indeed, this property might be useful as it makes the sensor particularly sensitive to low pressures, while it is still able to measure pressure as large as 130 kPa. Yet, with the experiments here it is not possible to determine whether the sensor also shows a linear response in a certain range. This is again due to the fact that the contact area and the viscosity of the silicone foam influence the measurements in an unquantified way.

In general, the sensor measurements presented here deviate from the results obtained with the final version of the fingertip, presented in Section 5.1.2. This could be due to the factors discussed above, or due the differences in the testing procedure and fingertip architecture. Also the unreliability of the ground layer (the conductive layer above the silicone foam that is connected to ground) could be a contributing factor (thereby, the material of the probe could start influencing the sensor measurements).

Concluding Remarks on the First Prototype

In this section, the first version of the fingertip sensor for iCub was presented. The desired shape was achieved, and the fingertip included the PCB with the electronics to perform the signal conditioning and digitization. Initial experiments were performed: while the initial results were promising, the experimental setup and the employed procedure did not allow a proper specification of the sensor characteristics.

The first prototype had the following problems: the PCB did not provide a connection to the ground layer and the position of the output connector was not compatible with the structural parts of the fingertip (the last metal phalange of the finger); this could easily be fixed by moving the connectors to a more suitable location. The chip for the capacitive pressure sensor was on the same side of the PCB as the receptive fields, which added noise to the signal. The production of each fingertip was a time consuming process and in addition prone to errors; in particular, the soldering spots for the 12 electrodes were very small and the wires tended to break off. Many of the problems could be solved by redesigning the PCB. In addition, a production method should be employed that involves less manual labour. Both aspects will be addressed in the next section.

4.4.2 Improvements to Version 1: Redesign of the PCB and Attachment through Soldering

Due to the experiences with the first prototype, the PCB was redesigned. The resulting PCB was bigger (as big as the outline of the fingertip) and also the connectors on the PCB to the 12 electrodes on the inner core were enlarged, see Figure 4.15. The PCB also included a pad connected to ground for the outer layer and the pads for the serial interface were moved to a more suitable location. The CDC chip was moved to the top side of the PCB to reduce the noise in the measurements. Using this new PCB and the production method described in the last section, a more reliable fingertip could have been produced. Nevertheless, another goal was to reduce the amount of manual labour required for each fingertip.

Therefore, a cooperation was entered with *Technimold Servizi* to produce a version of the inner support that could be soldered onto the PCB. The idea was to use a “pick and place” machine to position the inner support on the PCB and subsequently use reflow soldering to attach (both mechanically and electronically) the inner support. The 12 electrodes therefore had to continue on the bottom of the inner support (as shown in Figure 4.16). The whole inner support including the electrodes was to be automatically produced by *Technimold Servizi*.

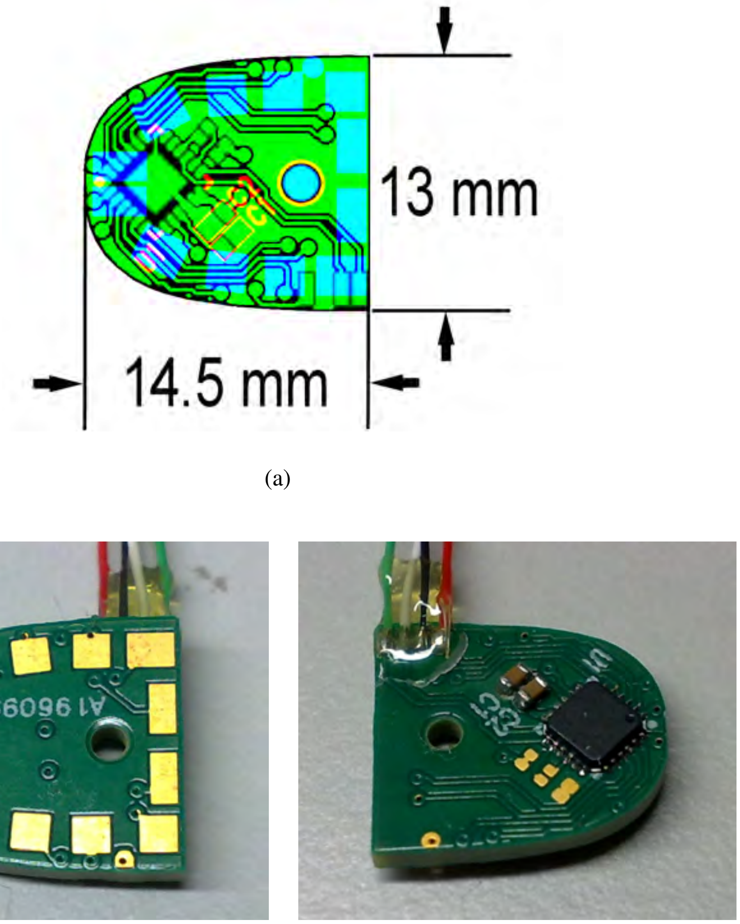

(a)

(b) (c)

Figure 4.15: **Enlarged PCB for the fingertip.** In **(a)** the schematic of the PCB shows the dimensions of the PCB. **(b)** and **(c)** depict the two sides of the PCB.

The first challenge was to find a material for the inner support that could be 3D printed (other production methods like injection moulding were not feasible due to the low amount of needed fingertips) and stand the high temperatures necessary during reflow soldering. After having tried several samples provided by *Technimold Servizi*, it could be confirmed that polyphenylene sulphide (PPS) can sustain the required temperature without melting. The electrodes were produced by sputtering copper in high vacuum, but it proved difficult to deposit the material only in the electrode areas. Several attempts were performed by *Technimold Servizi*, including using a mask, but ultimately failed. Finally, the whole inner support was covered with the conductive material and the electrodes had to be separated manually, as in the first version of the fingertip. Moreover, the con-

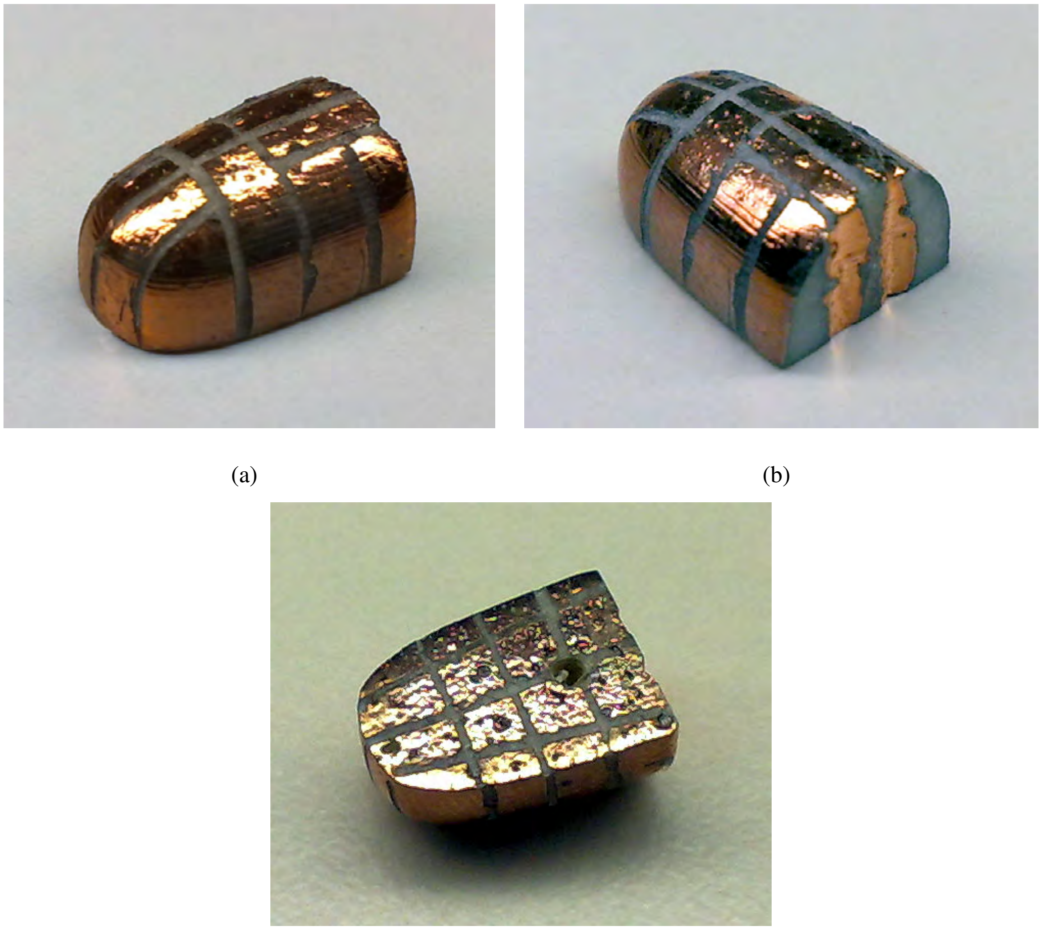

(a) (b)

(c)

Figure 4.16: **Inner support from *Technimold Servizi*.** In **(a)** from the front, in **(b)** from the back and in **(c)** from the bottom. The bottom part was designed to be soldered to the PCB.

ductive material could be deposited only as a very thin layer (0.003 *mm* thick). As a result, the production process was prone to errors: even in the final samples provided to us, only four out of eight inner supports worked as expected. In two, not all the electrodes were electronically connected to the bottom side of the inner support (the contact was discontinued at the edge); in one, two electrodes were connected to each other; in another one, a complete side was not covered with enough copper to be electrically conductive. Even in those samples for which all the electrodes worked as expected, the copper easily completely oxidized (especially if not handled with extreme care) and therefore lost its conductivity. Applying a protection above the electrodes proved to be not feasible. Most importantly, because the layer was so thin, it proved to be impossible to solder

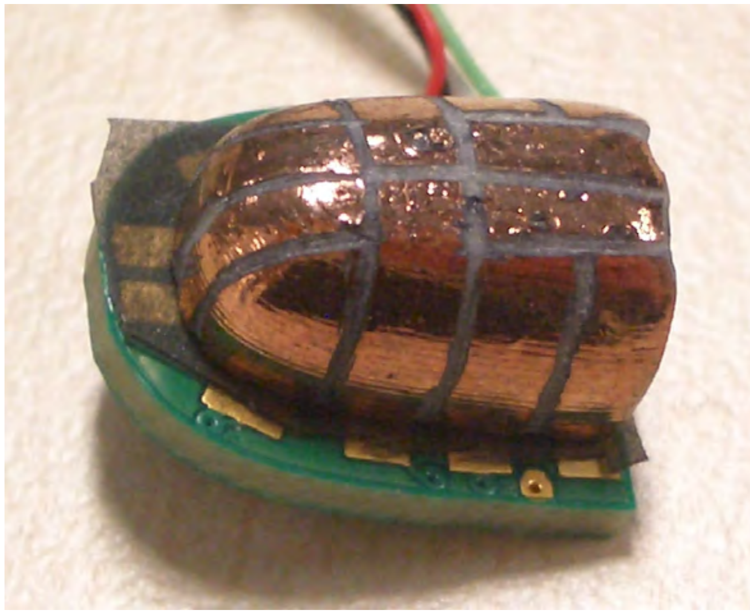

Figure 4.17: **An inner support form *Technimold Servizi* connected to the PCB with z-axis conductive foil.** One can clearly see the PCB with relatively big connection areas (gold) to the electrodes (copper). The z-axis conductive foil from Shin-Etsu, in this case *AF* type and not yet cut into shape, can be seen in black.

the inner support to the PCB. It was concluded that the conductive layer would have to be made thicker through electrolysis, but this process was made difficult by the spherical shape of the fingertip, which made it hard to electronically connect the fingertips. Finally, the efforts were concentrated on other solutions.

4.4.3 Improvements to Version 1: Z-Axis Electrically Conductive Foil

After concluding that soldering the inner support to the PCB was not a feasible approach, the electrodes were attempted to be electronically connected to the PCB with the help of an anisotropic electrically conductive foil. This foil is electrically conductive only in the z-axis; if conductors below and above it are pressed tightly against it, an electrical connection is established. Rather high forces are necessary for a good electrical connection. To establish a strong mechanical connection, a thread in the inner support enables to screw the PCB to the inner support. Because the inner supports provided by *Technimold Servizi* (see Figure 4.17) cannot be fabricated automatically and are not durable, the inner supports with the electrodes were again produced manually in-house (see Figure 4.18).

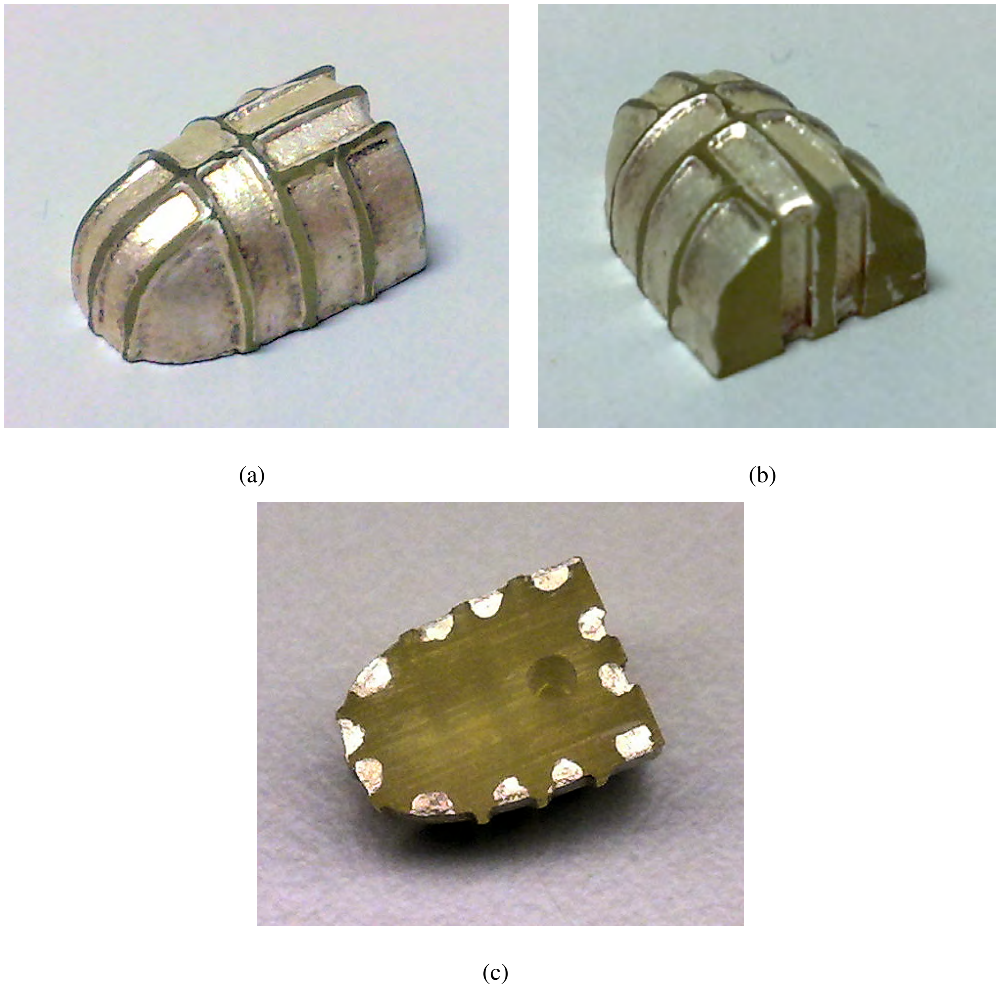

Figure 4.18: **Inner support with electrodes also on the bottom.** The electrodes are painted with silver conductive ink. The inner support is shown **(a)** from the top and **(b)** from the back. **(c)** The electrodes that extend to the bottom can be seen. Like this, they will face the pads on the PCB.

It is not feasible to cut the thread for the screw directly into the inner support. None of the materials the Eden 3D printer can provide, even with the support of *Loctite 243* threadlocker, is able to sustain the high forces necessary for establishing an electrical connection with the conductive foil. Therefore, *B-Lok* insert nuts from *Kerb Konus*, model 812 and 841 with an *M2* internal thread metric, were used to provide a stable thread. With superglue 431 from *Loctite* the insert nuts bonded strongly enough to the inner support. Even though the insert nuts provided a durable thread, finally another solution was preferred. Metal rods (see Figure 4.19) were inserted from the back into a hole in the inner support. Those rods have a threaded hole and can therefore be used to tighten the screw. In addition, they can also be used to attach the fingertip to the hand, if the rod is formed by

Figure 4.19: **Metal rod.** It includes a threaded hole to screw the inner support to the PCB.

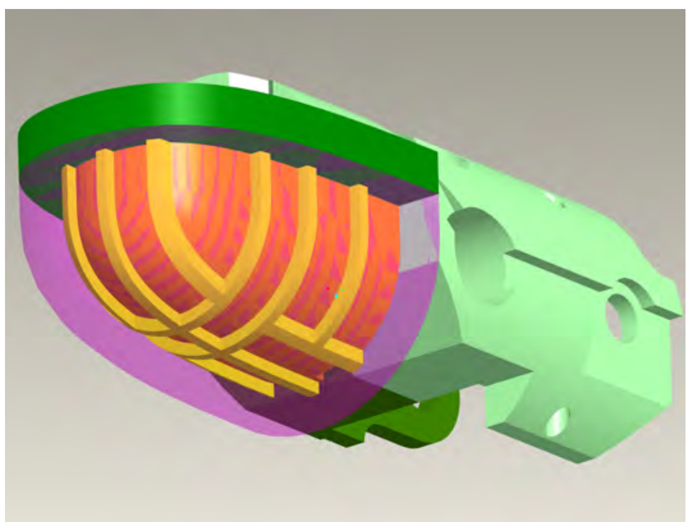

Figure 4.20: **Structure of the fingertip.** The inner core (yellow) with the electrodes (orange), the aluminium phalanx (light green), the PCB (dark green) and the cover silicone (purple) are visible.

a protrusion at the end of each finger. This solution was kept for the final version of the fingertip, as depicted in Figure 4.44 (originally the fingertip was planned to be installed by screwing it below a protrusion of the finger, as depicted in Figure 4.20 and Figure 4.21.).

Even with a good mechanical connection, steps were necessary to reduce the electrical resistance. Otherwise it could be observed that for each fingertip several of the connections to the PCB

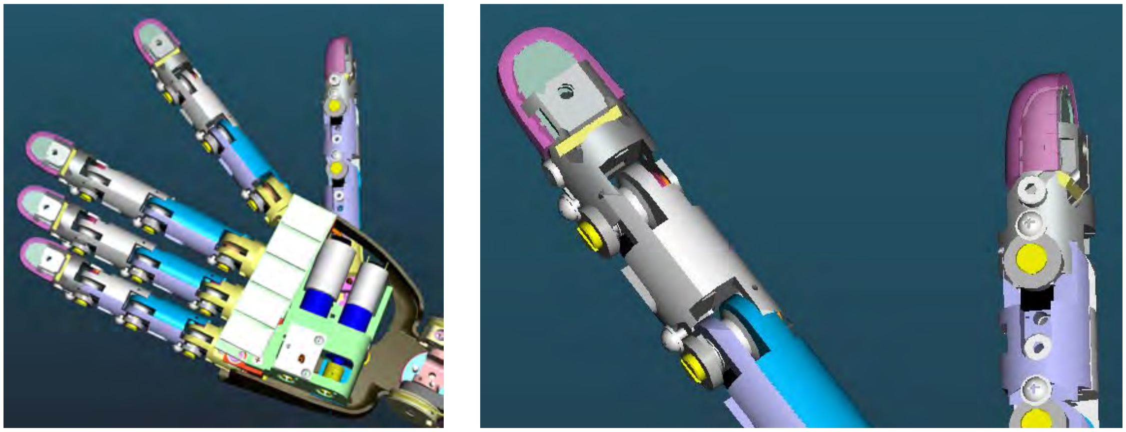

(a) (b)

Figure 4.21: **Original attachment of the fingertips to the hand.** Initially, the fingertips should have been installed under a metal protrusion of the fingers. **(a)** Image of the whole hand; **(b)** detail of the attachment structure.

had a very high resistance (more than 1 MΩ), especially for the front electrodes (probably due to the fact that the screw was not in the centre of the pads). Therefore, the centre part of the conductive foil was cut with a margin of about 2 *mm* so to focus the pressure on the places where electrical connections have to be established (see Figure 4.22). Other minor improvements were to tilt the hole for the metal rod 1°, as to push the front part of the inner support harder against the PCB, and to raise the areas of the inner support that would make contact with PCB, as to concentrate the pushing force in those areas. Still, even with all these improvements, it usually took several attempts for each fingertip to have good electrical connections to the PCB for all 12 electrodes. Initially, some of the 12 connections to the electrodes would have a too high resistance and the pads at the bottom of the inner support needed to be repainted to level them.

Several conductive foils were tested: 0.3 *mm* thick *AF* type, 0.2 *mm* thick *MAF* type, 0.5 *mm* thick *MAF type* and 1 *mm* thick *GB* matrix, all from *Shin-Etsu*. After having built several prototype fingertips with all those foils, it was concluded that the best results can be obtained with 0.2 *mm* thick *MAF* type. The 0.5 *mm* thick *MAF type* and 1 *mm* thick *GB* matrix made it more difficult to establish good connections with the PCB for the front electrodes: with the GB matrix it was visible with the naked eye that the inner support tilts upwards in the front when it got tightened to the PCB. For the 0.3 *mm* thick *AF* type, the best connections to the PCB had a resistance of about 10 Ω, while with 0.2 *mm* thick *MAF* type connections with a resistance of less than 1 Ω could be achieved.

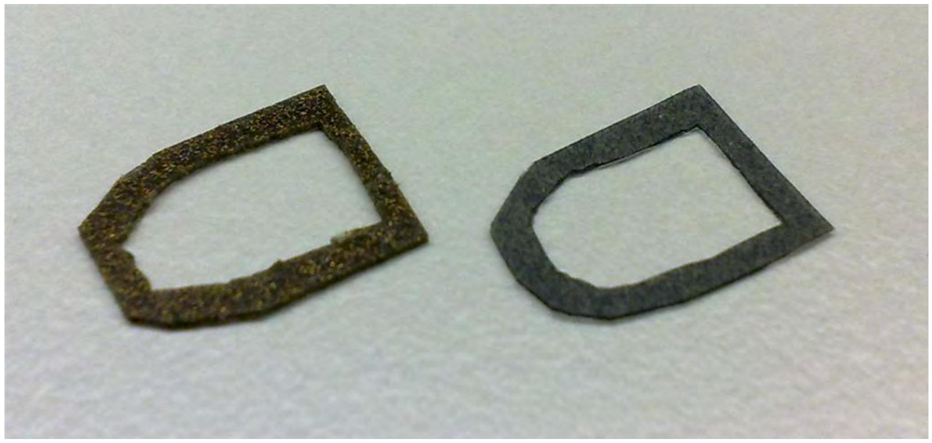

Figure 4.22: **Cut conductive foil.** The conductive foil (on the left 0.5 *mm* thick *MAF* type, on the right 0.3 *mm* thick *AF* type), was cut into a shape that allows to concentrate the pressure at the connection points between the inner support and the PCB.

Therefore, the production procedure is:

1. The 12 pads for the capacitive pressure sensor are painted with conductive ink on the inner support. Excessive paint between the electrodes is removed. Little pads on the bottom of the inner support will provide the connection to the PCB. The insert nut or the rod with a thread is inserted into the inner support.

2. 0.2 *mm* thick *AF* conductive foil is cut to fit the shape of the outline of the inner support. The centre part is cut out with a 2 *mm* margin, as depicted in Figure 4.22.

3. The inner support is screwed to the PCB, while paying attention to the alignment of the conductive foil. The result can be seen in Figure 4.23(a).

4. Adhesive is applied at the gap between the inner support and the PCB (which probably exists, as it is hard to align the conductive foil perfectly), because otherwise foam would enter in the space between the two, thereby pushing the inner support away from the PCB, resulting in a loss in electrical connectivity between the two.

5. Now the silicone foam layer can be moulded, as depicted in Figure 4.23(b). The procedure is the same as for the final version and described in detail in Section 4.4.5.5. The connector for the ground layer is manually cleared of silicone.

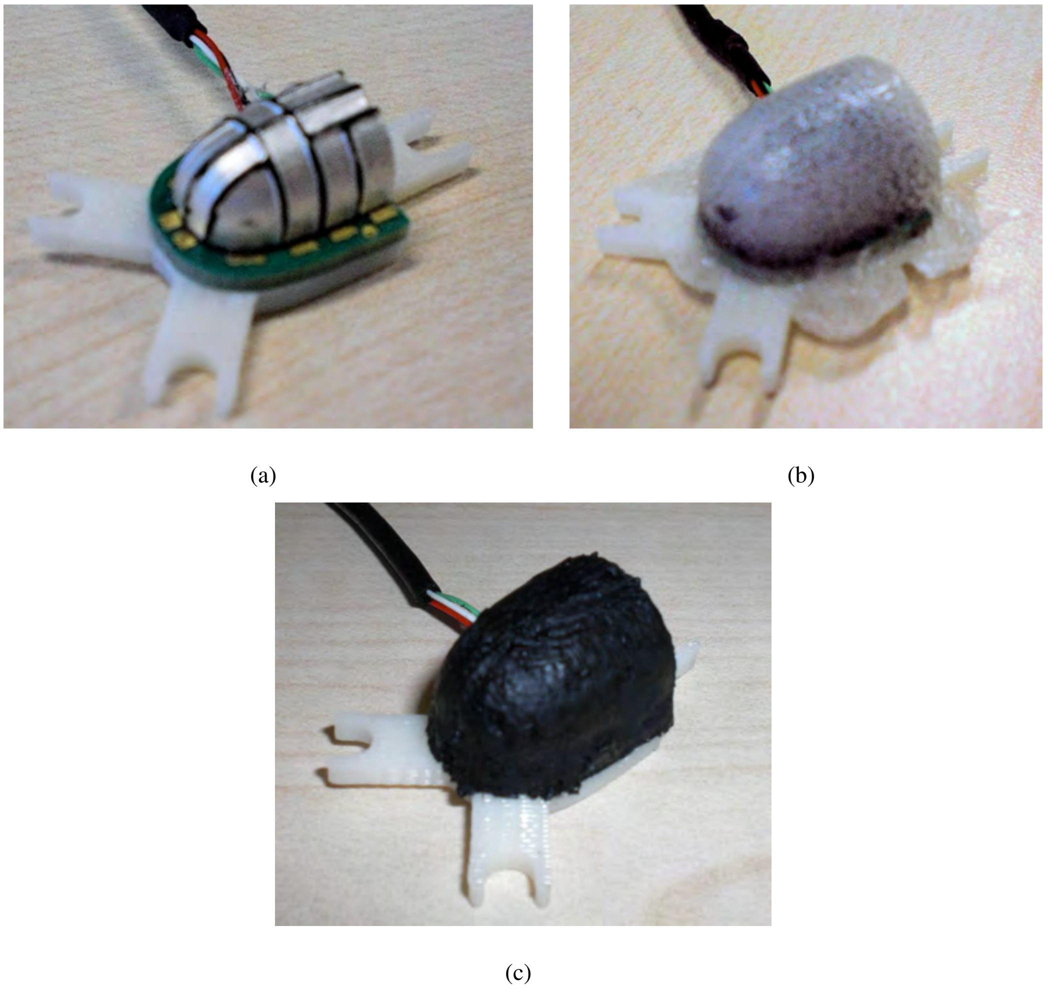

Figure 4.23: **Production process with conductive foil.** **(a)** The inner support has been screwed to the PCB, with the conductive foil sandwiched between the two of them. **(b)** The silicone foam has been moulded. **(c)** A conductive silicone layer has been deposited on top of the silicone foam.

6. The outer conductive layer can be applied, which is shown in Figure 4.23(c). Again, the procedure is the same as for the final version and described in detail in Section 4.4.5.7. A couple of finished fingertips can be seen in Figure 4.24.

Concluding Remarks on the Z-Axis Conductive Foil

Ten working fingertips were built with this approach. Yet the working process included a lot of manual labour. Moreover, within the course of a couple of months more and more of the electrical connections failed, and in 7 out of 10 fingertips some of the 12 taxels stopped working or delivered

(a)

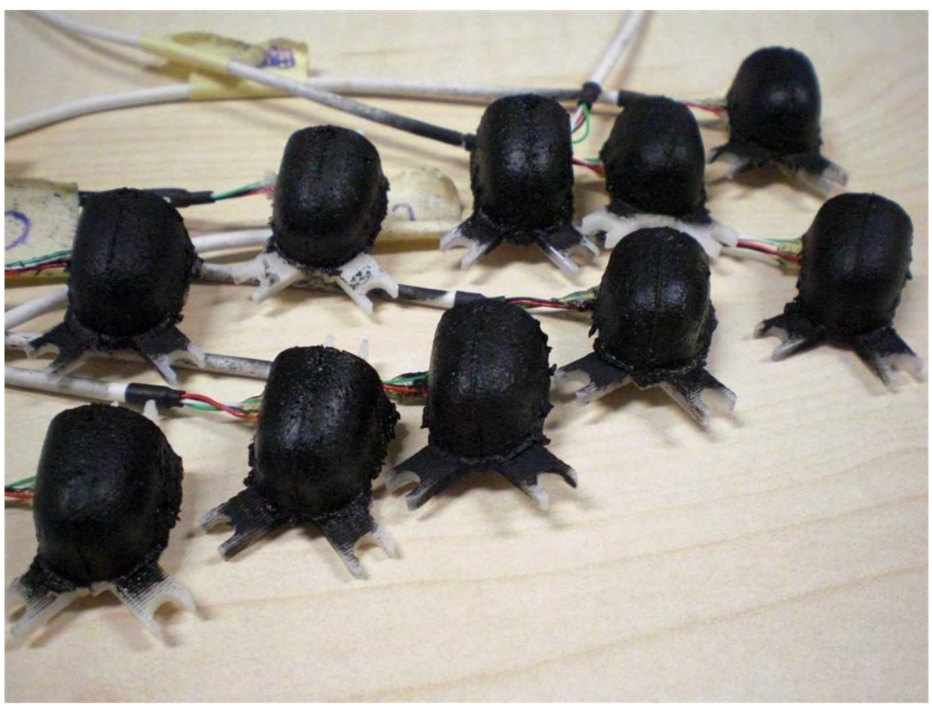

(b)

Figure 4.24: **Fingertips produced with the z-axis conductive foil. (a)** Several fingertips at different completion stages can be seen. **(b)** Ten finished fingertips. The version of the fingertip that uses the z-axis conductive foil was the first one to be produced beyond prototypes.

noisy measurements. Therefore, the design goals of finding a durable and fast way to produce the 12 electrodes and connect them to the PCB were not met. Possible improvements included moving the screw to centre of the electrodes, to provide a more even pressure for all electrodes, or even the use of anisotropic electrically conductive glue instead of foils (for example *Elecolit 3061* from *Panacol*, the working mechanism is explained in [144], page 230 - 232). Nevertheless, this approach became obsolete as the design with the flexible PCB, which is discussed in Chapter 4.4.5, showed good results.

4.4.4 Version 2: Soft Inner Support

The versions of the fingertips that were presented so far are already compliant due to the silicone foam layer. To increase the compliance even further, a fingertip was designed in which also the inner support is made from elastic material. Different silicones and latex were tested and finally *Ecoflex 00-30* silicone from *Smooth-On* was chosen because of its high elasticity, toughness and form stability (viscosity: 3000 cps, tear strength: 38 pli, elongation at break: 900%, tensile strength: 200 psi). Moreover, the 12 electrodes have to be elastic and are therefore made from conductive silicone, the same material that is used for the outer electrically conductive layer.

Like in the rigid version, covering only the electrode areas with conductive material proved to be difficult: applying the material with a syringe only in these areas was unfeasible, as they are rounded and too small. In analogy to the fingertips with a rigid inner support, the material was applied everywhere and subsequently manually cut away between the electrode areas (for a picture of the inner support at this stage please refer to Figure 4.25). In a first attempt, also the electrical connection to the PCB was achieved similar to the version of the fingertip described in Section 4.4.1: small wires were soldered to the 12 pads on the PCB; subsequently the wires are pressed against the corresponding electrodes on the inner support and are fixated with conductive silicone. As this process is work intense and not reliable, in an effort to facilitate the production, the inner core was first glued to the PCB and subsequently conductive silicone was sprayed on the whole structure. Afterwards, the conductive material between the pads on the PCB and the 12 electrodes was cut away.

The complete resulting production method is described in the following:

1. The inner support is made out of *Ecoflex 00-30* from *Smooth-On* with the help of a mould. After pouring the Ecoflex into the mould, trapped air is released by placing the mould into

Figure 4.25: **Soft inner support.** First the Ecoflex was moulded, then the conductive silicone with carbon black was sprayed upon it, and finally the electrodes were separated manually.

vacuum. Subsequently the part is cured in an oven. The shape of the inner support is depicted in Figure 4.26(a); it is raised between the electrode areas and also between the pads on the PCB.

2. The inner support is then glued to the PCB with *Sil-Poxy* silicone glue from *Smooth-On*. Before applying the glue, it is diluted with toluene or THF to decrease its viscosity. This is important to guarantee the inner support is placed completely flat on the PCB; otherwise parts of the PCB will be exposed in the next work steps. One also has to make sure not to cover the pads for the 12 electrodes on the PCB with silicone glue. For this purpose, a piece was designed that upholds the inner support while the glue is applied and the PCB is placed, which is also produced with the 3D printer, and it is depicted in Figure 4.26(b).

3. Conductive silicone is sprayed on the inner support and the exposed parts of the PCB (only the connection pads for 12 electrodes are not covered).

4. After the conductive silicone is fully cured the raised areas between the electrode areas and

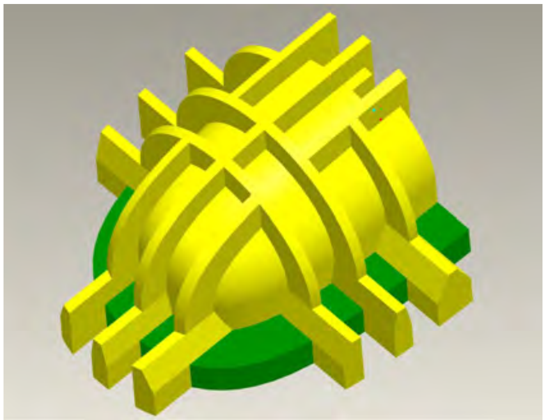

(a)

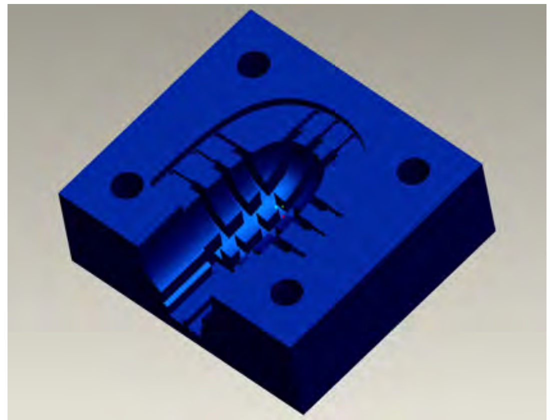

(b)

Figure 4.26: **The production of the fingertip with a compliant inner support.** **(a)** In this drawing the inner support is shown in yellow. It is raised between the electrode areas and also between the pads on the PCB (shown in green), so that they can be easily separated after the carbon black has been sprayed. **(b)** This part is used to uphold the inner support while the PCB is glued to it. It is shaped very similarly than a part of the mould for the compliant inner support.

the pads on the PCB are cut away, resulting in 12 elastic electrodes that are connected to the PCB.

5. Now the silicone foam layer can be moulded. The procedure is the same as for the versions with a rigid inner support and described in detail in Section 4.4.5.5. A slight difference is that PCB needs be glued to the upper mould. Moreover, if conductive silicone from the inner electrodes is exposed on the side of the PCB, it has to be manually covered with silicone. The connector for the ground layer is manually cleared of silicone.

6. The outer conductive layer can be applied. Again, the procedure is the same as for the versions with a rigid inner support and described in detail in Section 4.4.5.7.

Concluding Remarks on the Fingertips with a Soft Inner Support

Two fingertips were produced in this way, which were very soft. The production of the fingertips was work intensive and the fingertips were also not reliable: in the two fingertips produced with this method, not all the 12 sensors were working and even the working ones broke after some time. A possible explanation is the low conductivity of the conductive silicone. Due to this problem, this approach was not further investigated. Nevertheless, as it would be interesting to test whether increasing the compliance in this way is indeed beneficial for grasping, and how this additional compliance influences the sensor characteristics, it is intended to further pursue this research direction in the future.

4.4.5 Final Version: Flexible PCB

The final version of the fingertip is based on a flexible PCB. In comparison to the rigid PCBs used in former versions, the flexible PCB also includes 12 pads that act as electrodes for the capacitive pressure sensor. Therefore, there is no more need to connect these electrodes in an extra working step to the PCB. The flexible PCB is wrapped around an inner support (see Fig. 4.27). In addition, unlike in the previous versions, the 12 electrodes are circular.

The resulting structure of the fingertip is illustrated schematically in Figure 4.28(b). In brief, the fingertip is built up as follows: the flexible PCB surrounds the inner support. The flexible PCB is covered by a layer of soft silicone foam. A drawback of the final version of the fingertip is that the silicone foam layer does not have a uniform 2 *mm* thickness as before because the inner support only approximates the shape of the fingertip; yet, the variations in thickness are small. On top of the silicone foam is a thin layer of conductive silicone rubber, which is connected to ground. Another addition to previous versions is that a thin layer of silicone glue (Sil-Poxy from *Smooth-On*) is sprayed above the conductive silicone layer to protect the conductive layer (not visible in Figure 4.28, as this layer is thin and transparent).

Production Process of the Fingertips

In this section the production process of the fingertip is described step by step.

1. *3D printing of the parts:* an inner support and a fingernail have to be produced for each fingertip with a 3D printer (Eden 3D printer from *Objet*). Also the mould used for the silicone foam is fabricated with the 3D printer. The mould is split into three pieces which makes it easier to remove the fingertip from the mould after the moulding process. All the parts are depicted in Figure 4.29.

2. *Soldering the components on the PCB:* The AD7147 chip, the 10nF, the 100nF capacitor and the wires (AWG38, 25cm long) have to be soldered on the flexible PCB, as shown in Figure

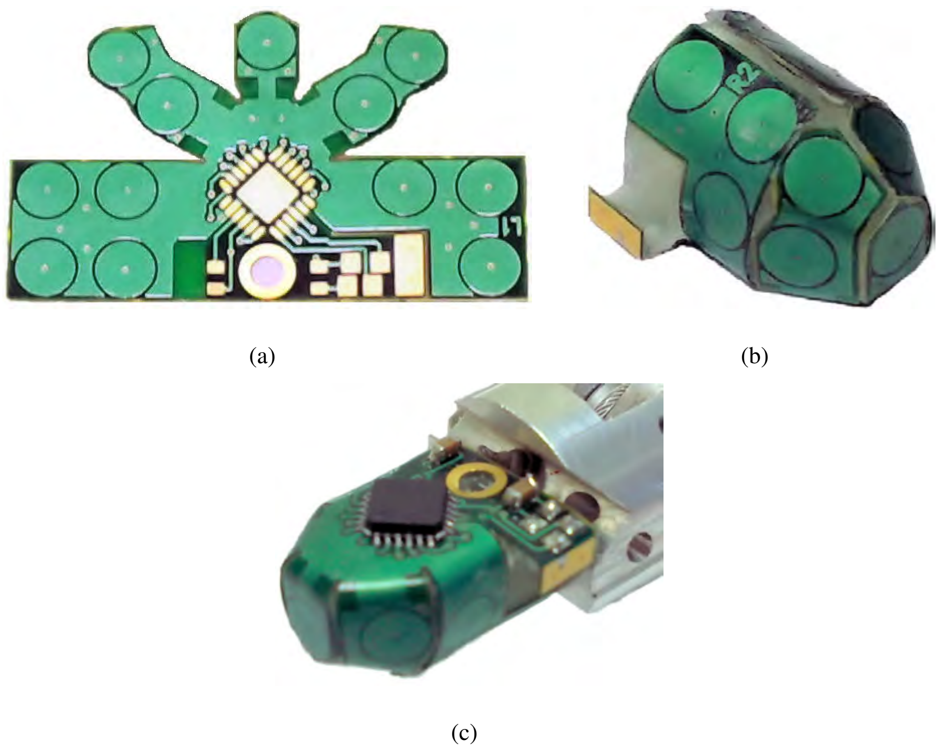

Figure 4.27: **The flexible PCB. (a)** The 12 pads for the capacitive pressure sensor system and the soldering points for the CDC chip, for the 2 capacitors and for the connector cables for the digital output are visible. **(b)** The flexible PCB is wrapped around the inner support. The inner support is produced with a 3D printer. **(c)** The flexible PCB is wrapped around the inner support and mounted on the last phalange of the finger. The AD7147 chip and the capacitors are soldered on the PCB.

4.30. Afterwards, a small amount of *Patafix* adhesive from *UHU* is put on the soldering of the wires, to protect the wires from breaking off in the following steps, see Figure 4.31.

Eight slightly different designs for the PCB have been designed: the CDC chip can be assigned with 4 different addresses for the serial bus, and the corresponding connections are hardwired in 4 different versions of the PCB. The hardwired solution has been adopted due to space limitations. Moreover, the fingers of the left hand of iCub are a mirrored copy of the right hand, with the wire duct either on the left or the right side of the finger, respectively. Therefore, also the PCB had to be produced with the connections for the wires either on the right or on the left side.

3. *Testing procedure:* a simple Matlab/Simulink model was programmed to test whether all electrodes are properly working. The test setup consists of the computer that runs this model,

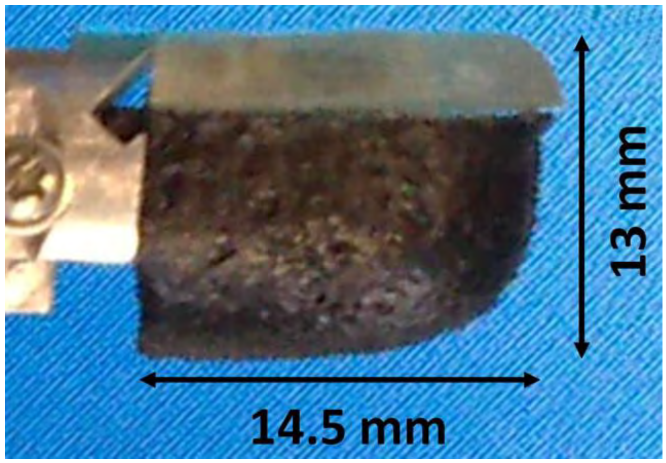

(a)

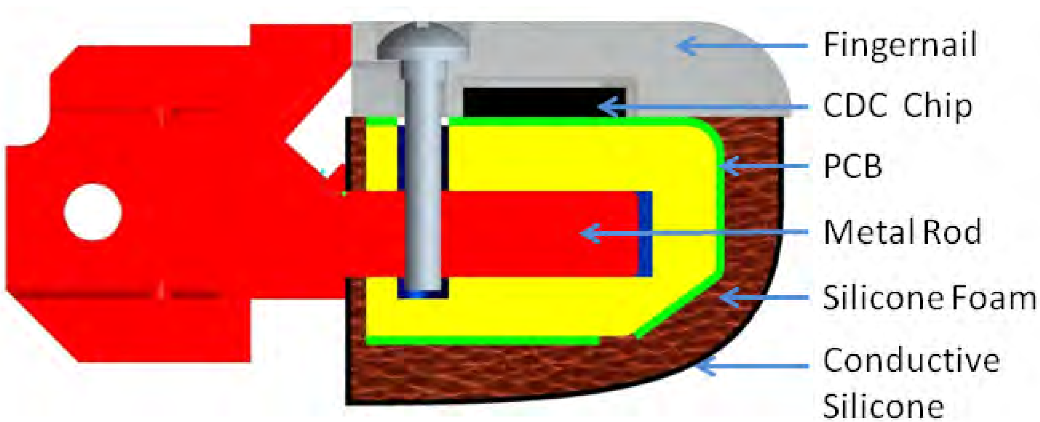

(b)

Figure 4.28: **Final fingertip. (a)** A close-up picture of the fingertip. **(b)** Longitudinal section of the fingertip. The inner support of the fingertip is shown in yellow, and the flexible PCB that is wrapped around it is depicted in green (see also Fig. 4.27). To mechanically attach the fingertip to the hand, the last phalange of each digit (shown in red) has a protrusion that fits inside a hole in the inner support. A screw is used to secure the fingertip and in addition the screw fixes a fingernail on top of the fingertip that covers the PCB. The dielectric made of silicone rubber foam is depicted in brown, and around the foam there is the carbon black layer. The AD7147 chip is also shown in black.

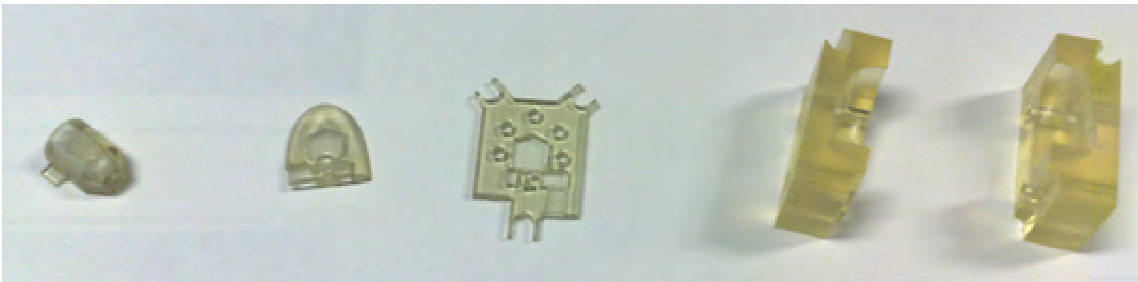

Figure 4.29: **Parts printed with the 3D printer.** From left to right: inner support, fingernail, upper mould, left mould, right mould.

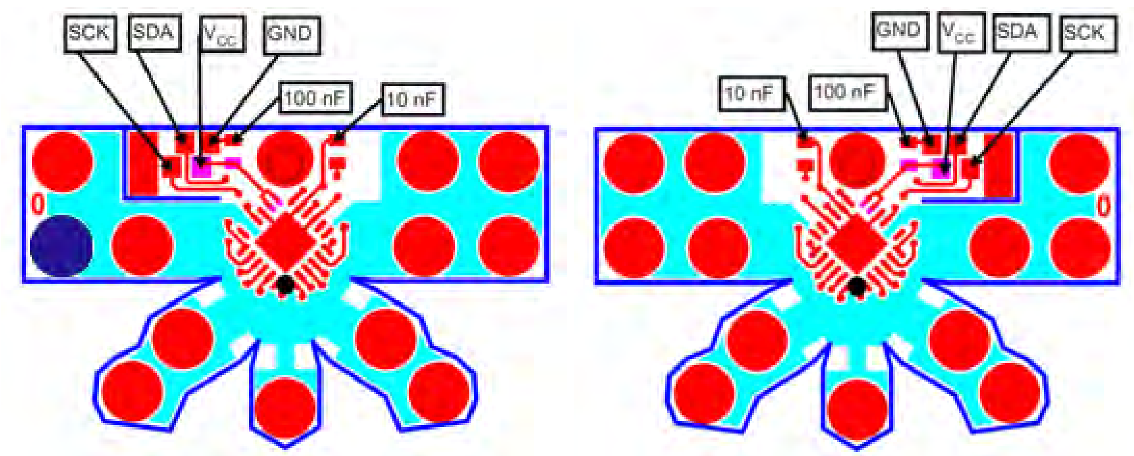

(a) Left

(b) Right

Figure 4.30: **Schemas of the flexible PCBs.** They show where the components and wires are soldered. The PCB for the left hand is depicted on the left (a), the one for the right hand on the right (b). The small number (in this case a "0") designates the address for the serial bus. The blue electrode corresponds to the taxel which was used for most of the experiments.

a power supply which provides 5V, a microcontroller board, a CAN2USB converter from *esd electronics* and a mechanism to connect the wires of the fingertip to the microcontroller board (see Figure 4.32(a)). After the fingertips have been connected, the Simulink model can be started. The fingertips can have four different addresses and for each one of those there is one scope (see Figure 4.32(b)). Each of the 12 round pads on the flexible PCB has to be touched with a metallic object; for each of the 12 pads there is one output in the relevant scope, which will respond strongly when touching the corresponding pad. If all 12 pads elicit a response, the fingertip has been successfully tested; otherwise, the soldering contacts on the PCB have

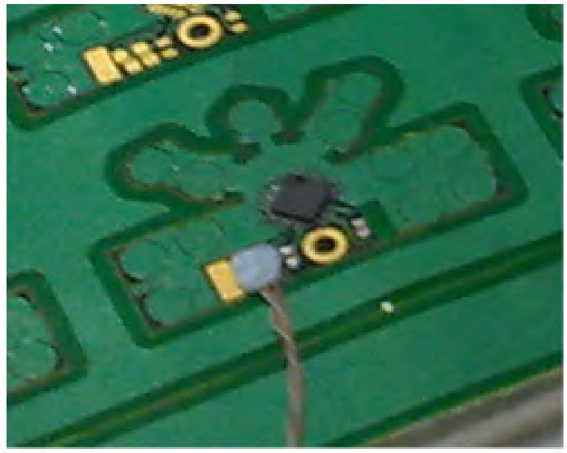

Figure 4.31: **Patafix.** The components have been mounted and a small amount of *Patafix* protects the wires from breaking off in the subsequent productions steps.

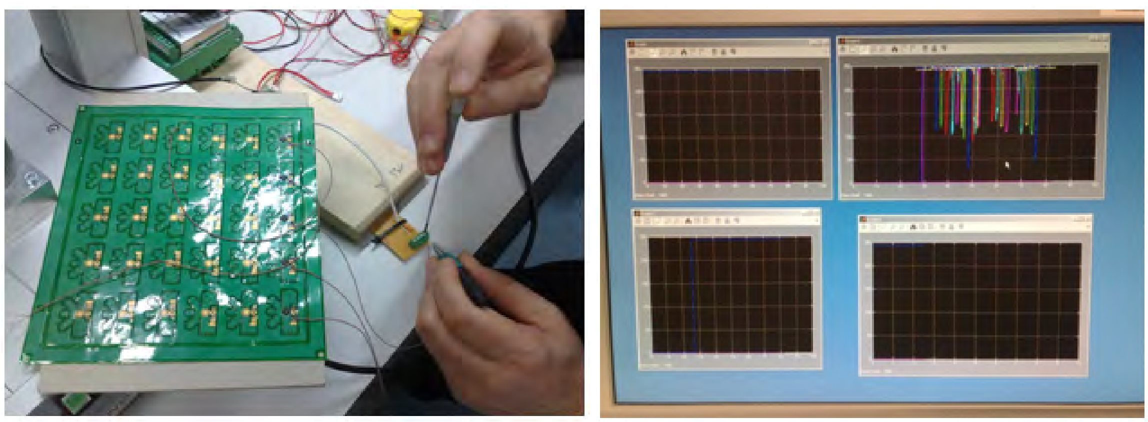

(a) (b)

Figure 4.32: **Testing. (a)** The mechanism to connect the wires of the fingertip to the microcontroller board. **(b)** Each of the four scopes is for one of the addresses that fingertip can have.

to be checked.

4. *Gluing the PCB on the inner support:* The PCB is wrapped around and glued to the PCB manually. The process is depicted in Figure 4.33: first the PCB is cut out of the panel, then the PCB is aligned with the inner support, and finally all the flaps of the PCB are glued to the inner support. The part of the PCB that will be connected to the ground layer has to be bent in a 90deg angle and fixated with superglue (see Figure 4.34).

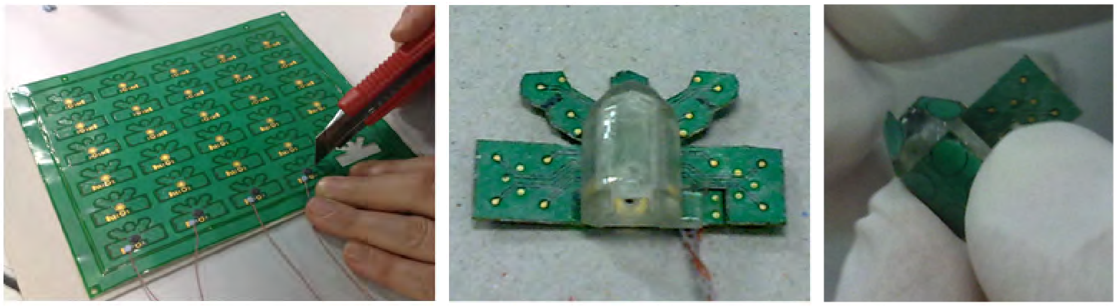

(a) (b) (c)

Figure 4.33: **Cutting and gluing of the PCB: (a)** cutting the PCB out of the panel, **(b)** gluing the PCB to the side of the inner support with the round hole and **(c)** gluing the other sides of the PCB to the inner support.

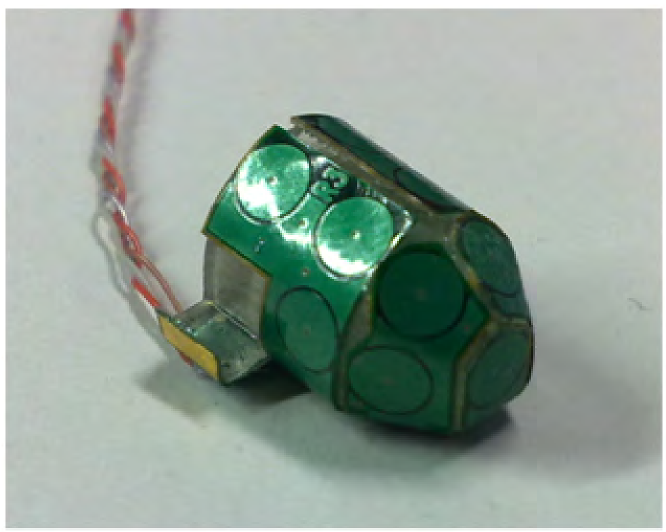

Figure 4.34: **Contact to outer electrode layer.** The contact to the outer electrode layer, visible in gold, has to bend $90deg$.

5. *Moulding the silicone foam layer:* before making the foam layer, several preparations are necessary. To prepare the fingertip, a metal rod (see Figure 4.35(a)) is put inside the inner support and the upper mould is screwed to the fingertip, as depicted in Figure 4.35(b). To ensure a better adhesion of the silicone foam to the fingertip, it is cleaned with isopropyl alcohol. Also the mould is cleaned and the left and right part of the outer mould are screwed together, see Figure 4.35(c). Subsequently, EasyRelease 200 from *Smooth-On* is sprayed into the inside of the mould. The EasyRelease 200 makes it easier to remove the fingertip later

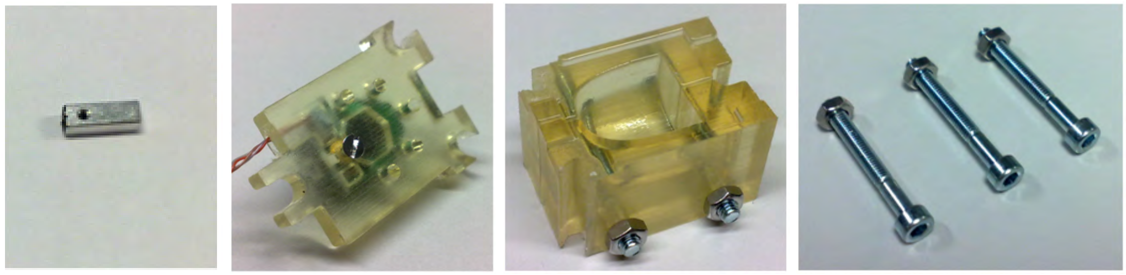

(a) (b) (c) (d)

Figure 4.35: **Preparations to mould the silicone foam layer.** **(a)** A picture of the metal rod that has to be inserted into the inner support. **(b)** The upper mould is screwed to the inner support. **(c)** The left and the right part of the mould have been screwed together. **(d)** These screws will be used to fixate the upper mould.

(a) (b)

Figure 4.36: **Preparation of the silicone foam.** **(a)** The two components of the silicone foam are shaken. **(b)** 2:1 parts (in weight) of silicone foam are put into a container and **(c)** mixed.

from the mould. It could be observed that *Soma Foama 15* that has spent extended time in the shelf before the moulding process will be less adhesive: in this case, Sil-Poxy silicone glue from *Smooth-On* was applied all over the fingertip, to ensure a better adhesion of the foam to the PCB.

Subsequently, 1.2 gram of Soma Foama part A and 0.6 gram of Soma Foama part B are dispensed into a container, see Figure 4.36(a). Soma Foama has a working time of only 50

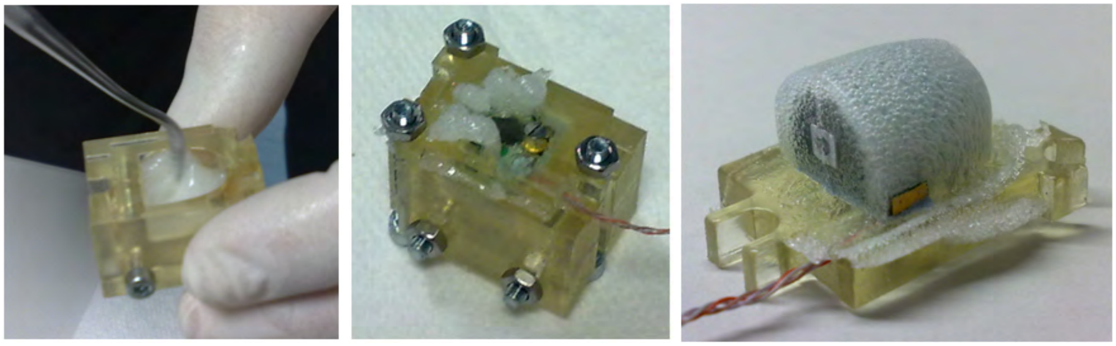

(a) (b) (c)

Figure 4.37: **Moulding the silicone foam layer. (a)** The Soma Foama is put into the mould. **(b)** The fingertip, attached to the upper mould, is tightened with screws. (c) This is the result after the moulding process.

seconds, depending on its age[9]. Therefore, the following part of the procedure is very time critical. The two parts are mixed manually for 20 seconds, see Figure 4.36(b). Even though the working time is short, one has to make sure that also the silicone on the bottom and the side of the container are well mixed. Immediately afterwards, the mixture is poured into the outer mould and the mixture is spread inside the mould, see Figure 4.37(a). One has to put enough Soma Foama into the mould so that when the fingertip is put into the mould, already a bit of Soma Foama gets pushed out: like this the density of the silicone foam for each fingertip can be made relatively similar one to another. Screws are used to fixate the fingertip in the correct position, which is demonstrated in Figure 4.37(b).

After some minutes the fingertip is removed from the mould, see Figure 4.37(c). It might be necessary to loosen the screws that hold together the left and right part of the mould. The easy release is wiped off from the fingertip and the foam on the part of the PCB that will be connected to the outer electrode layer has to be removed. The other excessive silicone and the upper mould are kept attached to the fingertip. They will cover and protect the PCB in the subsequent steps.

6. *Preparation of the carbon black composite:* 1 gram of carbon black (CB) is put into a container. 45 grams of THF are added and the mixture is stirred for a minute by hand.

[9]Old Foam cures faster and new foam slower. New foam expends also expands more than old foam and produces therefore softer and more sensitive fingertips.

(a) (b)

Figure 4.38: **Sonicator. (a)** The sonicator that is used to disperse the carbon black in the tetrahydrofuran. **(b)** The amplitude of the sonicator is set to 30 and the timer to 1 hour.

Subsequently, the CB is further dispersed with the help of a sonicator (Sonicator 4000 from QSONIX, see Figure 4.38) with an amplitude of 30 for 1 hour. Afterwards, about five grams of THF should have evaporated. After the mixture has been stirred quickly by hand, the homogeneity is checked by holding the mixture against a strong light source (see Figure 4.39). If the CB is not dispersed homogenous in the THF, half of the THF that has evaporated is added to the mixture and it is sonicated for another 30 minutes. The process is repeated until the mixture is homogenous. As a final product, one should have a mixture of around 1:40 of CB to THF, which will be called from now on “dispersed CB”.

In the next step, one has to find the right ratio of *CAF 4* to dispersed CB. Usually the right ratio is 1:7, but it varies slightly. To check it, 0.1 g of *CAF 4* is dissolved with sufficient THF; as a result, all the *CAF 4* has to be liquid (see Figure 4.40(a)). 0.7 g of the dispersed CB is added, and the mixture is stirred by hand for a minute (see Figure 4.40(b)). A bit of the mixture is put manually on a thin (about 1 mm) layer of *Ecoflex 00-30* from *Smooth-On*(see Figure 4.41(a)). Afterwards it has to dry; one should have put enough mixture on the Ecoflex so that when it is held now against a light source, no light should shine through. The resistance is measured (see Figure 4.41(b)): it should be around 10 $k\Omega$. If it is substantially higher (20 $k\Omega$ or more),

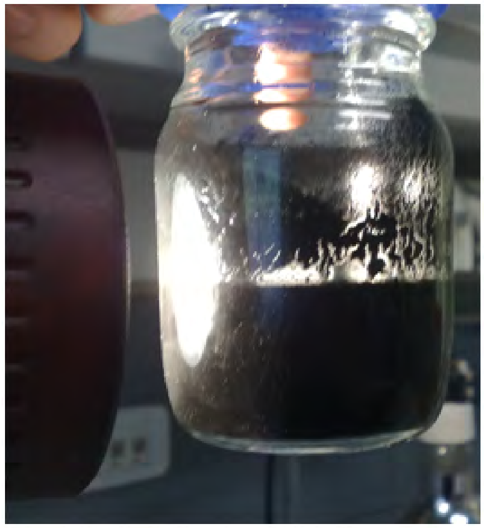

Figure 4.39: **Controlling the dispersion of the carbon black.** The homogeneity is checked by holding the mixture against a light source.

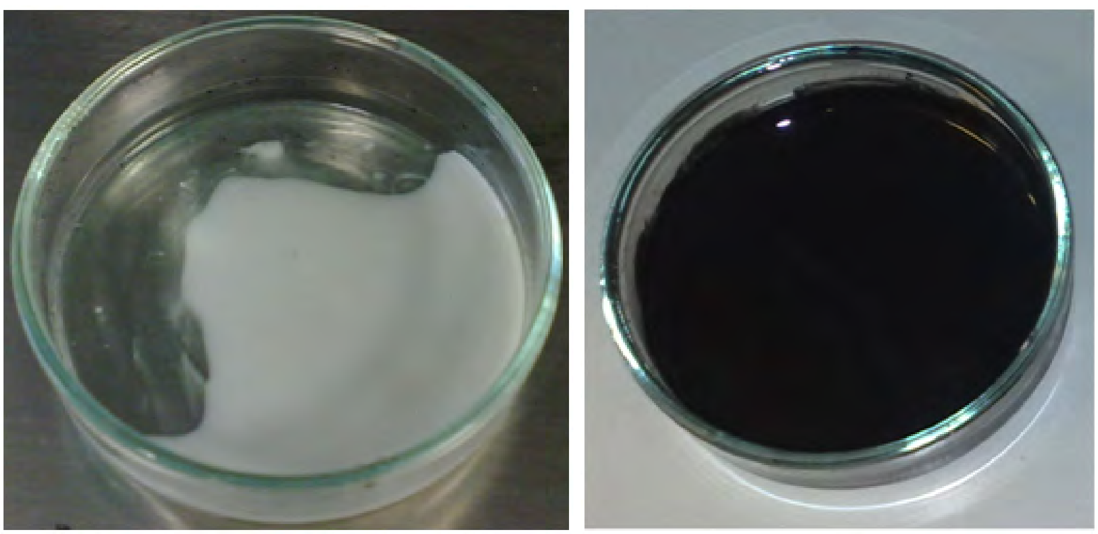

(a) (b)

Figure 4.40: **Preparations for the conductivity test of the conductive silicone. (a)** *CAF 4* has been solved in THF. **(b)** This picture shows how the mixture of *CAF 4*, CB and THF should look like.

the process has to be repeated with a ratio of 1:8. As a second test, the Ecoflex has to be held again against a light source and stretched: no cracks should appear (see Figure 4.42). If cracks appear, the ratio has to be reduced to 1:6. If the results are not satisfying even after the

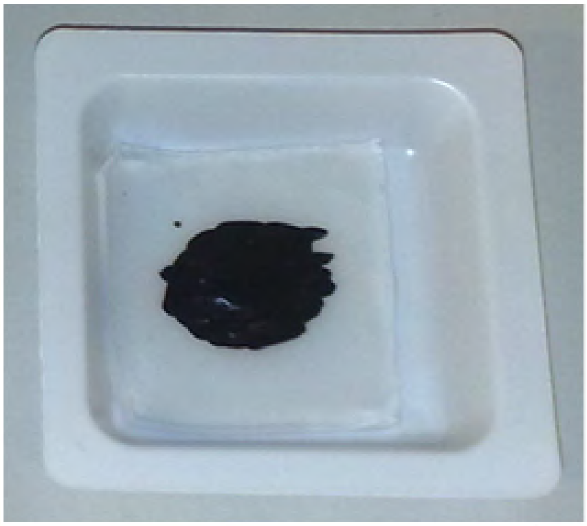

(a)

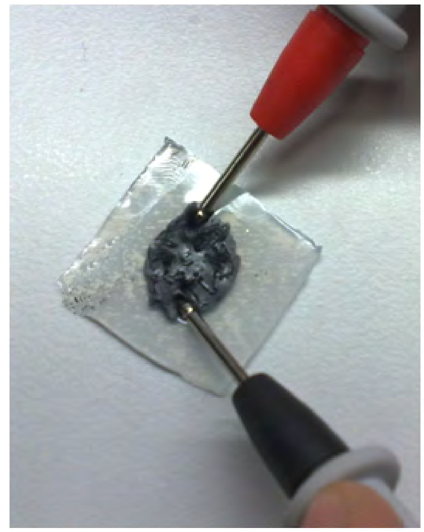

(b)

Figure 4.41: **Testing the conductivity.** **(a)** Some conductive silicone on *Ecoflex 00-30* is shown. **(b)** The testing of the conductivity of the conductive silicone is shown.

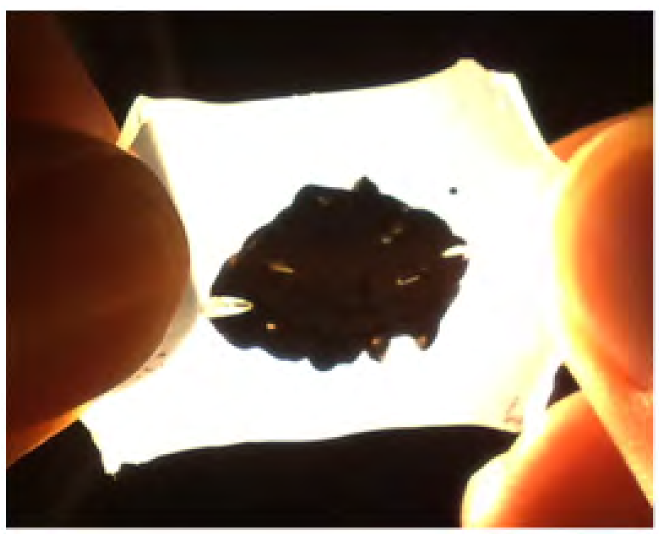

Figure 4.42: **Testing the elasticity.** The conductive silicone is held against a light source to see whether it is elastic. The light may shine through in some places because the conductivity was tested before, and because the silicone was not fully cured yet, it was thereby removed in some places. Yet, when the silicone is stretched, no additional cracks should appear.

changes, the carbon black is probably not well dispersed in the tetrahydrofuran.

After having found the right ratio, the final mixture is prepared. For five fingertips, about

3g of *CAF 4* are needed. A mixture with the corresponding amount of dispersed CB (as just determined) has to be prepared.

7. Spraying the CB composite: The fingertips (still attached to the upper mould) are now covered with the mixture that just has been prepared. The mixture is sprayed with the help of an airbrush under a fume hood. Good results can be obtained by spraying with short bursts and using a pressure of 3 *bar*. While spraying, the fingertips should have a distance of at least 20 cm to the airbrush, as demonstrated in Figure 4.43. Some remaining mixture should be used to make sure that a good contact with the PCB is established, as the conductive silicone tends to attach worse to it than to the silicone foam (the pad from the PCB should not be visible anymore). Subsequently, one has to wait for at least 24 hours for the conductive silicone to cure.

8. Spraying the Protective Layer: *Sil-Poxy* is dissolved in THF. The ratio is 1g *Sil-Poxy* for 6g THF. The fingertips are dipped quickly (less than a second) into the solution. Subsequently, they dry for one hour, the support facing down. The fingertips are shiny afterwards.

9. *Finalize the fingertips:* Now the metal rod can be removed with the help of a screw that can be screwed into the back side of the metal rod. Afterwards, the support and the excess foam are removed. In a final test, one has to check whether all the 12 sensor measurements are acquired and whether the fingertip responds also to plastic objects. Otherwise, there is a problem in the outer electrode layer and it has to be redone. The test of the fingertip is equal to the one described in point 3 apart from the fact that the probe must be made of non conductive material. Finally, the fingertips can be mounted on the hand of iCub.

4.5 Installation on iCub

To robustly attach the final version of the fingertip to the hand, the last phalange of each digit has a protruding rod that fits precisely inside a hole in the inner support of the fingertip, see Figure 4.28(b) and Figure 4.44. A screw is used to hold the fingertip in place. The screw also fixes a fingernail on top of the fingertip that covers the top side of the PCB. As discussed before, the PCB in each fingertip provides an I^2C serial interface. Therefore, only 4 wires have to be connected to the PCB,

Figure 4.43: **Spraying the conductive silicone.** There should be at least a distance of 20 *cm* from the airbrush to the fingertip.

which travel along the side of the fingers, as depicted in Figure 4.45. The fingertips mounted on the hand can be seen in Figure 4.46.

4.6 Conclusion

The implementation of the fingertip architecture was presented. Several production methods for the fingertip have been presented, which did not fulfil the expectations regarding ease of production and reliability. These issues were addressed in the final version of the fingertip, which is easier to produce and more durable. In the final version, the basis of the sensor is a flexible PCB, which includes 12 electrodes and a capacitance to digital converter. *Soma Foama 15* is used for the dielectric layer, and a self made mixture of carbon-black and silicone for the conductive layer.

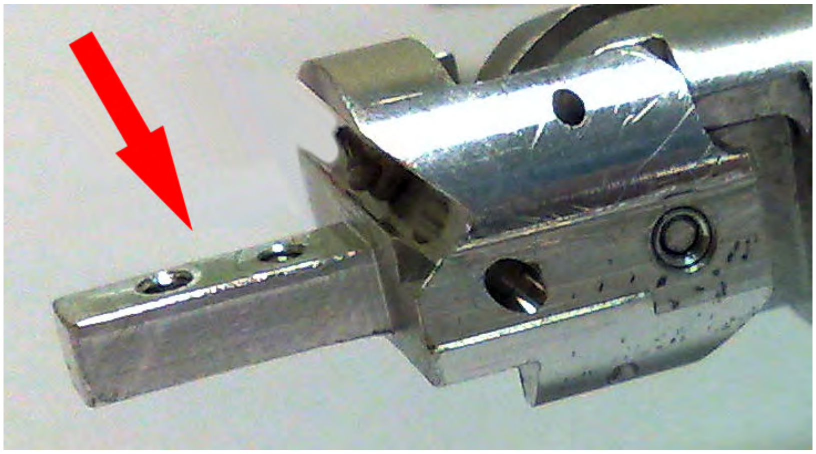

Figure 4.44: **Metal rod to fixate the fingertips.** The distal phalange of each finger has a metal rod that fits inside the sensorized fingertip.

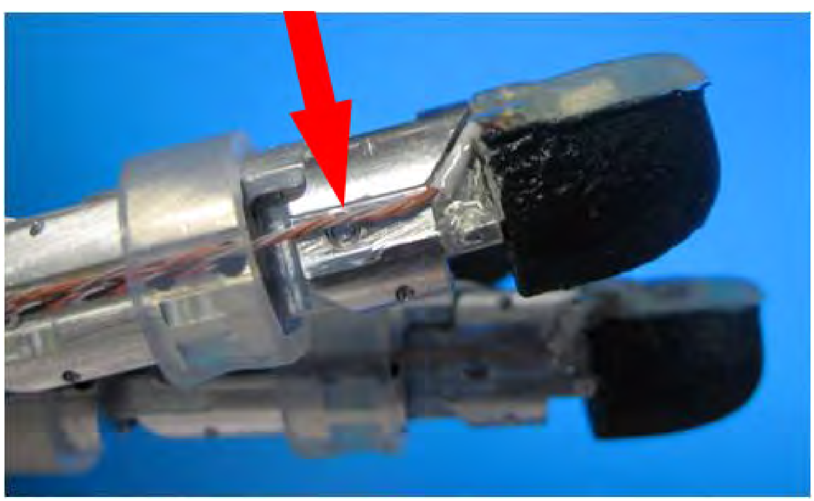

Figure 4.45: **Wiring of the fingertips.** As the digitization is performed in the fingertip, each fingertip is connected with only 4 wires.

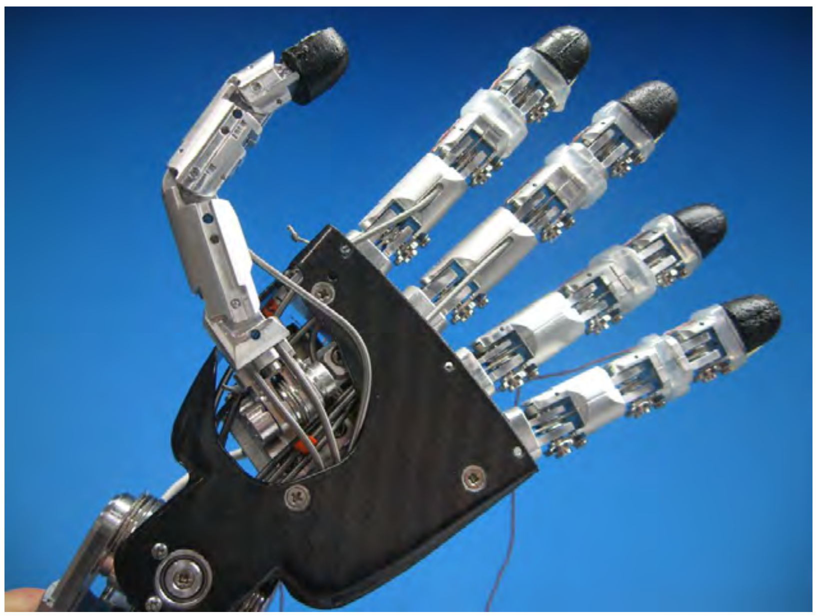

Figure 4.46: **The iCub hand with fingertips.** The fingertips mounted on the iCub hand can be seen.

Chapter 5

TESTING

This chapter presents tests that have been performed to determine the characteristics of the sensor. An overview of the outline of the chapter is shown in Figure 5.1. Using a specifically designed test setup, presented in Section 5.1.1, the following factors were examined, for both the palm and the fingertips: spatial sensitivity, dependence on the contact area, baseline drift, difference between different sensors, linearity, noise, stability, minimum detectable pressure and hysteresis. The experiments with the fingertips are described in Section 5.1.2 and the tests with the palm can be found in Section 5.1.3. The results are discussed in Section 5.1.4.

Furthermore, first experiments with the sensors installed on the robot's hand are presented in Section 5.2. Using predefined grasps, it could be shown that the sensor measurements are repeatable and can be used to detect touch (see Section 5.2.1). Moreover, the results show that the sensors can indeed help the robot in a real world scenario to grasp objects gently, as discussed in Section 5.2.2. The conclusions from all experiments are drawn in Section 5.3.

5.1 Tests with the Cartesian Robot

In this section, we evaluate several properties of the fingertip and palm, using a specifically designed experimental setup. An overview of the different characteristics that were evaluated can be seen as part of Figure 5.1.

5.1.1 Test Setup

To test the capacitive pressure sensor, a Cartesian robot (TT-C3-2020 from *IAI*) is used. The robot has a positioning repeatability of $\pm$ 0.02 mm, a maximal speed of 300 mm/s, a maximal portable weight of 2 kg and a work area of 200$\times$200$\times$100 mm. When controlled offline, the robot can reach 10 Hz for a 2 mm z-movement. The robot moves an off-centre load cell (0.5 kg AS series, from *Laumas*). At the end of the loadcell cylindrical probes of varying diameter can be attached to

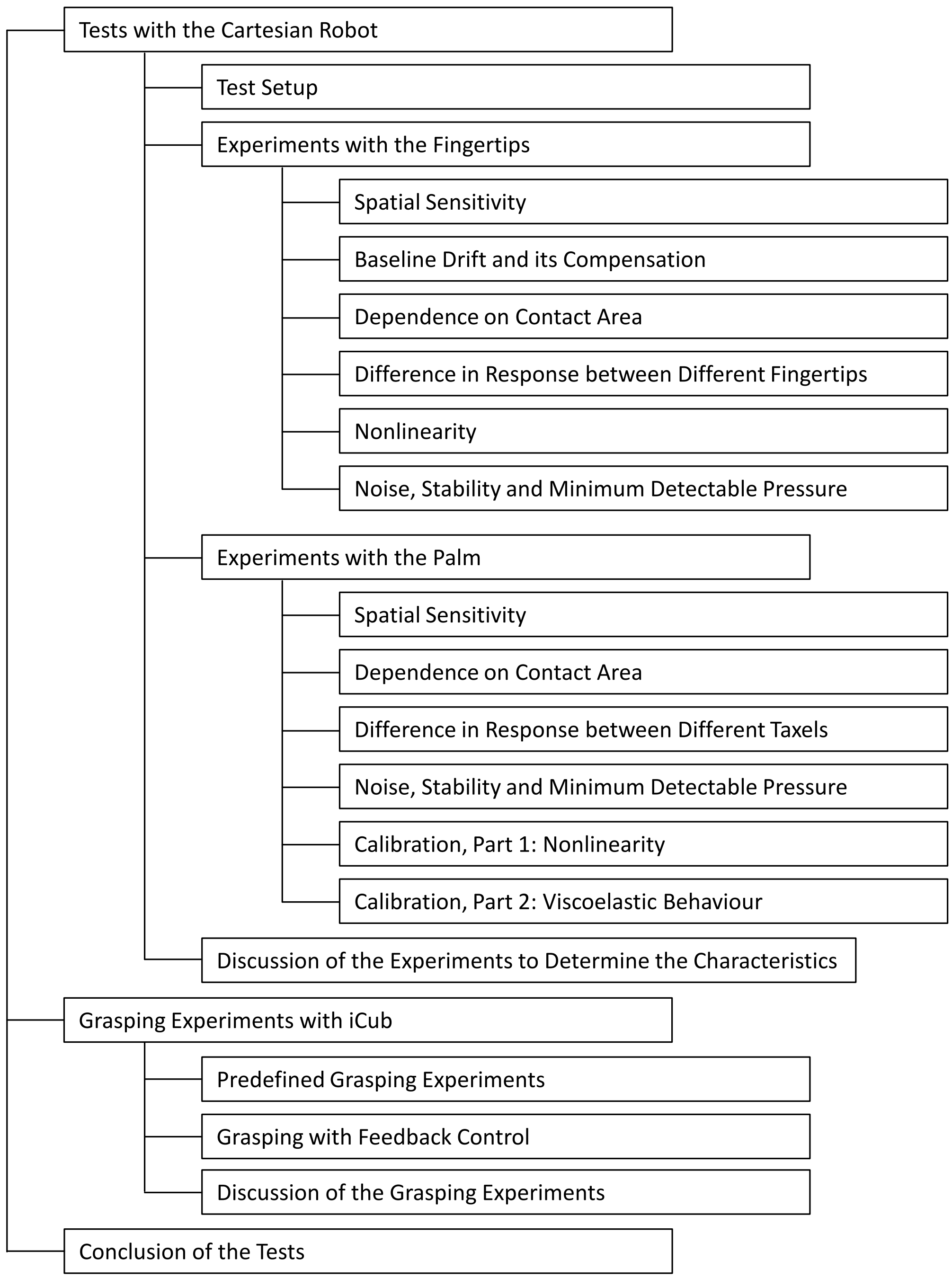

Figure 5.1: **Outline of Chapter 5.**

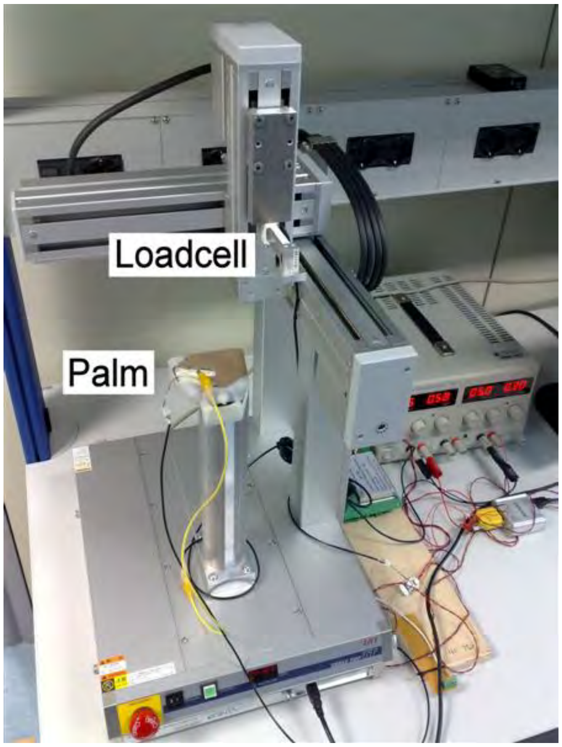

(a)

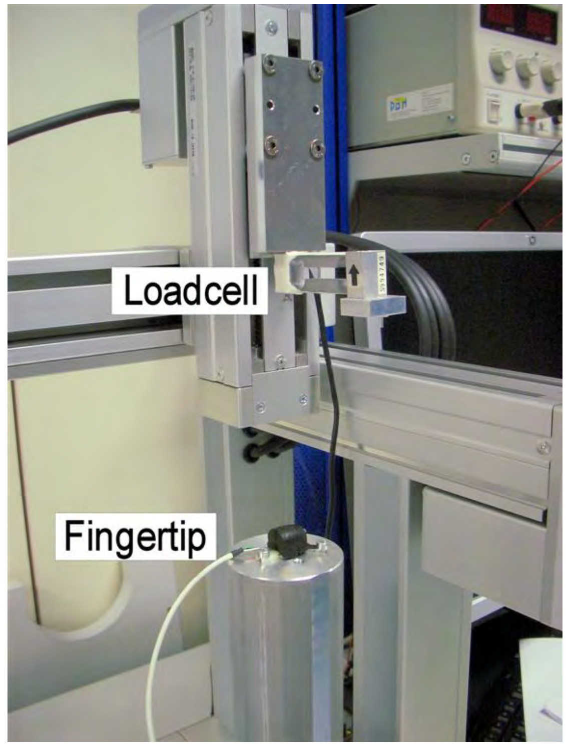

(b)

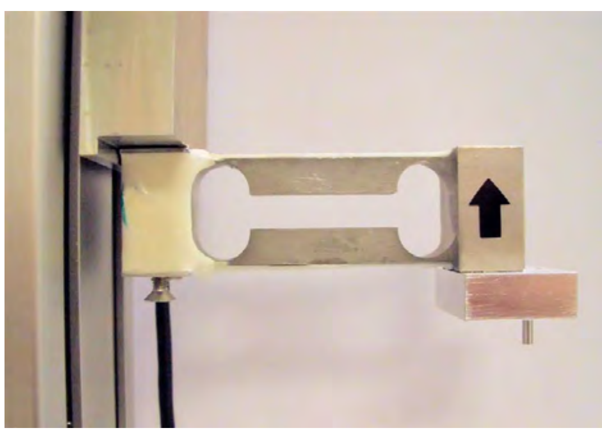

(c)

Figure 5.2: **Test setup.** The test setup that is used to test the characteristics of the sensor is shown. Either the palm or the fingertip is mounted on a platform, as shown in Figure **(a)** and **(b)**, respectively. A Cartesian robot (TT-C3-2020 from *IAI*) moves an off-centre loadcell (AS kg 0.5, from *Laumas*). In **(c)** a close-up of the loadcell and the probe that is used to push against the sensor can be seen.

the loadcell (see Figure 5.2). The Cartesian robot moves the loadcell with the probe in x, y and z direction and can therefore push the probe vertically at different locations against a fingertip or palm, respectively. The position of the loadcell can be determined via the serial interface of the robot, with a maximum frequency of 25 Hz. Therefore, we collect all measurements with a frequency of 25 Hz. The signal from the loadcell is amplified by an AT-10 from *Precise Instruments*. To digitize the signal, the same microcontroller board is used that also sends the measurements of the capacitive pressure sensor system to the PC. Therefore, synchronized data from the capacitive pressure sensor system and the loadcell can be acquired. The loadcell was calibrated with weights from *CIBE S.r.l.* The pressure applied to the palm is calculated as the force measured by the loadcell divided by the contact area. The measurements of the capacitive pressure sensor system are converted to Farad (1 measurement unit = 2.88 fF).

5.1.2 Experiments with the Fingertips

Spatial Sensitivity

To test the spatial sensitivity of the fingertip, a 2*mm* probe applied pressure to the fingertip at different positions, along a straight line from the back of the fingertip to the front. Along this line the surface of the fingertip is nearly perpendicular to the probe. For each position, the probe moved up and down several times, before moving towards the front of the fingertip, in steps of 0.1 mm each. The measurements of the 3 taxels are shown, which the probe traverses while going from the back to the front. In this plot the response of the sensor to a constant pressure is presented; to do this the data is filtered offline and only those values are plotted which correspond to a pressure of 87.5-100 kPa. The results presented in Figure 5.3 show that the fingertip can be used to localize where pressure is applied.

Baseline Drift and its Compensation

A baseline drift in the sensor measurements could be observed, with the drift affecting different taxels unequally (as depicted in Figure 5.4(a)). A probable cause is sensitivity to temperature, which is discussed in Section 3.5. Many methods for drift compensation have been studied, for example in [145]. For this thesis, a simple method was used, which was inspired by the compensation algorithm utilized in the CDC chip [127]. It is fast enough to be implemented in real-time:

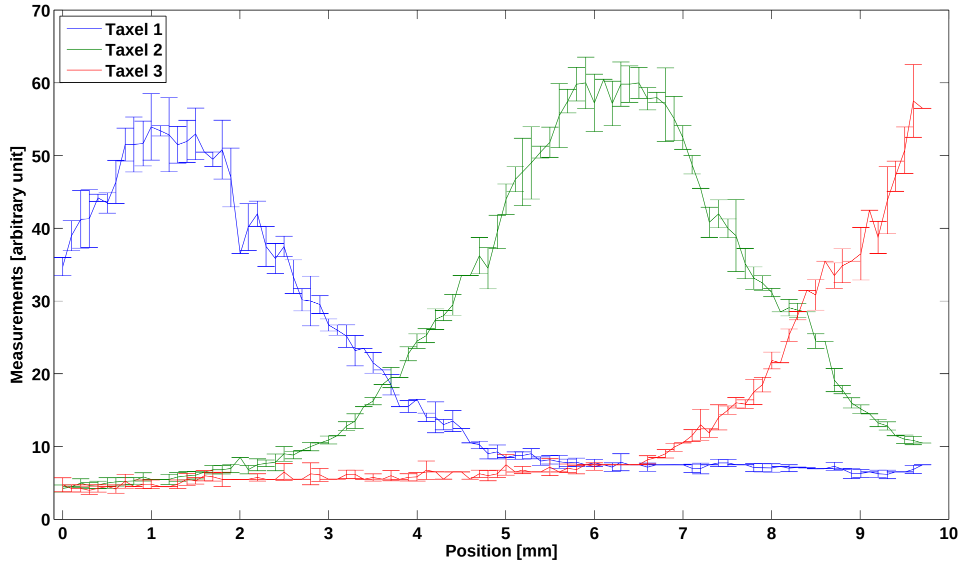

Figure 5.3: **Spatial resolution of the fingertip.** The probe (2 mm diameter) is pushing the fingertip at different positions (0.1 mm distance to each other), along a straight line from the back to the front of the fingertip. Along this line the surface of the fingertip is nearly perpendicular to the probe. For each position the probe moves up and down several times. The average measurement and standard deviation for 3 different taxels when the loadcell measures 28-32g are shown.

```
MAX_COMPENSATION_PER_SECOND = 0.1;
CHANGE = MAX_COMPENSATION_PER_SECOND / FREQUENCY;
at each timestep, for each taxel_j:
   // subtract the current baseline from the measurement
   measurement_j −= baseline_j;
   // if taxel not touched and more than 0.5 different, adapt baseline
   if measurement_j < touch_threshold_j:
      if measurement_j > 0.5:  baseline_j += CHANGE;
      if measurement_j < 0.5:  baseline_j −= CHANGE;
```

The initial baseline is calculated for each taxel individually: it is the average measurement during the calibration phase, which lasts for a couple of seconds before the sensor is used. Subsequently, the baseline of each taxel is adapted in small steps at every timestep. The maximum compensation

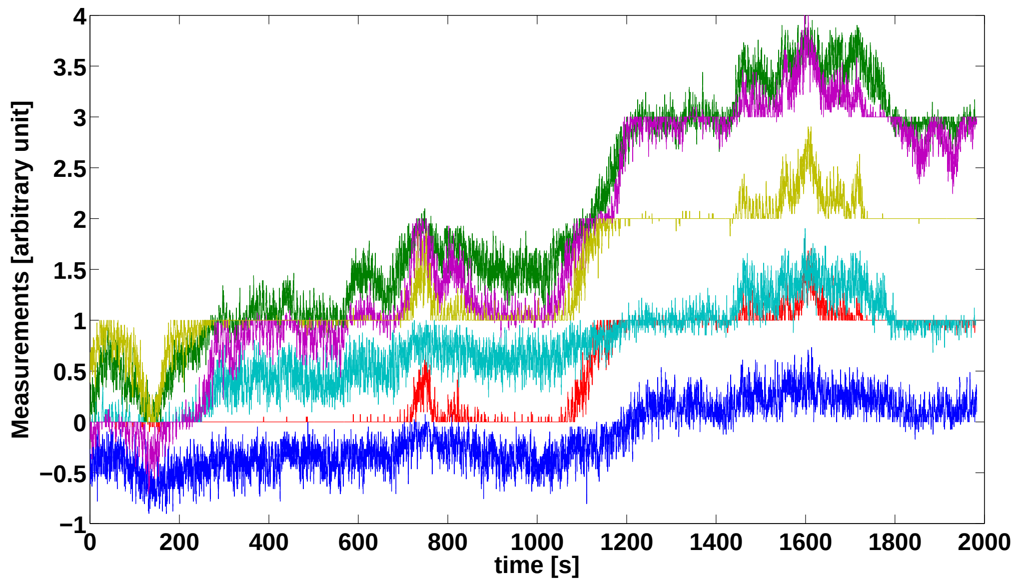

(a)

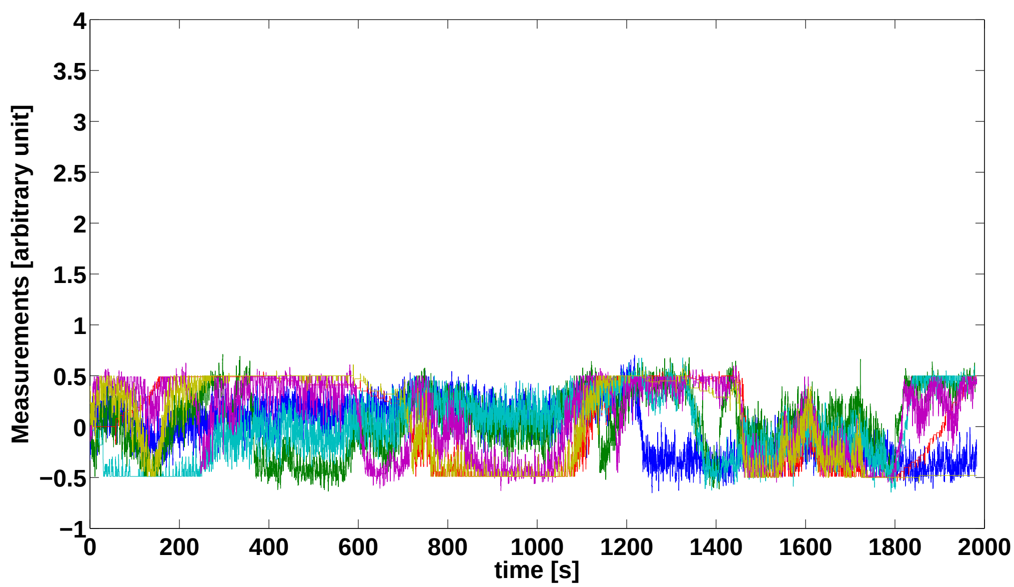

(b)

Figure 5.4: **Baseline drift.** The measurements of six taxels (moving average of the unprocessed sensor measurements) are shown. Their drift is clearly visible in **(a)**. In **(b)** the measurements are shown after the drift compensation has been applied. Each colour corresponds to a different taxel.

per second, `MAX_COMPENSATION_PER_SECOND`, was set to 0.1 (given in raw measurement units). This value is far higher than the maximum drift per second that was encountered in the experiments, yet is it low enough not to cause big oscillations in the baseline due to noise. The baseline is not changed if the measurements are within a margin of ± 0.5 of the baseline (given in raw measurement units). This margin is used as the measurements usually oscillate between two neighbouring values, as explained in Section 4.1.1; as a result, there are fewer fluctuations in the baseline.

The baseline is also not adapted if the taxel was touched. Therefore, one needs to differentiate the changes in the sensor measurements due to touch from those due to drift and noise. As already discussed in Section 4.1.1, the noise level is not the same for all taxels. Due to these differences between the taxels, the noise of each taxel is determined individually: in the calibration phase the 95% percentile of the sensor measurements for each taxel is calculated. The touch-threshold (if the value is larger or equal than this, it is defined that the taxel has come in contact with an object) is the 95% percentile plus a safety margin (which was empirically set as two measurement units). Due to the safety margin, the touch detection probably misses some very light touches, but for the drift compensation algorithm it is preferential to have some false negative touch detections than false positives: concerning false negative touch detections, as the baseline changes in very small steps, only very light touch that is applied for extended periods of time causes problems (it is mistaken for drift and will be erroneously offset). The results of false positive touch detections due to drift and noise are graver: the drift compensation algorithm stops to adapt the baseline, which could lead to a runaway drift. To avoid this, the safety margin accounts for small fluctuations in the measurements due to the drift that has not yet been compensated (but which the algorithm will eventually offset), and also accounts for additional noise that is not present in the calibration phase. With this safety margin practically no false positive touch detections could be observed during the experiments.

The drift compensation was employed in all the following experiments. As a result no drift in the sensor measurements could be observed (without causing a waveform distortion, a phase shift or a transient response). The effect of the drift compensation algorithm is shown in Figure 5.4.

Dependence on Contact Area

The influence of the contact area on the measurements was investigated. Probes of different diameter were pushed against the fingertip. In order to have a more constant contact area for each probe, the probes were concave in one dimension (radius: 13 *mm*) to conform more to the shape of the

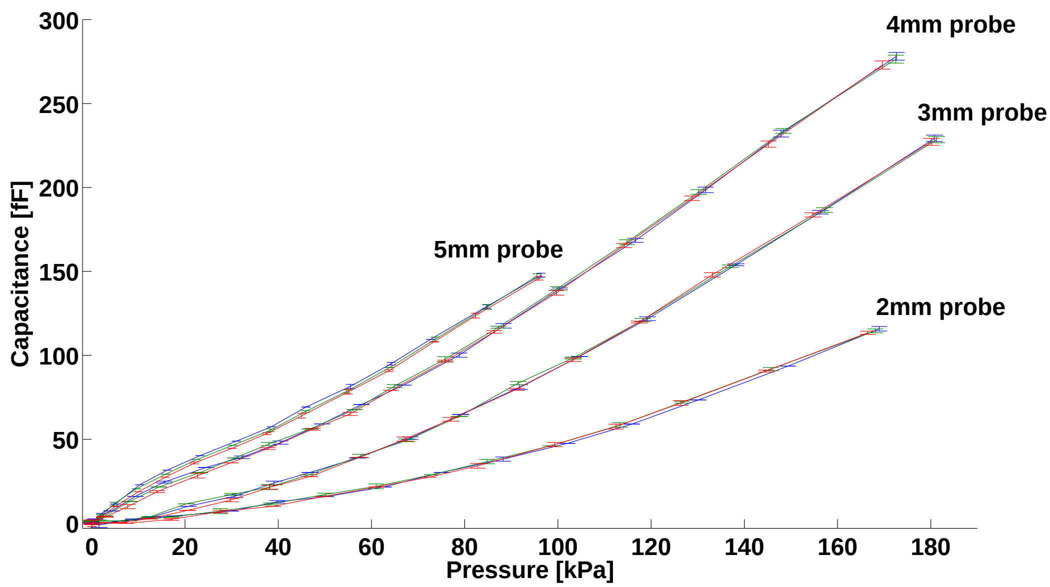

Figure 5.5: **Response of the sensor to varying pressure with different tip sizes.** Probes with different diameters were used to push against the fingertip. The average and standard deviation of the first second of measurements are shown. For each probe size three testing cycles were conducted, which correspond to different colours.

fingertip. In addition, the fingertip was tilted by 33 *deg*, in order to place the surface of the taxel, which is highlighted in Figure 4.30, as perpendicular as possible to the probe. The probe was then placed above the centre of the taxel. To apply pressure, the probe moved down to a certain depth as fast as possible, remained there and after two seconds moved up again to the non-contact position. The probe remained in this position for 20 seconds, to minimize the effects of hysteresis on the measurements. After that it moved down again, this time 0.1 *mm* deeper than before, and the whole process was repeated until the probe had pushed to the deepest defined point. These experiments were conducted with probes of different diameter, in particular 2, 3, 4, 5 *mm*. The size of the probes could not be increased more, because of the increasing influence of the second curvature of the fingertip, which was not being taken care of by the concavity of the probes. For each probe size three cycles were conducted. In Figure 5.5 the average and standard deviation of the first second of capacitance measurements are plotted. The pressure was calculated as the force measured by the loadcell divided by the contact area. It can be seen that for the same pressure the sensor measurements are higher while using probes of a bigger diameter.

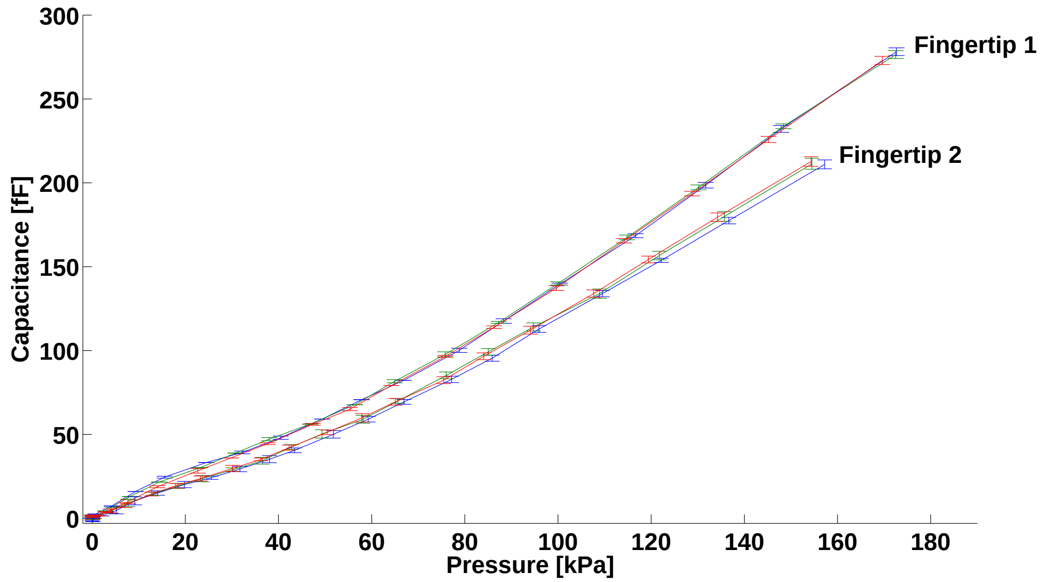

Figure 5.6: **Response of two fingertips to varying pressure.** The same taxel in 2 different fingertips was pushed with a 4 *mm* probe. The average and standard deviation of the first second of measurements are shown. For each fingertip three testing cycles were conducted, which correspond to different colours.

Difference in Response between Different Fingertips

In order to evaluate whether different fingertips have a different sensitivity, an experiment similar to Section 5.1.2 was conducted. The fingertip was pushed at different depths, again waiting 20 seconds in between. In Figure 5.6 the results for two different fingertips with a 4 *mm* probe are shown. The fingertips respond differently: for instance for 100 *kPa* fingertip 1 measured around 120 fF, while fingertip 2 measured around 140 fF. It can be concluded that in order to gain precise measurements, each fingertip would need to be calibrated individually. Yet, such a high precision might not be necessary for a humanoid robot during object manipulation.

Nonlinearity

To test whether the sensor has a nonlinear response, an experiment similar to Section 5.1.2 was conducted. The taxel indicated in Figure 4.30 was pushed with a 2 *mm* probe at different depths, again waiting 20 seconds in between. The result can be seen in Figure 5.7. Even though relatively high pressure was applied, the overall response of the sensor to varying pressure is rather linear.

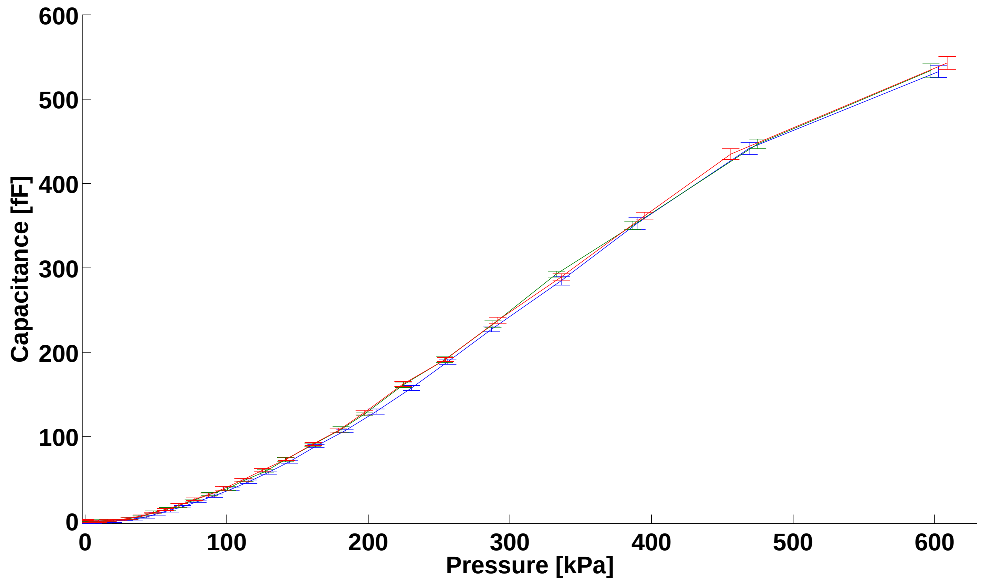

Figure 5.7: **Response to varying pressure with a 2 *mm* tip.** The average and standard deviation of the first second of measurements are shown. Three testing cycles were conducted, which correspond to different colours.

Moreover, in Figure 5.8 the response of the sensor is shown when the probe is positioned at different depths. The nonlinear relationship between position and capacitance is clearly visible.

Noise, Stability and Minimum Detectable Pressure

All the results presented so far show that there is low noise in the measurements, as the standard deviations as well as the differences between the repetitions are low. In Figure 5.9 the results are plotted, which were collected in 5.1.2, focusing on small pressure. It can be concluded that if the contact area has at least a 4 *mm* diameter, pressure differences of about 5 *kPa* can be detected. If only the taxel of fingertip 1 is considered, even 3 *kPa* could be reliably detected.

5.1.3 Experiments with the Palm

Spatial Sensitivity

The spatial resolution of the palm was tested in the following way: a probe with 3 *mm* diameter applied pressure to the palm at different positions, which have a distance of 0.5 *mm* to each other. Pressure was never applied to two adjacent positions one after another, to avoid the influence of

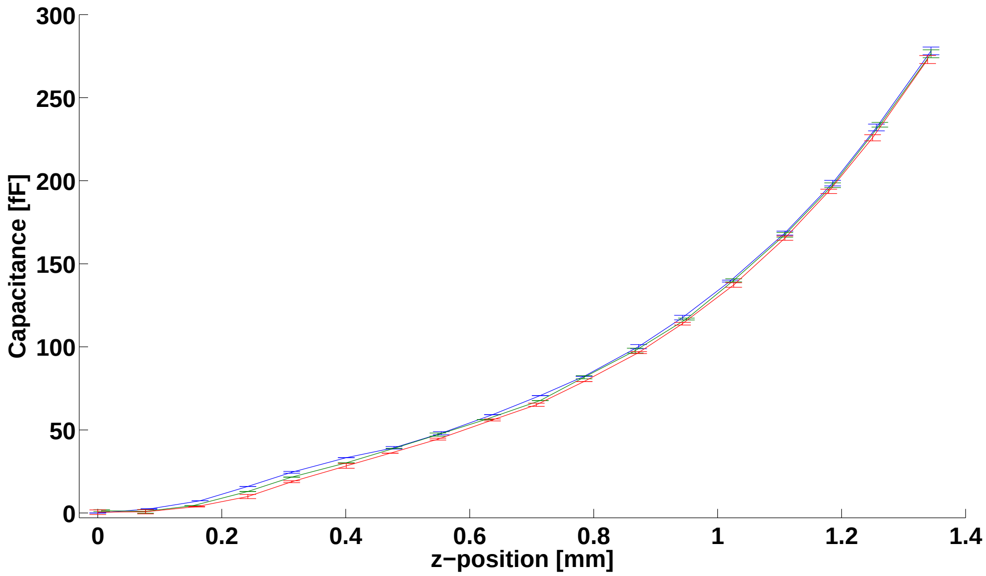

Figure 5.8: **Response to varying displacement with a 4 *mm* tip.** A 4 *mm* probe was used to push the taxel at varying depth. The average and standard deviation of the first second of measurements are shown.

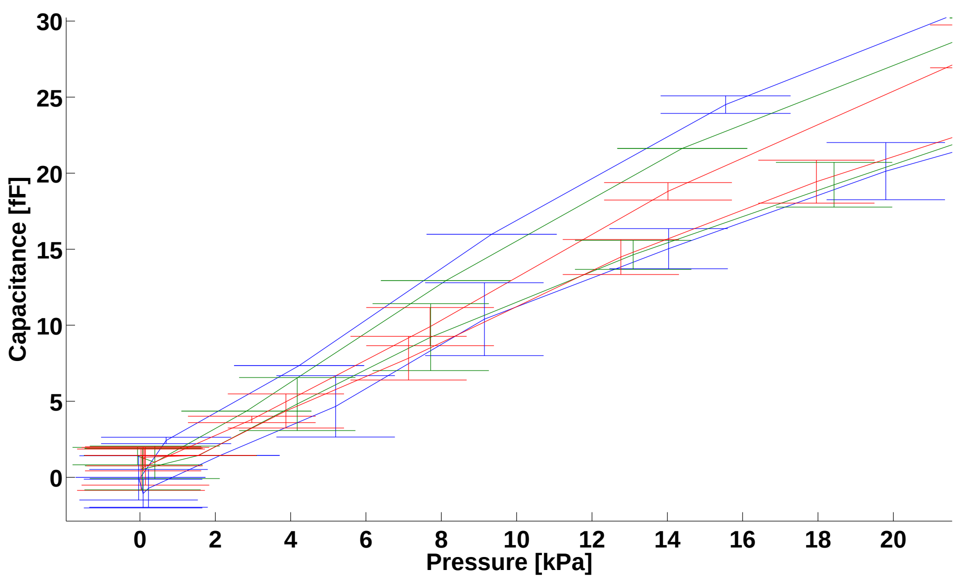

Figure 5.9: **Response of two fingertips to varying pressure with a 4 *mm* tip.** The same taxel in two different fingertips was pushed with varying pressure. The average and standard deviation of the first second of measurements are plotted.

hysteresis on the measurements, but instead the palm was covered in a pattern where each push is 5 *mm* apart from the next. At each position, the probe moved slowly down and then quickly up, and subsequently changed the position. After measurements for each position were obtained (which took a couple of hours), each position was subsequently tested a second time, to get more measurements and confirm the stability of the sensor measurements over time. In Figure 5.10 the response of all the taxels to a certain load is shown; to do this the data was filtered offline and only those values are plotted which correspond to a pressure of 150-160 *kPa*. To avoid the effects of hysteresis, only those measurements were used, while the probe was moving down. Furthermore, only a part of the surface area was tested, as only those positions can be compared, where the whole probe touches the palm nearly perpendicular. This is because, the response of all taxels to a certain pressure shall be shown; yet, if only a part of the probe touches the palm or if the probe is not perpendicular to

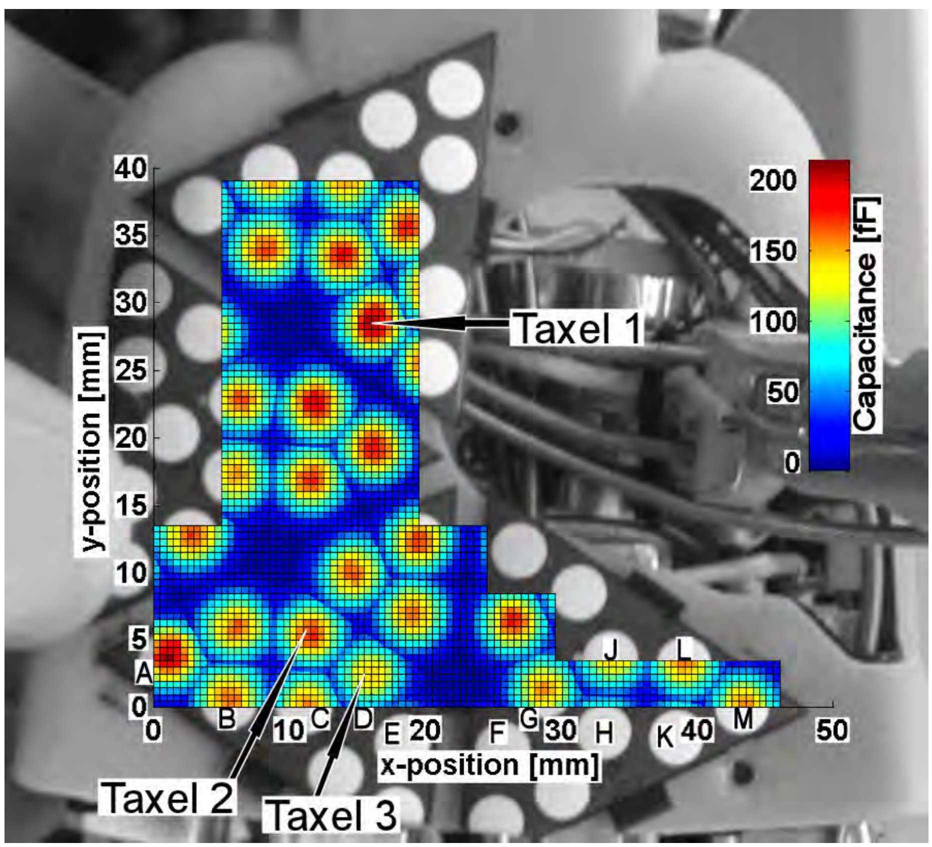

Figure 5.10: **Sensor response at different positions.** The superimposed responses of all taxels to a certain pressure (150-160 *kPa*) are shown. In the background a grayscale picture of the palm (without the silicone foam and the top conductive layer) can be seen, to demonstrate the correspondence of the sensitive areas to the round pads on the PCB.

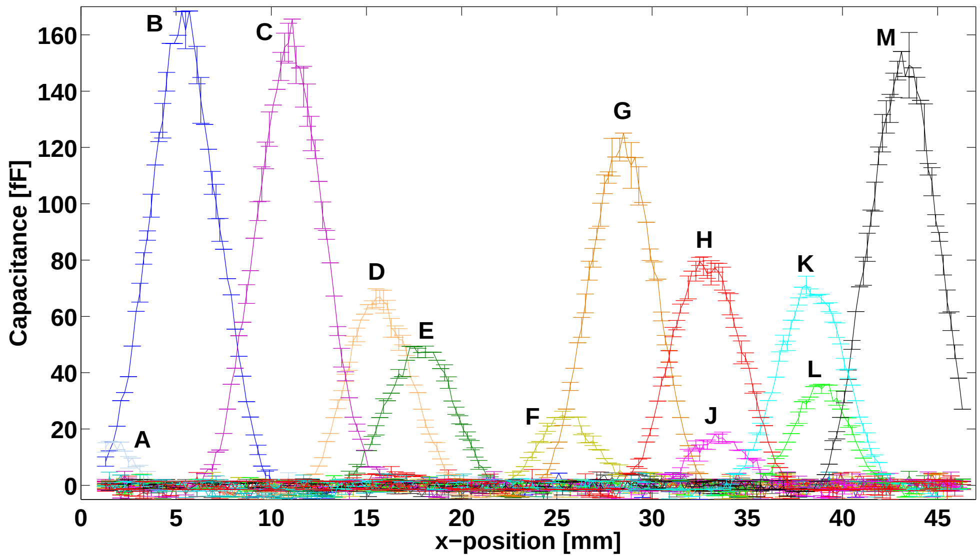

Figure 5.11: **Spatial resolution of the palm.** The probe (3 *mm* diameter) is pushing the palm at different positions (0.2 *mm* distance to each other), along a straight line (corresponding to Figure 5.10 where y-position = 0 *mm*). The average measurement and standard deviation of all taxels in both the triangular modules that the tip crosses are shown. Each colour corresponds to a different taxel and the letters show the correspondence of the activated taxels to the taxels in Figure 5.10.

the palm, the pressure applied to the palm varies, even if the loadcell measures the same force. The superimposed capacitance of all taxels and in the background a picture of the palm are shown. This demonstrates the correspondence of the sensitive areas to the round pads on the PCB.

In Figure 5.11 the results of another experiment are presented, in which the y-position of the probe is always zero and the x-positions have a distance of 0.2 *mm* to each other. The results demonstrate that the taxels respond in a bell shaped curve, little or no cross-talk occurs and that the responsive zones overlap. It can be concluded that the sensor can be used to localize where pressure is applied to it.

As a final consideration, it could be observed that even though the measurements presented here were taken while the robot was moving, they are similar to the ones obtained in static conditions, as will be discussed further in Section 5.1.3.

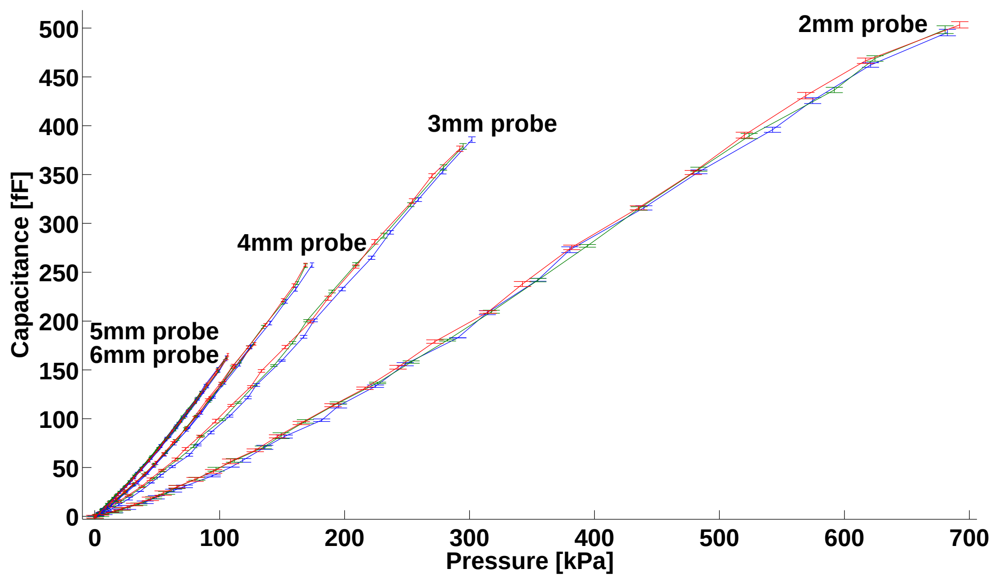

Figure 5.12: **Response of taxel 2 to varying pressure with different tip sizes.** Probes of different size were used to push the taxel with varying pressure. The average and standard deviation of the first second of measurements are shown.

Dependence on Contact Area

With the experiments presented here, the influence of the contact area on the measurements was investigated. The probe was placed above the centre of the taxel 2 (see Figure 5.10). The probe moved down to a certain depth as fast as possible, remained there and after two seconds moved up again to the non-contact position. The probe remained in this position for 20 seconds, to minimize the effects of hysteresis on the measurements. After that it moved down again, this time 0.1 *mm* deeper than before, and the whole process was repeated until the probe had pushed to the deepest defined point. These experiments were conducted with probes of different size, in particular 2, 3, 4, 5 and 6 *mm*. The probes up to 5 *mm* were made from aluminium, and the one with 6 *mm* diameter was made from plastic (when the sensor works correctly, the material does not influence the measurements). For each probe size 3 cycles were conducted. In Figure 5.12 the average and standard deviation of the first second of capacitance measurements are plotted. The pressure was calculated as the force measured by the loadcell divided by the contact area.

As it was to be expected, for the same pressure the sensor measurements are higher when using probes of a bigger diameter. Yet, the results from the probe sizes of 5 and 6 *mm* in Figure 5.12

overlap and cannot be distinguished, therefore it can be concluded that the response of the sensor is regardless of the probe size starting from 5 *mm* diameter. This shows once more (like in the previous section) that the taxels are only responsive to touches close to their corresponding pad on the PCB. This reduces the crosstalk between taxels and makes it easier to localize touch. Furthermore, as most objects that the robot will grasp are relatively big, at least some of the taxels can be expected to have contact areas that have a diameter larger than 5 *mm* and can therefore be used to measure pressure. Even if the contact area has a diameter of only 3 or 2 *mm*, the measurements are reasonably similar to judge the magnitude of the exerted pressure: as it can be seen in Figure 5.12, the measurements with a 3 *mm* probe are about half, and with a 2 *mm* probe still about a fourth as high as the measurements with a 5 or 6 *mm* probe.

Difference in Response between Different Taxels

When closely investigating the results of Figure 5.10, it can be seen that the maximum activation for different taxels is different. In particular, the maximum capacitance of Taxel 1 is 200.5 fF, Taxel 2 165.5 fF and Taxel 3 139 fF. Therefore, the maximum measurements of Taxel 1 are nearly $1.5\times$ higher than those of Taxel 3. To investigate this further, an experiment similar to Section 5.1.3 was conducted. The palm was pushed with a 3 *mm* probe at different depths, again waiting 20 seconds in between. In Figure 5.13 the results for the 3 different taxels indicated in Figure 5.10 (these correspond to a low, medium and high response taxel) are plotted. The results in Figure 5.13 correspond to the ones in Figure 5.10: for taxel 1 the response is higher than for the others and taxel 3 has the lowest response. This is probably due to the varying density of the silicone foam.

Yet, it is interesting to note that up to a certain pressure the responses overlap. Therefore, the experiment was repeated with a probe size of 6 *mm* and with a lower maximum pressure (the applied force is nearly the same, but the contact area is bigger), see Figure 5.14. While there are still differences between the taxels, they are small. It was concluded that while there are differences between the taxels, they become increasingly negligible with smaller pressure.

Noise, Stability and Minimum Detectable Pressure

All the results presented so far show that there is low noise in the measurements, as the standard deviations as well as the differences between the repetitions are low. The response of the sensor is stable: even though it took many hours to collect the results, given a certain probe size and a certain

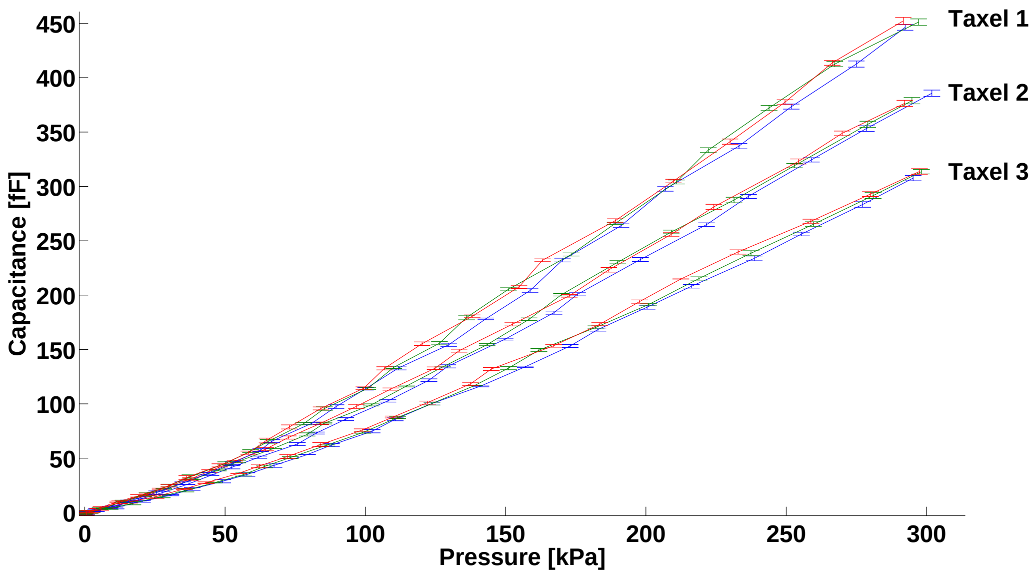

Figure 5.13: **Response of taxels 1, 2 and 3 to varying pressure with a 3 *mm* tip.** A 3 *mm* probe was used to push the taxel with varying pressure. The average and standard deviation of the first second of measurements are shown.

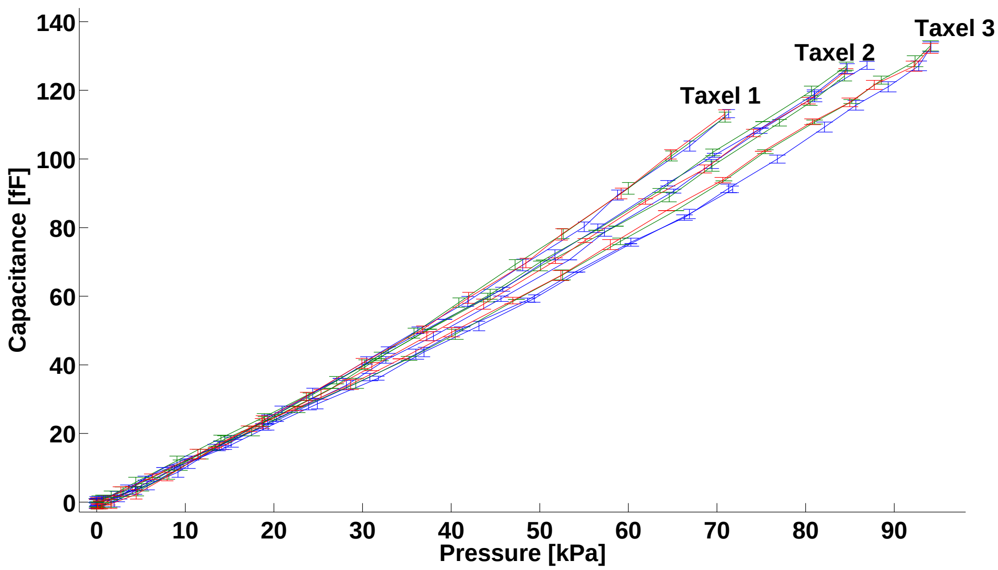

Figure 5.14: **Response of taxels 1, 2 and 3 to varying pressure with a 6 *mm* tip.** A 6 *mm* probe was used to push the taxel with varying pressure. The average and standard deviation of the first second of measurements are shown.

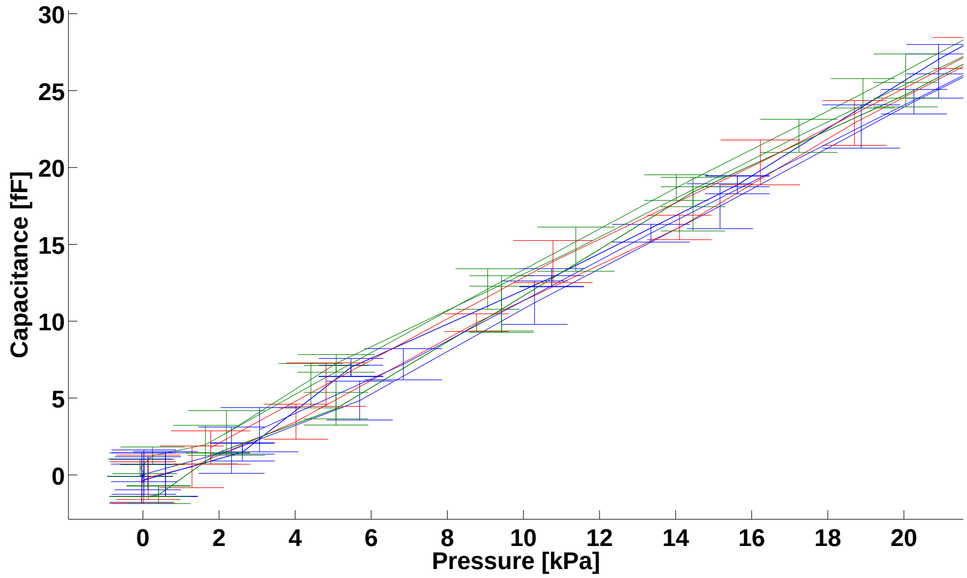

Figure 5.15: **Response of taxel 2 to varying pressure with a 6 *mm* tip.** A 6 *mm* probe was used to push the taxel with varying pressure. The average and standard deviation of the first second of measurements are shown.

location, the measurements of all testing cycles overlap.

In Figure 5.15 the results are plotted, which were collected in 5.1.3 and 5.1.3 for taxel 2 (see Figure 5.10) with a probe size of 5 and 6 *mm*, focusing on small pressure. It can be concluded that pressure differences of about 5 *kPa* can be reliably detected with this taxel.

Calibration, Part 1: Nonlinearity

The response of the sensor is slightly nonlinear and a quadratic function was used to convert the sensor measurements $S(t)$ at time t, given in fF, to pressure $C(t)$, given in *kPa* (without taking into account the relaxation of the silicone foam, which will be discussed later):

$$C(t) = aS(t)^2 + bS(t) \tag{5.1}$$

with $a = -0.001132$ and $b = 0.8141$. To compute these values, all the data was used, which has been collected in the previous sections for taxel 2 with a 5 or 6 *mm* probe. The quadratic term is quite small and the sensor can be assumed to respond linear to changing pressure if smaller precision is necessary.

Calibration, Part 2: Viscoelastic Behaviour

So far, pressure has been applied to the sensor only for short time intervals. In such short time frames the pressure can be assumed to be constant if the position of the probe is steady. But when the sensor is loaded for extended time periods, the pressure cannot be assumed anymore to be constant. This is due to the viscoelasticity of the silicone foam, as discussed in Section 3.5. Therefore, if the applied pressure is to be calculated out of the sensor measurements, this time dependent behaviour has to be taken into account. Many models exist to describe the relaxation behaviour of viscoelastic materials [146]. In our case, the sensor measurements $S(t)$ correspond to strain. $C(t)$ is used instead of $S(t)$, as it takes the nonlinear behaviour of the sensor into account. Therefore $P_{cal}(t)$, the calculated pressure, is

$$P_{cal}(t) = C(t) - relax(t) \tag{5.2}$$

$relax(t)$ is the time dependent relaxation. In a first approximation, it can be said that the stress decays exponentially with time. Suppose, due to a constant strain ε, a constant value for $C(t) = C$ is obtained. Then $relax(t)$ is

$$relax(t) = C\beta(1 - e^{-\frac{t}{\tau}}) \tag{5.3}$$

β is a scaling factor, and the relaxation approaches asymptotically the final value $C\beta$. The time constant τ is the time it takes to reach $1 - 1/e \approx 63.2\%$ of the final value. Furthermore, instead of just modelling the relaxation resulting from constant strain, changing sensor measurements should be taken into account. Consider a variable C(t), which is the sum of stepwise changes ΔC_1, ΔC_2... at times T_1, T_2... respectively. According to Boltzmann's superposition principle, the relaxation is a function of the entire history of the sensor. The total relaxation is therefore:

$$relax(t) = \sum_i \Delta C_i \beta(1 - e^{-\frac{t-T_i}{\tau}}) \tag{5.4}$$

where ΔC_i is the incremental change of C at time T_i. In this experimental setup the strain, and as a consequence of that C, changes slowly and monotonically even if the Cartesian robot is static. This is because the loadcell is slightly compliant, and the tip changes its position as the silicone foam is relaxing. A similar effect can be expected if the robot actuation system is compliant or the object that is in contact with the skin is soft. On the other hand, the sensor measurements also vary slightly at nearly every time step due to the digitisation and the noise, as discussed before; the resulting changes in C should not be considered, otherwise the algorithm becomes to computationally expensive. Therefore, ΔC_i is substituted with ΔD_i, obtained with a moving average and a threshold: every second the average of $C(t)$ is computed. If this average is more than 1.5 kPa different from the sum of all ΔD_i so far, a new ΔD_i is added.

Moreover, it could be observed that while unloading (ΔD is negative in this case), the relaxation term has slower dynamics, and therefore different parameters should be used in this case. This phenomenon has been described many times in the literature, for example [147]. Therefore, β_l and τ_l are used when ΔD is positive, and β_u and τ_u when ΔD is negative.

Finally, the model as described in (5.3) represents the relaxation behaviour of viscoelastic materials only to a first approximation, which can be better described with the superposition of several exponential functions. It was found that a sum of three exponential functions gives satisfying results. Therefore three β_l, τ_l, β_u and τ_u exist each. The final result is:

$$\begin{aligned} relax(t) = & \sum_{\Delta D_i > 0} \sum_{k=1}^{3} \Delta D_i \beta_{l_k} (1 - e^{-\frac{t-T_i}{\tau_{l_k}}}) \\ & + \sum_{\Delta D_i < 0} \sum_{k=1}^{3} \Delta D_i \beta_{u_k} (1 - e^{-\frac{t-T_i}{\tau_{u_k}}}) \end{aligned} \tag{5.5}$$

To get the parameters, a 6 mm probe was pushed with maximum speed against the palm and kept stationary for one hour. Subsequently, the sensor was quickly unloaded, and further data was collected for 75 minutes. The goal was to find the parameters so that $P_{cal}(t)$ matches $P^*(t)$, which is the pressure derived from the loadcell measurements divided by the contact area. First, the three β_l and τ_l were calculated by using the data between the first stress and the first release. To find the values, the curve fitting toolbox (method: "NonlinearLeastSquares") of Matlab was employed. Afterwards the data starting at the unloading until the end of the measurements was used: the relaxation due to the ΔD that happened before was subtracted (the parameters were used that had just been determined), and subsequently the three β_u and τ_u for unloading were calculated. The result can be seen in Figure 5.16(a). The parameters are reported in Table 5.1.

Subsequently, it was tested whether the model also works for calculating $P_{cal}(t)$ for other datasets, using the parameters that were just found: different time periods (Figure 5.16(b)), multi-step loading (Figure 5.17) and cyclic loading 5.18(a) were tested. The match of $P_{cal}(t)$ to $P^*(t)$ was generally satisfying. In Figure 5.18(b) the most difficult scenario and the worst result that was obtained is

Table 5.1: Parameters for Calculating the Relaxation.

Parameter	Value [s]	Parameter	Value
τ_{l_1}	2.17	β_{l_1}	0.0649
τ_{l_2}	117.42	β_{l_2}	0.0968
τ_{l_3}	909.04	β_{l_3}	0.4376
τ_{u_1}	3.22	β_{u_1}	0.1500
τ_{u_2}	202.28	β_{u_2}	0.1548
τ_{u_3}	750.91	β_{u_3}	0.2983

presented: in this experiment a different maximum pressure, different time periods, multi-step and cyclic loading were used. Moreover, the total time of pressure applied to the sensor is far higher than it can be expected to be usually the case in the humanoid robots. In this case, slight differences in $P_{cal}(t)$ and $P^*(t)$ could be seen. In general, this effect could be observed when applying pressures higher than the one in the original dataset. Nevertheless, it was concluded that this model is good enough for the task at hand.

Finally, it should be remarked that the initial response of the capacitive sensor to a change of displacement of the probe is fast: there is no delay between the initial change of the measurements of the capacitive sensor and the loadcell. This does not take into account the delay due to the microcontroller board and the subsequent CAN-bus.

5.1.4 *Discussion of the Tests with the Cartesian Robot*

It could be confirmed that the sensor can be used to localize touch and that the sensor response is dependent on the contact area. Unfortunately there are also slight differences in the response to pressure between different taxels, but the differences might be small enough for a humanoid robot in order to not require calibration for every single taxel. The sensitivity is satisfying and pressure of about 5 kPa can be detected. Furthermore, algorithms to compensate the drift and hysteresis in the sensor measurements, which commonly affect capacitive sensors, were presented.

In general, the round shape of the fingertips makes it more difficult to obtain conclusive results for the fingertips than for the palm: it is difficult to keep the contact area constant while pushing

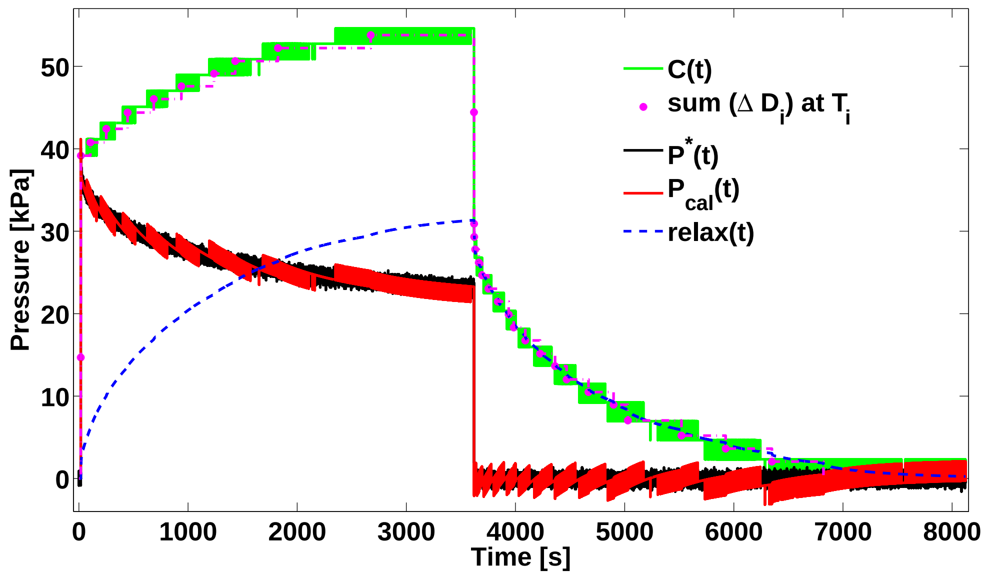

(a)

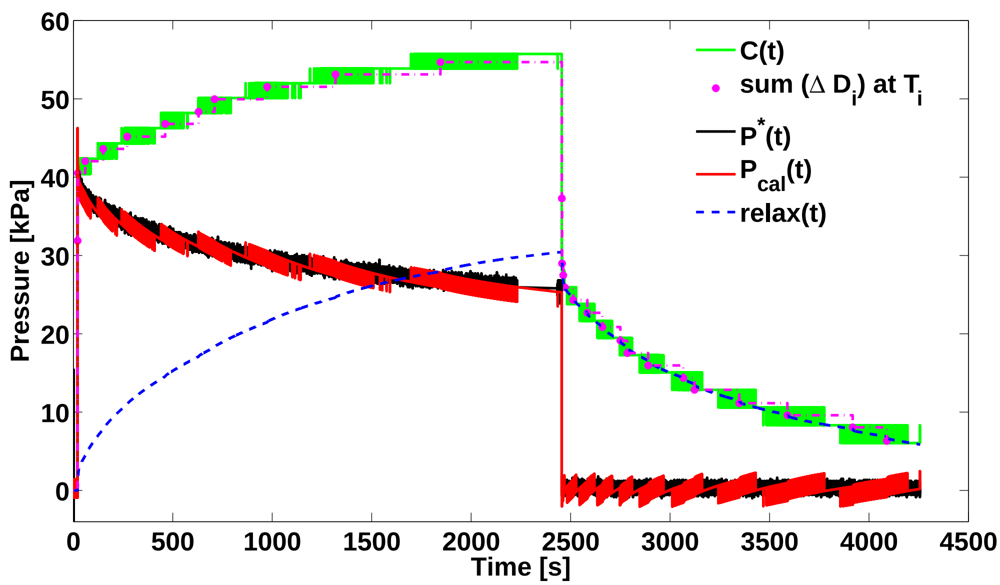

(b)

Figure 5.16: **Compensation of the relaxation of the silicone foam.** In **(a)** pressure was applied for one hour, in **(b)** for 30 minutes. $C(t)$ corresponds to the uncorrected sensor measurements, ΔD_i to their stepwise approximation, $relax(t)$ is the correction term and $P_{cal}(t)$ are the corrected measurements: $P_{cal}(t) = C(t)$ - $relax(t)$. $P^*(t)$ is the pressure as calculated from the loadcell.

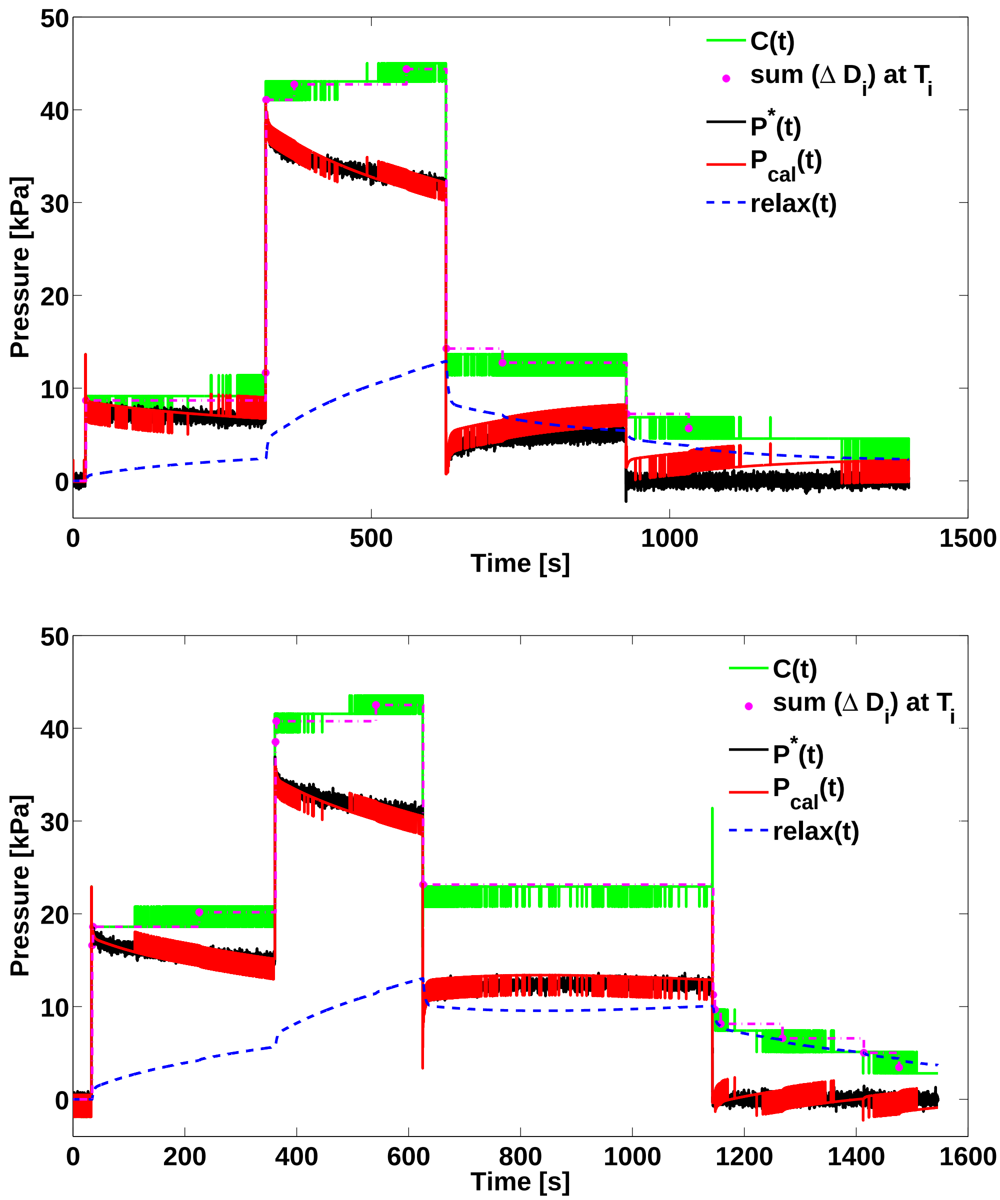

Figure 5.17: **Compensation of the relaxation of the silicone foam.** Multi-step loading was applied. $C(t)$ corresponds to the uncorrected sensor measurements, ΔD_i to their stepwise approximation, $relax(t)$ is the correction term and $P_{cal}(t)$ are the corrected measurements: $P_{cal}(t) = C(t)$ - $relax(t)$. $P^*(t)$ is the pressure as calculated from the loadcell.

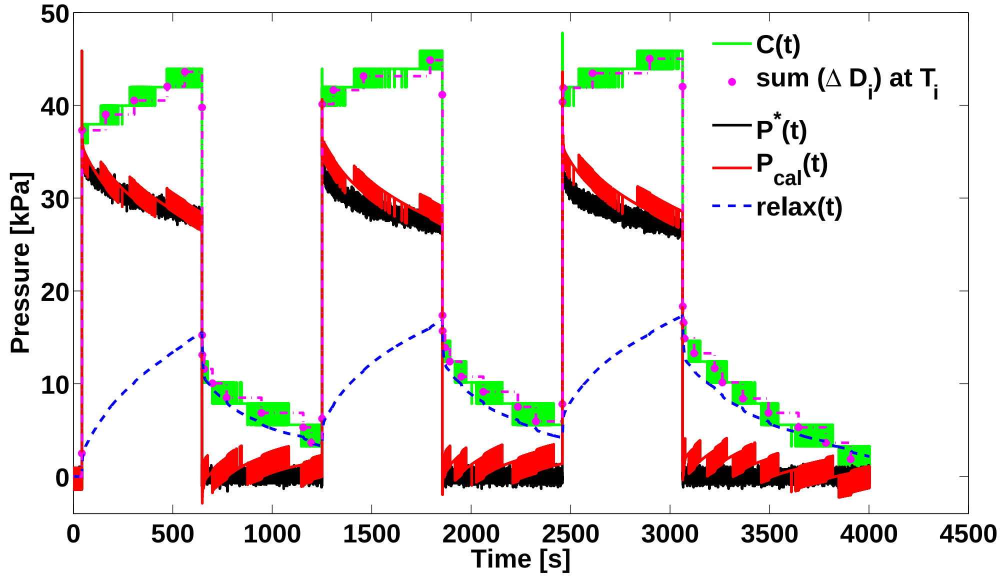

(a)

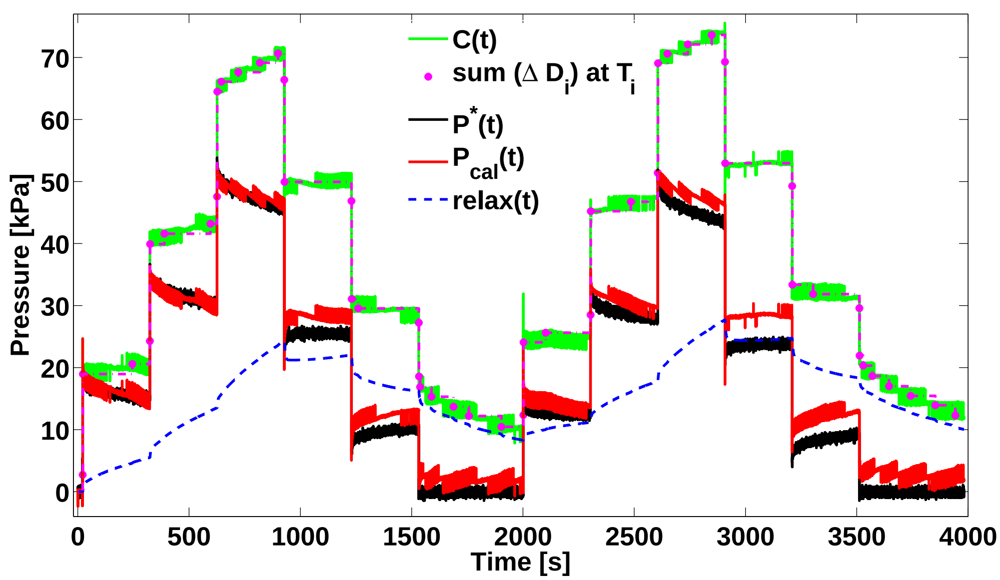

(b)

Figure 5.18: **Compensation of the relaxation of the silicone foam.** In **(a)** cyclic loading was applied, in **(b)** multi-step, cyclic loading. $C(t)$ corresponds to the uncorrected sensor measurements, ΔD_i to their stepwise approximation, $relax(t)$ is the correction term and $P_{cal}(t)$ are the corrected measurements: $P_{cal}(t) = C(t)$ - $relax(t)$. $P^*(t)$ is the pressure as calculated from the loadcell.

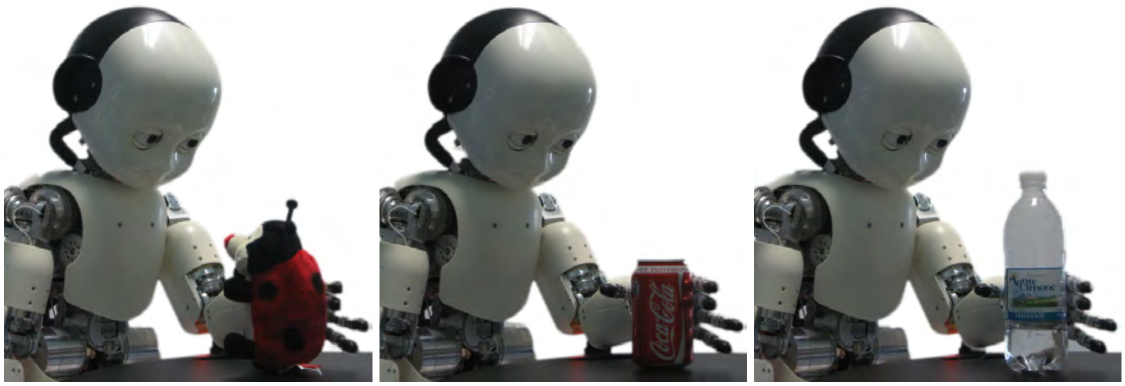

Figure 5.19: The iCub while grasping three different objects.

against the fingertip and in addition it is hard to keep the pushing angle perpendicular to the surface while pushing against the sensor at different positions. The relatively flat surface of the palm makes it easier to have clear experimental results.

Furthermore, for the fingertips it could be observed that the ground layer tends to fail, thereby influencing the sensor measurements. In particular, over time the fingertip sensors become less sensitive to plastic objects and more sensitive to human touch, also causing increased cross talk between the taxels. This effect has to be further investigated in the future and ultimately averted, as discussed in Chapter 6.1.

5.2 Grasping Experiments with iCub

In this section it will be shown that the fingertips can be used to aid grasping. First, an experiment will be presented in which the robot grasped three different objects with a predefined grasp (Section 5.2.1). The results show that the fingertip measurements are repeatable in a real world scenario and that the sensors can reliably detect touch. In the second experiment, a fragile plastic cup was grasped with the help of tactile feedback (Section 5.2.2). The amount of pressure exerted by the fingers was controlled and thereby the cup could be grasped without deforming it.

5.2.1 Predefined Grasping Experiments

The following experiment was conducted to test the reliability and repeatability of sensory data during a sequence of grasp movements: a set of objects was positioned in the same location on a table in front of the iCub. The robot performed a preprogrammed movement to reach for the objects shown in Figure 5.19: a plush ladybug, a coke can and a plastic bottle. Once the movement was completed, the iCub performed a grasping action. The latter was implemented as a predefined (position controlled) closure of the fingers. In this experiment, the hypothesis is that the same haptic stimulus can be produced on the sensors during different trials. This happens if (1) the object is in the same position/configuration with respect to the hand and (2) the fingers execute the same movement. The first hypothesis can be approximated by carefully positioning the object; the second was verified *a-posteriori* by measuring the variability in the position measurements of the joints of the hand. Table 5.2 reports the movement variability when four different grasping actions were repeated 20 times. Figure 5.20 and Figure 5.21 show the joint angle measurements while performing the grasp movement with an empty hand and with a plush ladybug, respectively. Results show that movements were repeatable, as the standard deviations of the recorded data are small: the maximum standard deviation was measured as 4.24° in the little finger DIP joint while grasping the can.

Given the assumption of repeatable haptic stimuli, the reliability of the tactile sensors in 20 repeated grasping trials was tested. In Figure 5.22 and 5.23, a toy bug is grasped; in Figure 5.24 and 5.25 a coke can; in Figure 5.26 and 5.27 a plastic bottle, as depicted in Figure 5.19. Red lines refer to the average sensor response when performing the grasping movement with no object; black lines and shaded regions represent respectively the average and standard deviation of the response while performing the grasping. Different rows refer to different fingers (from the top: thumb, index, middle, ring and little); the left column in each figure shows the fingertip response, while the right column refers to the grasp detector described in Appendix B. Among the 12 sensitive elements in each fingertip, in Figure 5.22, 5.24 and 5.26, the one with the strongest response (measured as the difference between the response corresponding to the condition in which the hand grasp each object or is left empty) is plotted. In Figure in Figure 5.23, 5.25 and 5.27 the taxel with the earliest detection time instant is plotted; this is the time when the average sensor measurement minus the standard deviation is higher than the 95% percentile of the empty grasp. The plots corresponding to the grasp detector show the output of the module, i.e. at time t the distance between the current hand configuration and the configuration predicted by the model, as explained in Appendix B.

Results clearly show the reliability of the fingertip sensors and demonstrate that their response can be used to detect the contact with the objects. The time of contact is indicated in the horizontal axis (time ticks in the horizontal axis are at 0, 5 and 10 seconds; if a contact is detected, an additional tick is added). It was inferred by monitoring the difference between the current response and

Table 5.2: **A tabular description of the movement variability in different grasping actions.** The standard deviation while grasping three different objects is shown for all the joints (carpometacarpal (CMC), metacarpophalangeal (MP), interphalangeal (IP), proximal interphalangeal (PIP) and distal interphalangeal (DIP) joint; see Fig. 2.19 for a detailed description).

	Joints movements variability during different grasping actions: standard deviation in degrees																		
Grasped	thumb				index				middle			ring				little			
object	CMC_1	CMC_2	MP	IP	MP_1	MP_2	PIP	DIP	MP_2	PIP	DIP	MP_1	MP_2	PIP	DIP	MP_1	MP_2	PIP	DIP
Empty hand	0.01	0.08	0.53	0.31	1.23	0.31	0.02	1.65	0.05	0.56	0.36	-	2.73	1.46	0.56	-	1.62	1.06	0.86
Ladybug	0.06	0.11	0.19	0.69	0.33	0.05	0.06	0.15	0.08	0.16	0.58	-	0.04	2.85	1.84	-	0.24	1.91	1.62
Coke can	0.05	0.29	1.81	2.07	1.14	0.1	0.13	0.87	0.13	1.48	1.77	-	0.04	3.94	3.08	-	0.5	2.26	**4.24**
Bottle	0.04	0.22	1.56	1.64	1.27	0.06	0.1	0.97	0.18	1.47	1.86	-	0.22	1.35	1.89	-	0.35	1.16	2.52

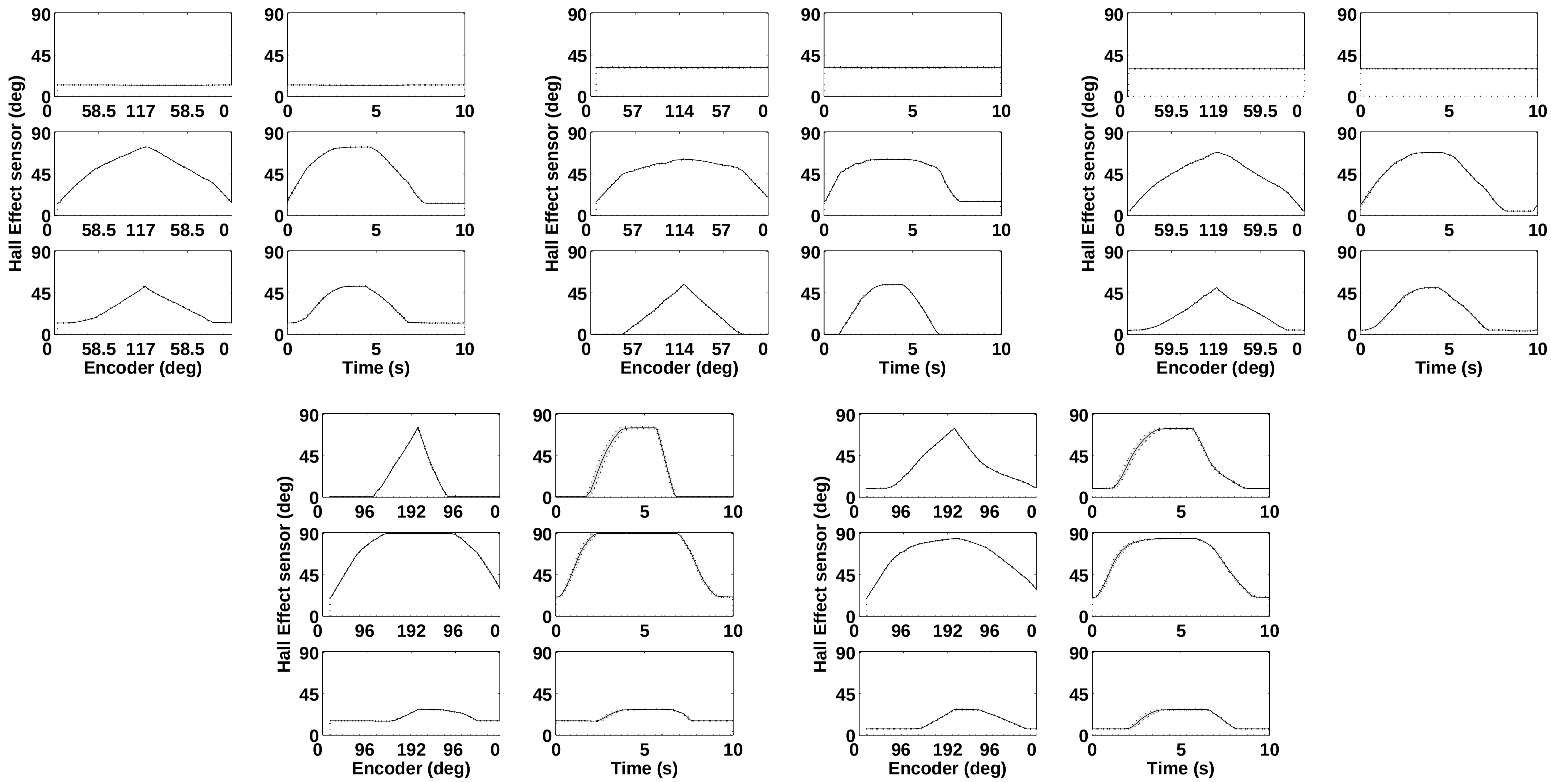

Figure 5.20: **Joint position sensor measurements when the hand is empty.** The hand is performing a predefined hand closure movement. In particular, the motors actuating the distal joints of all five fingers move with a given speed until they reach a predefined motor encoder value, and after 5 seconds they return to the original position. This process is repeated 20 times. The joint position sensor measurements are plotted against the respective motor encoder values (left columns) and against time (right columns). This is plotted for all five fingers, starting from the top left (reading direction): thumb, index, middle, ring and little finger. Three rows for each finger correspond to different joints for flexion, the top row corresponding to the most proximal and the bottom to the most distal joint. The black line is the average response in 20 trials. The shaded region is the standard deviation in 20 trials.

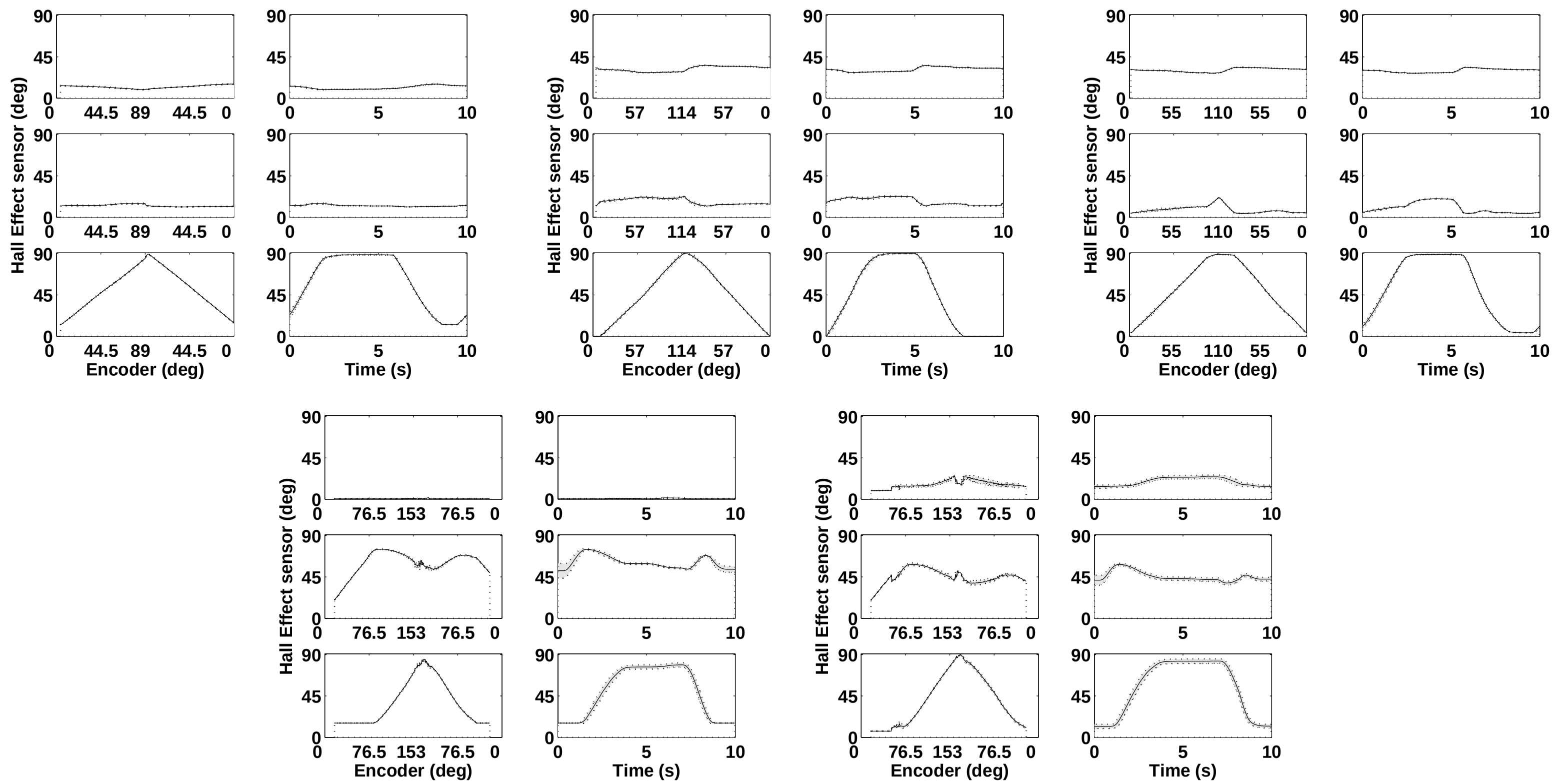

Figure 5.21: **Joint position sensor measurements when grasping a plush ladybug.** The hand is performing a predefined hand closure movement. In particular, the motors actuating the distal joints of all five fingers move with a given speed until they reach a predefined motor encoder value, and after 5 seconds they return to the original position. This process is repeated 20 times. The joint position sensor measurements are plotted against the respective motor encoder values (left columns) and against time (right columns). This is plotted for all five fingers, starting from the top left (reading direction): thumb, index, middle, ring and little finger. Three rows for each finger correspond to different joints for flexion, the top row corresponding to the most proximal and the bottom to the most distal joint. The black line is the average response in 20 trials. The shaded region is the standard deviation in 20 trials.

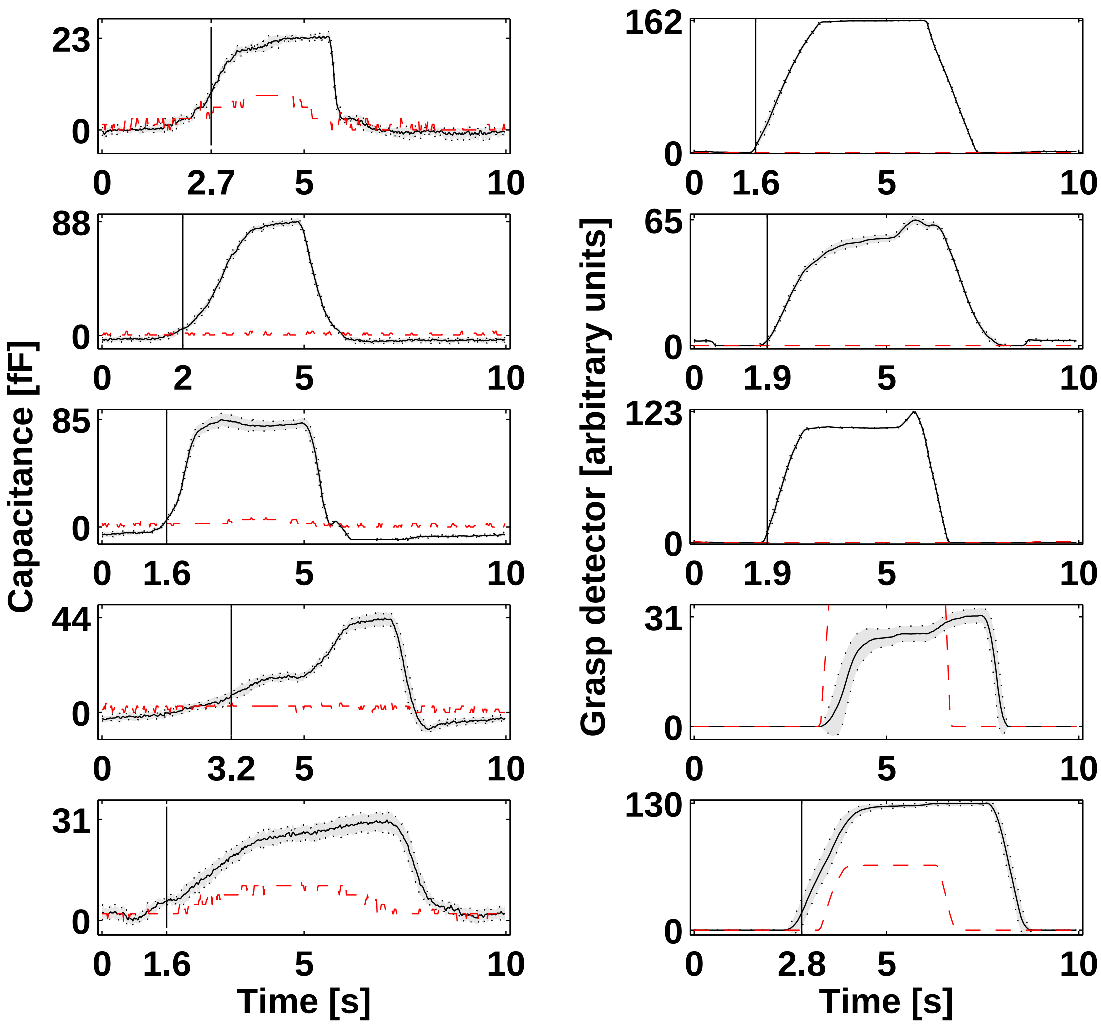

Figure 5.22: **Pressure sensor response (taxel shown with the maximum response) compared to grasp detector while grasping a ladybug toy.** A plot of the fingertips response (left column) and grasp detector response (right column). Rows correspond to different fingers: from the top to the bottom, thumb, index, middle, ring and little. The red line is the response when the grasp action is performed with no object. Thumb and little fingers mildly respond even if no object is present; these responses are due to imperfect grounding of the fingertip external conductive layer which produces a minor crosstalk disturbance. The black line is the average response in 20 trials. The shaded region is the standard deviation in 20 trials. The horizontal axis reports also the detection time instant; this is the time when the average sensor measurement minus the standard deviation is higher than the 95% percentile of the empty grasp. For each finger the taxel is shown which had the highest maximum response.

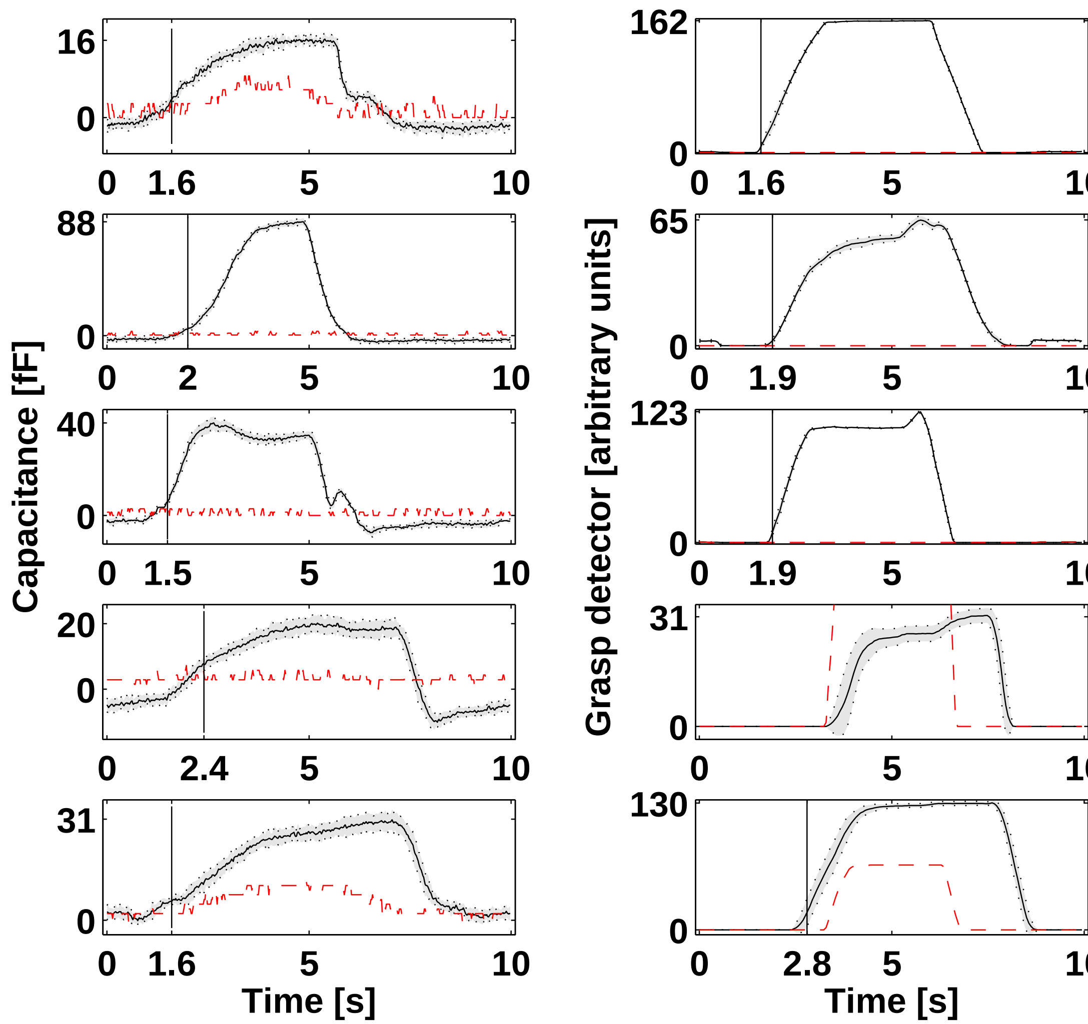

Figure 5.23: **Pressure sensor response (taxel shown with the earliest response) compared to grasp detector while grasping a .** A plot of the fingertips response (left column) and grasp detector response (right column). Rows correspond to different fingers: from the top to the bottom, thumb, index, middle, ring and little. The red line is the response when the grasp action is performed with no object. Thumb and little fingers mildly respond even if no object is present; these responses are due to imperfect grounding of the fingertip external conductive layer which produce a minor crosstalk disturbance. The black line is the average response in 20 trials. The shaded region is the standard deviation in 20 trials. The horizontal axis reports also the detection time instant; this is the time when the average sensor measurement minus the standard deviation is higher than the 95% percentile of the empty grasp. For each finger the taxel is shown which had the earliest detection time instant.

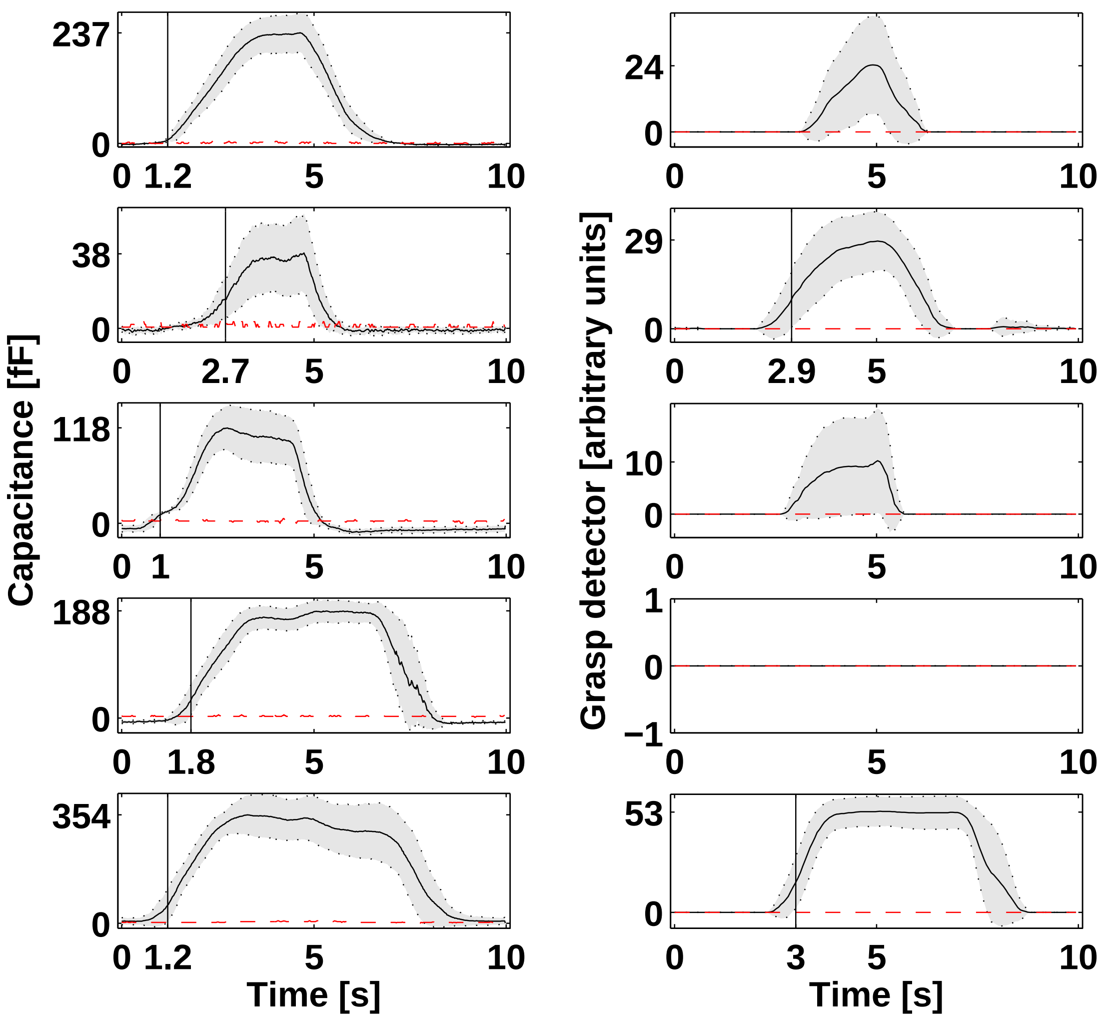

Figure 5.24: **Pressure sensor response (taxel shown with the maximum response) compared to grasp detector while grasping a coke can.** A plot of the fingertips response (left column) and grasp detector response (right column). Rows correspond to different fingers: from the top to the bottom, thumb, index, middle, ring and little. The red line is the response when the grasp action is performed with no object. The black line is the average response in 20 trials. The shaded region is the standard deviation in 20 trials. The horizontal axis reports also the detection time instant; this is the time when the average sensor measurement minus the standard deviation is higher than the 95% percentile of the empty grasp. For each finger the taxel is shown which had the highest maximum response.

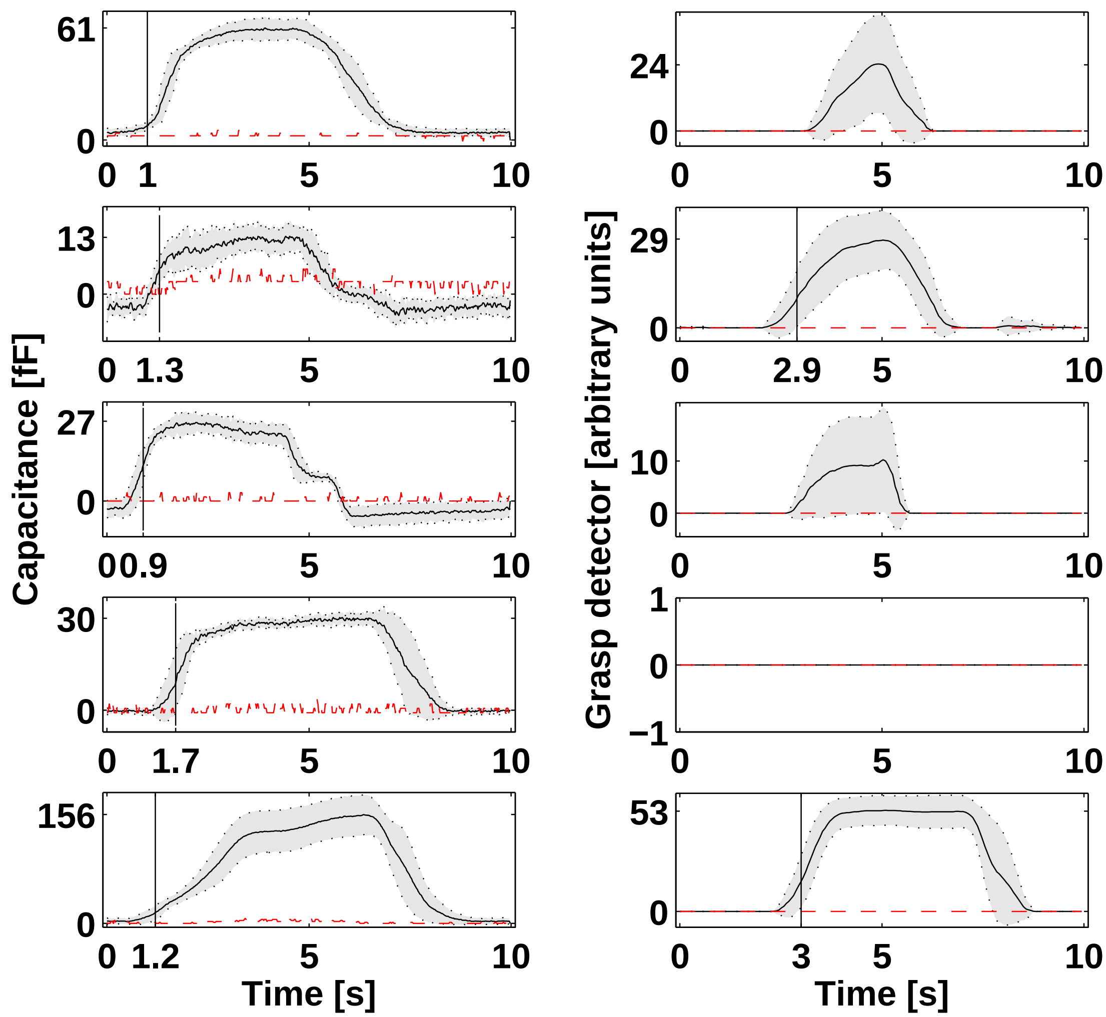

Figure 5.25: **Pressure sensor response (taxel shown with the earliest response) compared to grasp detector while grasping a .** A plot of the fingertips response (left column) and grasp detector response (right column). Rows correspond to different fingers: from the top to the bottom, thumb, index, middle, ring and little. The red line is the response when the grasp action is performed with no object. The black line is the average response in 20 trials. The shaded region is the standard deviation in 20 trials. The horizontal axis reports also the detection time instant; this is the time when the average sensor measurement minus the standard deviation is higher than the 95% percentile of the empty grasp. For each finger the taxel is shown which had the earliest detection time instant.

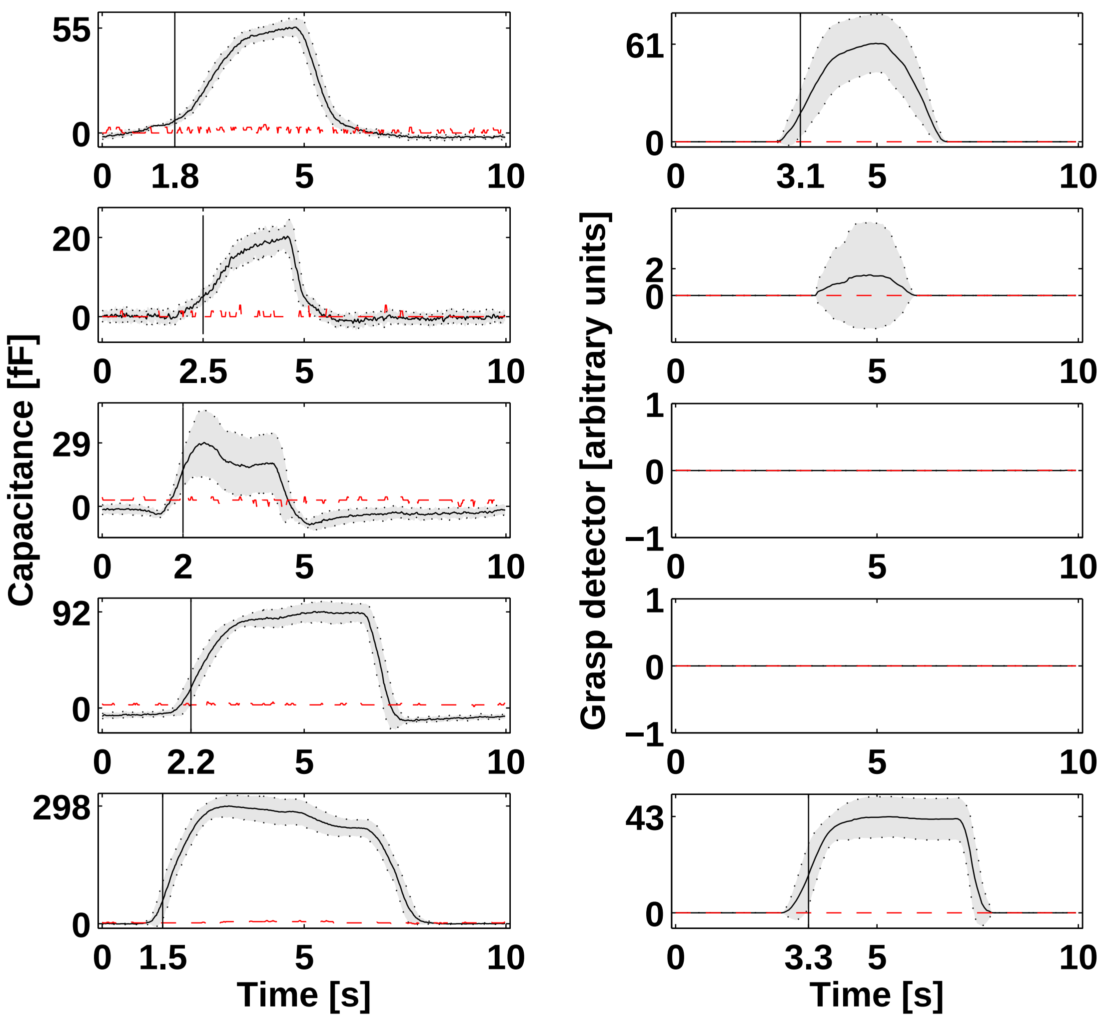

Figure 5.26: **Pressure sensor response (taxel shown with the maximum response) compared to grasp detector while grasping a plastic bottle.** A plot of the fingertips response (left column) and grasp detector response (right column). Rows correspond to different fingers: from the top to the bottom, thumb, index, middle, ring and little. The red line is the response when the grasp action is performed with no object. The black line is the average response in 20 trials. The shaded region is the standard deviation in 20 trials. The horizontal axis reports also the detection time instant; this is the time when the average sensor measurement minus the standard deviation is higher than the 95% percentile of the empty grasp. For each finger the taxel is shown which had the highest maximum response.

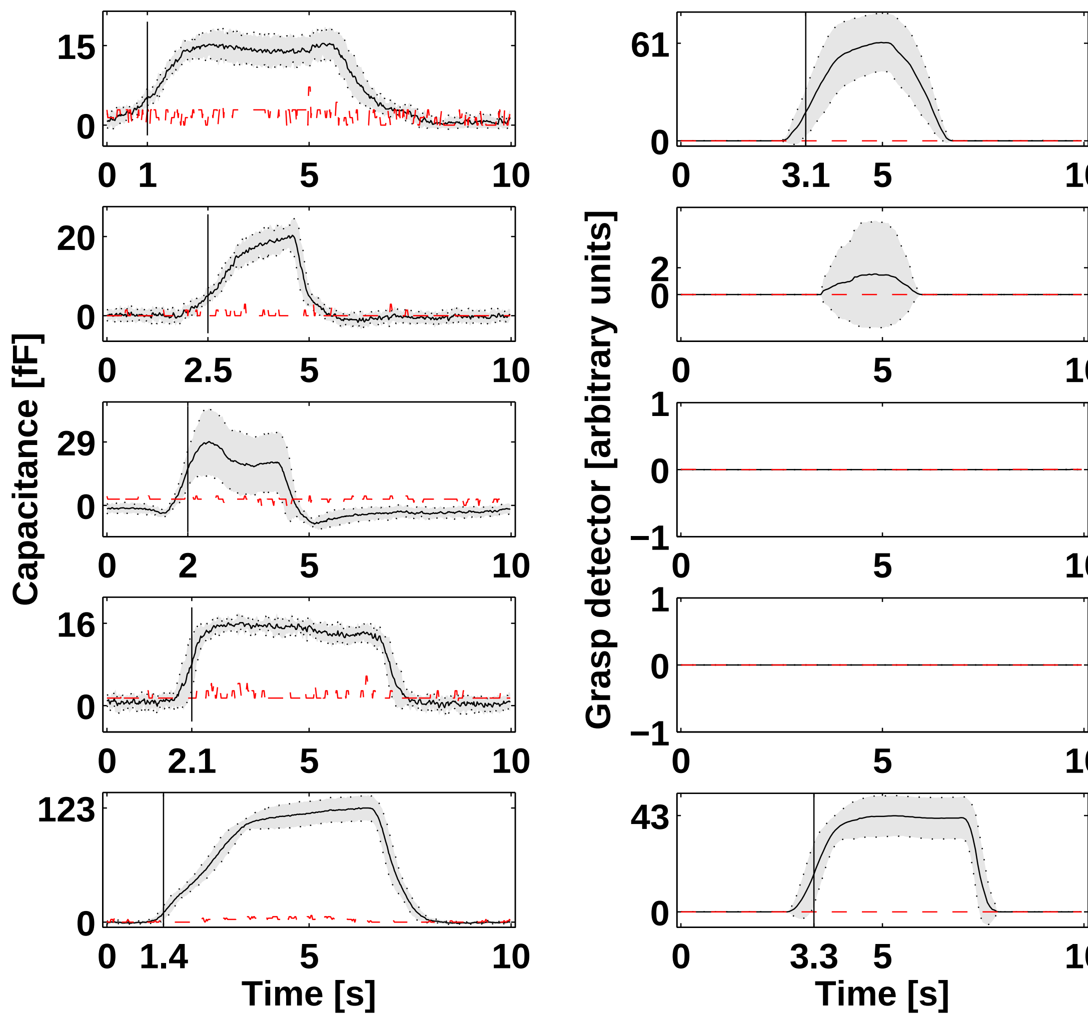

Figure 5.27: **Pressure sensor response (taxel shown with the earliest response) compared to grasp detector while grasping a .** A plot of the fingertips response (left column) and grasp detector response (right column). Rows correspond to different fingers: from the top to the bottom, thumb, index, middle, ring and little. The red line is the response when the grasp action is performed with no object. The black line is the average response in 20 trials. The shaded region is the standard deviation in 20 trials. The horizontal axis reports also the detection time instant; this is the time when the average sensor measurement minus the standard deviation is higher than the 95% percentile of the empty grasp. For each finger the taxel is shown which had the earliest detection time instant.

the 95% confidence interval on the response without object (red line). The grasp detector module sometimes fails to detect contact (for example, detection failed on the ring finger in the coke and the ladybug objects and on the middle and ring fingers during grasping of the coke and bottle). However, it is fair to say that in the experiments reported in this paper the model of eq. (B.2) was tuned using data from generic hand postures. The performance can be improved if the grasp detector is trained on the data obtained from the more specific movements performed in these experiments.

5.2.2 Grasping with Feedback Control

In the experiment described here the feedback provided from the sensors is used to grasp a fragile object, in particular a plastic cup. In the video [148] it is first shown that the iCub can crush the cup. Subsequently, with the help of the tactile sensors it grasps the same cup gently without deforming it (see Figure 5.28).

On startup iCub calibrates its sensors: it opens the hand completely and collects measurements for 5 seconds. In this way it can calculate the baseline and average noise for each taxel. To compensate for drift the algorithm described in Section 5.1.2 is employed. After the calibration, a plastic cup is placed in the hand of iCub and the grasping action is started. First, iCub grasps the cup without tactile feedback: the hand is position controlled, and the target posture was chosen to correspond to a fully closed hand. Subsequently, for the next grasping action, the robot uses tactile feedback. The algorithm is simple: for each finger, when one of the taxels in the fingertips detects touch, the movement stops; otherwise a closing movement is performed. To detect touch, the same function as for the drift compensation algorithm (see Section 5.1.2) is used: if one of the measurements minus the baseline (which is updated by the drift compensation algorithm) is bigger than the touch-threshold, it is assumed that the corresponding finger has come into contact with an object. In Figure 5.29, the resulting activation in all the taxels that reached their touch-threshold during the experiment is shown. The taxels are clearly more activated while iCub is crushing the cup then while it is grasping it gently. Ten such grasps were performed and in each case iCub grasped the cup without deforming it.

5.2.3 Discussion of the Grasping Experiments

In this section, first experiments are presented, in which the tactile fingertip sensors have been used on the iCub. In the first experiment, a predefined grasping movement was performed. The

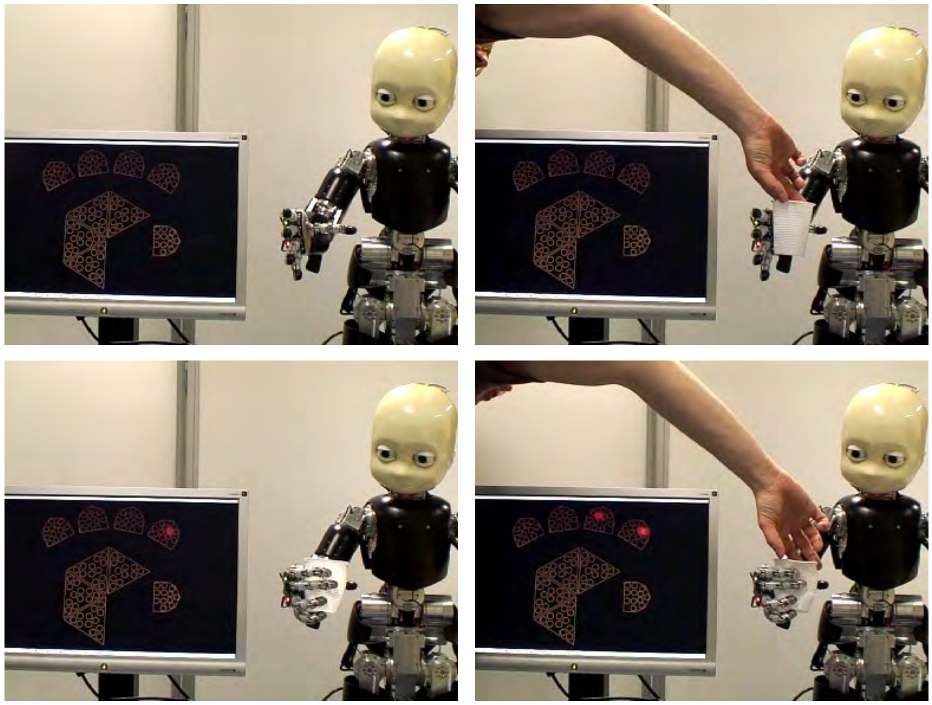

(a) Without control.

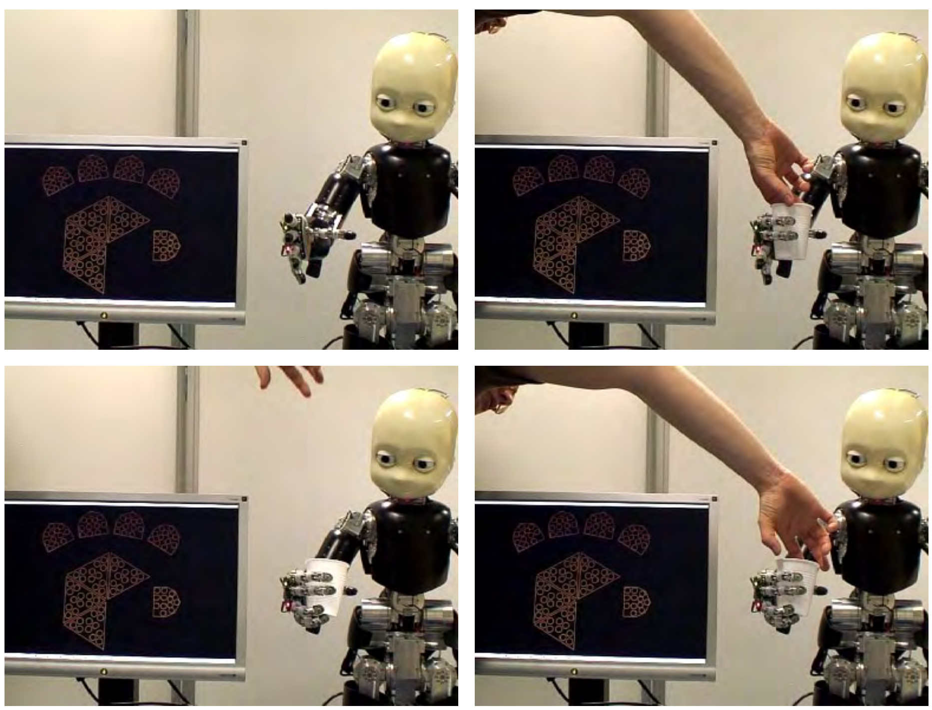

(b) With control.

Figure 5.28: **iCub is grasping a fragile plastic cup.** A picture is taken every 5 seconds from the video in [148] and the timeframe corresponds to Figure 5.29. In **(a)** the robot does not use tactile feedback and crushes the cup. In **(b)** it grasps the cup without deforming it, because it uses the tactile feedback from the fingertips. The resulting activation in the fingertips is shown; with feedback control the activation is so low that is not visible.

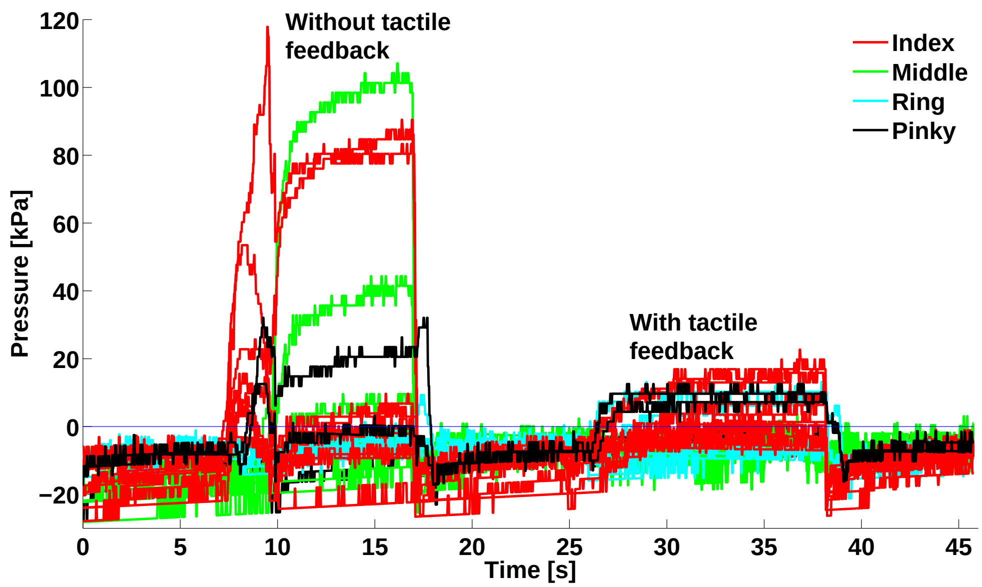

Figure 5.29: **The average activation of all taxels that reached their touch-threshold while iCub is grasping a cup with and without tactile feedback.** From each taxel its individual baseline (which includes the drift compensation) and its individual touch-threshold are subtracted; therefore, a taxel detects a touch if it measures more than 0 *Pa*. The taxels are clearly more activated when grasping the cup without tactile feedback.

tactile sensors could detect touch reliably. In the course of this experiment it is also shown that the iCub hand can reliably perform predefined movements. In the second experiment, iCub had to grasp a fragile plastic cup. Tactile feedback was used to control the grasping behaviour and the sensors proved to be sensitive enough to stop the movement before excessive force would have led to destruction of the cup. Therefore, it was concluded that the sensors can provide useful tactile feedback for iCub.

5.3 Conclusion of the Tests

The characteristics of the sensors are generally satisfying, and the sensors can be used to localize touch. The sensors are able to detect pressure of about 5 *kPa*, and can be used to gently grasp fragile objects. The measurements are repeatable, and using the drift and hysteresis compensation introduced in this chapter, the sensors can indeed be used to measure pressure within reasonable boundaries. For example, the sensitivity varies slightly between different taxels, but not to extend that would impede their usability for the humanoid robot. The biggest open problem remains the conductive ground layer of the fingertips, as it tends to fail, which will have to be avoided in the future and is being worked on, as discussed in 6.1.

Chapter 6

CONCLUSION AND FUTURE WORK

A distributed pressure sensor system with embedded digitisation was successfully incorporated into the limited dimensions of the iCub fingertip. In particular, each fingertip embeds 12 taxels and a capacitance to digital converter chip. Concerning the morphology, the fingertip has a curved shape similar to a human fingertip, and the fingertips are compliant (both factors make it easier to study and achieve human like grasping). Due to the integrated digitisation and as the same technology is used as in the triangular modules for the palm, the sensors could be readily integrated into the hand of the robot iCub. In particular, due the embedded electronics and distributed computation, few wires are necessary to connect all sensors. The fabrication of the sensors was optimized, which was important because the sensors are intended to be produced not only as prototypes but have to be (and indeed have already been) installed on a number of robots. Also the robustness of the sensors was an important design factor, but nevertheless the reliability of the fingertips has to be further improved in the future.

The sensors have been thoroughly tested. Pressure as low as 5 *kPa* or even less can be reliably detected, which is not as good as the sensitivity of humans, who can detect about 1 *kPa*, but close to. The measurements are repeatable, and using the drift and hysteresis compensation, the sensors can indeed be used to measure pressure within reasonable boundaries. For example, the sensors can clearly stand pressures higher than the 100 *kPa* that was aimed for, but with higher pressures there are increasing differences between the taxels.

Concerning the spatial sensitivity, the sensors can be used to localize touch, and for the palm the resolution nearly reaches a human level (5 *mm*). For the fingertips, the spatial sensitivity clearly lacks behind the required one to reach a human like performance (1 *mm*). Yet, the resolution is higher or at least equal to comparable tactile sensors for round fingertips, like the Shadow hand (for which otherwise few data is available) or the fingertips of TWENDY-ONE (but those fingertips are clearly bigger than the iCub fingertips and also few data concerning their performance was published).

Therefore, while the fingertips are clearly inferior to human fingertips in several aspects, most design goals (as presented in Section 1.3) have been achieved. Experiments have shown that the sensor has in general favourable characteristics and can aid the grasping process. The fingertips and palm were not only produced as prototypes, but have already been installed on numerous iCubs. Therefore, the sensors are clearly a step forward for the state of the art in robotic tactile sensing.

6.1 Future Work

A tactile sensor for the humanoid robot iCub has been presented. However, the sensor could be improved in several ways: some issues became evident in the current implementation and here possible solutions will be presented. The sensor could be also made more capable through certain modifications. In addition, not all the characteristics of the sensor have been fully investigated yet; especially the durability of the sensor has to be experimentally evaluated. Furthermore, the sensor still has to prove its use in many different grasping scenarios.

6.1.1 Improving the Reliability and the Production Process

1. In the next fingertips the components will be soldered automatically on the PCB. This is beneficial not only because it reduces the amount of manual work necessary for each fingertip, but more importantly, as reported in Section 4.1.1, imprecise soldering leads to increased measurement noise. When manually soldering the components on the PCB, slight imprecisions are unavoidable, but automatic soldering avoids this problem. The current PCBs are not ready for automatic soldering: due to the adhesive in the back of the PCBs, the panel with the PCBs is not completely flat, which makes it impossible to automatically place the components precisely. Moreover, the paper that covers the glue cannot stand the high temperatures necessary during reflow soldering. Therefore, the next version of the PCB will not have adhesive in the back: this makes it necessary to manually put a bit of glue on the PCB before aligning it with the inner support, but this work is easily achievable.

2. When using the fingertips for grasping tasks, even though the silicone foam is adhesive, it could be observed that the foam detaches from the PCB in some of the fingertips. In particular, the adhesion to the solder resist (the polymer coating the areas that should not be soldered) is

weak. Therefore, in the next version of the PCB solder resist will not be used for the areas that have to bond to the foam. In addition, if necessary, plasma bonding will be used, or if this does not work, silicone glue (which is more time consuming than the plasma bonding) to attach the foam more durably to the PCB.

3. The conductivity of the silicone and carbon black composite is rather low and the electrode layer made with it tends to fail after some time. Already in the past several other conductive materials have been tested (see Section 4.3), but so far without success. The conductive Lycra like material has proven to be a durable solution, and could be used with some modifications also for the fingertips: for example, silicone rubber should be sprayed above the Lycra like material to make it less slippery. Alternatively, other commercial products could be evaluated, for example good results have been shown in [121] with a combination of two products.

4. Other small improvements of the PCB include the electrical isolation of the hole for the screw[1] and the placement of the serial bus address designation in the front of the chip. There it will be still visible after the silicone foam has been applied.

6.1.2 Enhancing the Sensor

1. In [121] a silicone foam is used that is reported to cause less hysteresis in the sensor measurements than the one currently used. This foam will be explored for future use in the sensor.

2. Fillers in the silicone foam would increase the dielectric constant of the foam and thereby yield stronger sensor responses to the same displacement of the outer electrode layer. On the other hand, those fillers also change the mechanical characteristics of the silicone foam. For example, the fingertip could lose some of its compliance. Moreover, the gain in sensitivity due to the increased dielectric constant has to be gauged against the loss of sensitivity due to increased stiffness. Possible fillers include ionic liquid, titanium oxide, mesoporous silica (probably in combination with ionic liquid), strontium titanate and hafnium oxide. Some of the materials have already been acquired and an experimental setup has already been de-

[1] In the current implementation the edges of the hole are connected to ground and in this way the whole hand of iCub gets electronically connected to ground, which causes noise in the other components incorporated in the hand. Therefore, at the current state they have to be isolated in an extra working step.

veloped. Preliminary tests with an ionic liquid showed that the dielectric constant could be doubled without causing negative mechanical effects.

3. The other phalanges of the fingers could also be equipped with tactile sensors similar to the ones in the fingertip and the palm, which would be beneficial for the object grasping and manipulation capabilities of iCub. A preliminary layout for those sensors has already been designed.

4. A smaller version of the AD7147 chip, the AD7147A chip from *Analog Devices* is available. Using this chip, it would be possible to increase the number of taxels from 12 to 24. There would be enough space for 24 electrodes on the laps of the PCB if one reduces the diameter of each electrode to 3 *mm*. A preliminary layout for those sensors has already been designed.

5. A 3-axis force/torque sensor could be included into the fingertips, also using the capacitive technology. Basically, the metal stick that enters the fingertip would be surrounded by elastic silicone, and the fingertip could therefore slightly change its position relative to the last metal phalange of the finger. Additional flaps from the PCB could measure this displacement, which would give information about the shear forces that are acting on the fingertips.

6. The human skin can detect vibrations, temperature, air movement and pain in addition to touch. Additional sensors modalities could be added to the fingertip to detect those stimuli. Experiments using a microphone have been initiated but not concluded due to time constraints.

6.1.3 Further Testing of the Sensor Characteristics.

1. The delay due to the CAN bus should be evaluated.

2. The response of the sensor to stimuli of changing frequency should be investigated. A first indication to the frequency behaviour is provided by the study of the viscoelastic behaviour shown in Section 5.1.3.

3. Further tests regarding the repeatability and durability of the sensors should be performed. Several repetitions of the sensor measurements have been performed and the measurements are stable during this limited number of cycles. Yet, destructive tests would show how many

cycles the artificial skin can sustain before it starts to break or malfunction. For example, it has to be tested if there is a change in sensitivity over time. The aging of the sensor when not being utilized has to be compared to the one while the sensor is being used. Moreover, in the experiments so far only normal force has been applied to the sensor; the sensor should be also exposed to lateral forces, for example by rubbing it against surfaces. If aging occurs, it should be evaluated whether the sensor can be easily recalibrated.

4. While the minimum detectable pressure was measured, it would be also useful to measure the dimensions of the smallest imperfection on a surface that the robot can detect by sliding its fingers over the surface.

5. The differences in sensitivity from one fingertip to the next have to be fully explored. Differences within one sensor have already been tested, see Section 5.1.3. As every fingertip is produced by hand, variations are unavoidable and at least slight differences are probable, even though the production process has been optimized regarding the variability of the fingertips.

6.1.4 Using the Sensors

1. The robot could learn a skin to eye mapping: it could look at the areas of its skin that are touched. This could add to the sense of self of the robot.

2. The robot could perhaps use double touch to calibrate itself. For example, it could use a finger on its left hand to touch the right arm and calibrate its taxels.

3. iCub is able to reach for objects. This behaviour should be combined with the grasping based on feedback presented in this paper and would lead to a more complete behaviour.

4. The tactile sensors in the fingertips could be used to refine a grasp. The goal is that the centre of the contact with the object is in the middle of the fingertip. A possible scenario would be for example that the robot is grasping a can with two fingers, but the object is not placed correctly. As a result, the contact is not in the middle of the fingertip which would lead to an unstable grasp. Therefore, the grasp should be refined. This experiment fits into a bigger framework: visually guided reaching is error prone, and refining the grasp helps to make the behaviour more stable.

5. Features should be extracted out of the sensor measurements to aid reactive grasping. Possible features are softness/hardness, contact area (size, shape) and weight. These features could be also used for object recognition (which would be much harder to achieve on the raw sensor values).

6. Tactile following could be explored: a human touches the hand of the iCub and the robot has to follow the movements of the human.

REFERENCES

[1] M. H. Lee and H. R. Nicholls, "Tactile sensing for mechatronics: a state of the art survey," *Mechatronics*, vol. 9, pp. 1–31, 1999.

[2] R. Dahiya, G. Metta, M. Valle, and G. Sandini, "Tactile sensing: From humans to humanoids," *IEEE Transactions on Robotics*, vol. 26, no. 1, 2010.

[3] N. Tsagarakis, G. Metta, G. Sandini, D. Vernon, R. Beira, J. Santos-Victor, M. Carrazzo, F. Becchi, and D. Caldwell, "iCub - the design and realization of an open humanoid platform for cognitive and neuroscience research," *International Journal of Advanced Robotics*, vol. 21, pp. 1151–75, Oct. 2007.

[4] G. Metta, G. Sandini, D. Vernon, L. Natale, and F. Nori, "The iCub humanoid robot: an open platform for research in embodied cognition," in *PerMIS: Performance Metrics for Intelligent Systems Workshop*, (Washington DC, USA), Aug 19-21, 2008.

[5] G. Metta, D. Vernon, L. Natale, F. Nori, and G. Sandini, "The iCub humanoid robot: an open platform for research in embodied cognition," in *Proc. IEEE Workshop on Performance Metrics for Intelligent Systems*, 2008.

[6] A. Schmitz, M. P., M. Maggiali, L. Natale, G. Cannata, and G. Metta, "Methods and technologies for the implementation of large scale robot tactile sensors," *Transactions on Robotics, Special Issue on Robotic Sense of Touch*, 2011.

[7] E. S. Dellon., R. Mourey, and A. L. Dellon, "Human pressure perception values for constant and moving one- and two-point discrimination," *Plast Reconstr Surg.*, vol. 90, no. 1, pp. 112–117, 1992.

[8] R. L. Klatzky and S. J. Lederman, *Experimental Psychology*, ch. Touch, pp. 147–176. Volume 4 in I. B. Weiner (Editor-in-Chief) Handbook of psychology. New York: Wiley., 2002.

[9] S. C. B.Mannsfeld, B. C.-K. Tee, R. M. Stoltenberg, C. V. H.-H. Chen, S. Barman, B. V. O.Muir, A. N. Sokolov, C. Reese, and Z. Bao, “Highly sensitive flexible pressure sensors with microstructured rubber dielectric layers,” *Nature Materials*, vol. 9, pp. 859–864, 2010.

[10] A. Schmitz, M. Maggiali, M. Randazzo, L. Natale, and G. Metta, “A prototype fingertip with high spatial resolution pressure sensing for the robot iCub,” in *Proc. IEEE-RAS Int. Conf. on Humanoid Robots (Humanoids)*, 2008.

[11] A. Schmitz, M. Maggiali, L. Natale, B. Bonino, and G. Metta, “A tactile sensor for the fingertips of the humanoid robot iCub,” in *Proc. IEEE/RSJ Int. Conf. on Intelligent Robots and Systems (IROS)*, 2010.

[12] A. Schmitz, M. Maggiali, L. Natale, and G. Metta, “Integrating tactile sensors into the hands of the humanoid robot icub,” in *ICRA Workshop on Grasping*, 2010.

[13] A. Schmitz, M. Maggiali, L. Natale, and G. Metta, “Touch sensors for humanoid hands,” in *Proc. 19th IEEE Int. Symposium in Robot and Human Interactive Communication (Ro-Man)*, 2010.

[14] A. Schmitz, U. Pattacini, F. Nori, L. Natale, G. Metta, and G. Sandini, “Design, realization and sensorization of a dextrous hand: the iCub design choices,” in *Proc. IEEE-RAS Int. Conf. on Humanoid Robots (Humanoids)*, 2010.

[15] R. S. Johansson and J. R. Flanagan, “Coding and use of tactile signals from the fingertips in object manipulation tasks,” *Nature Reviews Neuroscience*, vol. 10, pp. 345–359, 2009.

[16] G. Robles-De-La-Torre, “The importance of the sense of touch in virtual and real environments,” *IEEE Multimedia*, vol. 13, no. 3, pp. 24–30, 2006.

[17] G. Westling and R. S. Johannson, “Factors influencing the force control during precision grip,” *Exp. Brain Res*, vol. 53, p. 277–284, 1984.

[18] H. Iwata, “Design of human symbiotic robot TWENDY-ONE,” in *Proc. IEEE Int. Conf. on Robotics and Automation (ICRA)*, 2009.

[19] A. Bierbaum, M. Rambow, T. Asfour, and R. Dillmann, "A potential field approach to dexterous tactile exploration of unknown objects," in *Proc. IEEE-RAS Int. Conf. on Humanoid Robots (Humanoids)*, 2008.

[20] S. Chitta, M. Piccoli, and J. Sturm, "Tactile object class and internal state recognition for mobile manipulation," in *Proc. IEEE Int. Conf. on Robotics and Automation (ICRA)*, 2010.

[21] J. Flanagan, P. Vetter, R. S. Johansson, and D. M. Wolpert, "Prediction precedes control in motor learning," *Current Biology*, vol. 13, pp. 146–150, 2003.

[22] A. Bierbaum, T. Asfour, and R. Dillmann, "Dynamic potential fields for dexterous tactile exploration," in *Human Centered Robot Systems*, vol. 6, pp. 23–31, Springer Berlin Heidelberg, 2009. HCRS Workshop, Bielefeld.

[23] L. Natale and E. Torres-Jara, "A sensitive approach to grasping," in *Proc. 6th Int. Conf. on Epigenetic Robotics*, 2006.

[24] J. J. Gibson, *The Theory of Affordances*. Lawrence Erlbaum, 1977.

[25] P. Cisek, "Beyond the computer metaphor: behavior as interaction," *Journal of Consciousness Studies*, vol. 6, no. 12, pp. 125–142, 1999.

[26] G. Metta and P. Fitzpatrick, "Better vision through manipulation," *Adaptive Behavior*, vol. 11, pp. 109–128, June 2003.

[27] R. Klatzky and S. Lederman, "Hand movements: a window into haptic object recognition," *Cognitive Psychology*, vol. 19, pp. 342–368, 1987.

[28] A. Clark, *Being There - Putting Brain, Body and World Together Again*. Cambridge, MA, USA/London, UK: MIT Press/Bradford Books, 1997.

[29] L. Natale, G. Metta, and G. Sandini, "A developmental approach to grasping," in *Proc. Developmental Robotics 2005 AAAI Spring Symposium*, 2005.

[30] M. A. Goodale, D. A. Westwood, and A. D. Milner, "Two distinct modes of control for object-directed action," *Prog Brain Res*, vol. 144, pp. 131–144, 2004.

[31] M. Lungarella, G. Metta, R. Pfeifer, and G. Sandini, "Developmental robotics: a survey," *Connection Science*, vol. 15, no. 4, pp. 151–190, 2003.

[32] A. M. Borghi, "Object concepts and action," in *Grounding Cognition: The role of perception and action in memory, language, and thinking* (D. Pecher and R. A. Zwaan, eds.), Cambridge, UK: Cambridge University Press, 2005.

[33] A. M. Glenberg, "What memory is for," *Behavioral and Brain Sciences*, vol. 20, no. 1, pp. 1–55, 1997.

[34] D. Wolpert, K. Doya, and M. Kawato, "A unifying computational framework for motor control and social interaction," in *The Neuroscience of Social Interaction* (C. Frith and D. M. Wolpert, eds.), pp. 305–322, Oxford, UK: Oxford University Press, 2004.

[35] J.-M. Jacob, P., "The motor theory of social cognition: a critique," *Trends in Cognitive Neuroscience*, vol. 9, pp. 21–25, 2005.

[36] M. Jeannerod, "Neural simulation of action: A unifying mechanism for motor cognition," *NeuroImage*, vol. 14, no. 1, pp. 103–109, 2001.

[37] J. Tani, "Articulation of sensory-motor experiences by 'forwarding forward model': From robot experiments to phenomenology," in *Proceedings of the 7th International Conference on Simulation of Adaptive Behavior (SAB'02)* (B. Hallam, D. Floreano, G. Hayes, J. Meyer, and J. Hallam, eds.), pp. 171–180, 2002.

[38] G. V., F. L., F. L., and R. G, "Action recognition in the premotor cortex," *Brain*, vol. 119, pp. 593–609, 1996.

[39] G. Rizzolatti, M. Fabbri-Destro, and L. Cattaneo, "Mirror neurons and their clinical relevance," *Nat Clin Pract Neurol*, vol. 5, no. 1, pp. 24–34, 2009.

[40] R. Pfeifer and G. Gomez, *Understanding Intelligence*. MIT Press Cambridge, MA, USA, 1999.

[41] S. H. Scott, “A motor learning strategy reflects neural circuitry for limb control,” *Nature Neuroscience*, vol. 6, pp. 399–403, 2003.

[42] L. Natale, F. Nori, G. Metta, and G. Sandini, “Learning precise 3d reaching in a humanoid robot,” in *Proc. IEEE Int. Conf. of Development and Learning*, 2007.

[43] M. Botvinick and J. Cohen, “Rubber hands ”feel” touch that eyes see,” *Nature*, vol. 391, p. 756, 1998.

[44] A. Maravita, C. Spence, and J. Driver, “Multisensory integration and the body schema: Close to hand and within reach,” *Current biology*, vol. 13, pp. 531–539, 2003.

[45] G. Rizzolatti, L. Fadiga, L. Fogassi, and G. V., “The space around us.,” *Science*, pp. 190–191, 1997.

[46] J. Bongard, V. Zykov, and H. Lipson, “Resilient machines through continuous self-modeling,” *Science*, vol. 314, pp. 1118–1121, 2006.

[47] M. Hersch, E. Sauser, and A. Billard, “Online learning of the body schema,” *International Journal of Humanoid Robotics*, vol. 5, no. 2, pp. 161–181, 2008.

[48] G. Cannata, S. Denei, and F. Mastrogiovanni, “Towards automated self-calibration of robot-skin,” in *Proc. IEEE Int. Conf. on Robotics and Automation (ICRA)*, 2010.

[49] T. M. Kubow and R. J. Full, “The role of the mechanical system in control: a hypothesis of self-stabilization in hexapedal runners,” *Philosophical Transactions of the Royal Society B: Biological Sciences*, vol. 354, pp. 849–861, May 1999.

[50] M. Desmurget and S. Grafton, “Forward modeling allows feedback control for fast reaching movements.,” *Trends in Cognitive Science*, vol. 4, pp. 423–431, November 2000.

[51] M. H. Dickinson, C. T. Farley, R. J. Full, M. A. R. Koehl, R. Kram, and S. Lehman, "How animals move: An integrative view," *Science*, vol. 288, pp. 100–106, April 2000.

[52] F. Iida, G. Gomez, and R. Pfeifer, "Exploiting body dynamics for controlling a running quadruped robot," in *Proc. 12th Int. Conf. on Advanced Robotics (ICAR)*, 2005.

[53] R. Pfeifer, F. Iida, and J. Bongard, "New robotics: Design principles for intelligent systems," *Artif. Life*, vol. 11, pp. 99–120, January 2005.

[54] L. Jamone, G. Metta, F. Nori, and G. Sandini, "James: A humanoid robot acting over an unstructured world," in *Proc. 6th IEEE-RAS Int. Conf. on Humanoid Robots (Humanoids)*, 2006.

[55] F. Lotti, P. Tiezzi, G. Vassura, L. Biagiotti, G. Palli, and C. Melchiorri, "Development of UB hand 3: Early results.," in *Proc. IEEE Int. Conf. on Robotics and Automation (ICRA 2005)*, pp. pp. 4488–4493, 2005.

[56] G. A. Kragten and J. L. Herder, "A platform for grasp performance assessment in compliant or underactuated hands," *Journal of Mechanical Design*, vol. 132, pp. 1–6, 2010.

[57] J. M. Loomis and S. J. Lederman, *Handbook of perception and human performance*, ch. Tactual perception., pp. 31–41. New York: Wiley, 1986.

[58] C. S. Sherrington, *The integrative action of the nervous system.* New Haven, CT: Yale University Press, 1906.

[59] R. S. Johansson and A. B. Vallbo, "Tactile sensibility in the human hand: relative and absolute densities of four types of mechanoreceptive units in glabrous skin," *Journal of Physiology*, vol. 286, pp. 283–300, 1979.

[60] J. C. Craig and K. B. Lyle, "A comparison of tactile spatial sensitivity on the palm and fingerpad," *Perception & Psychophysics*, vol. 63, pp. 337–347, 2001.

[61] H. Nicholls and M. Lee, "A survey of robot tactile sensing technology," *The International Journal of Robotics Research*, vol. 8, no. 3, pp. 3–30, 1989.

[62] P. Puangmali, K. Althoefer, L. D. Seneviratne, D. Murphy, and P. Dasgupta, “State-of-the-art in force and tactile sensing for minimally invasive surgery,” *IEEE Sensors Journal*, vol. 8, no. 4, pp. 371–381, 2008.

[63] R. D. Howe, “Tactile sensing and control of robotic manipulation,” *Journal of Advanced robotics*, vol. 8, no. 3, pp. 245–261, 1994.

[64] L. Biagiotti, F. Lotti, C. Melchiorri, and G. Vassura, “How far is the human hand? a review on anthropomorphic robotic end-effectors,” 2002.

[65] B. D. Argall and A. G. Billard, “A survey of tactile human robot interactions,” *Robotics and Autonomous Systems*, vol. 58, no. 10, pp. 1159–1176, 2010.

[66] H. Liu, P. Meusel, N. Seitz, B. Willberg, G. Hirzinger, M. Jin, Y. Liu, R. Wei, and Z. Xie, “The modular multisensory DLR-HIT-hand,” *Mechanism and Machine Theory*, vol. 42, pp. 612–625, May 2007.

[67] H. Liu, K. Wu, P. Meusel, N. Seitz, G. Hirzinger, M. Jin, Y. Liu, S.W.Fan, T. Lan, and Z. P. Chen, “Multisensory five-finger dexterous hand: The DLR/HIT Hand II,” in *Proc. IEEE/RSJ International Conference on Intelligent Robots and Systems (IROS)*, 2008.

[68] P. Dario, C. Laschi, A. Menciassi, E. Guglielmelli, M. C. Carrozza, M. Zecca, L. Zollo, G. Teti, L. Beccai, F. Vecchi, and S. Roccella, “A human-like robotic manipulation system implementing human models of sensory-motor coordination,” in *Proc. 3rd IEEE-RAS Int. Conf. on Humanoid Robots (Humanoids)*, 2003.

[69] ATI, “F/T sensor nano17.” [Online]. Available: www.ati-ia.com/products/ft/ft_models.aspx?id=Nano17. retrieved Nov. 6th, 2010.

[70] K. Kaneko, K. Harada, and F. Kanehiro, “Development of multi-fingered hand for life-size humanoid robots,” in *IEEE International Conference on Robotics and Automation (ICRA)*, 2007.

[71] R. Platt Jr, F. Permenter, and J. Pfeiffer, “Inferring hand-object configuration directly from tactile data,” in *Workshop on Mobile Manipulation, ICRA 2010*, 2010.

[72] B. Edin, L. Beccai, L. Ascari, S. Roccella, J. Cabibihan, and M. Carrozza, "Bio-inspired approach for the design and characterization of a tactile sensory system for a cybernetic prosthetic hand," in *Proc. IEEE International Conference on Robotics and Automation*, 2006.

[73] T. Mouri, H. Kawasaki, K. Yoshikawa, J. Takai, and S. Ito, "Anthropomorphic robot hand: Gifu Hand III," in *Proc. Int. Conf. on Control, Automation and Systems (ICCAS)*, pp. 1288–1293, October 2002.

[74] G. Cannata and M. Maggiali, "An embedded tactile and force sensor for robotic manipulation and grasping," in *Proc. IEEE-RAS Int. Conf. on Humanoid Robots (Humanoids)*, 2005.

[75] M. Zecca, S. Roccella, G. Cappiello, K. Ito, K. Imanishi, H. Miwa, M. Carrozza, P. Dario, and A. Takanishi, "From the human hand to a humanoid hand: Biologically-inspired approach for the development of robocasa hand 1," in *Proc. 16th CISM-IFToMM Symposium on Robot Design, Dynamics, and Control*, pp. 287–294, 2006.

[76] T. B. Martin, R. O. Ambrose, and J. M. Butzer, "Tactile gloves for autonomous grasping with the nasa/darpa robonaut," in *Proc. IEEE Int. Conf. on Robotics and Automation (ICRA)*, 2004.

[77] Interlink Electronics, "Force senors." [Online]. Available: http://www.interlinkelectronics.com/catalog/Force-Sensors.

[78] T. Iberall, G. Sukhatme, D. Beattie, and G. Bekey, "Control philosophy and simulation of a robotic hand as a model for prosthetic hands," in *Proc IEEE/RSJ International Conference on Intelligent Robots and Systems (IROS)*, 1993.

[79] H. Liu, P. Meusel, and G. A. Hirzinger, "A tactile sensing system for the three-finger robot hand," in *Proc. Int. Symposium on DLR Measurement and Control in Robotics*, pp. 91–96, 1995.

[80] T. H. Speeter, "A tactile sensing system for robotic manipulation," *The International Journal of Robotics Research*, vol. 9, no. 6, pp. 25–36, 1990.

[81] Tekscan, “Tekscan pressure sensors.” [Online]. Available: http://www.tekscan.com/pressure-sensors, December 2010.

[82] Tekscan, “Grip system.” [Online]. Available: http://www.tekscan.com/grip-pressure-measurement, December 2010.

[83] G. Cannata and M. Maggiali, *Sensors: Focus on Tactile Force and Stress Sensors*, ch. Design of a Tactile Sensor for Robot Hands, pp. 271–288. Croatia: InTech, 2008.

[84] H. Nakamoto, F. Kobayashi, N. Imamura, and H. Shirasawa, “Universal robot hand base equipped with tactile and joint torque sensors - development and experiments on stiffness control and object recognition,” *Journal of Systemics, Cybernetics and Informatics*, vol. 5, no. 2, pp. 79–84, 2007.

[85] H. Sugiuchi, S. Watanabe, Y. Hasegawa, and M. Nornoto, “A control system for multi-fingered robotic hand with distributed touch sensor,” in *26th Annual Conference of the IEEE Industrial Electronics Society (IECON)*, 2000.

[86] M. Shimojo, “A tactile sensor sheet using pressure conductive rubber with electrical wires stitched method,” *IEEE Sensor Journal*, vol. 4, no. 5, pp. 589–596, 2004.

[87] K. Weiss and H. Wörn, “Tactile sensor system for an anthropomorphic robotic hand,” in *Proc. IEEE International Conference on Humanoid Robots*, 2004.

[88] K. Weiß, D. Göger, and H. Wörn, “Reactive grasping in industrial automation,” in *Tagungsband der 4. Deutschen Robotik-Konferenz, München*, 2006.

[89] W. Robotics. [Online]. Available: www.weiss-robotics.de.

[90] G. Heidemann and M. Schöpfer, “Dynamic tactile sensing for object identification,” in *Proc. IEEE International Conference on Robotics and Automation (ICRA)*, 2004.

[91] A. J. Schmid, N. Gorges, D. Göger, and H. Wörn, “Opening a door with a humanoid robot using multi-sensory tactile feedback,” in *IEEE International Conference on Robotics and Automation*, 2008.

[92] D. Göger, N. Gorges, and H. Wörn, "Tactile sensing for an anthropomorphic robotic hand: Hardware and signal processing," in *Proc. IEEE International Conference on Robotics and Automation (ICRA)*, 2009.

[93] B. Choi, S. Lee, H. R. Choi, and S. Kang, "Development of anthropomorphic robot hand with tactile sensor : SKKU hand II," in *Proc. IEEE/RSJ International Conference on Intelligent Robots and Systems*, 2006.

[94] J. Jockusch, J. Walter, and H. Ritter, "A tactile sensor system for a three-fingered robot manipulator," in *Proc. IEEE International Conference on Robotics and Automation*, 1997.

[95] K. Hosoda, Y. Tada, and M. Asada, "Anthropomorphic robotic soft fingertip with randomly distributed receptors," *Robotics and Autonomous Systems*, vol. 54, no. 2, pp. 104–109, 2006.

[96] Shadow Hand Company, "The shadow tactile sensor - datasheet," April 2007.

[97] Shadow Hand Company, "Shadow tactile sensor." [Online]. Available: www.shadowrobot.com/tactile, 2010.

[98] Shadow Hand Company, "Shadow dexterous hand C5 - technical specification," May 2008.

[99] Y. Ohmura, Y. Kuniyoshi, and A. Nagakubo, "Conformable and scalable tactile sensor skin for curved surfaces," in *Proc. IEEE Int. Conf. on Robotics and Automation (ICRA)*, 2006.

[100] Y. Ohmura and Y. Kuniyoshi, "Humanoid robot which can lift a 30kg box by whole body contact and tactile feedback," in *Proc. IEEE/RSJ Int. Conf. on Intelligent Robots and Systems (IROS)*, 2007.

[101] T. Mukai, M. Onishi, S. Hirano, and Z. Luo, "Development of the tactile sensor system of a human-interactive robot "RI-MAN"," *IEEE Transactions on Robotics*, vol. 24, pp. 505–512, April 2008.

[102] O. Kerpa, K. Weiss, and H. Wörn, "Development of a flexible tactile sensor system for a humanoid robot," in *Proc. IEEE/RSJ International Conference on Intelligent Robots and Systems 2003*, 2003.

[103] D. Göger, K. Weiss, C. Burghart, and H. Wörn, "Sensitive skin for a humanoid robot," in *Human-Centered Robotic Systems (HCRS´06)*, 2006.

[104] I. Mizuuchi, T. Yoshikai, T. Nishino, and M. Inaba, "Development of musculoskeletal humanoid Kotaro," in *Proc. IEEE Int. Conf. on Robotics and Automation (ICRA)*, 2006.

[105] T. Miyashita, T. Tajika, H. Ishiguro, K. Kogure, and N. Hagita, *Robotics Research*, vol. 28, ch. Haptic Communication between Humans and Robots, pp. 525–536. Springer-Verlag, Berlin, Heidelberg, Germany, 2007.

[106] N. Mitsunaga, T. Miyashita, H. Ishiguro, K. Kogure, and N. Hagita, "Robovie-iv: a communication robot interacting with people daily in an office," in *Proc. IEEE/RSJ International Conference on Intelligent Robots and Systems (IROS)*, 2006.

[107] T. Tajika, T. Miyashita, H. Ishiguro, and N. Hagita, "Reducing influence of robot's motion on tactile sensor based on partially linear model," in *IEEE/RSJ International Conference on Intelligent Robots and Systems (IROS)*, 2008.

[108] T. Minato, M. Shimada, H. Ishiguro, and S. Itakura, "Development of an android robot for studying human-robot interaction," in *Proc. 17th international conference on Innovations in applied artificial intelligence*, pp. 424–434, 2004.

[109] D. Matsui, T. Minato, K. MacDorman, and H. Ishiguro, "Generating natural motion in an android by mapping human motion," in *Proc. IEEE/RSJ International Conference on Intelligent Robots and Systems (IROS)*, 2005.

[110] T. Minato, Y. Yoshikawa, H. Ishiguro, and M. Asada, "CB2: A child robot with biomimetic body for cognitive developmental robotics," in *Proc. IEEE-RAS 7th Int. Conf. on Humanoid Robots (Humanoids)*, 2007.

[111] T. Tajika, T. Miyashita, and H. Ishiguro, "Automatic categorization of haptic interactions-what are the typical haptic interactions between a human and a robot?," in *Proc. IEEE-RAS Int. Conf. on Humanoid Robots (Humanoids)*, 2006.

[112] T. Sekitani and T. Someya, “Stretchable, large-area organic electronics,” *Advanced Materials*, vol. 22, no. 20, p. 2228–2246, 2010.

[113] H. Alirezaei, A. Nagakubo, and Y. Kuniyoshi, “Development of a highly stretchable tactile sensor with easy wearability,” in *Proc. Humanoids 09 Workshop: Tactile Sensing in Humanoids - Tactile Sensors and Beyond*, 2009.

[114] H. Alirezaei, A. Nagakubo, and Y. Kuniyoshi, “A tactile distribution sensor which enables stable measurement under high and dynamic stretch,” in *IEEE Symposium on 3D User Interfaces*, 2009.

[115] S. Miyazaki and A. Ishida, “Capacitive transducer for continuous measurement of vertical foot force,” *Med. Biol. Eng. Comput.*, vol. 22, p. 309–316, 1984.

[116] Z. Chu, P. M. Sarro, and S. Middelhoek, “Silicon three-axial tactile sensor,” *Sens. Actuators A*, vol. 54, pp. 505–510, 1996.

[117] B. L. Gray and R. S. Fearing, “A surface micromachined microtactile sensor array,” in *Proc. Int. Conf. on Robotic Automation (ICRA)*, 1996.

[118] R. J. D. Souza and K. D. Wise, “A very high density bulkmicromachined capacitive tactile imager,” in *Proc. Int. Conf. Solid-State Sens. Actuators, Transducers*, pp. 1473–1476, 1997.

[119] D. Siegel, I. Garabieta, and J. Hollerbach, “An integrated tactile and thermal sensor,” in *Proc. IEEE International Conference on Robotics and Automation*, 1986.

[120] F. Castelli, “An integrated tactile-thermal robot sensor with capacitive tactile array,” *IEEE Transactions on Industrial Applications*, vol. 38, no. 1, pp. 85–90, 2002.

[121] J. Ulmen and M. Cutkosky, “A robust, low-cost and low-noise artificial skin for human-friendly robots,” in *Proc. IEEE Int. Conf. on Robotics and Automation (ICRA)*, 2010.

[122] P. A. Schmidt, E. Mael, and R. P. Wurtz, “A sensor for dynamic tactile information with applications in human-robot interaction & object exploration,” *Robot. Autonomous Syst.*, vol. 54, pp. 1005–1014, 2006.

[123] K. Wada and T. Shibata, "Social effects of robot therapy in a care house - change of social network of the residents for two months," in *Proc. IEEE International Conference on Robotics and Automation (ICRA)*, 2007.

[124] J. J. S. Johnston, D.; Ping Zhang; Hollerbach, "A full tactile sensing suite for dextrous robot hands and use in contact force control," in *Proc. IEEE International Conference on Robotics and Automation*, 1996.

[125] D. Siegel, S. Drucker, and I. Garabieta, "Performance analysis of a tactile sensor," in *Proc. IEEE International Conference on Robotics and Automation*, 1987.

[126] Apple Inc., "iPod Touch Technology." [Online]. Available: http://www.apple.com/ipodtouch/features/technology.html, 2009.

[127] Analog Devices Inc., "AD7147 technical datasheet," 2008.

[128] Pressure Profile Systems Inc., "PPS-products." [Online]. Available: http://www.pressureprofile.com/products.php, 2010.

[129] G. Stellin, G. Cappiello, S. Roccella, M. C. Carrozza, P. Dario, G. Metta, G. Sandini, and F. Becchi, "Preliminary design of an anthropomorphic dexterous hand for a 2-years-old humanoid: towards cognition," in *Proc. IEEE BioRob*, 2006.

[130] G. Stellin, C. Cipriani, F. Zaccone, M. Carrozza, and P. Dario, "Design of an anthropomorphic dexterous hand for a 2-years-old humanoid: Ongoing work," in *Proc. RoManSy*, 2008.

[131] L.-W. Tsai, *Robot Analysis: The Mechanics of Serial and Parallel Manipulators*. Wiley-IEEE, 1999.

[132] CarlStahl, "Stain-steel wires." [Online]. Available: http://www.carlstahl.de.

[133] Royal DSM, "Dyneema synthetic fiber." [Online]. Available: http://www.dyneema.com.

[134] M. Santello, M. Flanders, and J. F. Soechting, "Postural hand synergies for tool use," *Journal of Neuroscience*, vol. 18, pp. 10105–10115, December 1998.

[135] F. Reverter, X. Li, and G. C. M. Meijer, “Stability and accuracy of active shielding for grounded capacitive sensors,” *Measurement Science and Technology*, vol. 17, no. 11, p. 2884, 2006.

[136] Palmer, W., Analog Devices Inc., “Capacitance sensing in human body contact applications,” *Sensors*, July 1 2010.

[137] K. Staunton, “AC shield enhances remote capacitive sensing..” [Online]. Available: http://www.analog.com/library/analogdialogue/archives/42-05/AD7147_captouch.html.

[138] O. A. Shergold, N. A. Fleck, and D. Radford, “The uniaxial stress versus strain response of pig skin and silicone rubber at low and high strain rates,” *International Journal of Impact Engineering*, vol. 32, no. 9, pp. 1384 – 1402, 2006.

[139] M. Morton, *Rubber Technology*. Springer, 1987.

[140] V. Georgakilas, K. Kordatos, M. Prato, D. M. Guldi, M. Holzinger, and A. Hirsch, “Organic functionalization of carbon nanotubes,” *J. AM. CHEM. SOC.*, vol. 124, no. 5, pp. 760–761, 2002.

[141] T. Fukushima, A. Kosaka, Y. Ishimura, T. Yamamoto, T. Takigawa, N. Ishii, and T. Aida, “Molecular ordering of organic molten salts triggered by single-walled carbon nanotubes,” *Science*, vol. 300, pp. 2072–2074, 2003.

[142] M. Randazzo, R. Buzio, G. Metta, G. Sandini, and U. Valbusa, “Architecture for the semiautomatic fabrication and assembly of thin-film based dielectric elastomer actuators.,” in *Proc. Electroactive Polymer Actuators and Devices (EAPAD)*, 2008.

[143] R. Dahiya, M. Valle, L. Lorenzelli, and G. Metta, “Tactile sensing arrays for humanoid robots using piezo-polymer-fet devices.,” in *Proc. AISEM, 13th Nat. Conf. Sensors and Microsystems.*, 2008.

[144] G. Habenicht, *Kleben: Grundlagen, Technologien, Anwendungen*. Springer, 6., aktualisierte auflage ed., 2008.

[145] Z. Zeng, L. Zheng, and D. Ling, “A compensation method of the offset thermal drift of sensor using the neural network algorithm,” in *Proc. ICSP*, 2008.

[146] W. N. Findley, J. S. Lai, and K. Onaran, *Creep and relaxation of nonlinear viscoelastic materials*. Courier Dover Publications, 1989.

[147] M.-A. Lacasse, V. Duchaine, and C. Gosselin, “Characterization of the electrical resistance of carbon-black-filled silicone: Application to a flexible and stretchable robot skin,” in *Proc. IEEE Int. Conf. on Robotics and Automation (ICRA)*, 2010.

[148] A. Schmitz, “iCub grasps a fragile plastic cup with its tactile senors.” [Online]. Available: youtube, robotcub’s channel, www.youtube.com/watch?v=jQfX2SyxxXo, 2010.

[149] G. Cannata, R. S. Dahiya, M. Maggiali, F. Mastrogiovanni, G. Metta, and M. Valle, “Modular skin for humanoid robot systems,” in *Proc. 4th Int. Conf. on Cognitive Systems*, 2010.

[150] “iCub open source software repository documentation.” [Online]. Available: http://eris.liralab.it/iCub/dox/html/index.html.

Appendix A

TRIANGULAR MODULES FOR THE PALM

In parallel to the development of the fingertips, a “skin” has been developed by Dr. Marco Maggiali to cover large generic areas of humanoid robots. This skin uses the same capacitive technology that is also used for the fingertips. The expertise gained while designing the fingertips influenced the design of the palms and vice versa. Like in the final version of the fingertip, the basis of the skin is a flexible printed circuit board, which includes both 12 disc shaped pads that act as electrodes and the electronics to acquire 12 measurements and send of them over an I^2C serial bus. Unlike in the fingertips, the 12 pads have a diameter of 4 *mm*, electrically conductive fabric is used as the second conductive layer above the dielectric and the shape of the PCB is a triangle (all sides are 3 *cm* long). The triangular shape was chosen in analogy to polygonal modelling in 3D computer graphics, which uses triangles to describe the shapes of objects. The triangles can conform up to a certain degree to generic smooth curved surfaces [149], but not to the shape of the fingertip of iCub. The triangles can also communicate between themselves: three communications ports placed along the sides of the triangle relay the signals from one triangle to the adjacent ones. Up to 16 triangles can be connected in this way (4 serial buses with 4 different addresses each) and only one of them needs to be connected to a microcontroller board. These triangular modules have been used to sensorize the palms of iCub. Each palm incorporates four triangular modules. The triangular modules have also been incorporated into other parts of iCub and other robots [6]. The implementation steps for the palm are reported in Figure A.1.

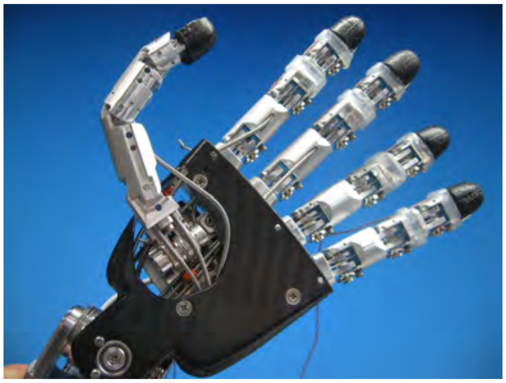

(a)

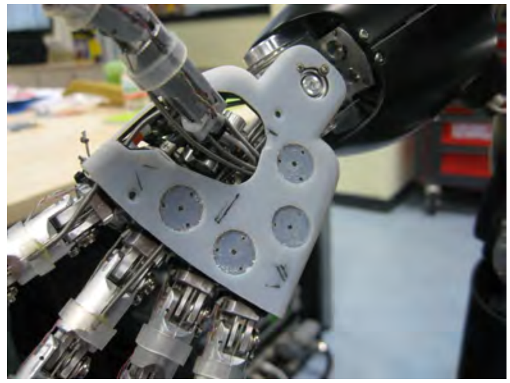

(b)

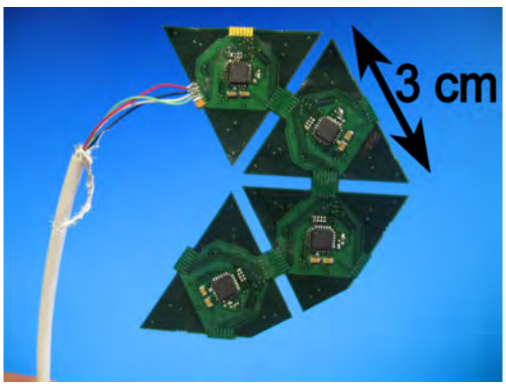

(c)

(d)

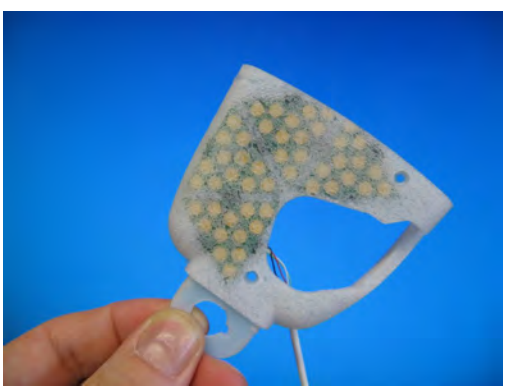

(e)

(f)

Figure A.1: **The production steps for the palm of iCub.** **(a)** The palm without the tactile sensor. **(b)** The housing for the electronics is produced with a 3D printer (Eden 3D printer from *Objet*). Shallow round holes provide space for the CDC chip and the other electronic components which are soldered on the PCB. **(c)** The mesh of flexible PCBs that is needed to cover the palm. The PCBs are shown from the back and their size is indicated. **(d)** Bonding of the PCBs on the part with bi-component glue and the help of a vacuum system. **(e)** The PCBs are covered with silicone foam. To this aim a specific purpose-built mould is employed. **(f)** The silicone foam is covered with conductive Lycra like material.

Appendix B

GRASP DETECTOR

The grasp dector described here, based on the tendons, is not part of this thesis, but is described as it was used as a reference for some of the experiments described within this thesis. Details can be found at [150], and the algorithm was published in [14].

Open-ended tendon drives such as the ones used in the iCub hand distal joints can be used to detect the presence of external forces. In practice, the coupling equations, "(2.2)" or "(2.3), (2.4) and (2.5)", hold only in absence of external forces. Therefore, exploiting the joints position measurement (θ_{mp}, θ_{ip}, θ_{pip}, θ_{dip}) for the different fingers, it is possible to determine the presence of external forces by checking the validity of the coupling equations. Remarkably, the coupling equations can always be written as a one dimensional linear space embedded in an n-dimensional space:

$$\mathbf{q} \in \mathbb{R}^n \text{ s.t. } \mathbf{q} = \mathbf{q}_1 \cdot t + \mathbf{q}_0, \qquad t \in [t_{min}, t_{max}]\,. \tag{B.1}$$

In the case of (2.2), $n = 2$:

$$\mathbf{q} = \begin{bmatrix} \theta_{mp} \\ \theta_{ip} \end{bmatrix}, \qquad \mathbf{q_1} = \begin{bmatrix} \frac{k_{ip}}{k_{mp}+k_{ip}} \frac{r_m}{r_{mp}} \\ \frac{k_{mp}}{k_{mp}+k_{ip}} \frac{r_m}{r_{ip}} \end{bmatrix}, \qquad t = \theta_m, \tag{B.2}$$

$[t_{min}, t_{max}]$ corresponds to the range of the motor rotation. $\mathbf{q}_0$ accounts for the springs rest-length and possible offsets in the motor position and/or in the joint measurements. Fitting (B.1) to a dataset of joint positions (collected in absence of external forces) requires simple linear algebra tools (see [150] for details). Once the model has been built, the distance of an arbitrary configuration $\mathbf{q}$ from the model (B.1) can reveal the presence of an external force on the finger. This distance gives also a qualitative idea of the intensity of the external force: the greater the distance from the model the higher the force. Exploiting this idea a grasp detector has been created; the associated software is available (together with other tools, modules, applications and further documentation) in the iCub open source repository [150].